
# The Role of Adenosine A2A Receptor Signalling in Cardiac Fibrosis

A Thesis Submitted for the Degree of Doctor of Philosophy

Michaelmas Term, 2014

**Alexander Stockenhuber**

Pembroke College

Radcliffe Department of Medicine

University of Oxford

Supervisors: Prof. Houman Ashrafian and Prof. Hugh Watkins

**The role of adenosine A2A receptor signalling in cardiac fibrosis**

Alexander Stockenhuber, Pembroke College, University of Oxford

A thesis submitted for the degree of Doctor of Philosophy, Michaelmas 2014

## Abstract

Myocardial fibrosis contributes to the pathogenesis of diverse forms of cardiac hypertrophy. Recent evidence suggests a crucial role for purinergic signalling in the formation of tissue fibrosis. In particular, inhibition of adenosine A2A receptors (A2AR) in animal models for hepatic and skin fibrosis resulted in a reduction of fibrosis formation. The specific hypothesis of this investigation was that myocardial stress results in increased interstitial levels of adenosine, which activate cardiac fibroblasts via adenosine A2AR. Accordingly, the specific objective of this investigation was to delineate the role of adenosine A2AR signalling in the development of myocardial fibrosis.

*In vitro,* isolated cardiac fibroblasts demonstrated a significant increase in collagen secretion into CCM upon specific A2AR stimulation. This stimulatory effect was inhibited by the addition of a specific A2AR inhibitor.

*In vivo*, models for cardiac hypertrophy including the transgenic cardiac actin E99K hypertrophic cardiomyopathy model, and a transverse aortic constriction (TAC) model of pressure overload, were investigated as murine models for myocardial fibrosis (MF). In cardiac actin E99K hearts the occurrence of cardiac fibrosis was associated with ventricular dysfunction, as well as energetic perturbations. In addition, a direct linear correlation between myocardial collagen content and interstitial adenosine levels was found in actin E99K hearts upon microdialysis experiments. Crossbreeding of actin E99K and A2AR knock-out (KO) mice resulted in a significant reduction of myocardial collagen content and fibrosis in E99K heterozygous A2AR KO animals compared to E99K heterozygous A2AR wild-type (WT) animals.

Further, adenosine A2AR KO mice undergoing transverse aortic constriction demonstrated significantly less fibrosis formation compared to constricted WT mice. This was associated with a significant rescue of cardiac function. In addition, pharmacologic adenosine A2AR inhibition using the antagonist ZM241385 demonstrated a partial rescue of myocardial fibrosis in both TAC and E99K animals.

These data suggest that adenosine the A2AR plays a crucial role in the formation of myocardial fibrosis in a variety of cardiac pathologies and that this pathway is susceptible to pharmacologic modulation. A2AR manipulation may contribute to further understanding of pathophysiological pathways in the development and progression of cardiac disease and represents an excellent therapeutic target for clinically available A2AR antagonists.

## Acknowledgments

I would like to express my special gratitude to both of my supervisors, Professor Houman Ashrafian and Professor Hugh Watkins for providing me with the opportunity to carry out my basic science doctoral studies in their laboratory at Oxford. Despite their extremely busy schedules they always found time to provide me with scientific guidance as well as career mentorship allowing me to grow as a research scientist. Both their continuous support and the opportunity to learn from their inspiring academic example have been invaluable. I am indebted to the British Heart Foundation Centre of Research Excellence and the Medical Research Council for funding my DPhil position. I would also particularly like to express my gratitude to Professor David Greaves whose scientific remarks at several DPhil student meetings proved remarkably insightful.

It is also with particular pleasure that I would like to express my sincere appreciation to all my friends and colleagues with whom I had the privilege to work with in the past three years. I would like to express immense gratitude to Dr Arash Yavari who took me under his wing when I first arrived in the laboratory. Since then his unparalleled enthusiasm and scientific prowess has been an incredible inspiration to me. I would also like to express very special thanks to Mrs Violetta Steeples, and Dr Gabor Czibik who taught me many basic biology techniques with extreme patience and provided me with valuable scientific advice on numerable occasions. Further I would like to thank Dr Mohamed Bellahcene for sharing his vast experience and his surgical expertise and Dr Matthew Kelly for his help with echocardiography and comradeship in- and outside the lab. I would also like to thank Mrs Sahar Ghaffari, Dr Katja Gehmlich, Dr Charles Redwood, Mr Cameron Turtle, Dr Paul Robinson, Dr Matthew Daniels, and Dr Theodosios Kyriakou for their kind help and advice. I would also like to thank Dr James Brown and Mr Phil Townsend, their work in the background ensures smooth running of the laboratory and their support and advice in the implementation new experimental procedures was immensely helpful.

I would like to thank Professor Craigh Lygate for providing his surgical expertise and Dr Damian Tyler for his kind help with investigating cardiac metabolism. I am also very grateful to Dr Nicolaj Støttrup for providing his vast expertise in cardiac physiology and for his amazing hospitality during my stay in Aarhus.

I would also like to express my sincere thanks to my little sister and my parents, their unfailing love and support even from afar has been and still is crucial on my quest to become a clinician scientist.

Finally I would like to thank my dearly loved partner Krista, who has been incredibly loving and supportive throughout the entire process. I also really enjoyed our common endeavours in the lab. Durch dich wird immer noch alles besser!

## Declaration of own work and attribution

Except where specifically outlined below the presented DPhil thesis is entirely my own work. It has not been submitted, either wholly or substantially, for another degree at the University of Oxford, or for a degree at any other institution.

The genotyping for preliminary mouse phenotyping experiments was performed jointly with Dr Katja Gehmlich and Dr Heena Lad.
Nuclear magnetic resonance spectroscopy experiments were performed jointly with Dr Damian Tyler and Dr Mohamed Bellahcene; analysis of the obtained readings was performed by Dr Damian Tyler.
Microdialysis experiments were performed jointly with Dr Nicolaj Støttrup; analysis of the obtained samples with mass spectroscopy was performed by Dr Nicolaj Støttrup.
Flow cytometry experiments were performed jointly with Dr Krista Adelmann.
Cardiac fibroblasts were isolated jointly with Dr Katja Gehmlich and Mr Cameron Turtle.
Invasive haemodynamic assessment was conducted by Dr Mohamed Bellahcene.
Tissue harvest was frequently performed jointly with Dr Mohamed Bellahcene.
Transverse aortic constriction operations were performed by Dr Mohamed Bellahcene and Prof Craig Lygate.
Echocardiography was performed jointly with Dr Matthew Kelly and Dr Arash Yavari; analysis of the obtained echocardiographic images was performed by Dr Matthew Kelly.
While the author performed the majority of intraperitoneal injections, Dr Mohamed Bellahcene, Dr Matthew Kelly, Dr Arash Yavari and Mrs Sahar Ghaffari kindly assisted with these.
Feeding, cleaning and daily checks of experimental animals were carried out by the staff of the Functional Genomics Facility.

# Table of contents

## Abbreviations

| | |
|---|---|
| A2A-R | adenosine A2A receptor |
| A2AR KO | adenosine A2A receptor knock-out |
| A2AR WT | adenosine A2A receptor wild-type |
| ACE | angiotensin-converting enzyme |
| Ado | adenosine |
| ADP | adenosine diphosphate |
| ANP | atrial natriuretic peptide |
| α-sma | α-smooth muscle actin |
| AT-1 | angiotensin II receptor, type 1 |
| ATP | adenosine triphosphate |
| BAPN | β-amino propionitrile |
| BNP | brain natriuretic peptide |
| BRDU | bromodeoxyuridine |
| BSA | bovine serum albumin |
| BW | body weight |
| CCM | cell conditioned medium |
| CFs | cardiac fibroblasts |
| Cxs | connexins |
| DCM | dilated cardiomyopathy |
| DDR-2 | discoidin domain receptor 2 |
| DMSO | dimethyl sulfoxide |
| EF | ejection fraction |
| EMT | epithelial to mesenchymal transition |
| EndMT | endothelial to mesenchymal transition |

| | |
|---|---|
| ENDO A | endocardial area |
| ENTPD | ectonucleoside triphosphate diphosphohydrolase |
| EPI A | epicardial area |
| FACS | fluorescence-activated cell sorting |
| $FADH_2$ | flavin adenine dinucleotide |
| FS | fractional shortening |
| FSC | forward scatter |
| gP38 | glycoprotein 38, podoplanin |
| HBSS | Hank's balanced salt solution |
| HCl | hydrogen chloride |
| HCM | hypertrophic cardiomyopathy |
| HR | heart rate |
| KHB | Krebs-Henseleit buffer |
| KI | knock-in |
| KO | knock-out |
| LOX | lysyl oxidase |
| LV | left ventricle |
| L | LV length in parasternal long-axis |
| MF | myocardial fibrosis |
| MLP | Muscle LIM protein |
| mM | millimolar |
| MMP | matrix metalloproteinases |
| MRI | magnetic resonance imaging |
| mRNA | messenger ribonucleic acid |
| MYBP-C | cardiac myosin-binding protein c |

| | |
|---|---|
| MYH7 | myosin heavy chain |
| NADH | nicotinamide adenine dinucleotide |
| NaOH | sodium hydroxide |
| nM | nanomolar |
| NMR-spec | nuclear magnetic resonance spectroscopy |
| OCT | optimal cutting temperature compound |
| OD | optical density |
| PAGE | SDS-polyacrylamide gel electrophoresis |
| Panx | pannexin |
| PBS | phosphate buffered saline |
| PCr | phosphocreatine |
| PCR | polymerase chain reaction |
| PFA | paraformaldehyde |
| Pi | inorganic phosphate |
| PVDF | polyvinylidene difluoride |
| qPCR | quantitative polymerase chain reaction |
| RAAS | renin-angiotensin-aldosterone system |
| RT-PCR | reverse transcription polymerase chain reaction |
| SSC | side scatter |
| t | LV wall thickness in diastole |
| TAC | transverse aortic constriction |
| TGF-β | transforming growth factor β |
| TIMP | tissue inhibitor of metalloproteinase |
| TNT | troponin-T |
| WGA | wheat germ agglutinin |

| | |
|---|---|
| WT | wild type |
| 31P-NMR | phosphorus-31 nuclear magnetic resonance |

# 1. Introduction

## 1.1. Myocardial fibrosis

### 1.1.1. Fibrosis definition

Fibrosis is the “dark side” of extracellular matrix formation in response to tissue damage (Varga, Brenner, & Phan, 2010). Physiological wound healing is an intricate and strictly regulated process, limited in its spatial and temporal extent. The heart stands out from many other organs, due to the particularly low regenerative capabilities of cardiomyocytes and functional myocardial tissue. As a result, scar formation in response to large-scale cardiomyocyte death, as occurs classically following ischemic insults is crucial to maintain a seal of the heart’s cavity (M. Zeisberg & Kalluri, 2013). Conversely, fibrosis occurs when this repair process is either activated in the absence of tissue necrosis, or when the repair is quantitatively disproportionate to the injurious stimulus, resulting in excessive accumulation of extracellular matrix, which is by itself pathological.

Such excessive extracellular matrix deposition can affect most organs and is commonly considered an irreversible end-stage result of various chronic pathologic processes. In any organ, fibrotic tissue demonstrates a loss of architecture leading to a loss of functional components, including tissue parenchyma as well as vasculature and innervation. These functional components are replaced by non-functional, homogeneous and progressively maturing scar tissue, consisting primarily of fibrillar collagens (type I & III), but also including other collagen subtypes as well as glycoproteins, proteoglycans and fibronectin (Varga et al., 2010). This structural

degeneration and loss of functional tissue components contributes progressively to dysfunction of the affected organ and ultimately results in its functional failure. These fundamental features of fibrosis formation are common to most organs affected by chronic diseases including the heart, kidneys, skin, lung and liver.

The histomorphologic and macroscopic similarities between affected organs have led to the concept of a common “fibrogenic cascade”, i.e. a conserved mechanistic pathway that contributes to fibrosis formation in common fashion in all affected organs. As a result, there is significant optimism that the effectors of this putative pathway could represent promising therapeutic targets across most organs affected by fibrosis (Wynn & Ramalingam, 2012; M. Zeisberg & Kalluri, 2013).

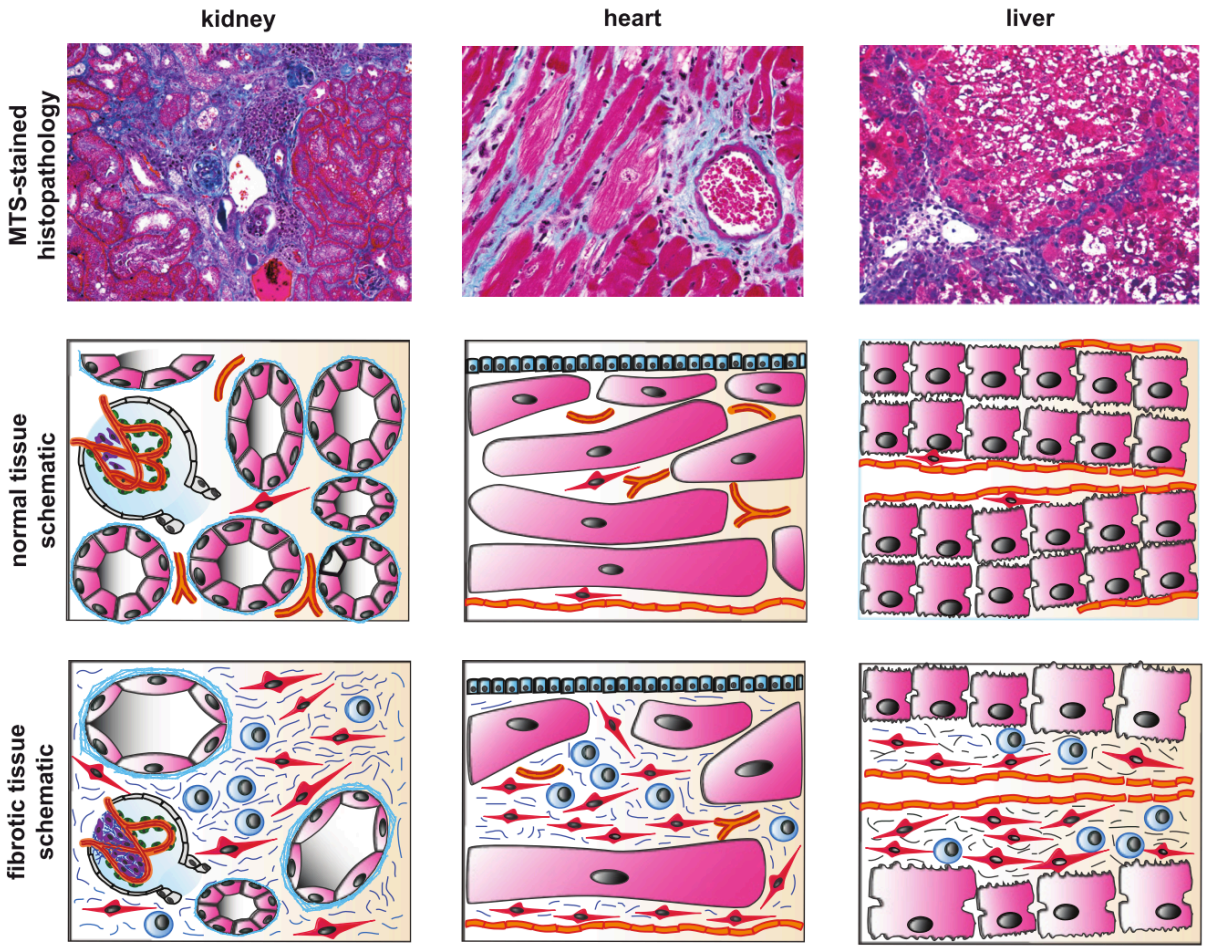


**Figure 1.1:** (Reproduced with permission from M. Zeisberg & Kalluri, 2013) Fundamental features of fibrotic tissue degeneration share many similarities between different organs and pathologies. The schematic figure displays the common effects of tissue fibrosis in the kidney, heart and liver. The top row depicts Masson's Trichrome stained sections of fibrotic animal models of these organs, respectively. The lower two rows demonstrate normal tissue organisation: parenchymal cells (pink) interspersed by the interstitium containing microvessels (orange) and resident fibroblasts (red). Fibrosis in all these organs involves the rarefication of parenchymal cells and vascularization, together with a reciprocal increase in activated fibroblasts, an infiltrate of immune cells and expansion of the interstitium due to accumulation of extracellular matrix (blue).

### 1.1.2. The physiological architecture of the extracellular matrix in the myocardium

Cardiac muscle has a distinct structural architecture, which is largely defined by its extracellular matrix. A thin layer of connective tissue, the pericardium, surrounds the heart. In addition, two thin connective tissue layers forming the myocardial epimysium border the ventricular wall on either side. The external layer is termed epicardium and the layer facing the ventricular cavity is termed endocardium. These two external linings branch into the myocardium forming the perimysium - a continuous network of collagen fibres that enwraps bundles of cardiomyocytes (Robinson, Geraci, Sonnenblick, & Factor, 1988; Rossi, Abreu, & Santoro, 1998). This perimysial network was first described in the papillary muscle of rat hearts and consists of 1-10 μm thick, coiled collagen fibres. Associated with these perimysial fibres are layers or bundles usually consisting of four cardiomyocytes. The first description of these perimysial fibres demonstrated a strongly coiled nature, i.e. describing them as long helices (Purslow, 2008; Robinson et al., 1988). However, more recent studies using confocal microscopy to create three-dimensional reconstructions of the cardiac stromal tissue reveal that these perimysial fibres form planar wavy structures rather than three dimensional coils (Hanley, Young, LeGrice, Edgar, & Loiselle, 1999; Pope, Sands, Smaill, & LeGrice, 2008).

The final arborisation of the myocardial collagen network, the endomysium, forms a weave that envelops each individual cardiomyocyte and each individual cardiac capillary (Macchiarelli et al., 2002; Purslow, 2008). This mesh-like structure is made up of wavy collagen fibrils that homogenously enwrap the entire circumference of the cardiomyocytes and capillaries (Macchiarelli & Ohtani, 2001). Earlier investigations describe twisted collagen bundles, termed “struts”, to connect cardiomyocytes within

the endomysium (Borg & Caulfield, 1981). Conversely, recent backscattered electron emission microscopy experiments demonstrate that endomysial collagen forms a continuous laminar network that spreads between neighbouring cardiomyocytes (Kanzaki et al., 2010), with computational models in support of this view (Intrigila, Melatti, Tofani, & Macchiarelli, 2007). It is therefore now believed that the collagen "struts" described originally were artefacts created by tissue fixation protocols less optimized to preserve the original structure of the myocardium. The myocardial collagen network contains largely fibrillar collagens, mainly collagen type I and type III, with collagen type I making up about 85% of total collagen expressed and collagen type III amounting to approximately 11% of total collagen (K T Weber, 1989).

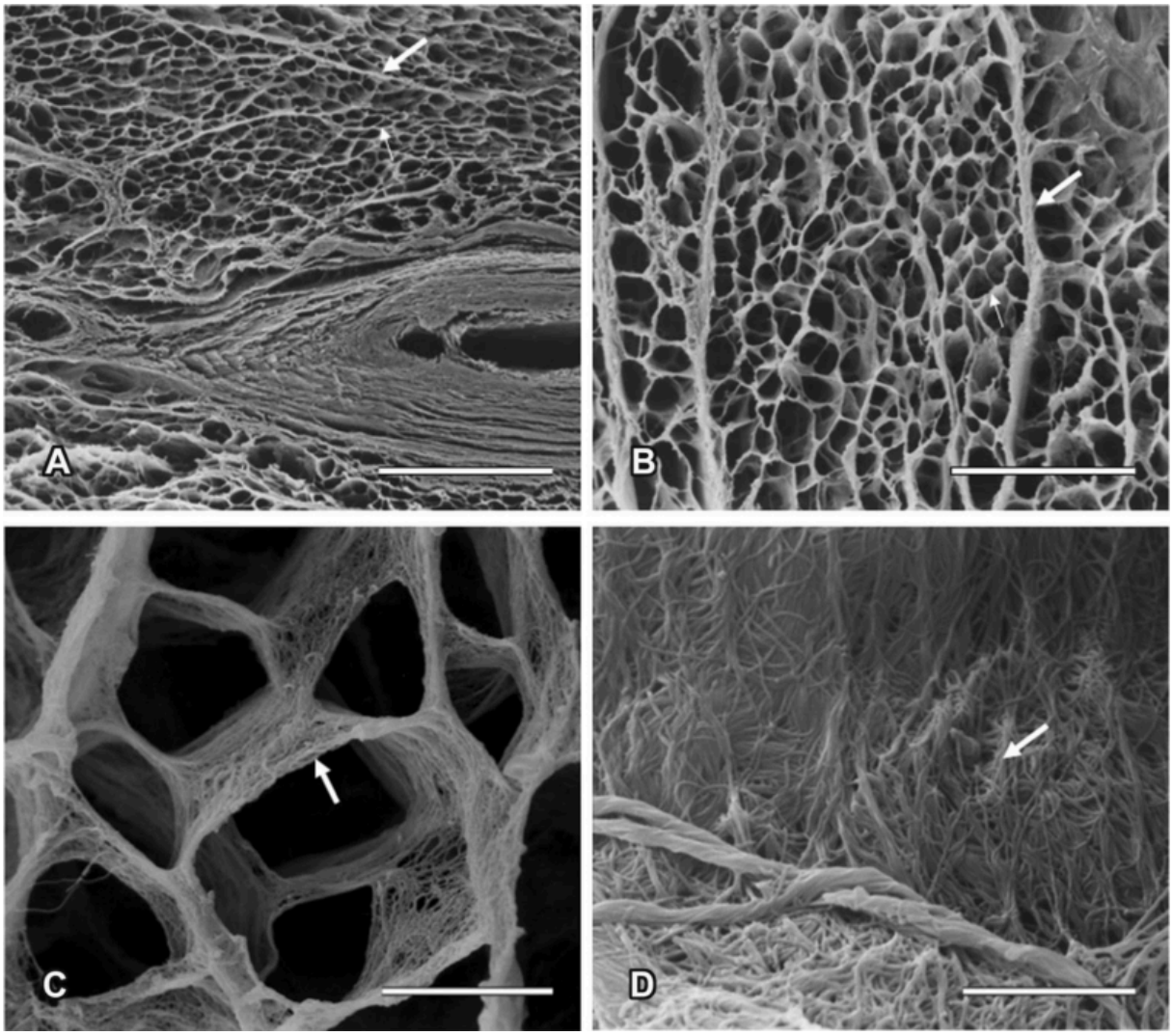


**Figure 1.2:** (Kanzaki et al., 2010) Backscattered electron emission microscopy of NaOH-digested human ventricle. (*A&B*) show the perimysial collagen fibres (thick arrows) and the endomysial network (thin arrows) of the myocardium at different magnifications. Bar=200μm and 100μm, respectively. (*C*) shows the endomysium forming myocyte and capillary lacunae. Bar=10μm. D, shows the endomysium as a planar network of fine collagen fibrils. Bar=3μm.

### 1.1.3 Mechanical functions of the myocardial extracellular matrix network

The primary purpose of the myocardial extracellular matrix network described above is to provide a structural scaffold that allows for efficient transmission of the contractile force developed by the myocyte component of the myocardium (Kong, Christia, & Frangogiannis, 2014).

However the role of the extracellular matrix in cardiac function, in particular in creating the necessary spatial arrangement of cardiomyocyte fibres, is far more complex. Throughout the myocardium cardiomyocytes are arranged into adjacent laminar sheets. These sheets are approximately four cells thick and are rendered a functional unit due to tight endomysial coupling. The perimysial matrix layer between these cardiomyocyte sheets forms a looser connection and contains wavy perimysial collagen strands (Costa, Takayama, McCulloch, & Covell, 1999). These undulating perimysial fibres are believed to be responsible for the non-linear resistance properties of the myocardium against passive displacement. Whereas low-level deformations at physiologic baseline length are met with least resistance, the collagen network provides high stiffness against deformation after a certain length threshold is surpassed.

These perimysial sheets are believed to form “slip planes”, allowing the sheets of cardiomyocytes to rearrange during ventricular contraction (Purslow, 2008). This arrangement permits for the shear strains that necessarily occur during ventricular contraction due to the simultaneous increase in ventricular wall thickness and decrease in ventricular wall plane area while individual myofibre sheets extend. Arts et al. (2001) state that these “*Layers of perimysial connective tissue, separating the*

*myofiber sheets, could be effective in permitting large shear strains without large shear stresses."*

### 1.1.4 Collagen production

As described above the myocardial collagen network consists primarily of fibril forming, i.e. fibrillar, collagen molecules. These collagen subtypes, namely collagen type I, type II and type III are characterized by the assembly into higher-order fibrils. The foremost feature of all collagens is the formation of triple helices formed from three separate polypeptide chains called α chains. The composition of these rope-like structures is facilitated by the protein sequence of the individual α chains. The amino acid glycine makes up every third residue, resulting in the repeating amino acid triplet Gly-X-Y with X and Y potentially being any amino acid. As a result, the glycine residues, which have only a hydrogen substituent as side chain, are small enough to be packed into the centre of the right-handed triple helical structure (Hulmes, 2008).

The triple helical structure of any collagen can be made-up of three identical α chains (homotrimeric) but can also consist of up to three genetically distinct α chains (heterotypic). In the myocardium both of these potential possibilities exist, with collagen type III made-up of three α1 chains whereas collagen type I consists of two identical α1 chains completed by one genetically distinct α2 chain (Hulmes, 2008).

#### *1.1.4.1 The biosynthesis of collagen*

The individual polypeptide α chains of fibrillar collagens are synthesized as precursors directly into the rough endoplasmic reticulum by membrane-associated ribosomes. These larger precursor proteins, called pro-α chains, contain a signal sequence responsible for directing the translating ribosome to the rough endoplasmic reticulum. In addition, however, pro-collagens also consist of larger N- and C-terminal pro-peptides responsible for preventing premature intracellular formation of higher-order collagen fibrils, which could have fatal effects on the cells (Alberts et al., 2002).

Post-translational modifications, in particular hydroxylation of proline and lysine residues as well as glycosylation, also occur within the endoplasmic reticulum. Proline is another amino acid that is very common in fibrillar collagens, making up about 20% of all amino acid components. Proline is thought to stabilise the helical structure of each α chain, thereby enhancing the formation of triple helices. In addition, hydroxylation of proline residues, primarily in the Y position of the Gly-X-Y amino acid repeats, is crucial to the stabilisation of the triple helical structure and has been shown to increase its *in vitro* melting temperature by 30°C. This stabilising effect is believed to be due to the formation of inter-chain hydrogen bonds. The enzymes responsible for proline hydroxylation are prolyl 4-hydroxylase and prolyl 3-hydroxylase. If these enzymes are prevented from proline hydroxylation, as occurs in dietary ascorbic acid (vitamin C) deficiency, scurvy develops. Ascorbic acid is required to return the active iron component of hydroxylases to its oxidised state necessary for hydroxylation. The absence of sufficient hydroxyproline residues prevents the intracellular assembly of stable triple helices, which results in the immediate intracellular degradation of the defective pro-α chains (Hulmes, 2008).

The abundance of hydroxyproline in collagen, compared to negligible incorporation in

other proteins can be utilised to measure the amount of collagen content in tissues, (described in more detail in the materials and methods section).

Following post-translational modifications, three collagen pro-α chains combine into triple helical pro-collagen molecules, in a zipper-like manner from the C-terminal to the N-terminal end. The pro-peptide molecules guide this process and the resulting triple helical structure is stabilised by the formation of intra molecular hydrogen bonds. These pro-collagen molecules then pass through the Golgi- apparatus of the cell, are accumulated in secretory vesicles and then released into the extracellular space by exocytosis. After secretion, the N- and C-terminal pro-peptides are removed by extracellular proteolytic enzymes. This conversion from pro-collagen to collagen molecules, i.e. the removal of pro-peptides, allows for the formation of large, higher-order collagen fibrils. Fibril-formation of fibrillar collagen subtypes is a largely self-driven process since these molecules are far less soluble after the removal of the pro-peptides and have a strong tendency to self-assemble into fibrils. However, the process of fibril formation occurs in the immediate vicinity of the cell surface, usually in deep infolds of the plasma membrane. As a result, the collagen producing cells, usually fibroblasts, can strongly regulate the speed, the direction and extent of fibril formation. The enzymes responsible for cutting of the N- and C-terminal pro-peptides of pro-collagen are active only in the extracellular space. Accordingly, collagen molecules and N- or C- terminal collagen pro-peptides are secreted by fibroblasts in a 1:1 ratio, respectively. As a result measuring these pro-peptides, in particular the C-terminal pro-peptide of pro-collagen type I, from blood samples has been established as a biomarker for increased collagen production. Even though the mechanism of collagen production is in no way specific to the heart (van Kuijk et al.

2010), in many cardiac diseases circulating collagen pro-peptide levels have been shown to reflect myocardial collagen production (López, González, and Díez 2010). This biomarker not only correlates with increased collagen production, but also with adverse patient outcomes in hypertension (Plaksej et al., 2009), heart failure (Barasch et al., 2011) and hypertrophic cardiomyopathy (Ho et al., 2010).

After collagen secretion and the extracellular aggregation into fibrils, collagen maturation, i.e. the formation of covalent intermolecular crosslinks, is considered the final step of collagen production. These covalent crosslinks are necessary for fibrillar collagens to generate mechanical resistance against tensile stress on the one hand and also resilience to degradation by extracellular proteinases on the other. Lysyl oxidase (LOX), an extracellularly expressed enzyme, is primarily responsible for the formation of these crosslinks. Lysyl oxidase catalyses the formation of highly reactive allysine aldehyde groups on lysine and hydroxylysine residues on collagen molecules. These aldehyde groups spontaneously form covalent crosslinks by condensing with other lysine residues. Such inter molecular connections are uniquely found in collagen and a failure in the production of crosslinks results in significant weakening of collagenous tissues.

Physiological expression of lysyl oxidase - and as a result the extent of collagen crosslinking - is variable between tissues and usually highest in tissues under the greatest mechanical stress, such as tendons. In the myocardium, an up-regulation of LOX expression - resulting in higher formation of collagen crosslinks and increased left ventricular stiffness - has been demonstrated in patients with chronic heart failure in several pathophysiological circumstances, such as hypertensive heart disease

(López B. et al. Hypertension 2009), aortic stenosis (Valencia F. et al. JACC 2010) and dilated cardiomyopathy (Sivakumar P. et al. Mol Cell Biochem 2008).

Collagen fibrils demonstrate a very particular pattern of cross striations (every 67 nm) under an electron microscope, which is due to the collagen molecules being arranged very regularly. This exact regular arrangement also results in the anisotropic optical properties of collagen after picro-sirius red staining when observed under polarized light microscopy.

### 1.1.5. The cardiac fibroblast

Fibroblasts in general are mesenchymal cells, existing in most tissues and organs containing connective tissue, being spatially and functionally associated with the extracellular matrix (Boor & Floege, 2012; Kalluri & Zeisberg, 2006). Fibroblasts are responsible for the formation and organisation of extracellular matrix under physiologic as well as pathologic circumstances. Fibroblasts were first described as early as 1858 by Virchow and other pioneer pathologists as spindel-shaped cells responsible for production of connective tissue (Virchow, 1858).

The myocardium consists of a number of cell types including contractile cardiomyocytes, cardiac fibroblasts (CFs) and immune cells. While cardiomyocytes comprise about two thirds of the myocardial volume, non-cardiomyocytes make up the majority of cells, constituting approximately 70% of the cells in the myocardium. Further, fibroblasts make up the majority of non-cardiomyocyte cells in the myocardium (Nag, 1980; Souders, Bowers, & Baudino, 2009; Zak, 1974). Alongside the cells constituting the heart's vascular system (endothelial cells, pericytes and smooth muscle cells) (Camelliti, Borg, & Kohl, 2005; Fan, Takawale, Lee, & Kassiri, 2012) these cellular components interact dynamically in response to developmental, homeostatic and pathophysiologic cues. Under physiologic circumstances, CFs provide a constant low-level collagen turnover maintaining the dynamic equilibrium of collagen synthesis and degradation, resulting in a collagen half-life of 80 to 120 days (Laurent, 1987).

CFs are therefore responsible for maintaining the three-dimensional, stress-tolerant collagen network throughout the myocardium, which in turn preserves tissue

architecture and chamber geometry (Porter & Turner, 2009; Sun & Weber, 2010). Following upon most pathologic stimuli in the myocardium, it is believed that CFs react with the increased production of extracellular matrix proteins, becoming “activated fibroblasts”. Signs of augmented biosynthetic properties, such as a prominent rough endoplasmatic reticulum, together with a prominent nucleolus and Golgi complex, characterize these activated fibroblasts.

In most models of cardiac disease processes this “activated fibroblasts” cell population further trans-differentiates over time from protomyofibroblasts into myofibroblasts. This differentiation step is defined by the intracellular expression of contractile proteins such as α-smooth muscle actin (α-sma). This cascade of activation and differentiation is accompanied by an increase in migratory, proliferative and secretory properties. This results in larger numbers of activated fibroblasts and increased release of extracellular matrix proteins and pro-fibrotic signalling molecules (Karl T Weber, Sun, Bhattacharya, Ahokas, & Gerling, 2013).

During embryological development the majority of resident cardiac fibroblasts originally arise from the proepicardium by undergoing epithelial to mesenchymal transition (EMT). However, there is still considerable debate concerning the origin of activated cardiac fibroblasts in the pathologically fibrotic myocardium. Resident cardiac fibroblasts are the most numerous individual cell type in the normal myocardium and are distributed ubiquitously throughout (Souders et al., 2009). As a result, the activation of resident cardiac fibroblasts is considered the primary source of activated CFs (Kong et al., 2014). This is further supported by the fact that pathologic changes in the myocardium induce a strong up-regulation of mediators,

which induce fibroblast activation and proliferation, such as transforming growth factor β (TGF-β).

However, recent evidence suggests several additional cellular sources for activated cardiac fibroblasts. Bone marrow-derived fibrocytes, recruited via the circulatory system, may represent an additional source of activated fibroblasts in the myocardium. These cells have been shown to accumulate in the myocardium after ischemic injury (Frangogiannis et al., 2007; Möllmann et al., 2006) and are believed to contribute to post-ischemic ventricular remodelling.

In addition to the activation of resident cardiac fibroblasts, the embryologic pathways that regulate the development of cardiac fibroblasts are reactivated under pathologic circumstances in the adult myocardium. The intricate epicardial-myocardial interactions from embryologic development thus appear to be redeployed. As a result, epithelial (epicardial) to mesenchymal transition contributes to the recruitment of activated cardiac fibroblasts in the adult heart (Von Gise & Pu, 2012).

Furthermore, a substantial portion of activated cardiac fibroblasts in fibrotic hearts appears to be of endothelial cell origin. Lineage tracing analysis, using *Tie1Cre;*R26RstoplacZ mice in models of cardiac pressure overload as well as chronic cardiac allograft rejection, have revealed that endothelial to mesenchymal transition (EndMT) partially drives the accumulation of activated fibroblasts (E. M. Zeisberg et al., 2007).

A potential primary vascular origin for activated fibroblasts in the myocardium, be it recruitment from the circulation or the endothelium, is favoured by many authors due

to the common perivascular localisation of activated fibroblasts in myocardial fibrosis (Kong et al., 2014). Similarly, pericytes can trans-differentiate into α-sma expressing, collagen-producing cells. However, the phenotypic similarities of pericytes and fibroblasts together with the absence of definitive differentiating markers, has hindered a clear investigation of the role of pericytes in myocardial fibrosis.

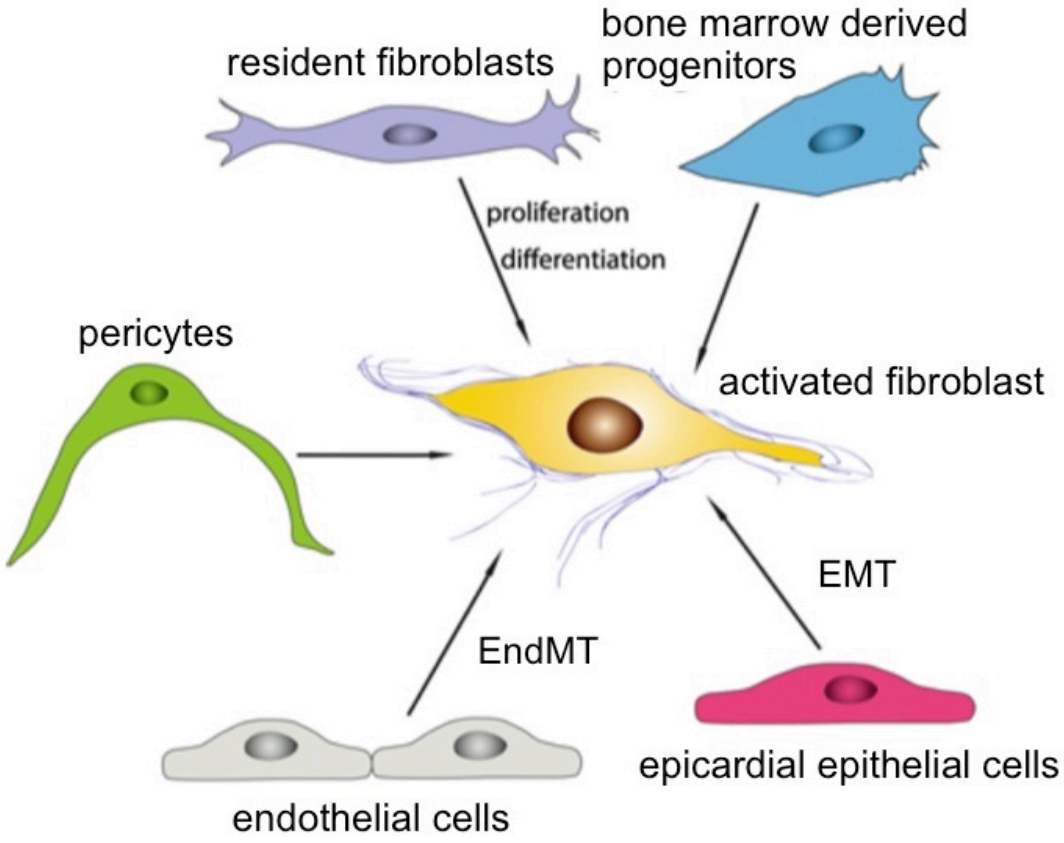


**Figure 1.3:** adapted with permission (Kong et al., 2014) Different cellular sources for activated cardiac fibroblasts in the myocardium. Bone marrow derived fibroblast progenitors, namely fibrocytes, are recruited to the myocardium via the circulation and contribute to myocardial fibrosis (top right). Epithelial/epicardial cells undergo epithelial-mesenchymal transition to become activated fibroblasts (bottom right). Further, various cellular components of the vasculature, including endothelial cells (bottom left) via endothelial to mesenchymal transition and also pericytes (left), contribute to the cellular pool of activated cardiac fibroblasts. Finally, resident fibroblasts are found in abundance throughout the myocardium, as a result their activation likely contributes a large portion of activated cardiac fibroblasts.

The proportional contribution of each of the potential cellular origins to the final pool of activated cardiac fibroblasts seems to be dependent on the nature of the pathological stimulus and also differs between experimental approaches (Kong et al., 2014). Whereas proliferation and activation of resident cardiac fibroblasts seems to play an important role in most cardiac pathologies, EndMT, EMT and haematopoietic progenitors play different roles dependent on the pathophysiologic context (Kong et al., 2014; Krenning, Zeisberg, & Kalluri, 2010).

However, very recent evidence from a mouse model of cardiac pressure overload suggests that the proliferative and activation response of cardiac fibroblasts is largely independent of their origin (Ali et al., 2014). Although it is the author's opinion that this paper's conclusions are limited by the choice of cell surface fibroblast markers and cannot be generalised to other cardiac pathologies, the work does suggest that there is a shared mechanism of activation between different fibroblast subsets.

### 1.1.5. Myocardial fibrosis

Myocardial fibrosis is the abnormal and adverse formation of extracellular matrix in the myocardium and plays an important role in most cardiac diseases (Brown, Ambler, Mitchell, & Long, 2005).

Biochemically, myocardial fibrosis can be delineated as an increase in the collagen specific amino acid hydroxyproline (Jugdutt & Amy, 1986).

However, the primary investigation finding that defines myocardial fibrosis is the microscopic histomorphological description of scar tissue formation. This scarring process can be either in response to tissue necrosis, i.e. replacement fibrosis following cardiomyocyte necrosis, or reactive due to more insidious injurious stimuli. In such cases, e.g. pressure overload, microscopic investigation reveals predominantly interstitial or perivascular fibrosis without tissue necrosis (Creemers and Pinto 2011).

Anderson et al. have suggested a histopathologic classification of myocardial fibrosis in 1979, dividing myocardial fibrosis into four distinct forms (Anderson et al., 1979).

1. *Scar formation.* Fibrosis visible to the naked eye is almost exclusively due to the replacement of diseased cardiomyocytes resulting in a gross macroscopic scar. In addition, the loss of cardiac tissue can also lead to the formation of microscopic scars, not readily visible. Such microscopic scars are focal in nature and occur in loci previously occupied by myocardium.

2. *Interstitial fibrosis* occurs as an increase of the extracellular matrix in the endomysial or perimysial component of the myocardium without a necessary

loss of the structure. Interstitial fibrosis can either be focal, involving only localised areas in the myocardium or, in more severe cases, can diffusely spread throughout the myocardium. As the collagen network envelops every individual cardiomyocyte, this process can lead to significant encasement of muscle cells, resulting in a thick “honeycomb” appearance of the extracellular matrix network.

3. *Perivascular fibrosis.* While the wall of large intracardiac vessels already contains collagenous connective tissue, its amount can be further increased in cardiac pathologies. This is usually also associated with the extension of collagen to the tissue surrounding more peripheral arborisations of the heart’s vasculature. In severe cases, the additional collagenous tissue surrounding these vessels can merge with the adventitia of other vessels and the perimysial collagen network. This accentuates the perimysial strands separating myocyte bundles, resulting in a “lobulated appearance” of the myocardium.

4. *Plexiform fibrosis* is the most specific form of myocardial fibrosis as it appears most commonly in hypertrophic cardiomyopathy, and only very rarely in other cardiac disease. The defining factor is the combined appearance of myocardial fibrosis and myocyte disarray without the replacement of cardiomyocytes.

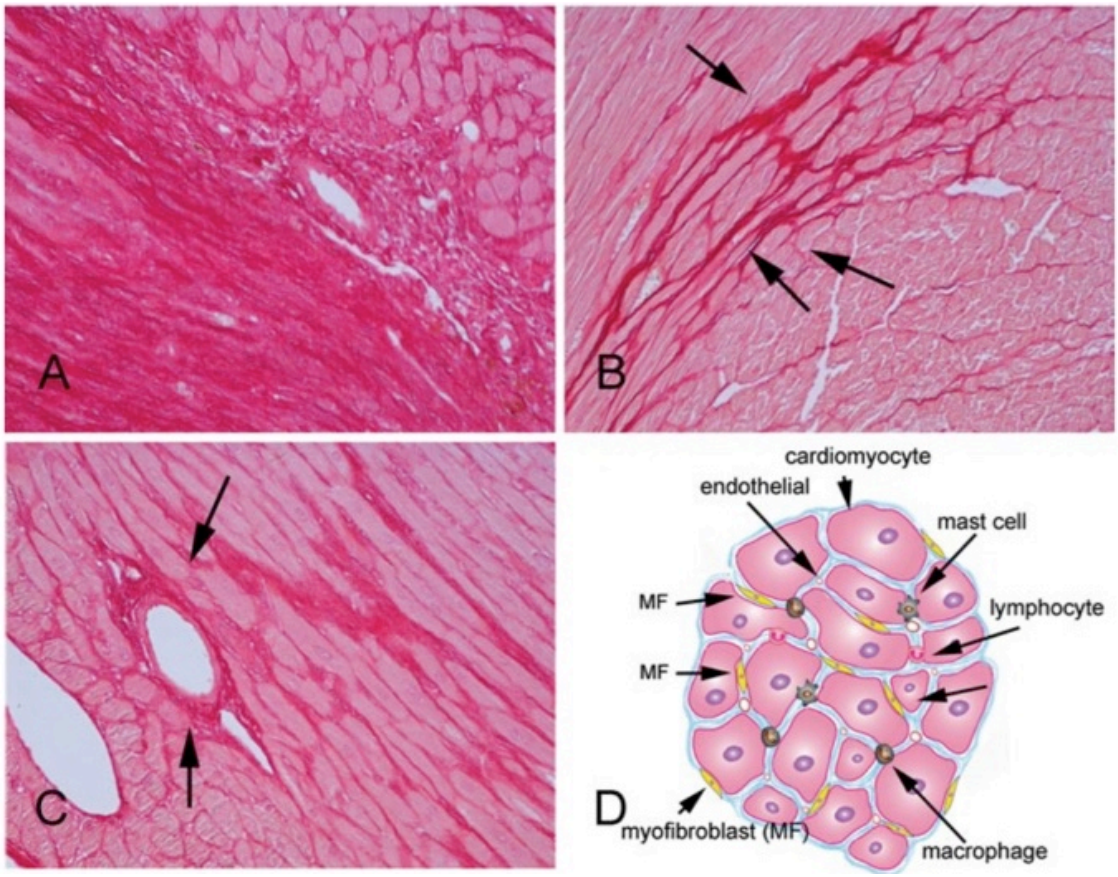


**Figure 1.4:** (Kong et al. 2014 with permission) Examples of different histologic subtypes of myocardial fibrosis demonstrated by Sirius-red stained histologic sections. *(A)* The sudden loss of cardiomyocytes due to ischemic insults results in the formation of replacement fibrosis, i.e. a scar. *(B)* Interstitial fibrosis is characterised by an increase in collagen signal between viable cardiomyocytes, either the endomysial or perimysial component. *(C)* Perivascular fibrosis constitutes an expansion of collagenous vascular adventitia. *(D)* Activated fibroblasts (myofibroblasts) are the cells primarily responsible for the formation of fibrosis.

#### *1.1.5.2. Myocardial fibrosis in pressure overload*

An increase in cardiac afterload is the common pathologic stimulus in many common cardiac diseases, including hypertension and aortic stenosis. Under such haemodynamic conditions the heart is required to develop higher intra-cardiac systolic pressures in order to maintain acceptable cardiac output. As a result of this, the heart undergoes maladaptive changes, including the development of hypertrophy and fibrosis (Kong et al., 2014).

Animal models reflecting the hearts pathophysiologic changes in response to induced pressure overload, in particular transverse aortic constriction (TAC), demonstrate a rapid development of hypertrophy and fibrosis both in primate (Abrahams, Janicki, & Weber, 1987) and murine models (K. T. Weber et al., 1988; Ying et al., 2009).
The response to ventricular pressure overload is typically biphasic: a hypertrophic and fibrotic, although functionally compensated, phase is eventually superseded by cardiac dilation and functional decompensation.

The primary pro-fibrotic mechanism in pressure overload is believed to be TGF-β up-regulation (Kuwahara et al., 2002), however low-level activation of pro-inflammatory pathways and angiotensin II activation also seem to be important (Kong et al., 2014). These pathways are responsible for regulating the early development of fibrosis and contribute to the hypertrophic phenotype.

Conversely, the exact mechanisms responsible for the detrimental dilative changes in ventricular geometry have not been fully elucidated. The structural weakening of the myocardial fabric, as a result of an increase in collagen degradation has been

suggested as a potential mechanism. In an animal model for left ventricular hypertrophy due to hypertension, the development of congestive heart failure was accompanied by the de-regulation of matrix metalloproteinases (MMP) (Iwanaga et al., 2002; Kong et al., 2014). However this does not prove a causal connection between MMP regulation and left ventricular chamber dilation per se.

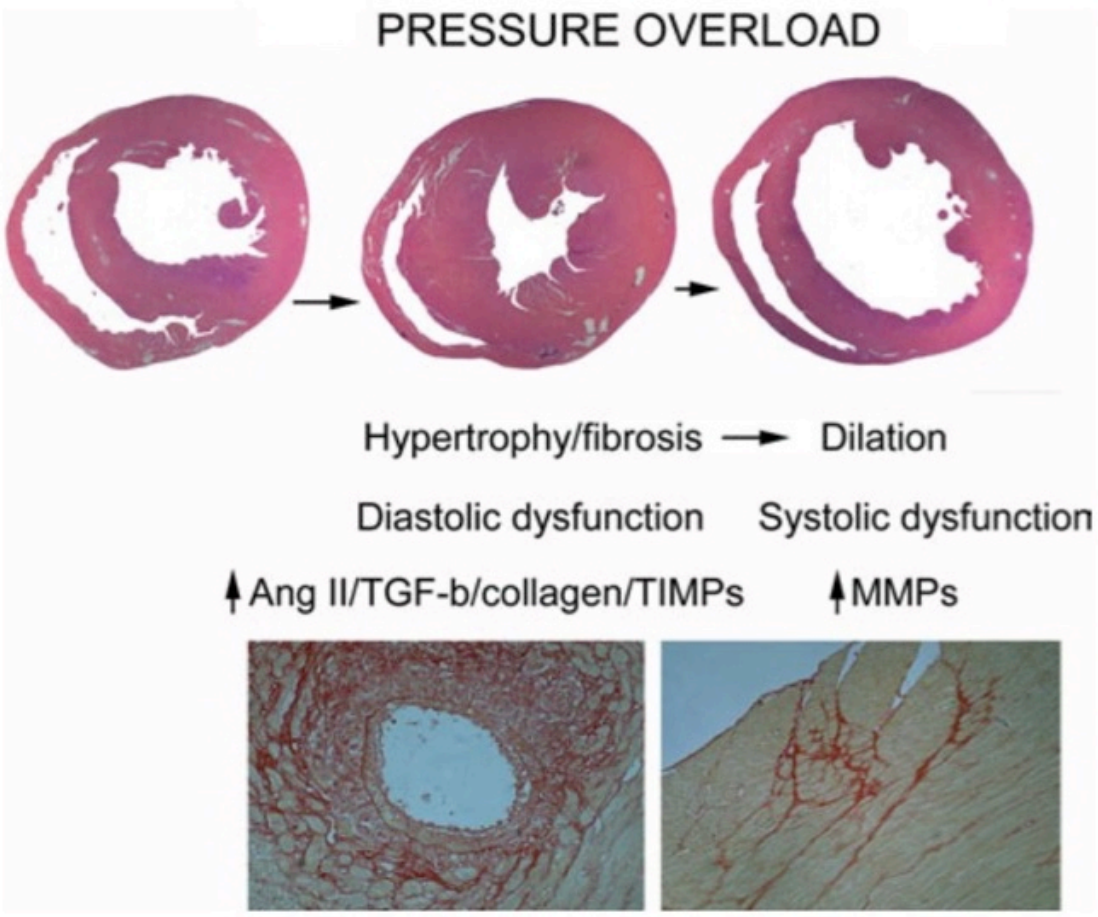


**Figure 1.5:** (Kong et al. 2014 with permission) Pressure-overloaded hearts demonstrate an early hypertrophic and fibrotic phenotype. This is accompanied by diastolic dysfunction with systolic function being mostly compensated. Pro-hypertrophic and pro-fibrotic signalling mechanisms, including angiotensin II and TGF-β mediate this early compensation. The compensated phenotype is typically followed by decompensation of systolic function and chamber dilation. The exact mechanism responsible for the development of heart failure due to pressure overload has not been elucidated, however, weakening of the myocardial scaffold due to an increase in interstitial proteolysis is deemed partially responsible. The deconstruction of matrix components is caused by the up-regulation of extracellular matrix metalloproteinases. Typical histopathologic changes in animal models for pressure overload are perivascular and interstitial fibrosis (*lower panel left and right, respectively*).

#### *1.1.5.3. Myocardial fibrosis in inherited cardiomyopathies*

Hypertrophic cardiomyopathy (HCM) is the most common monogenetic heart muscle disease. It has been termed a “disease of the sarcomere” since the large majority of disease-causing mutations involve genes encoding sarcomeric proteins (Watkins, Ashrafian, & Redwood, 2011). However, the pathophysiological processes involved in HCM are not limited to the cardiomyocyte (M. S. Maron et al., 2011). Typical hallmarks of HCM are asymmetric left ventricular hypertrophy and a dynamic pressure gradient within the left ventricle due to sub-aortic stenosis. This pressure gradient is typically connected to the movement of the anterior mitral leaflet towards the hypertrophied septum, which can result in endocardial thickening and subendocardial fibrosis, termed “impact lesion”.

Histopathologic hallmarks of HCM are cellular hypertrophy and disorganisation, the wall thickening of intramural coronary arteries, small vessel disease (B. J. Maron, Wolfson, Epstein, & Roberts, 1987) and myocardial fibrosis. The clinical course of patients with these cardiomyopathies is associated with the presence or absence of myocardial fibrosis on cardiac magnetic resonance imaging (MRI) such that those with higher levels of myocardial fibrosis demonstrate poorer cardiac outcomes, including a higher rate of arrhythmic events, heart failure and sudden cardiac death (Cho et al., 2010; Dweck et al., 2011; O’Hanlon et al., 2010).

Animal models of HCM manifest activation of pathways involved in cardiac collagen deposition and fibroblast activation in the early stages of disease. In the hearts of young mice bearing α-cardiac myosin heavy chain mutations, significant myocardial fibrosis is present before overt hypertrophy (Teekakirikul et al., 2010). A study of

human sarcomere mutation carriers demonstrated that cardiac collagen synthesis is significantly increased in gene carriers, even in the pre-hypertrophic stage (Ho et al., 2010). These findings suggest a potentially significant pathophysiological role for diffuse interstitial myocardial fibrosis in HCM.

### 1.1.6. Known signalling mechanisms contributing to myocardial fibrosis

#### *1.1.6.1 TGF-β*

As in other organs, TGF-β plays a crucial role in the development of fibrosis as the main mitogenic signalling factor in the myocardium. As a result TGF- β is perhaps the most investigated fibrogenic growth factor (Kong et al., 2014).

There are three distinct but structurally similar isoforms of TGF-β (TGF-β 1-3), which are encoded by separate genes. Even though these isoforms of TGF-β activate downstream signalling mechanisms via the same receptor, producing comparable results during *in vitro* studies, the *in vivo* effects of these isoforms are believed to be different (Dobaczewski, Chen, & Frangogiannis, 2011).

All isoforms of TGF-β are secreted as biologically inert complexes, consisting of three distinct parts: latent TGF-β binding protein, latency-associated peptide and the actual receptor activating TGF-β. These complexes are covalently bound to the extracellular matrix until proteolytic cleavage by proteases such as plasmin, MMP-2 or MMP-9 leads to the release of active, i.e. receptor-activating TGF-β. Because of this secretion and activating mechanism, latent TGF-β is stored in the interstitial matrix in relatively large amounts. As a result, activation of only a small portion of latent TGF-β can elicit a full-scale biologic response (Dobaczewski et al., 2011). The causal connection between proteolytic activity in the interstitium and activation of latent TGF-β indicates the latter's regulatory role linking extracellular matrix degradation and activation of signalling pathways, thereby prompting the formation and stabilisation of extracellular matrix (Kong et al., 2014).

Genetic gain- as well as loss-of-function approaches have been applied in order to

investigate causality for the role of TGF-β in myocardial fibrosis formation. Cardiac transgenic overexpression of TGF-β has been shown to result in pronounced left ventricular hypertrophy and interstitial fibrosis, coupled with alterations in expression and tissue activity of MMPs and their endogenous inhibitors (TIMP).

Inhibition of myocardial fibrosis by blocking the TGF-β response has been demonstrated in several models, including the pressure-overloaded heart (Kuwahara F. et al. Circulation 2002). In addition, pharmacologic treatment with a specific anti-TGF-β-antibody in a model for HCM resulted in a significant reduction in myocardial fibrosis and proliferation of non-cardiomyocytes (Teekakirikul P. et al. JCI 2010).
TGF-β has been shown to induce proliferation and activation of fibroblasts in the heart via the intracellular Smad signalling pathway, leading to increased production of collagen.

#### *1.1.6.3 Neurohumoral pathways*

There is extensive evidence connecting an activation of the renin-angiotensin-aldosterone system (RAAS) to the development of myocardial fibrosis, independent of the underlying cause (Kong et al., 2014). Several cell types in the myocardium, including activated fibroblasts and recruited immune cells express key enzymatic components of the RAAS including renin and the angiotensin-converting enzyme (ACE) (Karl T Weber et al., 2013). As a result, angiotensin II is created locally within the myocardium at the site of pathologic stimuli. *In vitro* studies have shown that angiotensin II activates cardiac fibroblast collagen production and proliferation (Sadoshima & Izumo, 1993; Schorb et al., 1993) via the type one angiotensin II receptor, type 1 (AT-1) (Crabos, Roth, Hahn, & Erne, 1994). In accordance with these findings, the inhibition of ACE or AT-1 significantly reduces myocardial fibrosis in animal models for myocardial infarction (Schieffer et al., 1994), pressure overload (Regan, Anderson, Bishop, & Berecek, 1997), and hypertrophic cardiomyopathy (Teekakirikul et al., 2010). In keeping with this, the beneficial effects of these widely used therapeutic interventions in human heart failure patients is considered to be partially mediated by an amelioration of pro-fibrotic mechanisms. However, both ACE inhibitors and angiotensin receptor blockers (sartans) have multifactorial effects on cardiac haemodynamics that may indirectly influence cardiac fibrosis.

In addition, the angiotensin II-regulated mineralocorticoid aldosterone has also been shown to elicit a pro-fibrotic mechanisms (Brilla, 2000; Lijnen & Petrov, 2000), potentially through a direct stimulatory effect on cardiac fibroblasts (Brilla, Zhou, Matsubara, & Weber, 1994; Neumann et al., 2002).

This is further evidenced by the fact that mouse models for myocardial fibrosis formation have been developed, which utilise angiotensin or aldosterone injections as pro-fibrotic mechanism. Continuous treatment of animals with aldosterone or angiotensin II leads to severe fibrosis formation after four weeks (Sun & Weber, 2010).

#### *1.1.6.4 Collagen production and maturation*

By enhancing the formation of lysine-derived covalent cross-linking of fibrillar collagen proteins, LOX strengthens the mechanical resilience of collagen fibrils and their resistance against degradation and removal by MMPs. This mechanism significantly correlates with left ventricular (LV) stiffness and consequently with the development or exacerbation of diastolic dysfunction. Mechanistically, it has been shown that TGF-β signalling leads to mRNA stabilisation of the protein LOX, thereby increasing the level of LOX protein expression in myocardium. This association of an increase in TGF-β signalling with an up-regulation of LOX expression - with resulting higher formation of collagen crosslinks and increase in LV-stiffness - has been demonstrated in patients with chronic heart failure in several pathophysiological circumstances, such as hypertensive heart disease (López B. et al. Hypertension 2009), aortic stenosis (Valencia F. et al. JACC 2010) and dilated cardiomyopathy (Sivakumar P. et al. Mol Cell Biochem 2008).

## 1.2. Energy deficiency in the hypertrophied myocardium

In the natural history of most progressive cardiac diseases heart failure is the inevitable disease endpoint. As in most organs, the development of heart failure is accompanied by the formation of pathological tissue fibrosis.

It is well recognised that deleterious alterations in cardiac metabolism and energetics are a principle pathophysiologic driving factor for the development of heart failure. This “energy-starvation hypothesis” of heart failure is supported by the finding that energetic-ameliorating therapeutic approaches such as beta-blockers (Packer et al., 1996), ACE inhibitors (Pfeffer et al., 1992) and angiotensin-receptor blockers (Cohn & Tognoni, 2001; Pfeffer et al., 2003) have a positive effect on prognosis in heart failure (Stefan Neubauer, 2007). Further, drugs that increase the myocardium’s energetic demand, such as phosphodiesterase-3-inhibitors or sympathomimetics, in spite of improving cardiac function in the short term, have demonstrated detrimental effects on patient outcome in long-term treatment studies (Cohn et al., 1998).

Cardiac energetics consist of three main aspects: substrate utilisation, oxidative phosphorylation and high energy phosphate metabolism (Stefan Neubauer, 2007). Substrate utilization entails the uptake of fatty acids and, to a lesser extent glucose, followed by beta-oxidation or glycolysis, respectively. The resulting intermediary products converge onto the citric acid cycle and consequently fuel the respiratory chain in the form of NADH and $FADH_2$ oxidative phosphorylation. The resulting biochemical energy in form of ATP is transformed into another high-energy phosphate, namely phosphocreatine, via the enzyme creatine kinase. Through this enzyme ATP can also be readily regenerated from phosphocreatine, typically at the

contracting myofibrils when required. Through this mechanism, phosphocreatine serves as an energy transporter and buffer in the acute vicinity of the contractile apparatus. As a result, during enhanced energetic demands ATP levels remain normal, while phosphocreatine levels drop due to utilisation to reform ATP (Stefan Neubauer, 2007).

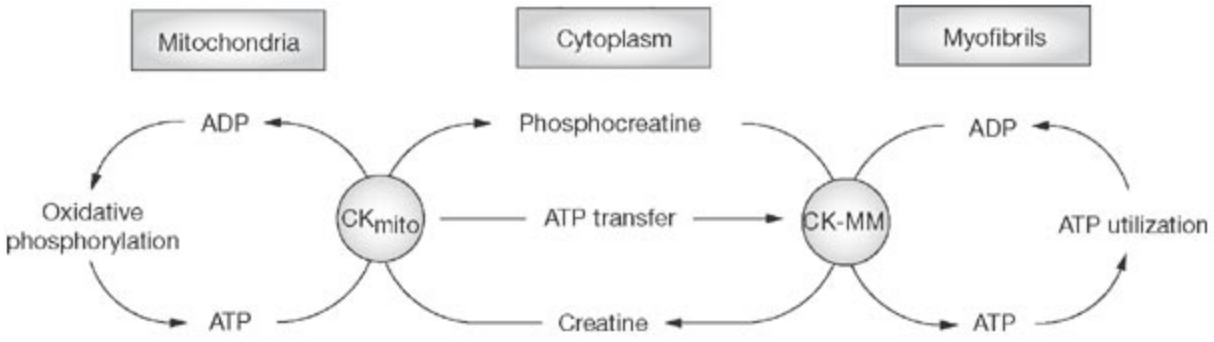


**Figure 1.6:** Reproduced with permission from (Hudsmith and Neubauer 2008). In the myocardium, biochemical energy is produced in the form of ATP, which is generated from substrate utilization (fatty acids and glucose) and subsequent oxidative phosphorylation within the mitochondria. The resulting biochemical energy is transferred onto phosphocreatine, which serves as energy transporter and buffer alike. Phosphocreatine diffuses more freely to the contractile apparatus where the biochemical energy can readily be reconverted into ATP, which is utilized by the myofibrils.

The metabolic state of the myocardium can be investigated in human patients and animal models alike. The classic analysis of obtained tissue, or plasma samples, for metabolites that define the metabolic state, such as ATP, ADP or phosphocreatine is flawed however, due to the rapid degradation of these molecules (Stefan Neubauer, 2007). As a result, phosphorus-31 nuclear magnetic resonance (31P-NMR) spectroscopy is regarded as the method of choice for investigating ATP and phosphocreatine levels in the myocardium and other tissues. This method can be applied with minimal invasiveness for human subjects (Hudsmith & Neubauer, 2008)

and large animals. In the case of murine models, however, this method has so far failed to produce consistent meaningful values due to the much smaller heart volumes and faster heart rate. As a result, 31P-NMR spectroscopy of murine hearts is usually carried out under Langendorff perfusion of explanted hearts (Schroeder et al., 2013; Zhang et al., 2008). Both of these methods produce 31P-NMR spectra, consisting of peaks for phosphocreatine, as well as three distinct peaks for each of the phosphate molecules on ATP. These peaks are directly proportional to the levels of phosphocreatine and ATP, which allows calculating the ratio of phosphocreatine and ATP concentrations in the myocardium. Under states of increased energy demand, the concentration of ATP is kept stable within the cardiomyocytes at the cost of phosphocreatine levels as a result of the creatine kinase equilibrium. Therefore, a decrease of the myocardial phosphocreatine:ATP ratio is the primary indicator for metabolic perturbation, while ATP levels remain unchanged until the phosphocreatine levels are exhausted (Stefan Neubauer, 2007). In patients with heart failure, a decrease in this ratio correlates with the clinical presentation according to the New York Heart Association classification (S. Neubauer et al., 1992), as well as functional parameters (S Neubauer et al., 1995) and patient outcome (Stefan Neubauer, 2007; Stefan Neubauer et al., 1997).

Perturbations of cardiac energetics can be found in a range of cardiac pathologies. Among these, HCM stands out as an exemplar for energy depletion as a causal driver of disease development (Ashrafian, Redwood, Blair, & Watkins, 2003; Watkins et al., 2011). HCM is caused by mutations of sarcomeric proteins, which lead to inefficient and profligate sarcomeric ATP consumption, myocardial hypercontractility, and ultimately excessive myocardial energy consumption. The pathophysiologic role

for energy deficiency in HCM is further supported by the observation that mutations affecting primary energy production or energy sensing mechanisms within the myocardium recapitulate the phenotype of classical sarcomeric HCM (Ashrafian et al., 2003). In particular, mitochondrial tRNA mutations, impeding mitochondrial energy production result in the development of a cardiac phenotype similar to that of patients with sarcomeric mutations (Merante, Tein, Benson, & Robinson, 1994). In addition, mutations in AMP activated protein kinase, an enzyme responsible for energy sensing and a central orchestrator of intracellular metabolism, cause a cardiac phenotype that recapitulates central features of HCM (Blair et al., 2001).

As described above, HCM is also characterised by the early development of myocardial fibrosis (Ho et al., 2010). A significant correlation has been found between impaired cardiac energetics and myocardial fibrosis (Esposito et al., 2009) suggesting a connection, albeit not proving a causal relationship.

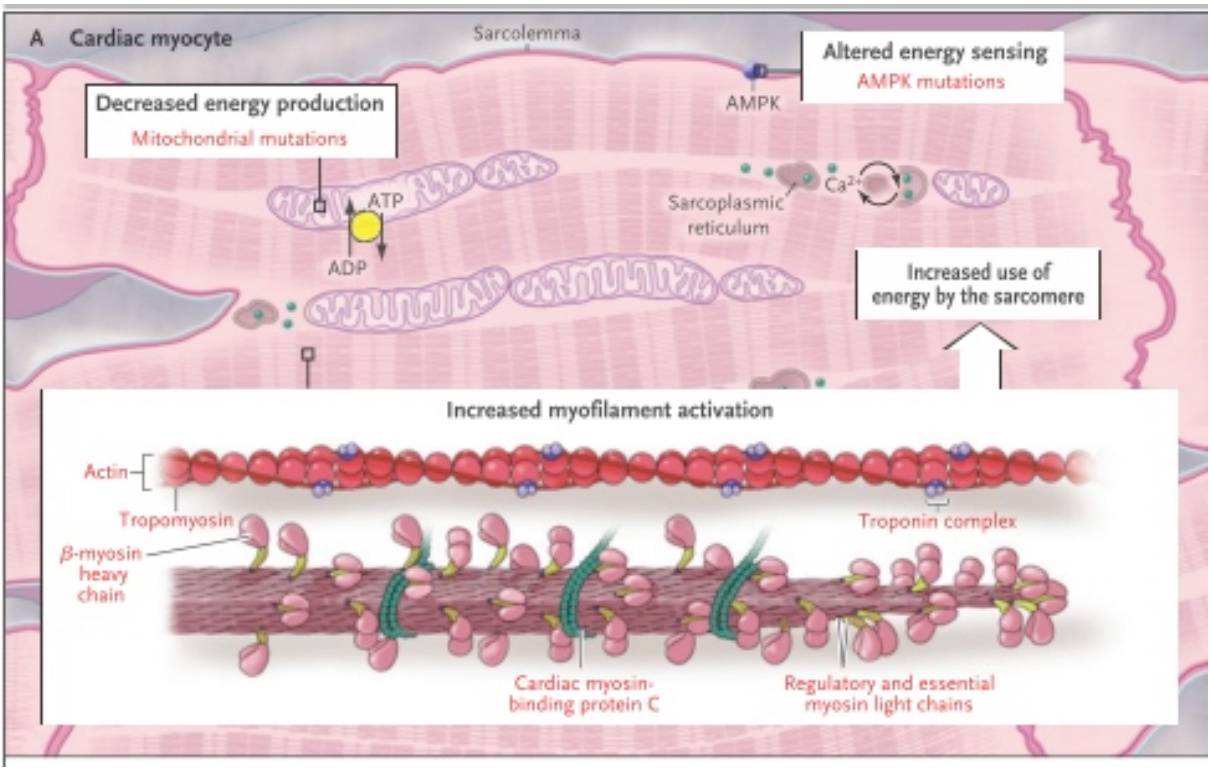


**Figure1.7:** Reproduced with permission from (Watkins et al., 2011), Copyright Massachusetts Medical Society. A deterioration in myocardial energy status, typically due to increased energy consumption, is the pathophysiologic hallmark of classic HCM caused by sarcomeric mutation. Further, mutations altering energy production within the myocardium, and also mutations disrupting energy sensing mechanisms recapitulate the disease pattern and phenotype of patients with sarcomeric mutations.

## 1.3 The role of purinergic signalling in the development of fibrosis

### 1.3.1 The purine signalling cascade

ATP can be found in every mammalian cell and has a critical role in cellular energy metabolism as a high-energy phosphate. In addition to this intracellular role, ATP can be released into the interstitial space where it acts as an autocrine and paracrine signaling molecule (Lu & Insel, 2014). This release of ATP, either through vesicle exocytosis or directly from the cytoplasm via pannexin channel proteins, initiates the so called "purinergic signaling cascade" (Bours, Swennen, Di Virgilio, Cronstein, & Dagnelie, 2006). This is considered a cascade, as not only ATP but also its metabolites, in particular adenosine (Ado) participate in the regulation of biological response to tissue injury, including vascular effects, inflammatory reactions and the transition to scar formation. These effects are mediated by several membrane-bound purinergic receptors, which mediate the different effects of changes in the interstitial concentration of ATP and Ado. Adenosine receptors belong to the family of P1 receptors, which is divided into A1, A2A, A2B, and A3 receptor subtypes. All of the Ado receptors belong to the family of G-protein coupled receptors, having seven transmembrane domains, however they demonstrate different affinities for Ado (Bours et al., 2006).

| Subtype | Physiologic affinity | Cardiac cell expression profile |
|---|---|---|
| **A1** | Ado $EC_{50}$: 0.18-0.53μM | **Cardiomyocytes**, CFs, smooth muscle cells, endothelial cells, macrophages |
| **A2A** | Ado $EC_{50}$: 0.56-0.95μM | Cardiomyocytes, **CFs**, endothelial cells, smooth muscle cells, macrophages, T&B-lymphocytes |
| **A2B** | Ado $EC_{50}$: 16.2-0.64μM | Cardiomyocytes, CFs, endothelial cells, smooth muscle cells, macrophages |
| **A3** | Ado $EC_{50}$: 0.18-0.53μM | Very low expression levels in the myocardium |

**Table 1.1:** (Bours et al., 2006) Adenosine receptor subtypes, estimated affinity for adenosine and cellular distribution across the myocardium.

The second family of purinergic receptors, namely the P2 receptors, are responsible for mediating ATP effects directly. P2 receptors are further divided into P2X and P2Y receptors. P2X receptors, expressed in most mammalian tissues, are ATP-gated ion channels which open upon ATP binding to its extracellular loop (Lu & Insel, 2014). Opening of these non-selective ion channels allows the flux of cations and ensuing changes in membrane potential, which is accompanied by an increase in cytoplasmic $Ca^{2+}$ concentrations and activation of $Ca^{2+}$-activated downstream signalling pathways (Kaczmarek-Hájek, Lörinczi, Hausmann, & Nicke, 2012; Lu & Insel, 2014). Conversely, P2Y receptors constitute a subfamily of ATP dependent G-protein coupled receptors. The individual contribution of these receptor subtypes to fibroblast activation appears to vary between tissues and to depend on the nature of the pathologic stimulus.

Multiple cellular mechanisms can lead to the release of intracellular ATP and Ado into the interstitial space. Cellular damage, for example during tissue necrosis, can result in the loss of cell membrane integrity, thereby causing the release of intracellular metabolites including nucleotides. Nucleotides released in this manner play an important role in the recruitment of inflammatory cells, wound healing and scar formation (Lu & Insel, 2014).

Further, cells can also actively release nucleotides as a metabolic danger signal indicative of perturbations in cellular energetics. Two families of trans-membranous hemi-channels (forming one-half of a gap junction) mediate this major route of nucleotide release, namely connexins (Cxs) and pannexins (Panx). Although structurally similar, Cxs typically form cell-cell connections, whereas Panx are more

likely responsible for providing a connection between the cytoplasm and extracellular space. In particular, the ubiquitously expressed Panx-1 channels serve as a major conduit for the release of nucleotides, particularly ATP (Lu & Insel, 2014). Such release initiates the purinergic signalling cascade which has been shown to regulate fibroblast activity in several organs including the heart (Dolmatova et al., 2012; Lu, Soleymani, Madakshire, & Insel, 2012; Nishida et al., 2008), kidneys (Campanholle, Ligresti, Gharib, & Duffield, 2013), liver (Mallat & Lotersztajn, 2013; Vaughn, Robson, & Burnstock, 2012) and lung (Bläsche et al., 2012; Riteau et al., 2010).

Although the aforementioned signalling cascade is primarily initiated by the release of ATP and exerts some of its effects directly via ATP receptors of the P2 family, Ado signalling has also been shown to be a major pro-fibrotic mechanism (Chan & Cronstein, 2010; Cronstein, 2011). Extracellular hydrolysis of ATP to Ado is the major source of interstitial Ado in most tissues. Two membrane bound enzymes catalyse the hydrolysis of extracellular ATP: ectonucleoside triphosphate diphosphohydrolases (ENTPDs) and ecto-5'-nucleotidase, also known as CD73. Hydrolysis of ATP by ENTPDs constitutes the first step of ATP metabolism, as it catalyses the hydrolysis of ATP and ADP to AMP and inorganic phosphate. As a subsequent step, CD73 hydrolyses AMP to Ado (Cronstein, 2011). These enzymes seem to be responsible for regulating the interstitial concentration of ATP via degradation and the levels of Ado via formation from ATP in many tissues (Fredholm, 2007), including the myocardium after ischemic injury (Bönner, Borg, Burghoff, & Schrader, 2012) and pressure overload (Xu et al., 2008).

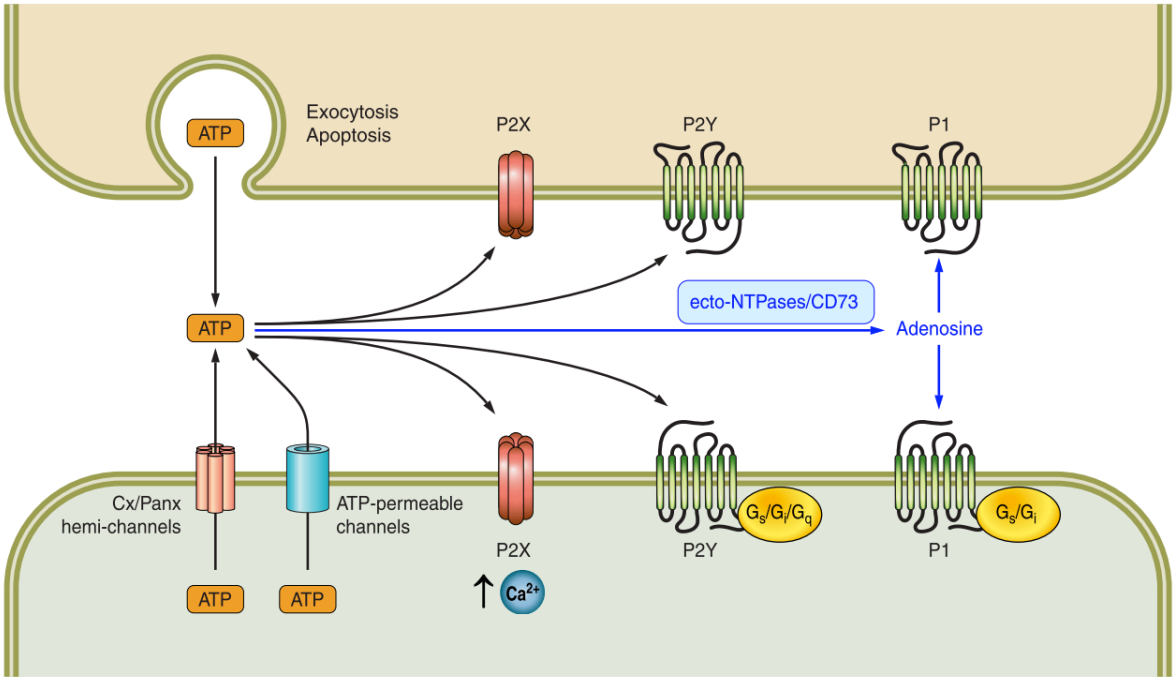


**Figure 1.7:** Reproduced with permission from (Lu & Insel, 2014) The purinergic-signalling cascade. ATP is released into the interstitium, as a sequel of cell damage or specifically via hemi-channels as a metabolic danger signal. Interstitial ATP functions as a autocrine and paracrine signal via P2 receptors. Further ATP is metabolised to adenosine by extracellular nucletidases CD73 and CD39. In many organs adenosine regulates fibroblast activation and extracellular matrix formation, via P1 receptors.

In addition to the described mechanism of Ado generation by extracellular hydrolysis of ATP, Ado can also be created within the cell in response to energetic perturbation. Intracellular ADP increases during heightened cellular energy demand or decreased energy supply. In such circumstances, the enzyme adenylate kinase catalyses the recycling of ATP (plus AMP) from two ADP molecules, thus leading to an increase in AMP and consecutively Ado (Dzeja & Terzic, 2009). As a result, the intracellular concentration of Ado is connected to the energetic state of the cell. Given that membrane transporters for Ado can translate intracellular concentration changes to the interstitium, this mechanism also links extracellular levels of Ado to intracellular metabolic perturbations.

### 1.3.2 Adenosine signalling and fibrosis

In several tissues adenosine has been shown to play a crucial role in the regulation of fibrosis formation. Mouse models of chronic diseases such as liver fibrosis and scleroderma have revealed that adenosine is responsible for the activation of fibroblasts and the pathological deposition of collagen. In particular, adenosine signalling via A2A receptors (A2ARs) plays a decisive role in fibrosis formation with pharmacologic or genetic disruption inhibiting fibrosis formation in chronic skin (Chan, Fernandez, et al., 2006) and liver disease models (Chan & Cronstein, 2010; Chan, Montesinos, et al., 2006) (Figure 1.8).

This finding might be considered at odds with the observations in the myocardium pointing to a protective role of adenosine A2ARs. Cardiomyocyte A2AR over-expression is protective against TAC-induced heart failure, and cardiac fibrosis (Hamad et al., 2012). However, the responses to tissue adenosine are influenced by the levels of ligand, the pattern of receptor expression on differing cell types and the effector systems coupled to these receptors. Substantial over-expression of A2AR vitiates physiological receptor sub-type regulation. Most importantly, the transgenic model employed is cardiomyocyte-specific with A2ARs expressed under a powerful inducible cardiac promoter, with the corollary that this model yields limited insights into the physiological role of A2ARs in cardiac fibroblasts. In contrast a knock-out strategy, similar to the studies undertaken on liver and skin fibrosis, is a therapeutically more pertinent model, reflecting the consequence of antagonists on endogenously expressed adenosine receptors in all cell types.

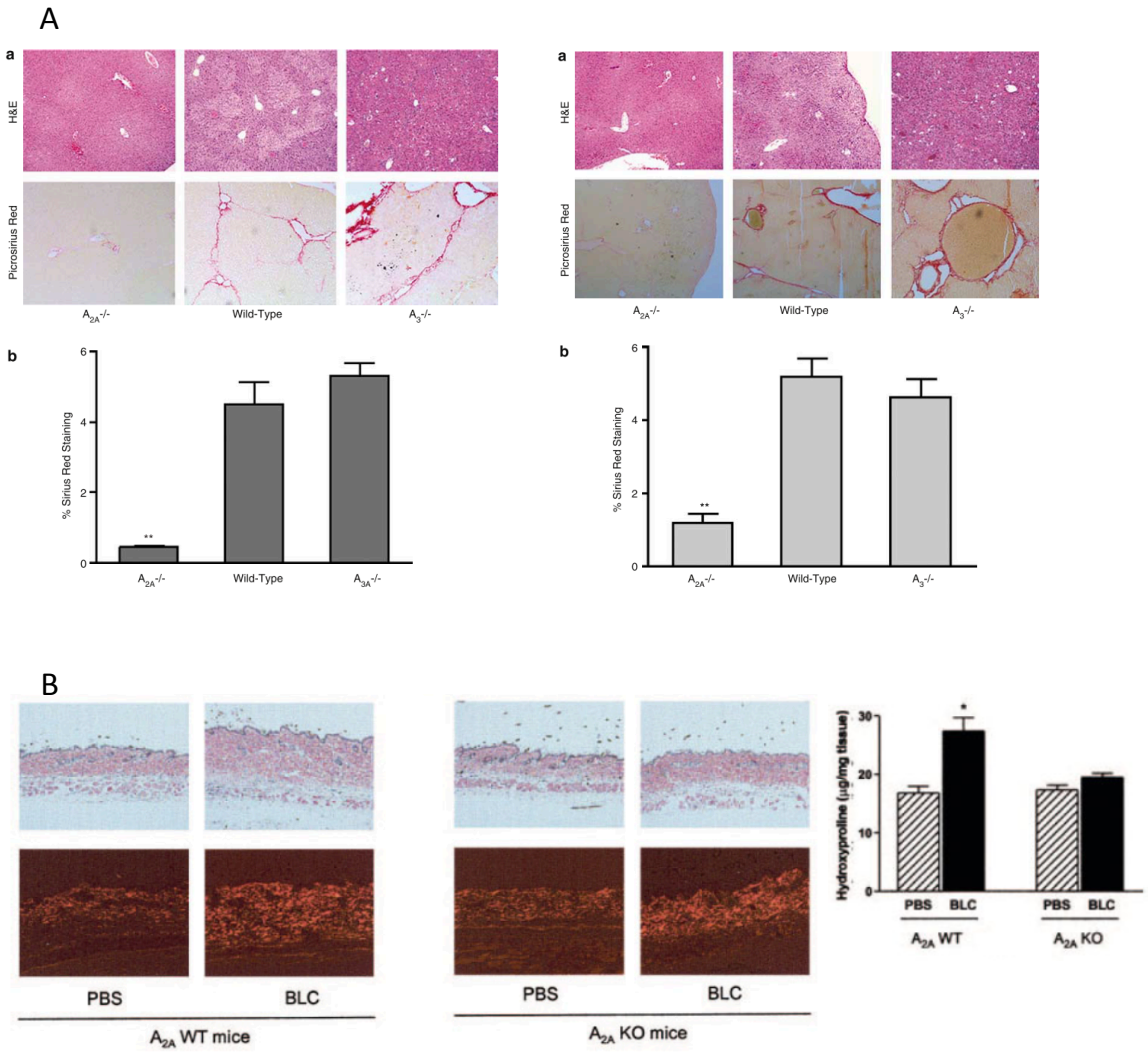


**Figure 1.8:** Reproduced with permission from (Chan, Fernandez, et al., 2006; Chan, Montesinos, et al., 2006). (*A*) Adenosine A2AR depletion prevented fibrosis formation in two distinct mouse models for hepatic fibrosis, namely thioacetamide- (top left) and $CCL_4$- (top middle) induced hepatic fibrosis. Treatment with the adenosine A2AR inhibitor ZM-241385 inhibited thioacetamide- and $CCL_4$- induced hepatic fibrosis as well (data not shown). (*B*) Bleomycin-induced dermal fibrosis was abrogated in mice lacking the adenosine A2AR, on bright field and polarized light microscopy, which correlated with a significant reduction in dermal hydroxyproline content. These findings demonstrate the important role of adenosine signalling, via the A2AR, in the development of tissue fibrosis in more than one organ.

### 1.3.3 Adenosine signalling in the myocardium

As described above, both HCM (Watkins et al., 2011) as well as pressure overload-induced left ventricular hypertrophy (Beer et al., 2002; Maslov et al., 2007) are characterised by compromised myocardial energetics. The biophysical consequences of mutant myofilament proteins, the consequent energy deficiency, the influence of wall tension, cellular hypertrophy per se and the sequelae of hypertrophic remodelling represent potent sources of myocardial stress. A variety of stimuli including mechanical strain, metabolic stress and cellular injury trigger a regulated nucleotide and/or nucleoside release in the myocardium. Regulated ATP release has been first characterised in neurones, but is well-recognised in epithelial cells and cardiomyocytes (Gödecke, Stumpe, Schiller, Schnittler, & Schrader, 2005; Nishida et al., 2008; Vial, Owen, Opie, & Posel, 1987). Under basal conditions, ATP is present intracellularly in the mM range. Once outside the cell, either being transported via transmembrane channels (pannexins) or due to disruptions of membrane integrity, ATP has a half-life measured in seconds due to a complex array of potent nucleotidases (e.g. ecto-nucleotidases CD39 and CD73) (Sinclair, Shepel, Geiger, & Parkinson, 2000) which degrade ATP and create Ado. These signalling moieties are present and active in the nM range. Cardiomyocytes (Germack & Dickenson, 2005; Mubagwa & Flameng, 2001) signal metabolic stress via the interstitial adenosine concentration (Meyer et al., 2001). This mechanism has been shown to be protective acutely (e.g. following ischemia reperfusion) (Sakaguchi et al., 2000) and in the context of short-term pressure overload (Xu et al., 2008), but has not been investigated in chronic cardiac disease models.

## 1.4 Therapeutic targets in fibrosis formation

The development of fibrosis is a common pathologic endpoint of organ failure and appears to play an important role in the pathophysiologic progression of disease in many organs. As a result, common pro-fibrotic pathways are considered to be promising therapeutic targets for the prevention or treatment of tissue fibrosis. However, specific pharmacologic agents modulating the progression of tissue fibrosis are not yet available for the heart or any other organ (M. Zeisberg & Kalluri, 2013). Considerable hope for the amelioration of fibrosis has been placed on therapeutic options modulating immunologic processes, such as anti-inflammatory or immunosuppressive drugs. However this approach has not led to the development of effective therapies yet.

In addition, there is considerable potential for side effects of systemic treatments specifically targeting pro-fibrotic pathways. For example, the agent β-amino propionitrile (BAPN) has been shown to inhibit the formation of LOX-mediated collagen crosslinks. As a result BAPN has shown promising results by inhibiting the formation of cardiac fibrosis with corresponding improvements in cardiac function (Bing, Fanburg, Brooks, & Matsushita, 1978; Creemers & Pinto, 2011). However, as with any agent that systemically inhibits collagen crosslinking, BAPN causes pronounced systemic side effects in collagen-containing tissues. This develops as progressive weakening of most collagenous components of the musculoskeletal system, described clinically as osteolathyrism.

The specific inhibition of TGF-β significantly reduces myocardial fibrosis with resulting functional improvements in animal models for pressure overload (Kuwahara

et al., 2002) and hypertrophic cardiomyopathy (Teekakirikul et al., 2010). However, TGF-beta specific inhibition in animal models of myocardial infarction led to a failure in acute compensation and were accompanied by increased mortality and worsening of myocardial function.

These findings emphasize the potential jeopardy of all therapeutic approaches modulating the formation of myocardial extracellular matrix. Most of these interventions have the risk of causing detrimental side effects in the context of acute myocardial ischemia.

## 1.5 Hypothesis and aims of this investigation

### 1.5.1 Hypothesis

The central hypothesis of this thesis is that in left ventricular hypertrophy resulting from sarcomeric mutations in HCM or from increased myocardial wall stress in TAC-related pressure overload, chronically elevated myocardial interstitial adenosine levels stimulate cardiac fibroblasts via A2AR activation. In particular, this work sets out a hypothesis that while adenosine secretion confers beneficial autocrine/paracrine effects in the heart in response to acute insults, chronic activation of adenosine A2ARs results in maladaptive changes, specifically the development of myocardial fibrosis.

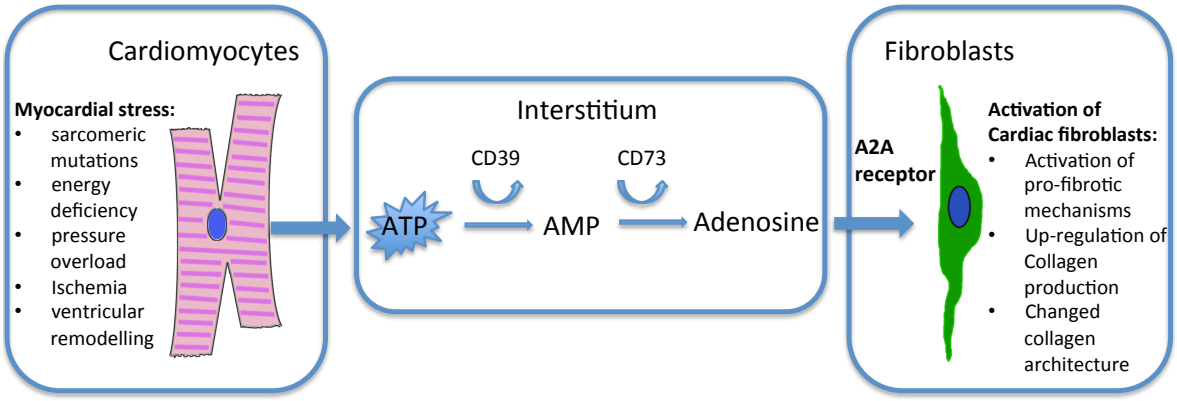


**Figure. 1.8**: Schematic summary of the main hypothesis: Myocardial stress leads to an increase in interstitial adenosine levels, which then activates pro-fibrotic mechanisms in cardiac fibroblasts as one of the initiating steps of fibroblast activation.

### 1.5.1 Aims

The primary hypothesis of this investigation is centred on the pro-fibrotic effect of adenosine A2AR in the myocardium. However, taking into account that the suggested pathway of fibroblast activation also entails myocardial energetics and associated changes in interstitial adenosine levels, the specific aims of the work set out in this thesis are:

- **Aim-1:** To demonstrate and define the fibrotic phenotype of several genetically distinct mouse models for inherited cardiomyopathies, in order to select the optimal model for subsequent rescue experiments (Chapter 3).
- **Aim-2:** To delineate the energetic state of the chosen fibrotic mouse model for inherited cardiomyopathy (Chapter 3).
- **Aim-3:** To gauge interstitial levels of adenosine and to correlate interstitial adenosine levels with the amount of myocardial collagen (Chapter 3).
- **Aim-4:** To describe the *in vitro* effects of adenosine A2AR stimulation and inhibition on isolated cardiac fibroblasts (Chapter 4).
- **Aim-5:** To investigate the role of the adenosine A2AR in the activation of myocardial fibroblasts in a fibrotic mouse model for inherited hypertrophic cardiomyopathy (Chapter 4). Two approaches will be utilized to address this:
    - Delineation of a potential rescue effect as a result of genetic deletion of the adenosine A2AR in the genetic model of cardiomyopathy
    - Investigate whether or not this mechanism is susceptible to post-natal pharmacologic modulation using a specific pharmacologic inhibitor of the adenosine A2AR .

- **Aim-6:** To demonstrate that the adenosine A2AR is a key node in a conserved pathway linking diverse myocardial pathophysiological stimuli to myocardial fibrosis formation (Chapter 4). Specifically:
    - The effect of pressure overload on cardiac function and fibrosis in adenosine A2A receptor-deficient mice will be explored in comparison to its effect on WT mice.
    - The effect of pharmacologic inhibition of the adenosine A2AR on the formation of myocardial fibrosis in response to TAC surgery will be investigated.

# 2. Materials and Methods

## 2.1 Animal

### 2.1.1 Mice general

Mice were kept and bred in individually ventilated cages (IVCs, Techniplast, Milan, Italy) in a specific pathogen-free facility under controlled environmental conditions 22°C temperature; stable humidity and a 12-hour light-dark cycle. Animals were fed a standard rodent chow diet (Teklad Global Diet: 16% protein, 4% fat; Harlan Laboratories, UK) and provided water *ad libitum.* All animal procedures were conducted in agreement with the 1986 British Home Office Animals Scientific Procedures Act.

| Mouse line/operation | Total number (N per genotype / breeders) | Used in experiments (N per genotype) | Mortality (%) | Sex | Age at harvest (weeks) |
|---|---|---|---|---|---|
| **Phython** | 10 / 0 | 10 | 0 | M | 12 |
| **MLP** | 5 / 0 | 5 | 0 | M | 12 |
| **MYBP-C** | 8-12 / 0 | 8-12 | 0 | M | 9 |
| **Cardiac TNT** | 4 / 0 | 4 | 0 | M | 8 |
| **E99K** | 33/ 150 | 33 | 0 | F | 9 |
| **E99K X A2A** | 25/ 150 | 20 | 25 | F | 9 |
| **TAC sham** | 20 / 0 | 19 | 5 | M | 13 |
| **TAC banded** | 40 / 95 | 31 | 15 | M | 13 |

**Table 2.1:** Delineation of the different mouse lines and operated animals, providing the numbers of experimental animals, mouse colonies and mortality rates.

### 2.1.2 Genotyping

#### *2.1.2.1 DNA extraction*

Murine tissue, typically mouse ear-notches were incubated overnight in 500µl of lysis buffer (containing 50mM Tris-HCl, 100mM ethylenediaminetetraacetic acid [EDTA], 100 mM NaCl, 1% sodium dodecyl sulphate [SDS]) supplemented with 0.2mg/ml proteinase K, in a water bath at 55°C. The next day, DNA was precipitated with isopropanol (500 µl) by placement at -20°C for 20 minutes. After that the precipitated DNA was pelleted by centrifugation at 13000g at 4°C for 15 minutes. The resulting supernatant was discarded and the DNA washed by addition of 500µl of 70% Ethanol. The DNA was again pelleted by centrifugation, the supernatant discarded and the DNA pellet was subsequently air dried at room temperature. Upon complete evaporation of the ethanol the pellets were resuspended in 50µl nuclease free water, by means of gentle shaking at room temperature. Genotyping PCR was then carried out according to the specifications explained below.

#### *2.1.2.2 Cardiac actin E99K genotyping*

Cardiac actin E99K animals were kindly provided by the laboratory of Professor Steven Marston (Song et al., 2011). The original PCR protocol utilized by the Marston laboratory was optimized until the conditions demonstrated below were reached, which produced consistent results. PCR reactions were set up on ice and performed using a thermal cycler (DNA Engine Tetrad 2 Peltier thermal cycler, Bio-Rad). The finished PCR products were mixed with 6x DNA loading buffer loaded on 1.5% agarose gels containing 0.002% ethidium bromide. The gels were visualized and imaged by ultraviolet transillumination.

Two separate PCRs were run, one demonstrating the presence or absence of the transgene in the DNA, the other a WT control PCR indicating the presence of DNA.

| ***Cardiac actin E99K* Genotyping** | | | | | | |
|---|---|---|---|---|---|---|
| **Primer** | | | **Sequence 5' → 3'** | | | |
| E99K_fw | | | TGACAGACAGATCCCTCCTATCTCC | | | |
| E99K_rv | | | GGCATCTTAGAAGCATTTGCGG | | | |
| **Reaction Mix** | | | **Reaction conditions** | | | |
| | | | Step | Temp. | Time | Cycles |
| **Genomic Mouse DNA** | 50 | ng | Denaturing | 94 °C | 3 m | **1 x** |
| **Primers** | 10 | pmol | Denaturing | 94 °C | 1 m | **35 x** |
| **dNTPs** | 0.20 | mM | Annealing | 60 °C | 1 m | |
| **Reaction Buffer** | 0.1 | Vol | Extension | 72 °C | 1 m | |
| **$MgCl_2$** | 1.5 | mM | | | | |
| **TaqPolymerase** | 1.0 | U | Final Extension | 72 °C | 10 m | **1 x** |
| **Reaction Volume** | 20.0 | µL | | | | |
| **Amplification Product** | | | **Size** | | | |
| E99K transgene | | | 800 bp | | | |

**Table 2.2:** The PCR primer sequences and thermal cycling conditions applied in the genotyping experiments of cardiac actin E99K animals to obtain signal of the transgene.

| **Genotyping** | | | | | | |
|---|---|---|---|---|---|---|
| **Primer** | | | **Sequence 5'→3'** | | | |
| WT_fw | | | TGAGGTTGTCTTCTGATCTGC | | | |
| WT_rv | | | TCCTGGACAAAGTAACCCTTG | | | |
| **Reaction Mix** | | | **Reaction conditions** | | | |
| | | | Step | Temp. | Time | Cycles |
| **Genomic Mouse DNA** | 50 | ng | Denaturing | 94 °C | 3 m | **1 x** |
| **Primers** | 10 | pmol | Denaturing | 94 °C | 1m | **35 x** |
| **dNTPs** | 0.20 | mM | Annealing | 55 °C | 1m | |
| **Reaction Buffer** | 0.1 | Vol | Extension | 72 °C | 45 s | |
| **$MgCl_2$** | 1.5 | mM | | | | |
| **Taq Polymerase (Immolase)** | 1.0 | U | Final Extension | 72 °C | 10m | **1 x** |
| **Reaction Volume** | 20.0 | µL | | | | |
| **Amplification Product** | | | **Size** | | | |
| Wildtype wt | | | 200 bp | | | |

**Table 2.3:** The PCR primer sequences and thermal cycling conditions applied in the genotyping experiments of cardiac actin E99K animals, to obtain wild type signal.

### *2.1.2.3 Adenosine A2A receptor knock out genotyping*

Adenosine A2AR KO mice (Chen et al., 1999) were obtained from Jackson Laboratories. The mice were originally produced by replacement of exon 2 and intron 2 of the adenosine A2AR by a neomycin selection cassette, resulting in the absence of functional protein. Genotyping was carried out by PCR according to specifications provided by Jackson Laboratories.

| **Genotyping Primer** | | | **Sequence 5' → 3'** | | | |
|---|---|---|---|---|---|---|
| A2A common_fw | | | GGGCTCCTCGGTGTACAT | | | |
| A2A wt_rv | | | CCCACAGATCTAGCCTTA | | | |
| A2A mutant_rv | | | CAT TTG TCA CGT CCT GCA CGA C | | | |
| **Reaction Mix** | | | **Reaction conditions** | | | |
| | | | Step | Temp. | Time | Cycles |
| **Genomic Mouse DNA** | 50 | ng | Denaturing | 94 °C | 10 m | **1 x** |
| **Primers** | 10 | pmol | Denaturing | 94 °C | 1m | **35 x** |
| **dNTPs** | 0.20 | mM | Annealing | 58 °C | 1m | |
| **Reaction Buffer** | 0.1 | Vol | Extension | 72 °C | 1m | |
| **$MgCl_2$** | 1.5 | mM | | | | |
| **TaqPolymerase (Immolase)** | 1.0 | U | Final Extension | 72 °C | 2m | **1 x** |
| **Reaction Volume** | 20.0 | µL | | | | |
| **Amplification Product** | | | **Size** | | | |
| A2A mutant | | | 550 bp | | | |
| Heterozygote | | | 550 bp and 365 bp | | | |
| A2A Wildtype | | | 365 bp | | | |

**Table 2.4:** The PCR primer sequences and thermal cycling conditions applied in the genotyping experiments of adenosine A2AR KO animals.

#### *2.1.2.4 Breeding strategy*

The cardiac actin E99K mouse line only exists as heterozygous and WT animals. Heterozygous animals develop the full phenotype, while homozygous animals are not viable. As a result the cardiac actin E99K line was maintained by crossing heterozygous males with WT females.

The adenosine A2A receptor mouse line was maintained by crossing homozygous mutants among each other.

Crossbreeding experiments in order to produce cardiac actin E99K, A2AR KO animals were carried out over 3 generations.

1. Cardiac actin E99K animals were crossed with A2AR KO animals. This resulted in the formation 100% A2A heterozygotes that were 50% E99K heterozygous.
2. Cardiac actin E99K, A2AR heterozygotes were crossed with cardiac actin WT, A2AR heterozygotes, resulting in the formation of 12.5% cardiac actin E99K A2AR KO animals; 12.5% cardiac actin WT, A2AR KO animals; 25% cardiac actin E99K, A2AR heterozygotes; 25% cardiac actin WT, A2AR heterozygotes; 12.5% cardiac actin E99K A2AR WT animals; 12.5% cardiac actin WT A2AR WT animals;
3. Cardiac actin E99K A2AR KO animals were bred with cardiac actin WT, A2AR KO animals, in order to generate sufficient numbers of cardiac actin E99K, A2AR KO animals

## 2.2 Investigations of the fibrotic phenotype

### 2.2.1 Collagen measurement

#### *2.2.1.1 Measuring the hydroxyproline content in the cardiac tissue*

The mice were sacrificed by cervical dislocation; the hearts were surgically extracted via thoracotomy and immediately snap frozen in liquid nitrogen. The heart tissue was then powdered in a frozen (≈ -80°C) state and divided into several aliquots of 10-20mg. One of these aliquots per mouse was then hydrolysed in 300µl of 6M HCl at 95°C for 20 hours. The hydrolysed samples were then allowed to cool to room temperature and centrifuged for 10 min at 13,000 x g. The supernatant was then taken and diluted 1:2 with 4M HCl. The amount of collagen in the samples was investigated by measuring hydroxyproline content using a kit (Quickzyme Biosciences©), modifying the hydroxyproline residues using chloramineT/DMBA, which results in a coloured product. Absorption measured at 570 nm OD. The concentration of myocardial collagen could then be calculated from a standard curve using the original tissue weight and the dilution factor. All the experiments were conducted in duplicates.

#### *2.2.1.2 Measuring soluble collagen levels*

Frozen aliquots of cardiac tissues (see above) were homogenized with a blender in 300-500µl 0.1N acetic acid containing 4mg/ml of pepsin and digested further for 16 hours. These samples were then spun (for 10 minutes at 10 000 x g) and the supernatants were evaluated according to manufacturers instructions using a Sirius-red detection assay (Quickzyme Biosciences©).

Insoluble collagen, which is calculated as the ratio of total collagen (measured as hydroxyproline content) to soluble collagen is a well-described marker of collagen maturation, i.e. the formation of covalent crosslinks between collagen triple helices by the enzyme LOX (Adam et al., 2011).

#### *2.2.1.3 Semi-quantitative collagen assay*

The hearts were kept in 4% para formaldehyde (PFA) for 48-62 hours, which was then changed to 70% ethanol for a maximum of 2 weeks until embedding, or embedded immediately post-fixation. Heart tissues were dehydrated in a series of increasing alcohol concentrations and then embedded in paraffin wax. Conversely to 7µm thick sections for microscopic evaluation, separate 15µm thick cardiac tissues sections were produced for this essay in order to increase the signal strength in consecutive measurements and mounted onto glass slides. The tissue sections were de-paraffinized in Histoclear© and rehydrated in a series of decreasing alcohol concentrations. The amounts of collagen as well as non-collagenous proteins were then measured by a method first described before by Marotta and Martino (Marotta & Martino, 1985). In brief, the tissue sections were incubated for 20 minutes in a staining solution (Chondrex©) containing Sirius-red, binding to all fibrillar collagens, and Fast-green, binding to all proteins but collagen. The sections were then washed with distilled water five times, consecutively the dyes eluted from the tissue sections in 1 ml of dye extraction buffer (0.1N NaOH and methanol 1:1). The resulting solutions, containing the eluted stains, were then investigated by UV/Vis spectrometer at wavelengths of 540nm (Sirius-red absorption) and 605nm (Fast-green absorption), respectively, using a POLARstar Omega micro-plate reader (BMG Labtech). To calculate the relative amounts of collagen and non-collagen proteins per section the following formulas were used:

Collagen (µg/section) =[OD 540 - (OD 605x0.291)]/37.8x1000

Non-collagen protein (µg/section) = OD 605/2.04x1000

#### 2.2.1.4 Evaluating fibrosis associated gene expression at mRNA level

Frozen tissue aliquots of the respective KO mouse hearts were homogenized with a blender and lysed in 300µl RLT buffer containing β-Mercaptoethanol. Messenger RNA was isolated using a column purification kit (Qiagen Rneasy©). The expression of pro fibrotic genes and collagen subtypes (*collagen type I alpha 1, collagen type III alpha 1, fibronectin, MMP-2, -9, TGF-β, LOX*) as well as cardiac stress response genes (*Nppa*, *Nppb*, *Myh7*) were evaluated by qPCR.

#### 2.2.1.5 Measuring total collagen by western blot

Frozen aliquots of heart tissues (see above) were homogenised and lysed in 500µl ice-cold RIPA buffer (1% NP-40, 0.5% sodium deoxycholate, 0.1% sodium dodecyl sulphate (SDS) in PBS). SDS-polyacrylamide gel electrophoresis (PAGE) was performed using 3-8% Tris-Acetate gels (NuPage®, Invitrogen) and the proteins were then transferred to polyvinylidene difluoride (PVDF) membranes. The membranes were blocked for 2 hours in 5% non-fat milk in PBS containing 0.1% Tween-20 and were subsequently stained with a primary polyclonal rabbit anti-collagen type I antibody (Novus, NB600-408) in 5% non-fat milk in PBS containing 0.1% Tween-20 at 4°C for 16 hours. The membranes were then washed (5 x 5 minutes in PBS 0.1% Tween) and stained for 50 minutes with a horseradish peroxidase labelled anti rabbit antibody. The labelled membranes were then developed on film using ECL.

#### *2.2.1.6 Histology experiments*

Tissue collection for consequent histologic experiments was conducted typically following haemodynamic measurements under terminal anaesthesia. The mice were culled under anaesthesia by cervical dislocation, followed by thoracotomy and removal of the heart. The hearts were then washed in ice cold phosphate buffered saline and kept in 4% para formaldehyde (PFA) for 48-62 hours, which was then changed to 70% ethanol for a maximum of 2 weeks until embedding, or embedded immediately post-fixation. The cardiac tissues were dehydrated in a series of increasing alcohol concentrations and cleared in histoclear solution followed by embedding in paraffin wax. The hearts were placed in paraffin to facilitate sectioning in a transverse plane and cut into 7μm thick transverse (short axis) sections of the heart's apical, mid-ventricular and basal area using a Leica RM2155 microtome. Cardiac sections from each of these areas were then mounted onto glass slides and stained with a Sirius-red staining kit (Polysciences Inc.) according to manufacturer's instructions. The sections were then mounted with Neo-Mount® and glass coverslips and imaged with a wide-field inverted Nikon TE2000U microscope under bright field and polarized light. Of each stained cardiac section three images were taken of the left ventricular free wall and one image was taken of the ventricular septum, using a 20x objective without additional zoom. Using MetaMorph v7.7 microscopy analysis software, the images were then analysed using threshold analysis for the total area of Sirius-red signal as well as the total area of myocardium on each image. These two values were then expressed as a percentage.

### 2.2.2 Immunofluorescence

Markers of cardiac fibroblast activation and proliferation were delineated by immunofluorescence experiments. Hearts were snap frozen in optimal cutting temperature (OCT) compound, using liquid nitrogen-cooled isopentane, sectioned into 8μm thick sections and mounted on glass slides. Staining was conducted against α-smooth muscle actin (Sigma), and ki-67 (Cell signaling), as markers for fibroblast activation and proliferation, respectively (Zhang et al., 2008). In addition antibody staining for the intercellular matrix components collagen type-1 (Novus), was used to stain and consecutively image myocardial collagen components, in particular endomysial collagen. Finally antibody staining for vimentin (Abcam) and discoidin domain receptor 2 (DDR-2, Santa Cruz) also serve as a cell marker for cardiac fibroblast, both within cardiac tissue sections but also in tissue culture stainings. (Camelliti et al., 2005).

Immunofluorescence staining was conducted according to the following protocol. Frozen sections were removed from storage at -20°C and immediately fixed, either in -20°C acetone for 10 minutes or in 4% PFA for 15 minutes at room temperature. The slides were then washed in PBS and mounted onto shandon coverplates (Thermo scientific). Blocking solution (PBS plus 5% goat serum) was added onto the slide and left on for one hour. Primary antibody solution (PBS plus 1% BSA, containing the primary antibody in a dilution of 1:100) was then added directly and left on at 4°C over night. Following over night incubation, the slides were washed three times for five minutes with PBS. Consecutively, secondary antibody staining solution (PBS plus 1% BSA, containing fluorescently labelled secondary antibodies in a dilution of 1:400, and HOECHST nuclear stain in a dilution of 1:1000) was added on the slides

for one hour. The slides were then washed and mounted with glass coverslips over night, using ProLong Gold mounting medium.

The same protocol was applied for the immunofluorescence staining of cultured fibroblasts. The resulting slides were imaged with a Zeiss 510 MetaHead confocal microscope.

### 2.2.4 Flow cytometry experiments

Hearts were harvested from mice and flushed with cold HBSS. The heart were then cut into two halves and stored in HBSS on ice until initiation of the digestion procedure. In order to achieve full digestion the two halves were transferred into a gentleMACS C tube to which 5ml digestion media containing 600 U/ml Collagenase II (Worthington, CLS-2) and 60 U/ml DNase I was added. The tubes were attached to a gentleMACS dissociator and the programme m_heart_01 was run once for each tube. The tubes were then incubated for 30 min at 37°C under constant shaking at 200 rpm. At the end of this incubation period the tubes were again transferred to the gentleMACS dissociator and the programme m_heart_02 was run once for each tube. 10ml of ice cold HBSS was added to halt further digestion. The digested sample was pressed through a 70um filter and washed twice with HBSS containing 0.2% BSA.

Immediately after digestion, the cells were plated in a 96 well plate and the appropriate mix of antibodies against surface molecules suitable for flow cytometry, diluted in PBS containing 0.2% BSA was added for 30 minutes. Cells were washed with PBS containing 0.2% BSA and used for flowcytometric analysis or for further intracellular staining. For intracellular staining the cells were fixed using a BD lysis buffer and permeabilized by washing with PBS containing 0.2% BSA and 0.05% saponin. Intracellular antibodies were diluted in PBS containing 0.2% BSA and 0.05% saponin. Cells were incubated with the antibody mix for 30 minutes and washed with PBS containing 0.2% BSA. All cells solutions were recorded on a BD LSR II or BD Fortessa flow cytometer. The resulting cell data was analysed and presented in a blinded fashion using FlowJo vX.0.7 FACS analysis software.

| Antibody | Fluorophore | Dilution |
|---|---|---|
| **L/D** | APC Cy7 | 1000 |
| **CD31** | PerCp eF 710 or FITC | 200 |
| **CD45** | AmCyan or NC 650 | 400 |
| **CD45** | NC 650 | 600 |
| **gp38** | APC | 400 |
| **Thy1.2** | PE Cy7 | 200 |
| **CD39** | PE | 200 |
| **CD73** | BV605 | 200 |
| **Thy1.2** | PeCy7 | 300 |
| **Vimentin** | APC | 600 |
| **Vimentin** | purified | 800 |
| **ki67** | eF 450 | 100 |
| **DDR2** | purified | 75 |
| **secondary** | AF 594 | 500 |
| **secondary** | AF 488 | 500 |
| **secondary** | AF 647 | 500 |

**Table 2.5:** Antibody list for FACS experiments stating antigen, the fluorophore and the applied antibody dilution.

## 2.3 In-vitro experiments investigating the response of cardiac fibroblasts upon Adenosine receptor stimulation

### 2.3.1 Neonatal rat cardiac fibroblasts

Neonatal cardiac rat fibroblasts were isolated from 2-4 days old rat pups. The rats were culled by cervical dislocation, the hearts removed, minced and exposed to collagenase digestion. The cells subsets were then isolated by adhesion procedures (Walsh, Zhang, Fuseler, Hilliard, & Hockerman, 2007). As fibroblasts are the only cardiac cell population with proliferative potential, cultivating the cells for at least three passages before any experiments were performed further purified the fibroblast subpopulation.

The purity of these fibroblast isolations was then investigated using immunofluorescence staining against well-described cardiac fibroblast markers: DDR-2, collagen1 and vimentin. After three passages the fibroblast cultures were >98% positive for these markers.

The neonatal rat fibroblasts were further evaluated for the expression of adenosine receptors. The cells were plated in 6-well plates and mRNA of the fibroblasts extracted using a column purification kit (Qiagen Rneasy©) according to the manufacturer's instructions. The following primers were used in a touch down polymerase chain reaction (PCR) protocol:

Adenosine A1 receptor fw.: TACATTGGCATCGAGGTGCT;

rv.: AGGTGTGGAAGTAGGTCTGT.

Adenosine A2A receptor fw.: CTCACGCAGAGTTCCATCTT;

rv.: TCCATCTGCTTCAGCTGTCT.

Adenosine A2B receptor fw.: CTTCTGCACGGACTTTCACA

rv.: GGTGGCACGGTCTTTACTGT.

Adenosine A3 receptor fw.: ATATGGCTATTCCTGGGCCT

rv.: ACCAGAAACAGGGACTTAGC.

The PCR products were then run on a 1% agarose gel and visualized by trans illumination with ultraviolet light.

The cells were then plated in six well plates and stimulated in groups of four wells with different dosages of the adenosine A2AR agonist, CGS-21680, in DMEM containing 10% fetal bovine serum, 0.1% dimethyl sulfoxide (DMSO). Further the specific adenosine A2AR antagonist ZM-241385 was added to stimulated wells in order to test the specificity of agonist effect. The amount of collagen in the purified CCM was evaluated after 48 hours of stimulation.

The CCM samples were concentrated 10 fold with Polyethylene glycol solution (Chondrex®) according to manufacturers instructions as collagen levels in tissue culture medium are generally lower culture media. The collagen in the purified CCM content was then investigated either by anti-collagen Western blot as described above), or by Sirius-red absorption assays (Chondrex®) according to manufacturers instruction.

### 2.3.2 Adult mouse cardiac fibroblasts

In order to delineate the effect of adenosine A2A receptors on fibroblasts isolated from adult cardiac tissue, stimulation experiments were recapitulated on fibroblasts isolated from wild type adult mouse hearts.

Cardiac fibroblasts were isolated from adult mouse hearts by retrograde Langendorff perfusion. The mice were culled by cervical dislocation, subsequently the hearts were extracted surgically and placed into pre-cooled (4°C) Tyrode's solution. The aortic roots of these hearts were then cannulated using a pre-filled 22G needle with cut tip. The hearts were then connected to a Langendorff-style rig and perfused by means of gravity with pre-warmed (about 37°C) and pre-oxygenated Ca-free Tyrode's solution at about 100 cm H2O pressure. After three minutes of perfusion the solution was changed to digestive enzyme enriched Tyrode's solution and continuously perfused for nine minutes, resulting in the breakdown of extracellular connective tissue. The hearts were then removed from the perfusion rig, minced and subsequently incubated in collagenase solution at 37° while gently shaking. Filtering of the resulting cell solution through a monofilament nilon filter cloth mesh (Cadisch premium meshes Ltd, London,UK) ensured the generation of solution containing primarily single cells. The resulting cell solution was diluted immediately with enzyme stopping solution.

Cardiomyocytes and cardiac fibroblasts were then roughly separated by means of centrifugation. Cardiomyocytes were pelleted by centrifugation at 30g for 2 minutes, the remaining cells the resulting supernatant were the pelleted by centrifugation at 250g for 8 minutes. The resulting cells were then cultured under standard tissue

culture conditions: In Dubecco's Modified Eagles Medium (DMEM) supplemented with 10% fetal bovine serum (FBS) and 1% penicillin-streptomycin solution at .

After three to four cell passages the cells were evaluated for the expression of fibroblast markers using immunofluorescence experiments.

The cardiac fibroblasts were then plated in six well plates and stimulated in groups of four wells with increasing dosages of, CGS-21680, the adenosine A2AR agonist in DMEM containing 10% fetal bovine serum, 0.1% dimethyl sulfoxide (DMSO). Further the specific adenosine A2AR antagonist ZM-241385 was added to stimulated wells in order to test the specificity of agonist effect. The amount of collagen in the purified CCM was evaluated after 48 hours of stimulation.

The collagen of the CCM was then purified as above. The amount of collagen was then evaluated either by Sirius-red absorption assay (Chondrex®) according to manufacturers instructions, or by measurement of the Hydroxyproline content.

No obvious differences were found between neonatal rat cardiac fibroblasts and murine adult cardiac fibroblasts upon phase contrast microscopy, and upon immunofluorescence staining against vimentin. However, while neonatal rat cardiac fibroblasts demonstrated a modest, approximately 1.5 fold increase in collagen production, murine adult cardiac fibroblasts demonstrated an at least two fold increase in collagen content in the CCM.

## 2.4 Investigation of myocardial energetics

The primary hypothesis of this project is that comprised energetics in the myocardium leads to an increase in interstitial adenosine, which is responsible for fibroblasts activation. Accordingly, experiments were conducted aiming to outline the energetic myocardial metabolism, in our primary mouse model for myocardial fibrosis, the cardiac actin E99K mouse model.

Myocardial energetics were delineated using magnetic resonance spectroscopy and. First, high-energy phosphates were measured by $^{31}$P-magnetic resonance spectroscopy in an established collaboration with Dr Damian Tyler (Schroeder et al., 2013; Zhang et al., 2008). Hearts from E99K and WT mice (n = 6-8 per genotype) were isolated and Langendorff perfused with Krebs-Henseleit buffer (KHB). $^{31}$P spectra were acquired to quantify phosphocreatine (PCr), inorganic phosphate (Pi) and ATP resonances.

### 2.5 Microdialysis experiments: Measurement of interstitial adenosine

Interstitial levels of adenosine were quantified using microdialysis in an established collaboration with Dr Nicolaj Støttrup (Birkler et al., 2010; Povlsen et al., 2013; Støttrup et al., 2010). Cardiac actin E99K mice ("N"=8, 8 weeks of age) were anaesthetized by intra-peritoneal injection of ketamine and midazolam and quickly ventilated by tracheostomy. The mice did then undergo thoracotomy and a micro-dialysis probe was introduced into the myocardial tissue of the apical left ventricular free wall. Microdialysate samples were obtained from within the myocardium using a microsampler (Univenter U820) and a pump (Univenter U801, Zejtun, Malta), combined with microdialysate catheters (CMA 20 Elite probe) covered with a 20 kDa molecular weight cut off semipermeable membrane, using a flow rate of 1µl/min. Aliquots of microdialysates were collected in 10-minute or 10µl intervals for 60 minutes, stored at -80°C and separated by ultra-performance liquid chromatography using a Waters Xevo TQ-S triple quadrupole tandem mass spectrometer (Waters Corp.)

## 2.6 Genetic rescue experiments

### 2.6.1 Cardiac actin E99K – adenosine A2A receptor knock out – crossbreeding experiment

Given the putative key role of the A2AR in fibroblast activation, we used genetic and pharmacological approaches designed to inhibit A2AR signalling in order to rescue the fibrotic phenotype of the E99K mice. Accordingly, E99K mice were crossbred with adenosine A2A receptor knock-out (A2AR KO) mice (Chen et al., 1999) (Jackson laboratories) to obtain four groups of animals: E99K WT and A2A WT; E99K het and A2A WT; E99K WT and A2A WT; E99K het and A2AR KO. The hearts of these mice were then be evaluated for cardiac fibrosis (see experiment and its effects on myocardial function.

Left ventricular haemodynamics (n = 8 per genotype, age 9 weeks) was measured *in vivo* using a 1.4F Millar Mikro-tip catheter inserted into the left ventricle via the carotid artery; measurements include the contractile and chronotropic reserve in response to dobutamine (4-16 ng/g BW/min).

### 2.6.2 Transverse aortic constriction – adenosine A2A receptor knock out

We utilized a well-established model of pressure overload and MF, namely transverse aortic constriction (TAC), whereby banding of the aortic arch to a defined diameter leads to heart failure as well as the formation of MF after 5 weeks (Ying et al., 2009). TAC hearts develop interstitial and perivascular fibrosis from early time points, throughout the left ventricle, in addition to microscopic scars during the transition to heart failure (Chapman, Weber, & Eghbali, 1990; Heymans et al., 2005). Energetic perturbations have been implicated in this model, including significant alterations in PCr/ATP ratio (Maslov et al., 2007) as well creatine kinase activity (Aksentijević et al., 2010; Lygate et al., 2007). We therefore hypothesized that our findings on the role of adenosine signaling in the activation of myocardial fibroblasts and induction of MF in the E99K model would be reflected in this pressure-overload model of MF. Accordingly, TAC experiments were carried out on A2AR KO mice. The development of the fibrotic phenotype in banded homozygous A2AR KO animals will be compared to banded WT type animals of the same background (BALB/c; n=15 per genotype) and sham-operated mice of both genotypes. At 6 weeks post-surgery, hearts were extracted and investigated for their fibrotic phenotype by molecular measurement of collagen at protein and mRNA level (see above, n=6). This was supplemented by immunofluorescence experiments (see above, n=5) for fibroblast activity (α-sma) and proliferation (ki-67) as well as histology (picrosirius red and H&E, n = 4) as described in detail above. These experiments on the one hand served to validate our findings in the E99K model, and on the other hand provided evidence of potential dissimilarities in the mechanisms leading to myocardial fibrosis caused by different pathophysiologic conditions in the E99K and the TAC model.

### 2.7 Pharmacologic rescue experiments actin E99K mice

Injection experiments were performed with the specific adenosine A2AR antagonist ZM-241385. The drug was diluted in PBS containing 15% DMSO and 15% Cremophor® freshly at least every 48 hours, and in injected into the peritoneal cavity of the mice twice daily at a dose of 25mg/kg. The injections were started after weaning the mice, at the age of 28 days of age and continued for five weeks until the mice were nine weeks of age.

There were four groups of mice in total: WT mice on vehicle control (N = 7), WT mice on drug treatment (N = 6, one mouse died during the third week of treatment), actin E99K mice on vehicle control (N = 11) and actin E99K mice on drug treatment (N = 11).

During the last week of treatment, the mice were investigated by echocardiography under isoflurane anaesthesia. Several functional (systolic and diastolic) parameters were evaluated, such as the ejection fraction from M-mode images, the flow intervals and velocities through the mitral valve, and myocardial tissue velocities were investigated at heart rates optimal for systolic (HR ~475-500/min) or diastolic (HR permitting E'/A' separation, typically ~300-350/min) imaging.

At the end of the treatment period, haemodynamic measurements were obtained under terminal anaesthesia. A Millar® catheter was inserted into the left ventricle via the carotid artery and left ventricular pressure measurements undertaken at baseline as well as during the administration of increasing dosages of dobutamine (4 and 16 ng/g BW/min).

Hearts were then harvested, and cut into an apical section, measuring about 1/3$^{rd}$ of the heart and a basal section. The apical section was snap frozen in liquid nitrogen and used for molecular experiments, whilst basal two thirds of the hearts was fixed in 4% PFA for 48 -72 hours and used for collagen assays, as well as microscopic experiments as described above.

## 2.8 Experiments evaluating cardiac function

### 2.8.1 Echocardiography

Following the induction of general anaesthesia mice were placed and fixated supine on a custom built, heated echocardiography stage. Following positioning, the left side of the chest was shaved in order to facilitate imaging. Anaesthesia of the animal was maintained by passive administration of approximately 1.2% isoflurane through a nosecone. The appropriate range of heart rate for echocardiographic image acquisition (400-430 beats per minute) was obtained and stabilised by careful titration of the isoflurane concentration. Acquisition of the echocardiographic images was carried out with a 6-15 MHz linear array ultrasonic transducer (Agilent Sonos 5500) with minimal thoracic compression. Parasternal short and long axis images were obtained followed by recovery of the mice in a heat incubator.

Analysis of the obtained images was performed on a Vevo 2100 Imaging System (VisualSonics, Toronto, Canada) in a blinded fashion. Several parameters were analysed in order to gauge cardiac function. First, M-mode images were analysed in order to gauge ventricular dimensions, by averaging 3-5 cardiac cycles. Left ventricular end-diastolic diameter (LVEDD); left ventricular end-systolic diameter (LVESD); were obtained from the parasternal short axis view at mid-papillary level. These parameters served to calculate a parameter evaluating left ventricular systolic function: Left ventricular fractional shortening (FS):

$$\%FS = [(LVEDD - LVESD)/LVEDD] \times 100$$

An additional parameter demonstrating systolic function, the Teicholz ejection

fraction (EF) (Stypmann et al., 2009) was calculated from Left ventricular end systolic volume (LVESV), and left ventricular end diastolic volume (LVEDV).

$$\text{LV EF} = [(\text{LVEDV} - \text{LVESV})/\text{LVEDV}] \times 100$$

In addition parameters evaluating ventricular size, and potential hypertrophy were evaluated. Estimated left ventricular mass was calculated using, epicardial area (EPI A) endocardial area (ENDO A), LV length in parasternal long-axis (L); LV wall thickness in diastole (t)

$$\text{LV mass} = 1.05 \times ([5/6 \times \text{EPI A} \times (L + t)] - [5/6 \times \text{ENDO A} \times (L)])$$

### 2.8.2 *In vivo* measurement of left ventricular invasive haemodynamics

At the final time-point of genetic and pharmacologic treatment experiments invasive recordings of left ventricular haemodynamic pressures were conducted under terminal anaesthesia. After induction of the anaesthetic protocol the mice were placed on an operating table and continuously passively ventilated with oxygen and 2% isoflurane. The right carotid artery and right jugular vein were surgically exposed and a ultra-miniature 1.4F pressure catheter (Millar Mikro-tip, ADInstruments, UK) was inserted into the carotid artery. The catheter was further retrogradely inserted into the left ventricular cavity through the aortic valve. Correct placement of the catheter within the left ventricular cavity was verified by a change in pressure recording. In addition venous access was gained via cannulation of the jugular vein. Following the described surgical procedure, isofluorane concentration was reduced to 1.5% followed by a 15 minutes equilibration period. Subsequently, left ventricular pressures, heart rate, as well as derived parameters, such as rates of pressure change was continuously obtained via a PowerLab data acquisition system acquisition system (ADInstruments). These unstimulated baseline values were recorded for 15 minutes, after that the inotropic reserve of each heart was assessed by continuous infusion of two increasing dobutamine dosages (4 and 16 ng/g BW/minute) for 5 minutes each. After the finalisation of this protocol the animals were culled by cervical dislocation, followed by organ harvest and the obtaining of morphometric measurements, including heart-, lung- and liver weight and tibia length. Analysis of the obtained pressure tracings was carried out in a blinded fashion using LabChart Pro software.

# 3. Results: Delineation of the fibrotic phenotype of mouse models for cardiac hypertrophy (genetic, and pressure overload)

## 3.1 Introduction

The experiments set out in this chapter are primarily of a descriptive nature and were carried out to address several questions. First of all, the fibrotic phenotype of a number of murine models for inherited cardiomyopathy was delineated. This served as a screening experiment to select for models with a pronounced fibrotic phenotype. Given that the primary aim of this thesis was to investigate pro-fibrotic mechanisms, it was crucial to obtain a clear picture of the fibrotic phenotypes of these models, all of which had been described as "fibrotic" in the literature. As a result of these screening experiments, the cardiac actin E99K mouse model for HCM was ultimately chosen as the platform for follow-up experiments (addressed both in this and the following chapter). This model, regarded as faithfully reflecting the human disease phenotype caused by cardiac actin E99K mutations, demonstrated a robust fibrotic phenotype (Song et al., 2011).

While the role of adenosine A2A receptors in fibroblast activation is not directly addressed in this chapter, the experiments presented serve to describe the fibrotic phenotype and metabolic state of the cardiac actin E99K mouse model. This model was further investigated for interstitial adenosine levels in order to investigate whether changes in adenosine levels are associated with the degree of myocardial fibrosis.

### 3.1.1 Hypothesis

The experiments in this chapter were carried out to address the following hypotheses: i) The fibrotic phenotype of different mouse models for inherited cardiomyopathies differs dependent on the causative mutation; ii) The fibrotic phenotype of these models is accompanied by alterations in cardiac cell populations, in particular by enhanced proliferation and activation of resident cardiac fibroblasts; iii) Further, that myocardial energetics are disturbed in the cardiac actin E99K mouse model, and that the interstitial adenosine level in the myocardium correlates with the development of myocardial fibrosis.

### 3.1.2 Aims

The experimental aims of this chapter are:

- To carry out screening experiments in several well-described mouse models for inherited cardiomyopathies to find an example of a pronounced cardiac fibrosis phenotype.
- To compare fibrotic phenotypes and collagen biology in these mouse models.
- To attain a more detailed delineation of the fibrotic phenotype of the cardiac actin E99K mouse model for hypertrophic cardiomyopathy by:
    - Obtaining a more detailed conception of collagen structure in order to recapitulate the fibrotic phenotype;
    - Delineating cell populations in the myocardium, using immuno-fluorescence and flow cytometry experiments, in order to define the cellular phenotype associated with myocardial fibrosis.
- To investigate the cardiac metabolic state of the fibrotic E99K mouse model.
- To demonstrate a correlation between interstitial adenosine levels and myocardial fibrosis.

## 3.2 Description of the fibrotic phenotype of several cardiomyopathy models

Hearts from murine models of inherited cardiomyopathy were investigated for myocardial collagen content by hydroxyproline measurements or semi-quantitative collagen assay and for cardiac fibrosis by histologic examination utilizing Sirius-red staining under bright-field as well as polarized-light microscopy.

### 3.2.1 The fibrotic phenotype of the Python mouse model

A mouse model for dilated cardiomyopathy (DCM) caused by a mutation in the mitochondrial fission gene Dnm1l, also known as the Python mutant, was investigated for changes in collagen biology. This model has been shown to display myocardial fibrosis and demonstrated enhanced deposition of extracellular matrix (Ashrafian et al., 2010). As a result it served as a positive control for myocardial fibrosis during the investigation of subsequent models (see below).

Collagen measurements of Python hearts (Figure 3.1) (N=7; three month old mice) demonstrated a statistically significant ($p < 0.002$) two-fold increase in the amount of total collagen content compared to WT controls. In order to quantify the amount of pepsin soluble collagen as a measure for the soluble, i.e. not covalently cross-linked, collagen subfraction, a Sirius-red assay was performed after overnight digestion in pepsin. WT and Python hearts did not differ significantly in the amount of soluble collagen. This signal for enhanced collagen crosslinking was associated with an up-regulation of LOX, the enzyme responsible for collagen crosslink formation. A significant five-fold increase in LOX mRNA expression ($p < 0.0001$) measured by

reverse transcription polymerase chain reaction (RT-PCR).

Histologic examination of Python mutant hearts (Figure 3.1 *C&D*) demonstrated marked interstitial and perivascular fibrosis, as well as myocardial disorganisation. This observation was supported quantitatively by a significant increase ($p = 0.0002$) in the fraction of Sirius-red signal normalised to total myocardial area using computational analysis.

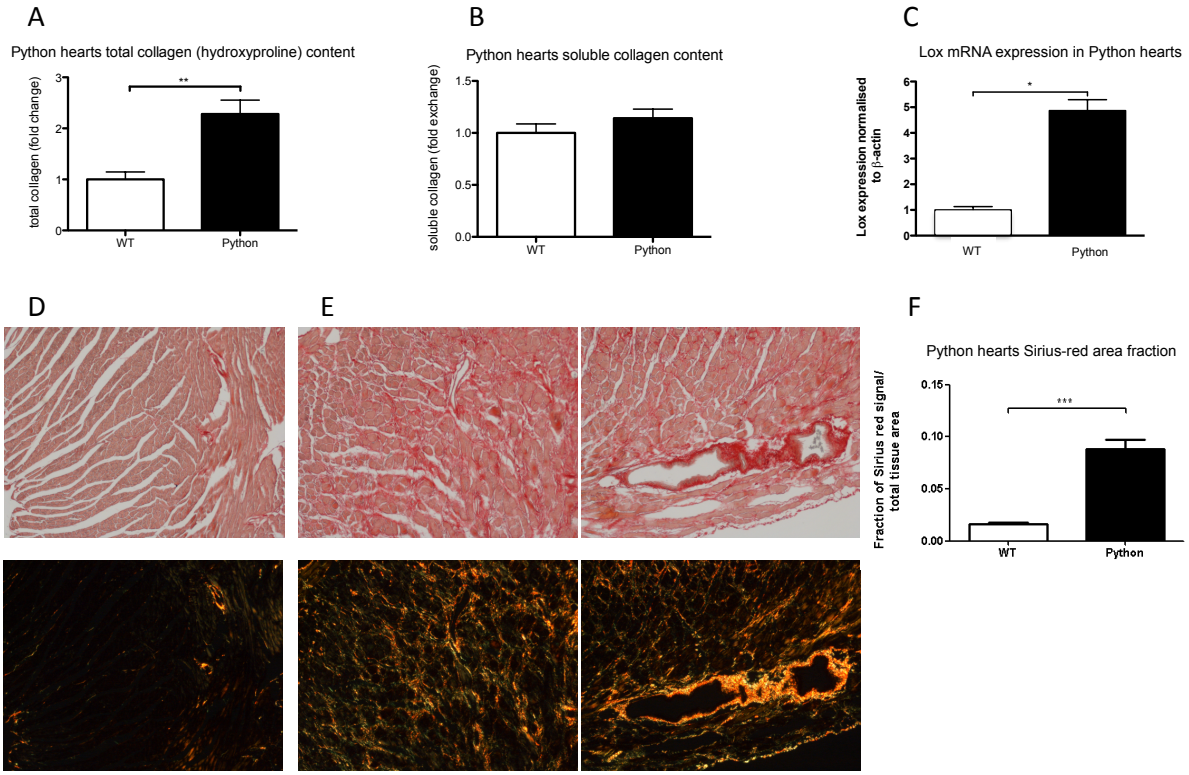


**Figure 3.1:** Collagen measurements in Python mutant hearts. (N=7; three month old mice). (*A*) The amount of total collagen in cardiac tissue shows a statistically significant ($p < 0.002$) two fold increase in the mutant hearts. (*B*) The amount of pepsin soluble collagen, measured by a Sirius-red assay after overnight digestion in pepsin, does not differ between WT and Python mutant hearts. (*C*) At mRNA level, measured by RT-PCR, there is a significant five-fold increase in *Lox* expression in Python hearts ($p < 0.0001$). (*D&E*) Upon histologic examination of WT and Python mutant hearts, significant fibrotic changes were evident. Representative images of the left ventricular wall of (N = 3) Python heterozygous (*E*) and WT mouse hearts (*D*) demonstrating normal cardiac architecture and collagen content in the WT hearts vs. pronounced interstitial and perivascular fibrosis in Python mutants. The hearts were stained with picro-sirius red and imaged under bright field microscopy (upper row) and under polarized light (lower row). (*E*) Computational analysis of these images revealed a significant increase ($p = 0.0002$) in the fraction of Sirius-red signal normalised to the total myocardial area.

### 3.2.2 The fibrotic phenotype of MLP knock out hearts

The fibrotic phenotype of a mouse line deficient in a LIM-only protein in terminally differentiated muscle (MLP), considered to be a classic genetic model of DCM, was also investigated (Arber et al., 1997). Although not primarily investigated with a focus on myocardial fibrosis so far, MLP KO mouse hearts have been described as "fibrotic" in the literature (Arber et al., 1997; Heineke et al., 2010).

Collagen measurements in MLP KO hearts (Figure 3.2) (N=5; three month-old mice) showed no significant change compared to WT in the amount of total collagen in cardiac tissue. The amount of soluble collagen, evaluated by overnight digestion in pepsin, followed by a Sirius-red assay, did not differ between WT and MLP KO hearts. These findings suggest that that, if present, there is only a weakly fibrotic phenotype present in MLP KO model, with in particular no induction of collagen production or maturation. Supporting this, there was also no significant increase in collagen-Ia1 or LOX mRNA expression.

Histologic examination of MLP KO and WT hearts demonstrated scarce areas of enhanced interstitial fibrosis formation, in particular there were several areas where perimysial collagen fibres appeared thickened and more common than in WT hearts (Figure 3.2; *D&E*). However, this phenomenon was mild and the affected areas were interrupted by large areas of normal appearing myocardium. As a result, even though the electronic quantification of the histologic images revealed an approximately 1.5 fold increase in the fraction of Sirius-red signal to total myocardial area, this did not reach statistical significance due to the variability in collagen signal.

Accordingly, while the collagen network of this model is qualitatively abnormal, it did not provide the optimal model for subsequent experiments aimed at modulating fibrosis.

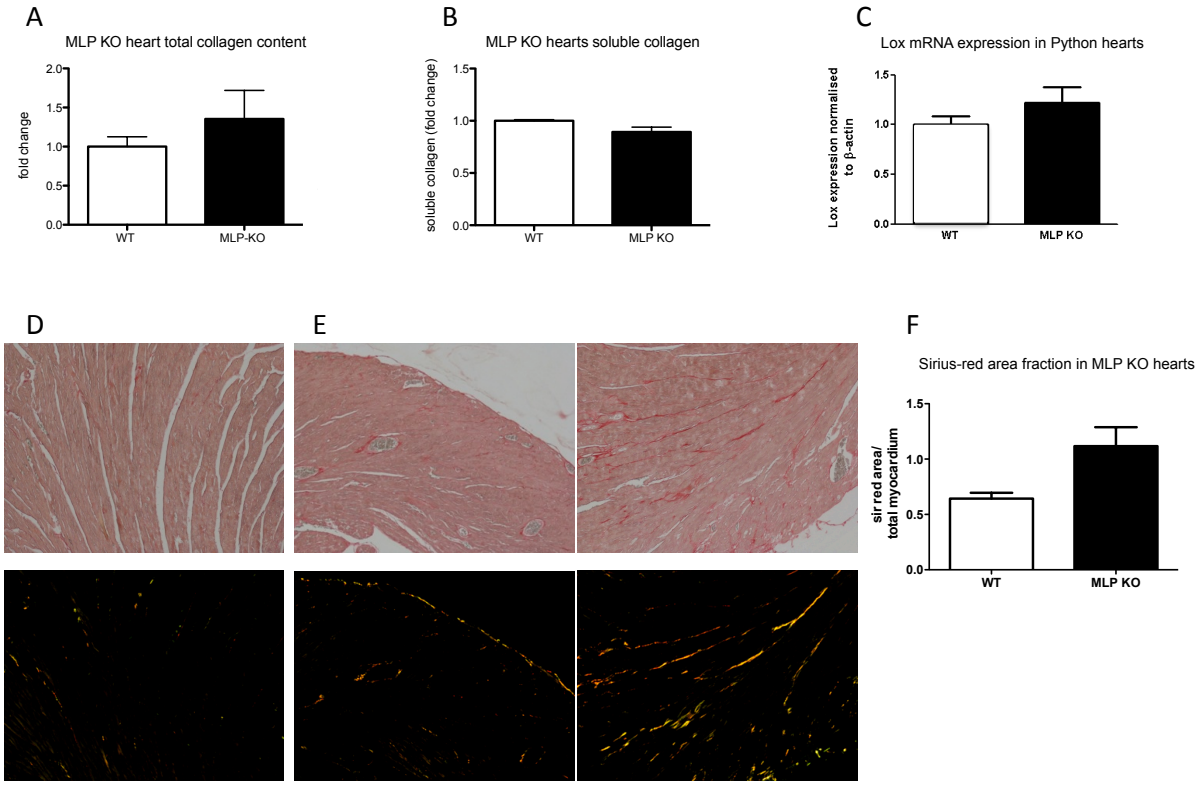


**Figure 3.2:** Description of the fibrotic phenotype in MLP KO hearts (N=5; three month old mice). (*A*) There was no significant change in the amount of total collagen in cardiac tissue. (*B*) The amount of pepsin soluble collagen, did not differ between WT and MLP KO hearts. Accordingly, the mRNA expression of LOX was not altered in MLP KO hearts compared to WT hearts (*C*). (*D&E*) Histologic examination of MLP KO and WT hearts did identify infrequent areas of mild interstitial fibrosis in MLP KO hearts. (*D*) A representative image of the left ventricular wall of a WT heart demonstrates normal myocardial structure and collagen deposition, and (*E*) showing two areas of MLP KO myocardium, one with normal myocardial collagen content (left) and the other with mildly pronounced perimysial collagen fibres (right). The hearts were stained with picro-sirius-red and imaged under bright field microscopy (upper row) and under polarized light (lower row). (*F*) Computational analysis of these images revealed a non-significant increase in the fraction of Sirius-red signal normalised to the total myocardial area.

### 3.2.3 The fibrotic phenotype of cardiac troponin T R92Q hearts

As the first of three models for HCM, the fibrotic phenotype of a transgenic mouse bearing an R92Q mutation in cardiac troponin-T (TNT) was investigated. This model is considered a model for HCM even though it does not demonstrate significant cardiac hypertrophy. However it has been described to recapitulate other aspects of the HCM phenotype, including myocardial fibrosis and myocardial disarray (Oberst et al., 1998).

Collagen measurements from the hearts of TNT mice (Figure 3.3) (N=4; 8-9 week old mice) did not demonstrate a significant change in the amount of total collagen in cardiac tissue. Furthermore the amount of pepsin soluble collagen measured by a Sirius-red assay after overnight digestion in pepsin did not differ significantly between TNT WT and TNT R92Q hearts. Accordingly, there was no significant increase in collagen 1a1 mRNA expression found, and only a minor, albeit statistically significant, increase in LOX expression at mRNA level. However the biologic significance of this approximately 1.1 fold increase in mRNA expression is questionable. Histologic examination of TNT WT and TNT R92Q (N=3; 8-9 weeks of age) hearts revealed normal myocardial collagen staining in both groups and largely unaltered myocardial architecture. Accordingly, computational analysis of these images demonstrated no significant difference in the fraction of Sirius-red signal normalised to the total myocardial area (Figure 3.3; (*D&E*)).

In conclusion, the findings presented did not replicate the described fibrotic phenotype of this mouse model. A possible explanation for this disparity is the use of

an earlier time-point for the present work (8 weeks of age vs. 3 months). In addition it is known that the phenotype of genetic mouse models can be altered between multiple generations. As a result, the cardiac troponin T R92Q mouse model was not used for subsequent experiments.

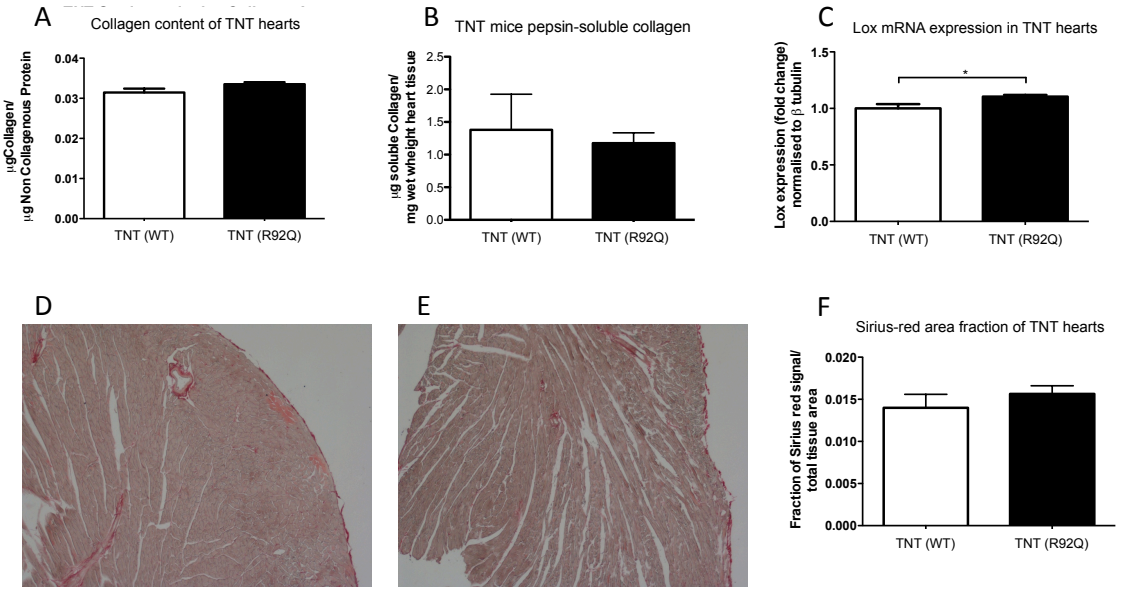


**Figure 3.3:** Collagen measurements in cTNT hearts. (N=4; three month old mice). (*A*) There is no significant change in the amount of total collagen in cardiac tissue. (*B*) The amount of pepsin soluble collagen, measured by a Sirius-red assay after overnight digestion in pepsin, does not differ between WT and TNT R92Q hearts. (*C*) Further, upon investigation of mRNA levels, a minor albeit significant increase in LOX expression was found. (*D&E*) The histologic examination of TNT R92Q and WT hearts revealed no differences between the two groups including no obvious formation of myocardial fibrosis in either group. (*D*) A representative image of the left ventricular wall of TNT WT hearts and (*E*) depicting a representative for the left ventricular wall of TNT R92Q hearts. (*F*) Accordingly, computational analysis of these images revealed no significant difference in the fraction of Sirius-red signal normalised to the total myocardial area.

### 3.2.4 The fibrotic phenotype of MYBP-C KI hearts

An additional mouse model for HCM, the cardiac myosin-binding protein c (MYBP-C) knock-in model, was investigated for the development of myocardial fibrosis. Homozygous MYBP-C knock-in mice, carrying a G>A point mutation on exon 6 on both alleles, have been shown to develop a strong hypertrophic phenotype and functional changes that recapitulate the disease pattern of human patients with HCM (Vignier et al., 2009). In the description of this model, Vignier et al. also demonstrate myocardial fibrosis, evidenced by Sirius-red staining, although without quantification.

In the present study, collagen measurements in MYBP-C KI hearts (Figure 3.4) (N=8-12; 9 weeks old mice) demonstrated a significant reduction in total myocardial collagen content compared with WT(genetically identical but lacking the point mutation) mice. The amount of pepsin soluble collagen did not differ significantly between WT and MYBP-C KI hearts. However, there was a significant, approximately 2-fold increase in collagen-1a1 and LOX mRNA expression in MYBP-C KI hearts compared to MYBP-C WT measured by RT-PCR. This data indicates that there is an increased expression of pro-fibrotic genes in these hearts. Concerning the observed reduction in total tissue collagen, however, it is necessary to take into account that this value is normalized to tissue weight. MYBP-C KI hearts demonstrated significant cardiac hypertrophy (mean heart weight was 85mg in MYBP-C WT hearts, compared to 155mg heart weight in MYBP-C KI). One interpretation of these findings is that the modest increase in collagen expression is diluted by the more pronounced hypertrophic response of the MYBP-C KI hearts, resulting in a net decrease in collagen per milligram heart weight. This finding was also recapitulated by a statistically significant decrease in semi-quantitative collagen content, measuring

collagen via the absorption of Sirius-red solution that was bound to, and subsequently eluted from, a paraffin embedded tissue section. As the collagen value in this assay is normalized to the total amount of protein, measured by fast-green absorption, the ‘diluting’ effect of cardiac hypertrophy is similar in this assay, albeit less pronounced.

Histologic evaluation revealed a marked disruption of myocardial organisation and cardiomyocyte disarray in the MYBP-C KI hearts, however only few and localised areas of interstitial myocardial fibrosis could be found (Figure 3.4 (*D&E*)).

In summary, MYBP-C KI hearts demonstrate a potential pitfall in the evaluation of myocardial fibrosis since they are characterised by a decrease in total collagen content per unit heart weight, while simultaneously exhibiting an up-regulation of collagen expression. As discussed, the marked cardiomyocyte hypertrophy in combination with the mild and unevenly distributed fibrotic phenotype is potentially responsible for these findings. Taken together with the mild fibrotic phenotype evident on histology, the MYBP-C KI mouse model was not considered sufficiently robust for experiments aiming to modulate the cardiac fibrotic phenotype.

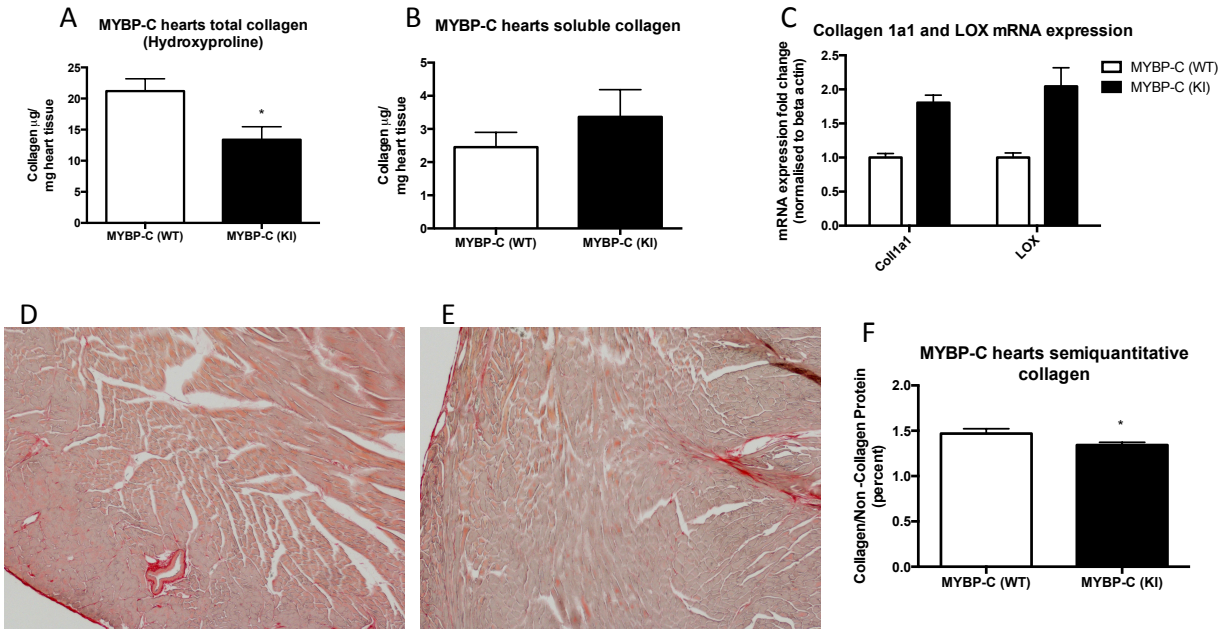


**Figure 3.4:** Description of the fibrotic phenotype of MYBP-C KI compared to WT hearts. (*A*) The total collagen content normalised to heart weight was significantly reduced ($p < 0.05$) in MYBP-C KI vs WT hearts. (*B*) There was no significant difference in the amount of pepsin-soluble collagen between the two groups. Conversely, (*C*) collagen 1a1 and LOX mRNA were significantly up regulated in MYBP-C KI hearts. (*D&E*) Histologic examination of MYBP-C WT and KI hearts revealed marked myocardial disorganisation in the KI group, with rare localized areas of interstitial fibrosis. (*F*) This was associated with a significant reduction in collagen content measured by a semi-quantitative collagen assay, which measures Sirius-red and Fast-green absorption after staining and subsequent elution from paraffin embedded tissue sections.

### 3.2.5 The fibrotic and metabolic phenotype of cardiac actin E99K hearts

The cardiac actin E99K model for HCM, a transgenic mouse bearing an E99K mutation in cardiac actin (ACTC E99K), was investigated for its fibrotic phenotype (Song et al., 2011). The causal mutation in this model has been described to cause apical hypertrophy in human patients, leading to a spade-like deformation of the ventricular cavity on ventriculography. The cardiac actin E99K model recapitulates this phenotype, as it is characterized by predominantly apical hypertrophy as well as myocardial fibrosis affecting mainly the apex and left ventricular free wall (Figure 3.5). The myocardial septum is typically unaffected by the fibrotic changes, whereas the apex and apical two thirds of the left ventricular free wall consistently demonstrate marked interstitial fibrosis. Fibrotic changes of the left ventricular free wall are typically gradually ameliorated towards the base of the heart (Figure 3.6). While mice homozygous for the transgene are not viable, heterozygous mice develop the described phenotype consistently.

Collagen measurements from ACTC E99K mice (Figure 3.7) (N=8; 8-9 weeks old) demonstrated a highly significant ($p < 0.0001$), approximately three fold-fold increase in the amount of total collagen in cardiac tissue in the mutant hearts. In addition there was no significant difference in the amount of pepsin soluble collagen. As a result, the measure for collagen crosslinking, i.e. the ratio of insoluble to soluble collagen, demonstrated a statistically significant three-fold increase. This was accompanied by a significant four-fold increase in collagen-1a1 mRNA as well as LOX mRNA expression ($p < 0.001$) (Figure 3.7). In addition the expression of MMPs was significantly altered, indicating a change in extra cellular matrix turnover, with potential effects on TGF-β release from its latent tissue bound form. Finally, an up-

regulation of well-described myocardial stress and hypertrophy markers, namely atrial natriuretic peptide (ANP), brain natriuretic peptide (BNP) and myosin heavy chain (MYH7) was identified in actin E99K hearts compared to actin WT hearts. The latter indicate myocardial stress, atrial stretch and activation of pro-hypertrophic counter-regulatory mechanisms. Given that atrial stretch is one of the primary stimuli for the production of these markers, these findings are consistent with the marked atrial enlargement observed in actin E99K mouse hearts (Figure 3.5).

The consistent fibrotic phenotype in the actin E99K mouse model, in association with only a mild hypertrophic phenotype, rendered it an appropriate model for experiments aiming to modulate fibrosis formation. Further, the phenotype of actin E99K hearts closely recapitulates the phenotype of human mutation carriers. For these reasons the actin E99K mouse model was chosen for further experiments: First, a more detailed investigation of the fibrotic phenotype as well as the functional, cellular, and metabolic phenotype was carried out; Secondly, rescue experiments aimed at preventing the formation of myocardial fibrosis were undertaken.

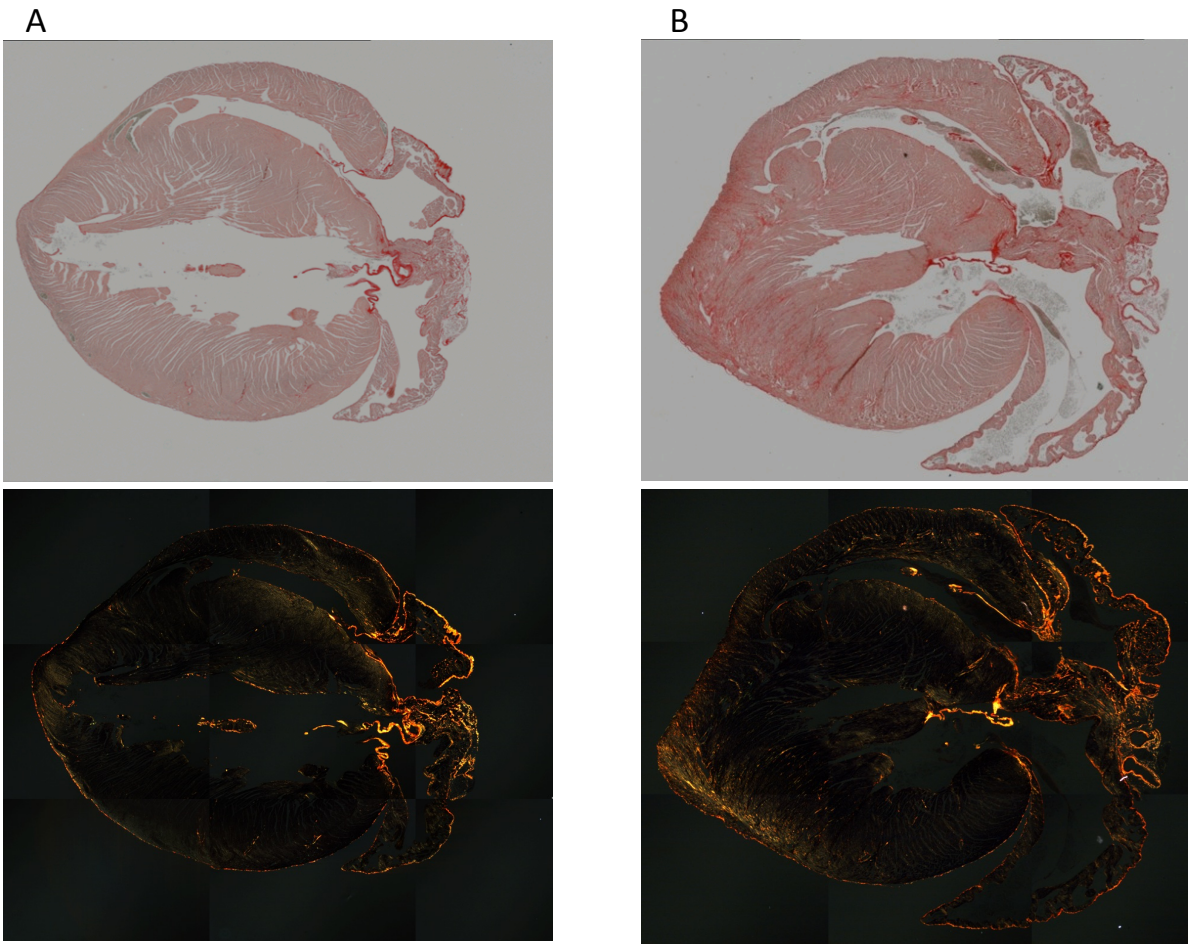


**Figure 3.5:** Multiple image alignment of Sirius-red stained ventricular sections of an actin WT heart (*A*), and an actin E99K heart (*B*). The top pictures are imaged under bright-field microscopy, while the lower images are taken under polarised light. These images demonstrate the apical focus of the pathologic changes in actin E99K mutant hearts, mainly hypertrophy and myocardial fibrosis. In addition there is marked enlargement of the left and to a lesser extent the right atrium, pointing to increased ventricular filling pressure followed by atrial remodelling. These morphologic changes, in particular the apically focused hypertrophy and fibrosis, recapitulate the disease pattern of human cardiac actin E99K mutation carriers.

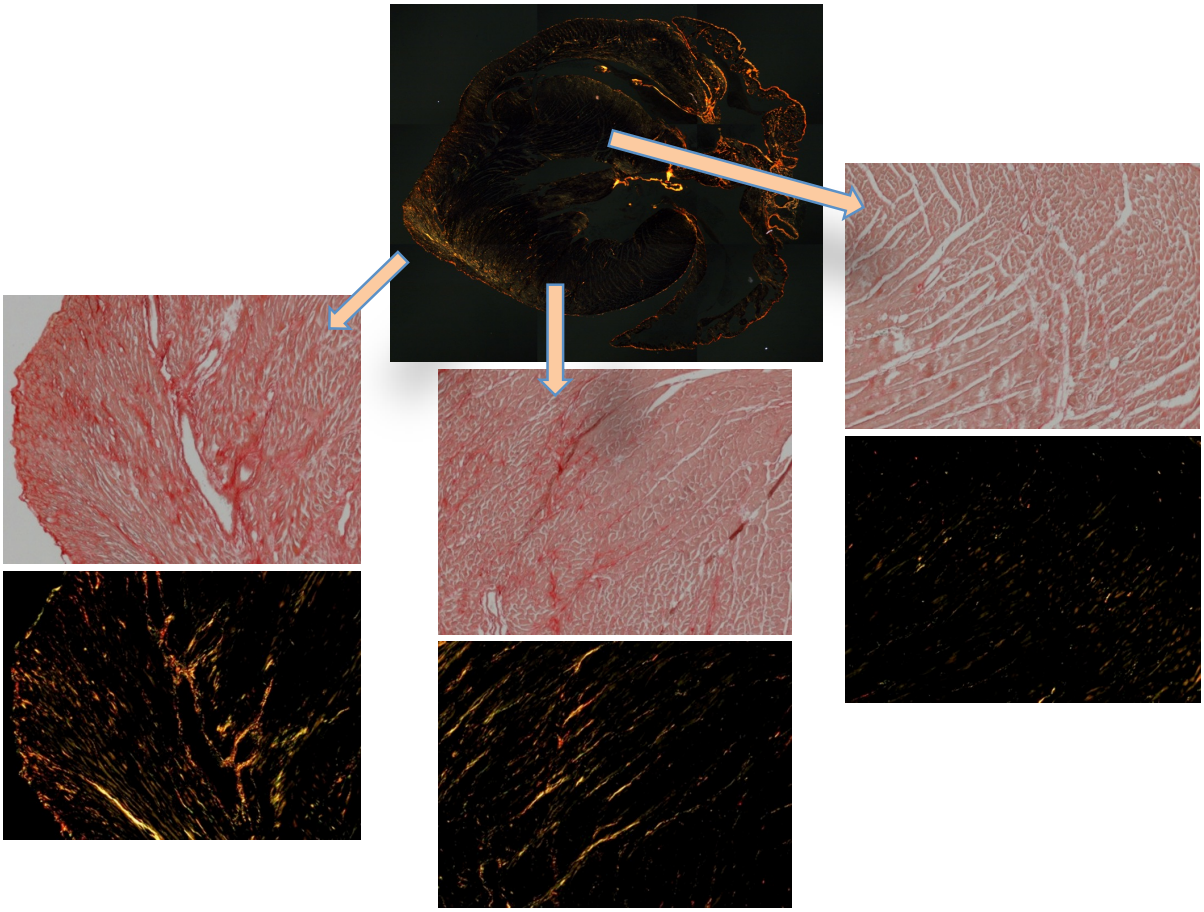

**Figure 3.6:** The localised apical fibrosis is a specific and consistent feature of the phenotype of the actin E99K heart model. In all the cardiac actin E99K hearts evaluated, demonstrable fibrosis was limited to the apex and left ventricular free wall, while the ventricular septum was unaffected by fibrotic changes demonstrable by Sirius-red histology. The primary type of fibrosis in these hearts was interstitial fibrosis, entailing the perimysial as well as endomysial collagen component. Perivascular fibrosis was scarce in this model and no replacement fibrosis was observed.

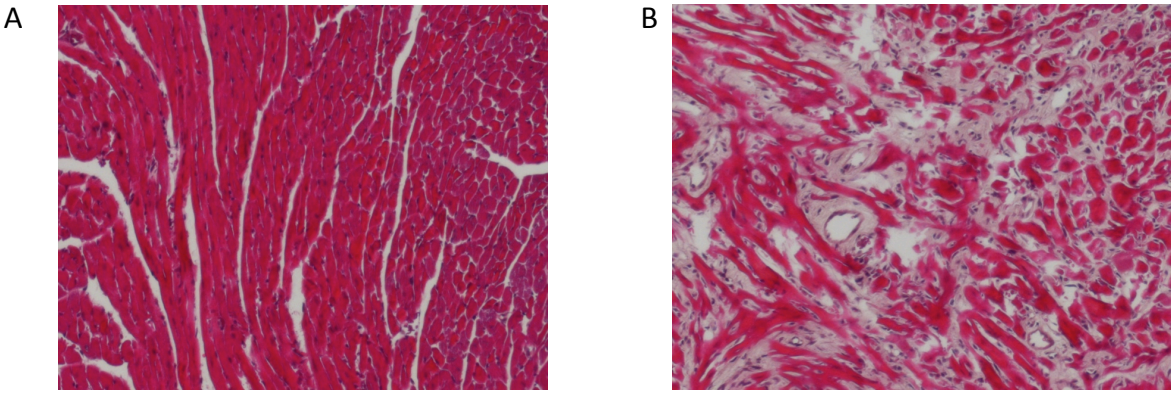


**Figure 3.7:** In addition to the fibrotic phenotype, myocardial disorganisation could be demonstrated in the left ventricular free wall of actin E99K hearts (*B*) compared to actin WT hearts (*A*), demonstrated by haematoxylin and eosin staining.

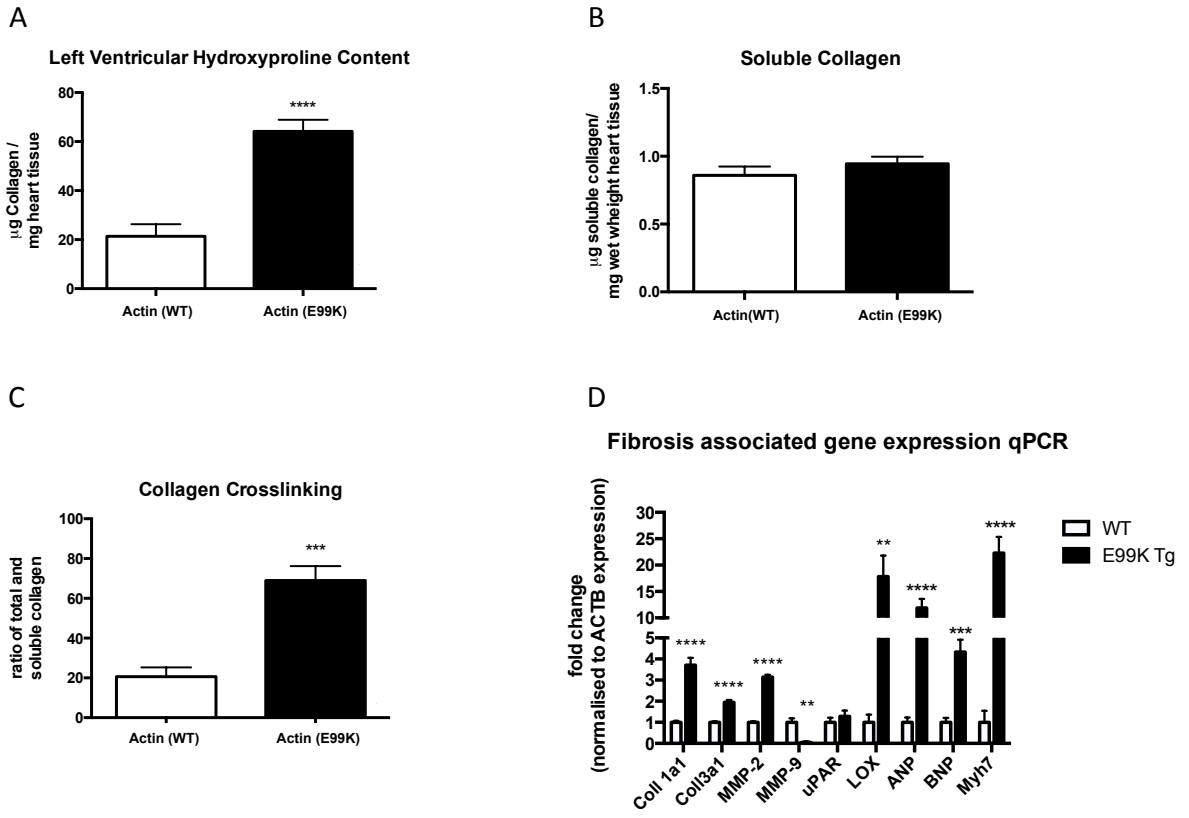


**Figure 3.8:** Collagen measurements in ACTC E99K. (N=8; 9-10 week old mice). (*A*) The amount of total collagen in cardiac tissue shows a significant ($p < 0.0001$) near four-fold increase in the transgenic actin E99K cohort. (*B*) The amount of pepsin soluble collagen did not differ significantly between WT and E99K mutant hearts. As a result, (*C*) a well-described marker for collagen crosslinking, the ratio of total and soluble collagen was significantly increased (*D&E*). At mRNA level there is a significant increase in several fibrosis-associated genes measured by RT-PCR: collagen-1a1, collagen-3a1 ($p < 0.0001$, respectively) as well as LOX expression ($p < 0.01$). The expression patterns of MMP-2 and -9 are divergently regulated; with MMP-2 being significantly up regulated ($p < 0.0001$) while MMP-9 is significantly down regulated ($p < 0.01$). Further, the expression of several genes, indicating myocardial stress, namely ANP, BNP and MYH7 were significantly up-regulated.

### 3.3 Detailed description of the functional and fibrotic phenotype of cardiac actin E99K hearts

Preliminary investigation of actin E99K hearts demonstrated a reproducible pronounced fibrotic phenotype, primarily in the apical and left ventricular free wall region of the myocardium. In order to delineate this fibrotic phenotype in more detail, additional staining for collagen, i.e. immunofluorescence staining, was carried out. Further, immunofluorescence microscopy experiments were conducted in order to investigate the changes in the cellular composition of actin E99K hearts, the results of which were confirmed by flow cytometry experiments after collagenase digestion.

In addition, the cardiac actin E99K mouse model was investigated in detail for abnormalities in cardiac function in order to investigate whether or not the fibrotic phenotype is associated with altered myocardial performance.

Finally, the metabolic state of E99K hearts was investigated by nuclear magnetic resonance spectroscopy (NMR-spec) and the amount of interstitial adenosine gauged and correlated to myocardial collagen content.

The overall aim of these experiments was to obtain a more detailed understanding of the functional and fibrotic phenotype of the actin E99K heart. Of particular importance was the assessment of the role of metabolic perturbations and adenosine signalling in the formation of myocardial fibrosis as a prelude to experiments seeking to rescue the fibrotic phenotype by modulating adenosine receptor signalling.

### 3.3.1 Functional studies

The myocardial function of actin E99K hearts was investigated using Langendorff perfused hearts. Hearts were extracted, cannulated, and perfused retrogradely in Langendorff mode. A hand made balloon was inserted into the left ventricular cavity and used for live measurement of intra-ventricular pressures (N=8-10; 10 weeks old). In actin E99K hearts, the maximal rate of pressure increase during systolic contraction was significantly reduced ($p<0.05$) compared to actin WT hearts, indicating systolic dysfunction (Figure 3.9). This was further supported by the finding of a significant reduction in the maximal developed intra ventricular pressure ($p<0.01$).

In addition, the minimal rate of pressure decrease during diastolic relaxation (expressed in negative mmHg/sec) was significantly reduced ($p<0.01$) in actin E99K hearts. This slowing of cardiac relaxation provides evidence that both diastolic and systolic function is impaired in cardiac actin E99K hearts.

The impaired systolic and diastolic cardiac function of actin E99K hearts was also reflected by an increase in lung weight consistent with cardiac congestion (Figure 3.9).

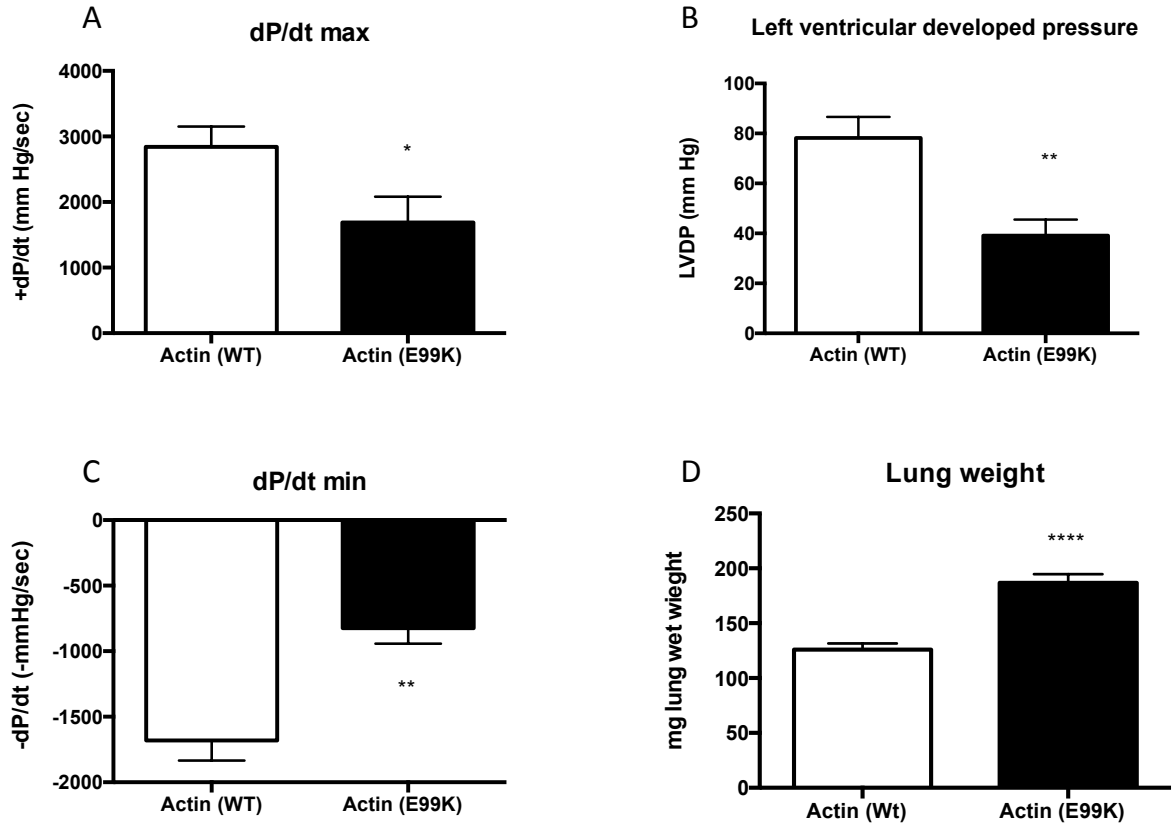


**Figure 3.9:** Functional analysis of actin E99K hearts compared to actin WT hearts during Langendorff perfusion. (*A&B*) Demonstrate the investigation of systolic cardiac function. (*A*) The maximal rate of pressure increase (+dP/dt max) during systolic contraction was significantly decreased in actin E99K hearts ($p<0.05$). (*B*) Maximal developed left ventricular pressures during systole were significantly reduced in actin E99K hearts compared to actin WT hearts. The alterations of both these parameters indicate systolic dysfunction. (*C*) In addition, the minimal rate of pressure decrease (-dP/dt min) was significantly reduced in actin E99K hearts, indicating a slower rate of left ventricular relaxation and thereby indicating diastolic dysfunction. (*D*) An increase in wet lung weight in actin E99K hearts suggestive of cardiac decompensation and ensuing pulmonary congestion.

### 3.3.2 Delineation of collagen deposition and cellular phenotype

In order to further delineate the fibrotic phenotype of actin E99K hearts, immunofluorescence microscopy and flow cytometry experiments were carried out. The aims of these experiments were to further validate findings from Sirius-red staining by immunofluorescence staining for collagen.

In addition immunofluorescence staining for cellular markers served to investigate changes in the cellular composition of actin E99K hearts. The cellular phenotype of actin E99K hearts was also investigated by flow cytometry to reiterate findings from immunofluorescence staining.

#### *3.3.2.1 Immunofluorescence microscopy for collagen*

Immunofluorescence staining with anti-collagen I antibodies demonstrated a marked increase in collagen signal in actin E99K hearts compared to WT hearts (N=5). In actin WT control hearts (Figure 3.10), collagen staining revealed a thin but continuous endomysial collagen layer, inter-lining individual cardiomyocytes and capillaries. In actin E99K hearts there was an increase in collagen signal throughout the myocardium, which appeared to be primarily caused by thickening of the endomysial collagen component. Interestingly, this phenomenon was distributed continuously throughout the myocardium and was not limited to the apical region.

The collagen network surrounding cardiomyocytes also appeared to encase them, evidenced by the cardiomyocytes being pushed into a more round form in actin E99K hearts. Such an encasement of cardiomyocytes has been demonstrated in the literature, and has been suggested to contribute to myocardial dysfunction in spontaneously hypertensive rats (LeGrice et al., 2012).

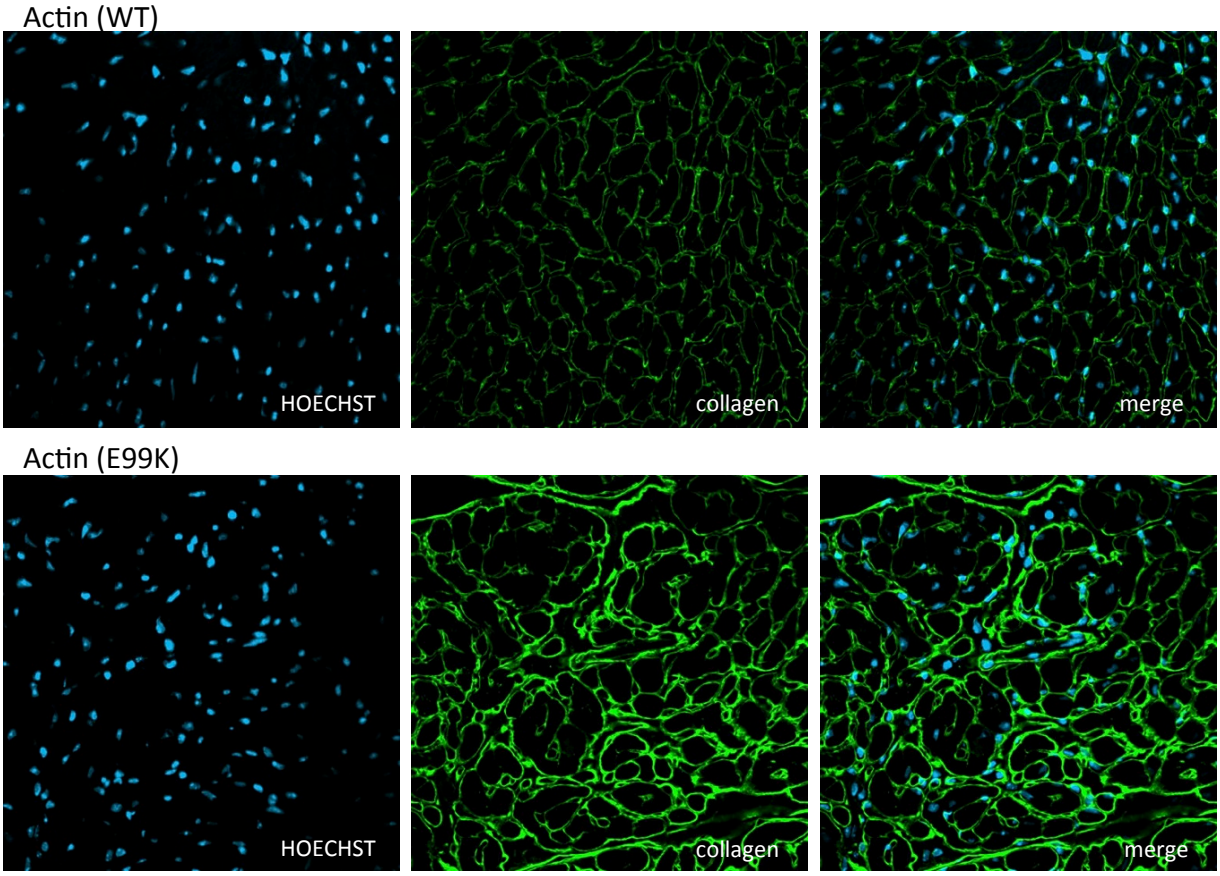


**Figure 3.10:** Immunofluorescence images cross-sections of actin WT and E99K hearts were stained with an anti-collagen I antibody. In actin WT control hearts (top row), collagen staining revealed a thin continuous interstitial collagen network, inter-lining individual cardiomyocytes and capillaries (endomysial collagen). In actin E99K hearts (bottom row) there was an increase in collagen signal throughout the myocardium, primarily caused by a thickening of endomysial collagen. Nuclear staining (blue) on the left; collagen I antibody staining (green) in the middle; merged image (right); actin WT heart (top row); actin E99K (bottom row).

#### *3.3.2.1 Immunofluorescence microscopy for cellular markers*

Different cellular populations that can potentially contribute to the fibrotic phenotype in the actin E99K heart were investigated by immunofluorescence microscopy using antibody staining for different cellular markers.

Using anti-vimentin and anti-CD68 antibodies, actin E99K hearts demonstrated a marked increase in vimentin signal as well as in CD68 positive cells compared to actin WT hearts (Figure 3.11,*A*). Vimentin expression is considered to be a marker for fibroblasts, although it is also expressed to a lesser extent by endothelial cells. CD68 expression is used in the literature to identify cells from a monocyte/macrophage lineage. These findings indicate a marked increase in fibroblasts (i.e. vimentin expressing cells) and recruitment of inflammatory cells, in particular macrophages, into actin E99K hearts.

Interestingly, the increase in vimentin expressing cells was not accompanied by an up-regulation of α-sma in actin E99K hearts. As evidenced by the presented images (Figure 3.11*,B)* vascular smooth muscle cells surrounding the larger ventricular vasculature clearly expressed α-sma. However, in neither actin WT nor E99K hearts was any α-sma signal found in the spaces between cardiomyocytes, where most of the vimentin positive cells were located. This finding indicates that the development of cardiac fibrosis in models for HCM is not necessarily associated with the emergence of myofibroblasts, which has also been demonstrated in other HCM models (Teekakirikul et al., 2010).

In addition, an increase in non-cardiomyocyte cells demonstrating Ki-67 positive

nuclei (as a cellular marker for proliferation) on immunofluorescence staining was found in actin E99K hearts (Figure 3.11,*C*), supporting a role for active proliferation in the multiplying of cardiac fibroblasts.

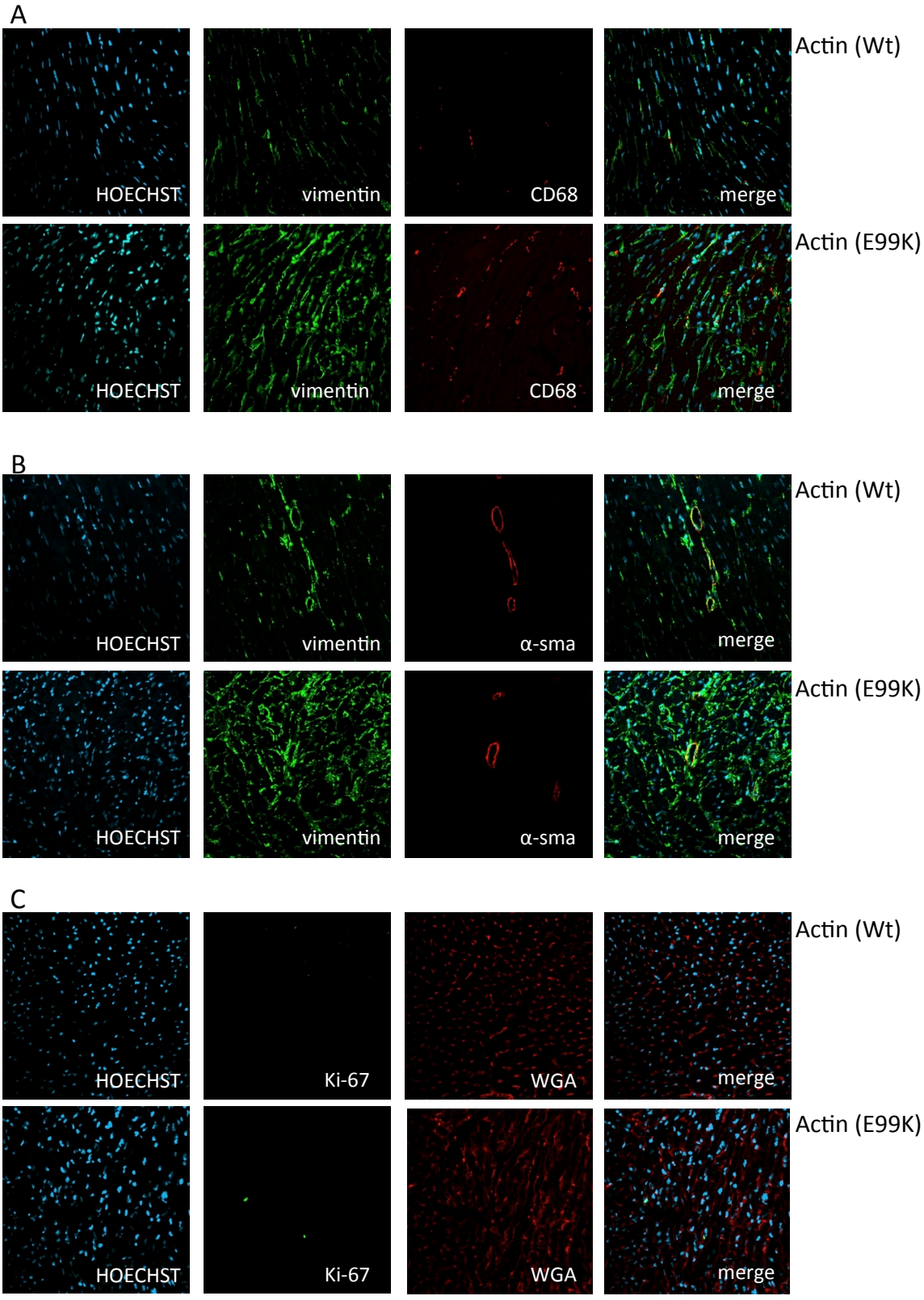


**Figure 3.11:** Immunofluorescence images of actin WT and E99K hearts. (*A*) Actin WT and E99K hearts were stained with anti-vimentin and anti-CD68 (tissue macrophages) antibodies. Actin E99K hearts demonstrated a marked increase in vimentin as well as CD68 positive cells. (*B*) Interestingly, the increase in vimentin expressing cells was not accompanied by an up-regulation of α-sma in actin E99K hearts. (*C*) In addition there was an increase in Ki-67 positive nuclei in non-cardiomyocytes, and the increase in non-cardiomyocytes was also evidenced by an augmented wheat germ agglutinin (WGA staining).

#### *3.3.2.2 Fluorescence-activated cell sorting (FACS)*

In order to further validate the results of the immunofluorescence microscopy experiments, as well as to more precisely define the cell population involved, flow cytometric experiments were conducted. The potential to readily obtain quantifiable measurements of cell number rendered FACS the method of choice in addressing this aim.

FACS experiments depend on the disruption of tissues into single cell solutions. In order to achieve this, the hearts were disrupted mechanically, as well as digested chemically, using a cardiac specific gentleMACS® setup and protocol.

In order to define the population of cardiac fibroblasts, a specific gating strategy was applied during the FACS experiments (Figure 3.12). In the forward scatter versus side scatter plot, the area of interest was selected based on cell size and granularity. From the resulting cells, duplicates and dead cells (primarily cardiomyocytes) were excluded from further analysis. The remaining live cells were plotted and differentiated according to CD45 and CD31 expression, defining bone marrow derived cells and endothelial cells, respectively. The double negative cell population of this plot, expressing neither CD45 nor CD31 was then further investigated. A large proportion of this population was double positive for DDR-2 and vimentin, two well-described markers for fibroblasts. Therefore, the CD45 negative, CD31 negative, vimentin positive ($CD45^-/CD31^-/vimentin^+$) cell population was considered to represent the cardiac fibroblast population in the myocardium and was further analysed in actin E99K hearts compared to WT hearts.

The major descriptive findings obtained by FACS experiments recapitulated the

marked increase in vimentin expressing fibroblasts observed in immunofluorescence microscopy (Figure 3.13). Actin E99K hearts demonstrated a marked increase in $CD45^-/CD31^-/vimentin^+$ cells, both as a percentage of total live cells as well as in the percentage of $CD45^-/CD31^-$ cells. In addition absolute cell numbers were gauged by the use of counting beads. Using this method, the resulting total numbers of $CD45^-/CD31^-/vimentin^+$ cells, considered to represent cardiac fibroblasts, were highly significantly ($p<0.0001$) increased in actin E99K hearts (Figure 3.13),

This prominent cell population was further evaluated for the expression of several fibroblast activation markers, as well as ectonucleotidases. The latter enzymes are responsible for extracellular hydrolysis of ATP and of particular interest given that they have been shown to regulate interstitial myocardial adenosine concentrations (Bönner et al., 2012; Headrick, Matherne, & Berne, 1992; Xu et al., 2008).

The fibroblast population (i.e. $CD45^-/CD31^-/vimentin^+$ cells) demonstrated a marked increase in podoplanin (gp38) expression in actin E99K hearts. Both the percentage of fibroblasts that were podoplanin positive, as well as the absolute cell number of podoplanin positive fibroblasts were markedly increased ($p<0.0001$). Podoplanin, a ligand for the CLEC-2 receptor, is a marker of a subpopulation of stromal fibroblast which is believed to be responsible for intercellular communication between stromal cells and immune cells via CLEC-2 signalling (Acton et al., 2012). Podoplanin has been described to play an important role in synovial fibroblast activation in models of rheumatoid arthritis inflammation and also in cancer-associated fibroblasts (Pula, Witkiewicz, Dziegiel, & Podhorska-Okolow, 2013).

Thy1 is another well-described marker for fibroblasts and has been utilised by several investigators as the primary cellular marker for cardiac fibroblasts. In the present study, a large proportion of cardiac fibroblasts ($CD45^-/CD31^-/vimentin^+$ cells in the myocardium) were Thy1 positive in actin WT animals. However, in actin E99K hearts a substantial fraction of cardiac fibroblasts (about 25%) did not express Thy1. Accordingly, even though there was a significant increase in Thy1 positive fibroblasts in actin E99K hearts ($p<0.0001$), a substantial portion of fibroblasts appears to be missed by using this marker alone.

In addition, a significant increase in Ki67 positive fibroblasts ($p<0.001$) was observed in actin E99K hearts. This up-regulation of nuclear Ki67 staining indicates a contribution of cellular proliferation in the development of the observed cardiac fibroblast expansion.

Finally, cardiac fibroblasts demonstrated the expression of ATP hydrolysing enzymes, ecto-nucleotidases CD39 and CD73. As a result, a significant increase in CD73 and CD39 expressing fibroblasts was observed in actin E99K hearts. The expression levels of these enzymes have been shown to regulate myocardial adenosine content (Bönner et al., 2012).

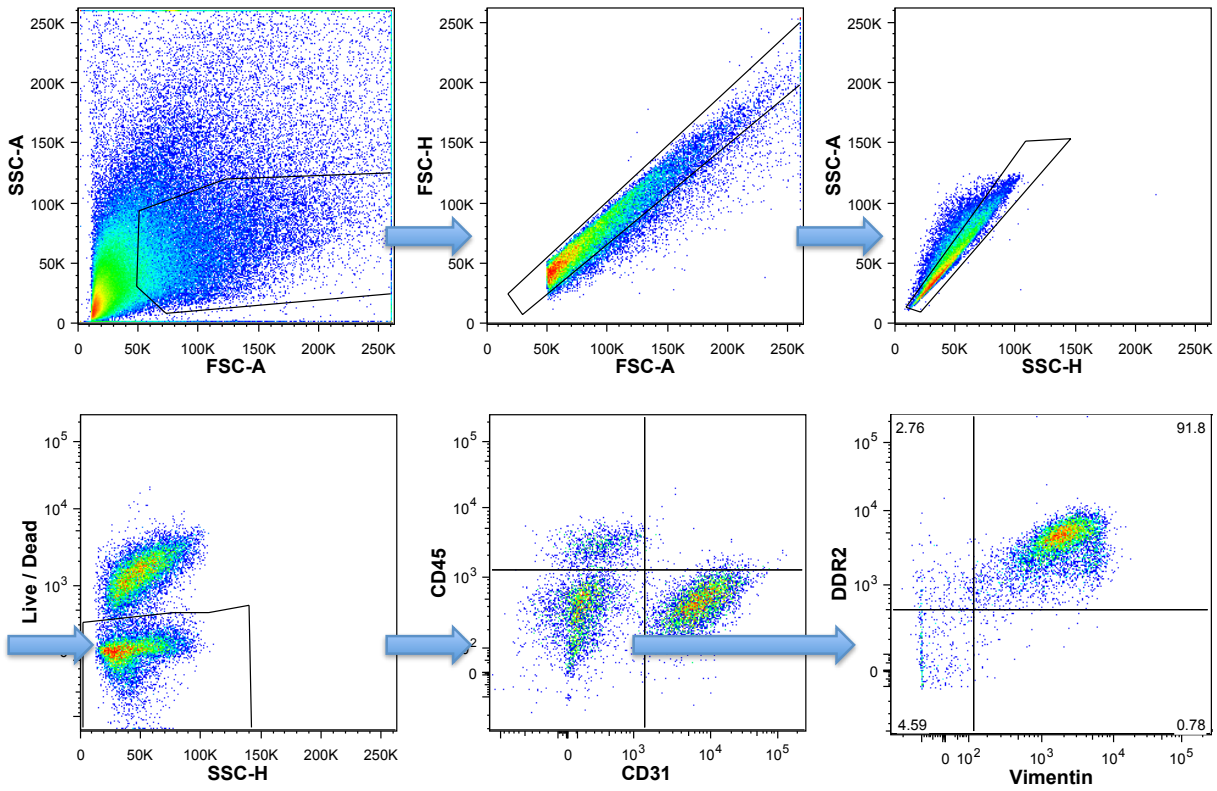


**Figure 3.12:** Demonstration of the gating strategy applied for flow cytometry experiments. In the forward scatter (FSC-A; x-axis) versus side scatter plot (SSC-A; y-axis) the area of interest based on cell size and granularity was selected (top left). From the resulting cells, duplicates (top middle and top right) and dead cells (bottom left) were excluded from further analysis. From the resulting live cells, the CD45 (bone marrow derived cells) and CD31 (endothelial cells) negative population was chosen for further investigation (bottom middle). The resulting cell population was largely double positive for DDR-2 and vimentin, two well-described fibroblast markers. Therefore, this cell population was considered to represent cardiac fibroblasts and further analysed.

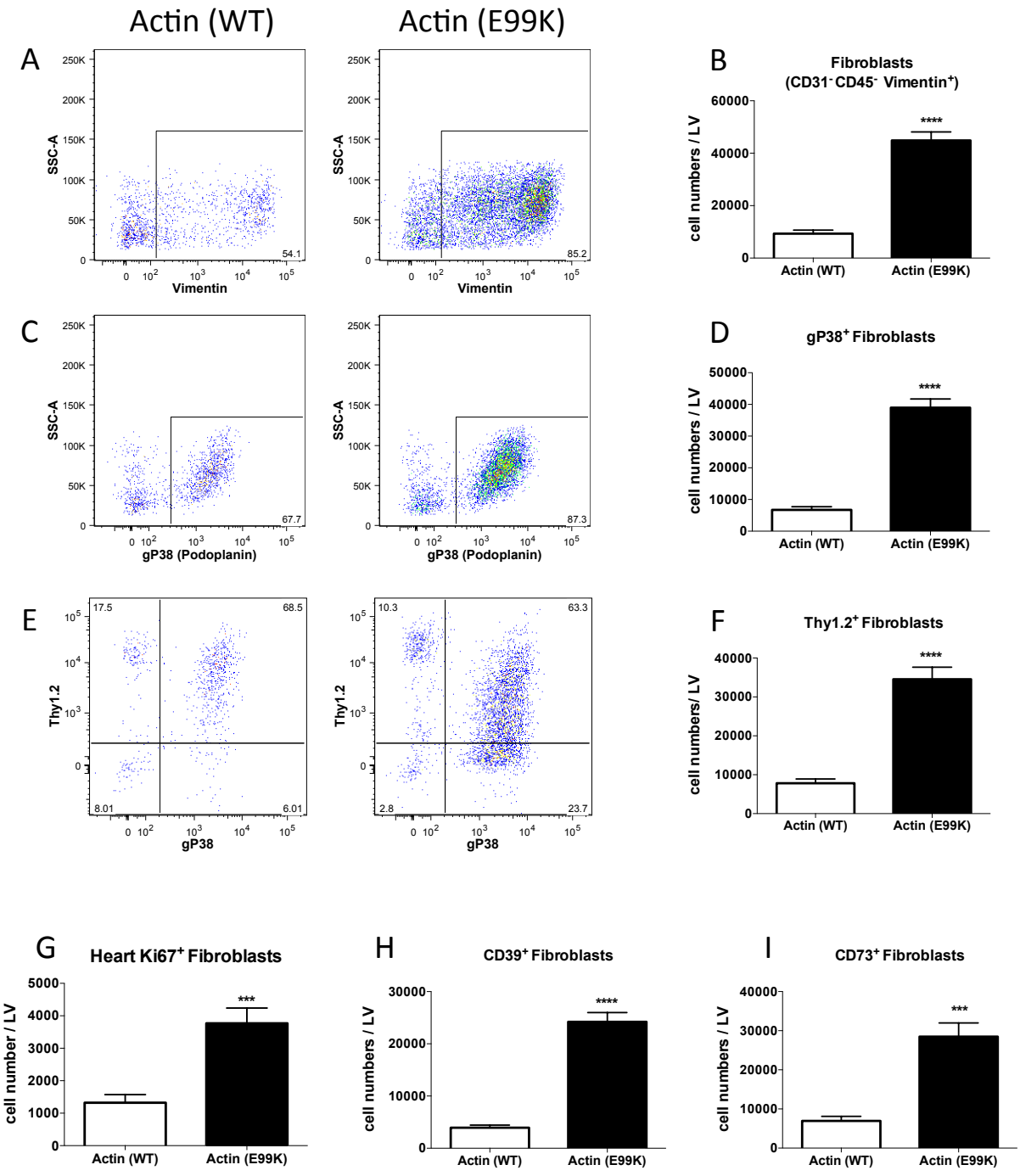


**Figure 3.13:** Major findings in FACS experiments. (*A&B*) Actin E99K hearts demonstrated a marked increase in CD45$^-$CD31$^-$vimentin$^+$ cells in percentage of all live cells as well as in the percentage of all CD45$^-$CD31$^-$ cells (*A*). In addition, the total cell number of CD45$^-$CD31$^-$vimentin$^+$ cells, which were considered cardiac fibroblasts, was significantly ($p$<0.0001) increased in actin E99K hearts (*B*). This fibroblast population demonstrated a marked increase in podoplanin (gp38; *C&D*) expression in actin E99K hearts, both in the percentage of fibroblasts (*C*) as well as in absolute cell numbers ($p$<0.0001; *D*). Thy1 is a well-described marker for fibroblasts and in the present study a large proportion of fibroblasts (CD45$^-$/CD31$^-$/vimentin$^+$ cells) were Thy1 positive in actin WT animals (*E&F*). Even though there was a significant increase in Thy1 positive fibroblasts in actin E99K hearts ($p$<0.0001; *F*). In addition, actin E99K hearts demonstrated a significant increase in Ki67 positive fibroblasts ($p$<0.001; G) indicating a role for cell proliferation in the observed increase in cardiac fibroblast numbers. Finally, cardiac fibroblasts demonstrated the expression of ATP hydrolysing enzymes, ecto-nucleotidases CD39 and CD73 (*H&I).* There was a significant increase in CD73 and CD39 expressing fibroblasts in actin E99K hearts.

## 3.4 Delineation of the metabolic state of cardiac actin E99K hearts and a correlation of interstitial adenosine with collagen content

### 3.4.1 Assessment of myocardial energetics

The primary hypothesis of this project was that metabolic perturbations of the myocardium initiate a purinergic-signalling cascade responsible for activation of cardiac fibroblasts. Based on the existing literature, adenosine signalling via the adenosine A2AR, being responsible for fibroblast activation in several organs (see Introduction), appeared the most likely signalling mechanism.

In order to verify that actin E99K hearts feature a disruption in cardiac energetics, the metabolic state of these hearts was investigated and compared to actin WT hearts using nuclear magnetic resonance spectroscopy.

Hearts were explanted, cannulated, retrogradely perfused (Langendorff) with oxidised Krebs solution and inserted into a magnet. Nuclear magnetic resonance spectroscopy demonstrated marked perturbations of myocardial energetics in actin E99K hearts. ATP peaks for all three phosphate residues were unchanged in actin E99K hearts, consistent with published data that ATP is kept at stable levels within cardiomyocytes until very late stages of cardiac failure (Stefan Neubauer, 2007). Conversely, there was a marked decrease in PCr signal in actin E99K hearts ($p<0.001$), as well as an increase in inorganic phosphate. As a result, the PCr to ATP ratio, a well-recognised indicator for energetic perturbations in the myocardium, was markedly decreased in actin E99K hearts (Figure 3.14, *A and B*).

### 3.4.2 Correlation of interstitial adenosine and myocardial collagen content

The in-situ interstitial levels of adenosine in cardiac actin E99K mouse heart were gauged using microdialysis. Cardiac actin E99K mice (N=6, 8 weeks old), under terminal anaesthesia, underwent thoracotomy followed by introduction of a micro-dialysis probe into the left ventricular free wall. Microdialysis catheters were perfused with Krebs solution (1µl/minute) and the microdialysate collected in 10-minute intervals for 70 minutes and analysed by mass spectrometry.

Adenosine levels in microdialysate samples from E99K hearts showed a typical drop in adenosine concentrations after dialysis probe insertion (Figure 3.14,*C*). The high adenosine levels in the early aliquots obtained are considered to reflect cellular injury due to insertion of the microdialysis probe. Continuous microdialysis leads to wash out of the released interstitial metabolites such that after 30-40 minutes baseline levels were reached. As is the nature of microdialysis samples, these baseline levels do not represent a direct measurement of interstitial adenosine concentrations. However, the resulting measurements are directly correlated to interstitial adenosine concentrations (Figure 3.14,*D*). The adenosine concentrations in the microdialysate samples collected at baseline (at 40 minutes past probe insertion) were observed to correlate significantly with myocardial collagen content, determined by hydroxyproline measurements ($r^2$=0.8613; $p<0.05$).

While these results do not prove a causal connection between adenosine and myocardial collagen formation, the significant correlation between interstitial adenosine and myocardial collagen content suggests an association.

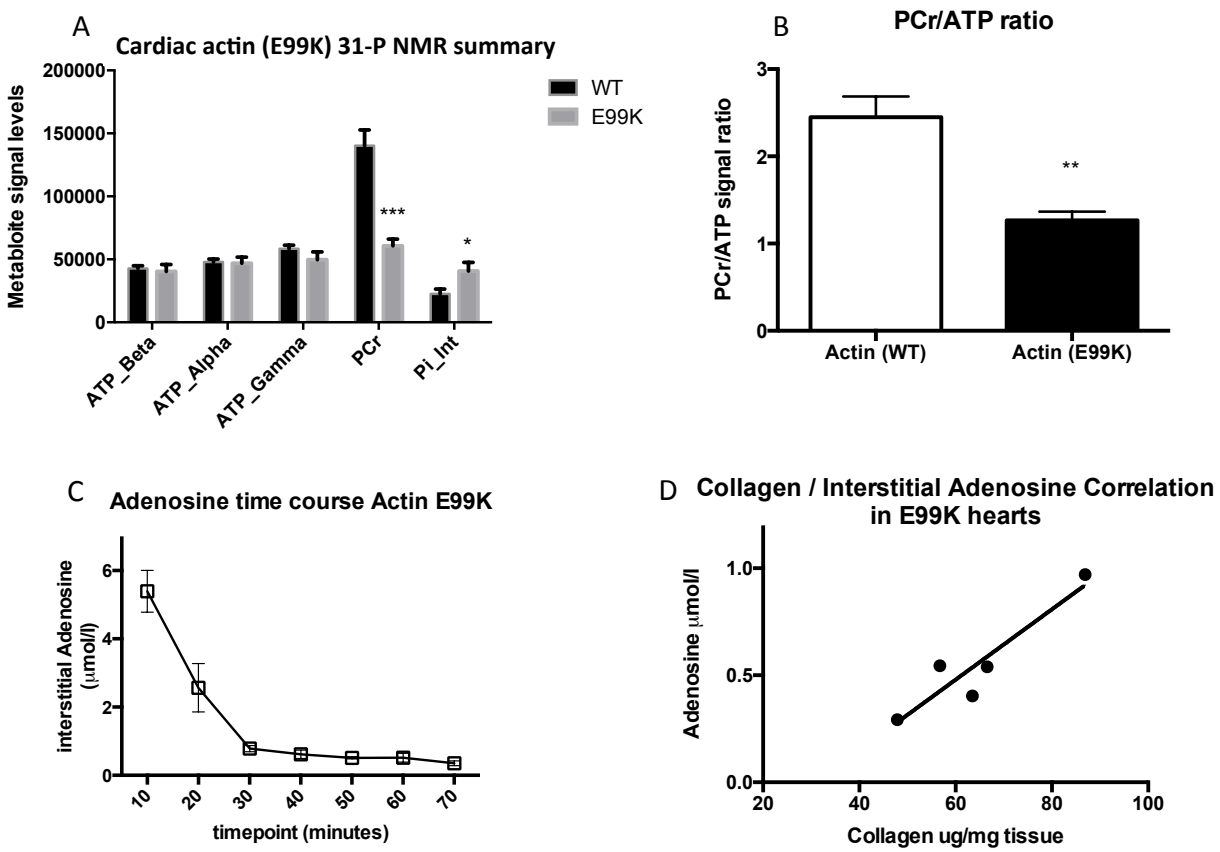


**Figure 3.14:** Delineation of the metabolic phenotype of cardiac actin E99K hearts. (*A&B*) Nuclear magnetic resonance spectroscopy revealed a marked perturbation of myocardial energetics in actin E99K hearts. (*A*) While there was no change in any of the ATP peaks, there was a marked decrease in phospho-creatine (PCr) levels in actin E99K hearts. As a result, the PCr to ATP ratio was markedly decreased in actin E99K hearts. In addition there was a significant increase in inorganic phosphate signal in actin E99K hearts ($p<0.05$). (*C&D*) Adenosine levels in microdialysate samples from E99K hearts showed a typical drop of adenosine concentrations after dialysis probe insertion, after 30-40 minutes baseline levels were reached (*C*). These baseline adenosine levels are directly correlated to interstitial concentrations. (*D*) The adenosine concentrations in the microdialysate samples collected at baseline (40 minutes past probe insertion) correlated significantly with myocardial collagen content, determined by hydroxyproline measurements ($r^2=0.8613$; $p<0.05$).

## 3.9 Discussion

### 3.9.1 Primary conclusions of Results chapter one

1. There are marked differences in the development of fibrotic phenotypes in mouse models that have been described as fibrotic in the literature.

2. The cardiac actin E99K mouse model develops consistent marked myocardial fibrosis at an early time-point.

3. The fibrotic phenotype in cardiac actin E99K mice is associated with a significant increase in cardiac fibroblast number.

4. The development of myocardial fibrosis in cardiac actin E99K hearts is associated with marked myocardial dysfunction and impaired myocardial energetics.

5. In cardiac actin E99K hearts there is a strong positive linear correlation between interstitial adenosine concentrations and myocardial collagen content.

### 3.9.2 Summary of chapter findings and resulting conclusions - fibrotic phenotypes

Detailed investigations of the fibrotic phenotype of five separate genetic mouse models of inherited cardiomyopathies revealed marked differences in the extent of myocardial fibrosis (Table 2). All of these models have been described to develop myocardial fibrosis in the literature. In our experiments, two mouse models developed fibrotic changes at the age of three months. While other models for inherited cardiomyopathies have been described in the literature to develop a fibrotic phenotype, these models had already been established at our facility, and the import of further models was not deemed necessary.

| **DCM** | | **HCM** | | |
|---|---|---|---|---|
| **Python** | **MLP** | **MYBP-C** | **E99K** | **TNT** |
| Total coll. ↑ | Total coll. = | Total coll. ↓ | Total coll. ↑ | Total coll. = |
| Collagen Crosslinking ↑ | Collagen Crosslinking = | Collagen Crosslinking = | Collagen Crosslinking ↑ | Collagen Crosslinking = |
| Fibrosis on Histology ↑ | Fibrosis on Histology = | Fibrosis on Histology ↑ | Fibrosis on Histology ↑ | Fibrosis on Histology = |
| Collagen I mRNA ↑ | NA. | Collagen I mRNA ↑ | Collagen I mRNA ↑ | Collagen I mRNA = |

**Table 2:** Summary of the observed changes in collagen expression, histology and LOX expression. (↑ increased; = unchanged)

One model for DCM, the Python mouse and one model organism for HCM, the actin E99K mouse model, developed overt myocardial fibrosis that was readily detectable on histology and upon hydroxyproline measurement. In addition, the increase in total collagen in these mouse hearts did not coincide with an increase in soluble collagen. These findings point towards an increase in the insoluble collagen fraction in these hearts, i.e. an increase in collagen crosslinking, which correlates with a significant increase in LOX expression, the enzyme responsible collagen crosslinking. These

results indicate that in these models, in addition to up-regulated production of extra cellular matrix, the mechanism for matrix maturation is simultaneously up regulated. These findings concur with descriptions in the literature (Ashrafian et al., 2010; Song et al., 2011) and as a result the cardiac actin E99K model was chosen for further descriptive and intervening experiments.

Other investigated mouse models, in particular the MLP KO mouse model for DCM and the cardiac TNT mouse as a model for HCM, did not demonstrate obvious fibrotic changes. Neither on histologic evaluation nor upon collagen measurements a fibrotic phenotype could be demonstrated. The absence of detection of myocardial fibrosis does not necessarily indicate its complete absence. In MLP KO mouse hearts mild interstitial fibrosis was observed on histology and upon quantification a trend towards myocardial fibrosis was found, albeit it did not reach statistical significance. In cardiac TNT mice, however, no evidence of a fibrotic phenotype was observed. Both of these models are described as developing myocardial fibrosis in the literature (Arber et al., 1997; Oberst et al., 1998). A possible explanation for the difference between our observations and the described phenotypes in the literature is that in our investigation was carried out at an earlier time-point. This comparatively early time-point was chosen as these experiments were also screening experiments, carried out to find a mouse model suitable for rescue experiments by genetic and pharmacologic interventions. Accordingly, it was considered paramount to choose a model that consistently develops a prominent fibrotic phenotype at an early age.

In addition, it has been shown that the phenotype of genetic mouse models can be altered between multiple generations. As a result, a large proportion fibrotic

phenotype could have been lost in the generations since the descriptive experiments by the respective authors.

The phenotype of MYBP-C hearts stands out from the phenotypes of the other investigated mouse models. Even tough MYBP-C hearts did demonstrate a decrease in myocardial collagen content, scarce focal areas of interstitial myocardial fibrosis were observed upon histologic examinations. In addition collagen mRNA expression was significantly increased in MYBP-C hearts. The author believes that these seemingly contradictory results can be explained by the prominent hypertrophy of MYBP-C hearts. Measurements of collagen by investigating hydroxyproline content are normalized to tissue weight. As a result, hypertrophy of the myocyte component of the myocardium impacts on the normalized collagen values. In conclusion, pro-fibrotic mechanisms are initiated in MYBP-C hearts as evidenced by investigation of collagen mRNA levels, and minor fibrotic changes on histology. But this up-regulation does not result in an increase of collagen when normalised to either tissue weight or total protein because it is diluted by the more prominent hypertrophic response. For this reason, even though this model recapitulates several aspects of the typical HCM phenotype, the fibrotic phenotype of MYBP-C hearts was considered too weak for investigating fibrosis specific pathways.

Two primary findings resulted from these screening experiments. First, actin E99K hearts were shown to develop a marked and consistent fibrotic phenotype at an early time-point and were therefore chosen for further phenotyping and genetic and pharmacologic interventions. Second, a large variation was observed in the extent of myocardial fibrosis in different model organisms for inherited cardiomyopathies. This

finding demonstrates that the binary fashion in which myocardial fibrosis is typically described in research papers may fall short to describe fibrotic phenotypes in their full variability.

### 3.9.3 Summary of chapter findings and resulting conclusions – actin E99K hearts

#### *3.9.3.1 Cardiac function and collagen staining*

Cardiac actin E99K hearts demonstrated a clear fibrotic phenotype using a variety of methods of investigation. Using both histologic examination and by measurement of hydroxyproline content, a significant increase of extracellular matrix was found. Therefore, the actin E99K mouse model was chosen for more detailed investigation of its fibrotic as well as the functional cardiac phenotype.

In association with severe myocardial fibrosis, actin E99K hearts displayed significant myocardial dysfunction. Both systolic contraction and diastolic relaxation were both significantly poorer in actin E99K hearts compared to WT hearts. Importantly, the functional experiments were carried out using pressure measurements obtained from balloons inserted into the left ventricle of Langendorff perfused hearts. Given that these results were obtained from explanted cannulated hearts, they are not necessarily representative of true pressure values achieved in vivo. However, subsequent intra-thoracic invasive haemodynamic measurements carried out for the evaluation of actin E99K mice crossbred with adenosine A2A receptor KO mice (results chapter 3), was seen to produce comparable values. In addition, the marked increase in lung weight of actin E99K mice indicated congestion and was consistent with overt cardiac decompensation.

Immunofluorescence staining against collagen revealed a marked increase of collagen signal in actin E99K hearts. Morphologically, endomysial collagen was markedly thickened in actin E99K hearts, appearing to encase individual cardiomyocytes. This has been suggested as a potential contributor to myocardial dysfunction, in particular to systolic dysfunction (LeGrice et al., 2012). The thicker, stiffer layer of endomysial collagen encases individual cardiomyocytes or groups of cardiomyocytes and constitutes a physical restriction to the increase in diameter of cardiomyocytes during systole (Janicki & Brower, 2002). Taking into account the marked thickening of endomysial collagen observed in actin E99K, hearts this mechanism may potentially contribute to cardiac dysfunction. In particular, the marked systolic dysfunction, which characterizes actin E99K hearts, could be potentiated by cardiomyocyte encasement.

#### *3.9.3.2 Cellular phenotype of actin E99K hearts*

In order to investigate changes in cell populations of actin E99K hearts, immunofluorescence microscopy experiments were conducted. Upon vimentin staining a marked increase in non-cardiomyocyte cells was observed in actin E99K hearts. Cellular expression of vimentin is considered a fibroblast marker, however, vimentin is also expressed to a lesser extent by endothelial cells. As a result, a definitive conclusion regarding whether an increase of vimentin positive cells constitutes an increase in fibroblasts is not possible using this approach alone. In order to address this question further, non-cardiomyocyte cells were further defined using FACS experiments (see below). Interestingly, however, the increase in vimentin positive cells was not accompanied by an increase in α-sma expressing cells. In conclusion, while fibroblast numbers and collagen production are up-regulated in cardiac fibroblasts of actin E99K hearts, the cellular activation does not appear to initiate the transdifferentiation of fibroblasts to myofibroblasts. The myocardium naturally contains vascular smooth muscle cells as a positive control for α-sma expressing cells. The fact that these cells demonstrated clear α-sma staining in the absence of other α-sma positive cells provides convincing evidence that cardiac fibroblasts are not activated to the degree of transdifferentiating into myofibroblasts. While in most models that develop cardiac fibrosis this transdifferentiation does occur, such an absence of myofibroblasts has been reported in other fibrotic mouse models of HCM (Teekakirikul et al., 2010). The formation of myofibroblasts in humans with sarcomeric mutations leading to HCM has not been sufficiently investigated.

In addition, an increase in Ki67 positive nuclei was observed actin E99K hearts. It

should be noted that Ki67 expression does not necessarily stain all cells undergoing the various steps of the cell cycle (Scholzen & Gerdes, 2000). However, Ki67 has been shown to correlate significantly with other measurements of cell proliferation within the myocardium, such as nuclear incorporation of bromodeoxyuridine (BRDU) (Teekakirikul et al., 2010). Therefore, even though it is not possible to draw definitive conclusions on the precise numbers of proliferating cells from such staining, the finding of an increase in Ki67 positive nuclei in actin E99K hearts is consistent with raised cell proliferation. Ki67 staining was performed jointly with wheat germ agglutinin (WGA). The combination of the two revealed that Ki67 positive nuclei were most likely not indicating the proliferation of non-cardiomyocytes. These results were again recapitulated by more quantifiable flow cytometric results (see below).

Finally, immunofluorescence experiments demonstrated a marked increase in CD68 positive cells in the myocardium of actin E99K hearts. This finding indicates that inflammatory cells, in particular monocytes/macrophages, are recruited into the myocardium and most likely contribute to the pathophysiologic process, as has been shown in human HCM mutation carriers (Kuusisto et al., 2012). The influx of such inflammatory cells and the activation of pro-inflammatory pathways has also been suggested as a potential driver of myocardial fibrosis in HCM (Westermann, 2012).

In order to verify the findings obtained by immunofluorescence microscopy and in particular to obtain quantifiable cell numbers of fibroblasts, FACS experiments were conducted. A specific gating strategy was developed in order to characterize the cardiac fibroblast population with the highest possible sensitivity and specificity. After standard FACS procedures to gate for the cells of interest according to cell size and

cell granularity and to exclude cell doublets from single cells, CD45 positive bone marrow derived cells and CD31 expressing endothelial cells were excluded. The resulting cells were divided according to vimentin expression, with the $CD45^-/CD31^-/vimentin^+$ population considered to entail a large proportion of cardiac fibroblasts. This was also demonstrated by the fact that over 90% of $CD45^-/CD31^-/vimentin^+$ fibroblasts were also DDR-2 positive, a well described marker for cardiac fibroblasts (Goldsmith et al., 2004). Thy-1, another marker commonly used to define cardiac fibroblasts (Ali et al., 2014) also showed approximately 90% positivity in actin WT hearts. However, in actin E99K hearts a substantial portion (about 25%) of $CD45^-/CD31^-/vimentin^+$ did not demonstrate Thy-1 expression. This recapitulates data from other organs, where the presence or absence of Thy-1 expression defines distinct fibroblast subsets, including in the lungs (Hagood et al., 1999; Phipps et al., 1989), spleen (Borrello & Phipps, 1996) and the uterus (Koumas, Smith, Feldon, Blumberg, & Phipps, 2003). Taking these reports as well as data from our FACS experiments into account it appears that relying solely on the expression of Thy-1 falls short in defining the entirety of the cardiac fibroblast population. While the large majority of cardiac fibroblasts in actin WT hearts expressed Thy-1, actin E99K hearts demonstrated a marked subpopulation of Thy-1 negative fibroblasts. These findings underline that fibroblasts in the myocardium, as in most organs, constitute a heterogeneous cell population that is hard to define by individual cellular markers.

However, there was a clear and marked increase in $CD45^-/CD31^-/vimentin^+$ cells, which arguably represent a large majority of cardiac fibroblasts. The observed increase in E99K hearts could be demonstrated both as a percentage of live cells, as well as in absolute cell numbers per left ventricle. The marked, approximately four

fold increase in absolute cell numbers of cardiac fibroblasts cannot be explained by left ventricular hypertrophy alone, as the left ventricular tissue used for these assays did not differ in weight (65-70mg) significantly. This finding recapitulates the increase in vimentin signal observed in immunofluorescence microscopy experiments. In addition, given that this increased cell population was CD31 negative, the FACS results indicate that the majority of vimentin positive cells observed in immunofluorescence images of actin E99K hearts were likely fibroblasts, rather than endothelial cells.

In addition, cardiac fibroblasts were further examined for the expression of markers of cellular activation and proliferation. Podoplanin expression, a CLEC-2 receptor ligand which has been described to be responsible for the interaction of stromal cells and immune cells (Acton et al., 2012), was markedly increased in the fibroblasts of actin E99K mice. Furthermore, the number of cardiac fibroblasts expressing Ki67, a marker for proliferating cells, was also markedly increased in actin E99K hearts. Both of these findings recapitulated those obtained by immunofluorescence microscopy, and support a role for proliferation in the accumulation of cardiac fibroblasts in the murine actin E99K cardiomyopathy model. While there is no optimal single marker for cardiac fibroblasts, the combination of the aforementioned markers makes the quantitative investigation of cardiac fibroblasts possible. This is similarly the case in most tissues, as there are different subsets of fibroblasts in most tissues, expressing the described markers including vimentin, Thy-1 and podoplanin. However the proportions of fibroblast subpopulations may differ between different tissues.

Finally a significant proportion of cardiac fibroblasts in both actin WT and E99K

hearts were characterized by the expression of ectonucleotidases CD39 and CD73. As a result the amount of ectonuclotidase expressing fibroblasts was markedly increased in actin E99K hearts. The primary role of these enzymes is the hydrolysis of extracellular ATP to adenosine. These enzymes play a crucial role in the regulation of interstitial adenosine concentrations (Bönner et al., 2012). The result that cells expressing these enzymes are more numerous in the myocardium of actin E99K hearts supports the possibility of an important role of adenosine in pathophysiologic signalling.

#### *3.9.3.3 Metabolic phenotype and interstitial adenosine levels of actin E99K hearts*

The primary premise of this projects' hypothesis is that a disruption in the energetic state of the myocardium initiates signalling mechanisms, which activate cardiac fibroblasts leading to myocardial fibrosis. In order to verify this assumption, the metabolic state of cardiac actin E99K hearts was investigated using nuclear magnetic resonance of Langendorff perfused hearts. These experiments revealed a marked decrease in the ratio of PCr and ATP, representing a classic marker for impaired cardiac metabolism. ATP levels are rarely altered in the myocardium and fall only very late in the progression of cardiac failure. PCr, as the buffer of high-energy phosphates in the myocardium, is consumed during states of increased metabolic demand as the enzyme creatine kinase utilizes it to replenish ATP. As a result the fall in PCr levels and consequently reduction in the PCr to ATP ratio in the actin E99K hearts is a strong indicator of important metabolic perturbation in the myocardium. However, the level of PCr is related to the total amount of Creatin in the myocardium, therefore a change in total Creatin could also explain the observed alteration in PCr in actin E99K mice (Wallis et al., 2005). As total Creatin levels were not measured in this study, an alteration in total Creatin cannot be excluded as a contributor to altered PCr levels in this model.

Of note, hearts were explanted and retrogradely perfused with oxidised Krebs solution and so the values obtained are not necessarily directly representative of the metabolic state of the myocardium pre-explantation. While in vivo high-energy phosphate measurements using cardiac 31P NMR spectroscopy is well-established in human subjects, the size and rapidity of movement of the murine myocardium are posing a not yet surpassed technical challenge in mice. An equilibration period of 20

minutes of perfusion with oxidised Krebs solution within the magnet was used for the myocardium to recover from the temporary ischemia incurred during cannulation.

In order to investigate a potential connection between adenosine signalling and myocardial fibrosis, microdialysis experiments were carried out. Microdialysis experiments are well suited to the investigation of interstitial metabolites. A microdialysis probe is covered by a semi-permeable membrane with a particular weight cut-off for free osmosis. Upon insertion of the microdialysis probe, all interstitial metabolites below the molecular weight cut-off diffuse freely into the perfusate. The probe insertion itself causes cellular injury leading to the release of intracellular metabolites, which are typically washed out by the probe perfusion within 30-40 minutes. As a result, the measurements of metabolite concentrations in the perfusate by mass spectroscopy, after 40 minutes of continuous perfusion when baseline levels are reached, can be considered representative of interstitial levels. Even though no causal relationship can be concluded from this data, the significant correlation between interstitial adenosine levels and myocardial collagen content supports a potential connection between adenosine and myocardial fibrosis.

# 4. Results: Inhibiting adenosine A2A receptor signalling in cardiac fibroblasts *in vitro* and *in vivo*

## 4.1 Introduction

The work presented in this chapter addresses the role of adenosine A2AR in myocardial fibrosis formation. While the role of adenosine A2ARs in the activation of hepatic stellate cells (Chan, Montesinos, et al., 2006), as well as skin- (Chan, Fernandez, et al., 2006) and other fibroblasts has been well established (Chan & Cronstein, 2010), their role in myocardial fibrosis has not been elucidated.

### 4.1.1 Hypothesis

We hypothesize that adenosine A2AR signalling plays a crucial role in cardiac fibroblast activation, specifically that: collagen production of cardiac fibroblasts can be activated *in vitro* by adenosine A2AR stimulation; that genetic deletion of the adenosine A2AR in the cardiac actin E99K mouse model will rescue its fibrotic phenotype; finally, that pharmacologic inhibition of this receptor will recapitulate the phenotypic rescue found by A2A genetic deletion.

### 4.1.2 Aims

The aims of the experiments conducted in this chapter were:

- To isolate and characterize cardiac fibroblasts, as well as to delineate their response to adenosine A2AR stimulation and inhibition.
- To characterise the effect of adenosine A2AR deletion on the fibrotic phenotype of cardiac actin E99K mouse hearts.
- To determine the effect of pharmacologic adenosine A2AR antagonism on the development of fibrosis in cardiac actin E99K mouse hearts.

## 4.2 Isolation of cardiac fibroblasts and evaluation of the response to adenosine A2A receptor stimulation

In order to assess the response of cardiac fibroblasts to adenosine A2AR stimulation, *in vitro* experiments were performed on neonatal cardiac rat fibroblasts as well as on adult mouse cardiac fibroblasts.

### 4.2.1 Neonatal cardiac rat fibroblasts

Neonatal cardiac rat fibroblasts were isolated by digestion and adherence protocols and the resulting cell populations were shown to express several markers for cardiac fibroblasts: vimentin, collagen-1, and DDR-2, which have been described as specific markers for fibroblasts in cardiac tissue (Fan et al., 2012). The combined and marked expression of these markers in more than 98% of the cells obtained is consistent with the resulting cell population being comprised predominantly of cardiac fibroblasts (Figure 4.1, *A*).

In addition, as preparatory work for subsequent receptor stimulation experiments, the resulting neonatal cardiac rat fibroblasts were investigated for the expression of adenosine receptors at mRNA level. Un-stimulated, cultured cardiac fibroblasts were harvested and messenger RNA was isolated. End-point PCR demonstrated clear amplification of adenosine A1, A2A and A2B receptor gene products. Neonatal rat brain tissue, which has been described to express these genes, was used as a positive control (Figure 4.1, *B*). Given the evidence for the expression of adenosine receptors, in particular the adenosine A2AR, these neonatal cardiac fibroblasts were deemed potentially suitable to pharmacologic intervention with an adenosine A2AR agonist (CGS-21680) followed by investigation of the cellular response.

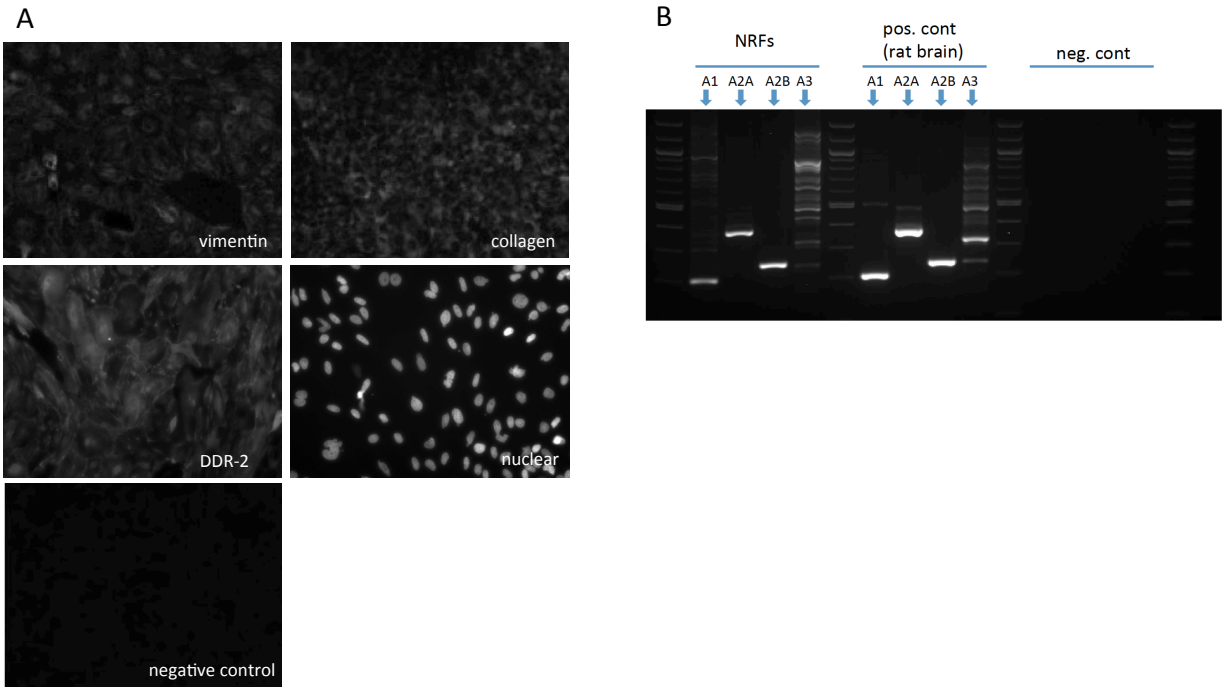


**Figure 4.1.:** Cardiac fibroblasts isolated from neonatal rats. (*A*) The isolated cells express well-described markers for cardiac fibroblasts, vimentin (top left), collagen 1 (top right) and the most specific marker for fibroblasts isolated from cardiac tissues, DDR-2 (middle left), nuclear staining (middle right) and a negative, no primary antibody control (lower left). (*B*) End-point PCR revealed the expression of adenosine A2ARs. The neonatal rat cardiac fibroblasts express the Adenosine A1, A2A and A2B receptor at mRNA level.

Accordingly, cell stimulation experiments (Figure 4.1) to investigate the response of neonatal rat cardiac fibroblasts to stimulation with an adenosine A2AR agonist were carried out. The fibroblasts were cultivated on tissue culture treated plastic in six-well plates and were stimulated by addition of the specific adenosine A2AR agonist CGS-21680 and followed by Sirius-red assays conducted on purified CCM from control treated and CGS-21680 treated cells. A significant 1.5 fold increase in collagen content was found in the CCM of CGS-21680 treated cells compared to the CCM of vehicle treated fibroblasts.

Anti-collagen western blot experiments undertaken on purified CCM showed a significant, dose-dependent increase in collagen concentration upon stimulation with CGS-21680. In order to test whether the effects of CGS-21680 were specific for adenosine A2AR stimulation, the experiments were performed with or without the specific adenosine A2AR inhibitor ZM-241385. Addition of the adenosine A2AR inhibitor ZM-241385 at a concentration of $10^{-5}$M prevented a significant stimulatory response in collagen production.

The results of these experiments demonstrate in principle that cardiac fibroblasts increase collagen production upon activation of the adenosine A2AR. Further, the observed abrogation of the stimulatory response upon addition of the specific adenosine A2AR antagonist provides supporting evidence that the observed effect is indeed due to adenosine A2AR signalling. However, the use of neonatal cardiac fibroblasts has been criticized, as they are not considered representative of fully developed adult cardiac fibroblasts. Therefore, similar experiments were performed in cardiac fibroblasts isolated from adult mouse hearts.

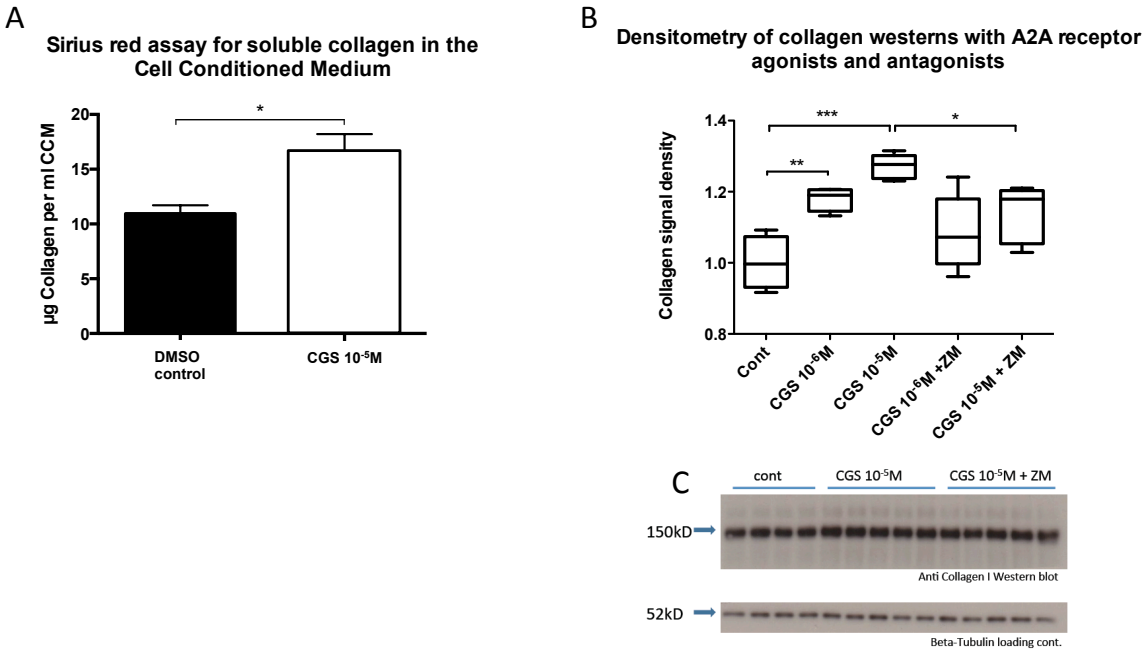


**Figure 4.2:** Cell stimulation experiments investigating the response of neonatal rat cardiac fibroblasts towards stimulation with adenosine A2AR agonists. (*A*) Sirius-red assay with purified CCM of stimulated neonatal rat cardiac fibroblasts demonstrated a significant increase in collagen concentration ($p<0.05$). (*B*) Densitometry results of anti-collagen western blots of purified cell-conditioned media after the stimulation of neonatal rat cardiac fibroblasts with the specific A2AR agonist CGS-21680 with or without the inhibitor ZM-241385. (*C*) Representative western blot.

### 4.2.2 Adult mouse cardiac fibroblasts

In order to investigate the response of cardiac fibroblasts isolated from adult mouse hearts to adenosine A2AR stimulation, *in vitro* cell stimulation experiments were conducted. Mouse hearts were extracted, cannulated and retrogradely perfused with collagenase solution in order to obtain a single cell solution containing all contents of the myocardium. Fibroblasts, when cultured on plastic under standard tissue culture conditions, are the only cell population with proliferative potential within the myocardium. As a result, tissue culture for at least four passages of the resulting cardiac cell population resulted in the formation of cardiac fibroblast cultures. This cell population was characterized by immunofluorescence microscopy staining for cardiac fibroblast markers, DDR-2 and vimentin. At the time the cell stimulation experiments were carried out, at cellular passage four to five, at least 95% of the cells expressed both of these markers, and were therefore considered fibroblasts isolated from cardiac tissue (Figure 4.3, *A*).

Cell stimulation experiments of the resulting cardiac fibroblast population revealed a clear dose-dependent response upon stimulation with the specific adenosine A2AR agonist CGS-21680. Thus, hydroxyproline content in the CCM of CGS-21680 stimulated cardiac fibroblasts demonstrated a significant dose dependent increase in collagen secretion. Upon stimulation of the cardiac fibroblast population with the highest dose of CGS-21680 ($10^{-5}$Molar) a highly significant ($p$ <0.0001) more than two-fold increase in collagen content was observed in the CCM (Figure 4.3, *B*).

Similar findings were obtained using Sirius-red collagen measurements from CCM of stimulated cardiac fibroblasts. These experiments demonstrated a significant, dose-

dependent increase in collagen content in the CCM, which was inhibited by co-addition of the specific adenosine A2AR antagonist ZM-241385 (Figure 4.3, *C*).

These experiments demonstrated that cardiac fibroblasts isolated from adult mouse hearts increase collagen production and secretion into CCM upon activation of adenosine A2AR signalling, similar to neonatal rat cardiac fibroblasts. Also comparable to the response of neonatal rat cardiac fibroblasts, the stimulatory effect of CGS-21680 on adult mouse cardiac fibroblasts was inhibited by addition of the specific adenosine A2AR inhibitor ZM-241385.

The primary conclusion drawn from these cellular experiments is that adenosine A2AR stimulation specifically activates neonatal as well as adult cardiac fibroblasts. The fact that this stimulatory response to adenosine A2AR stimulation was conserved between different species and developmental stages of cardiac fibroblasts emphasizes the potential biological significance of this effect.

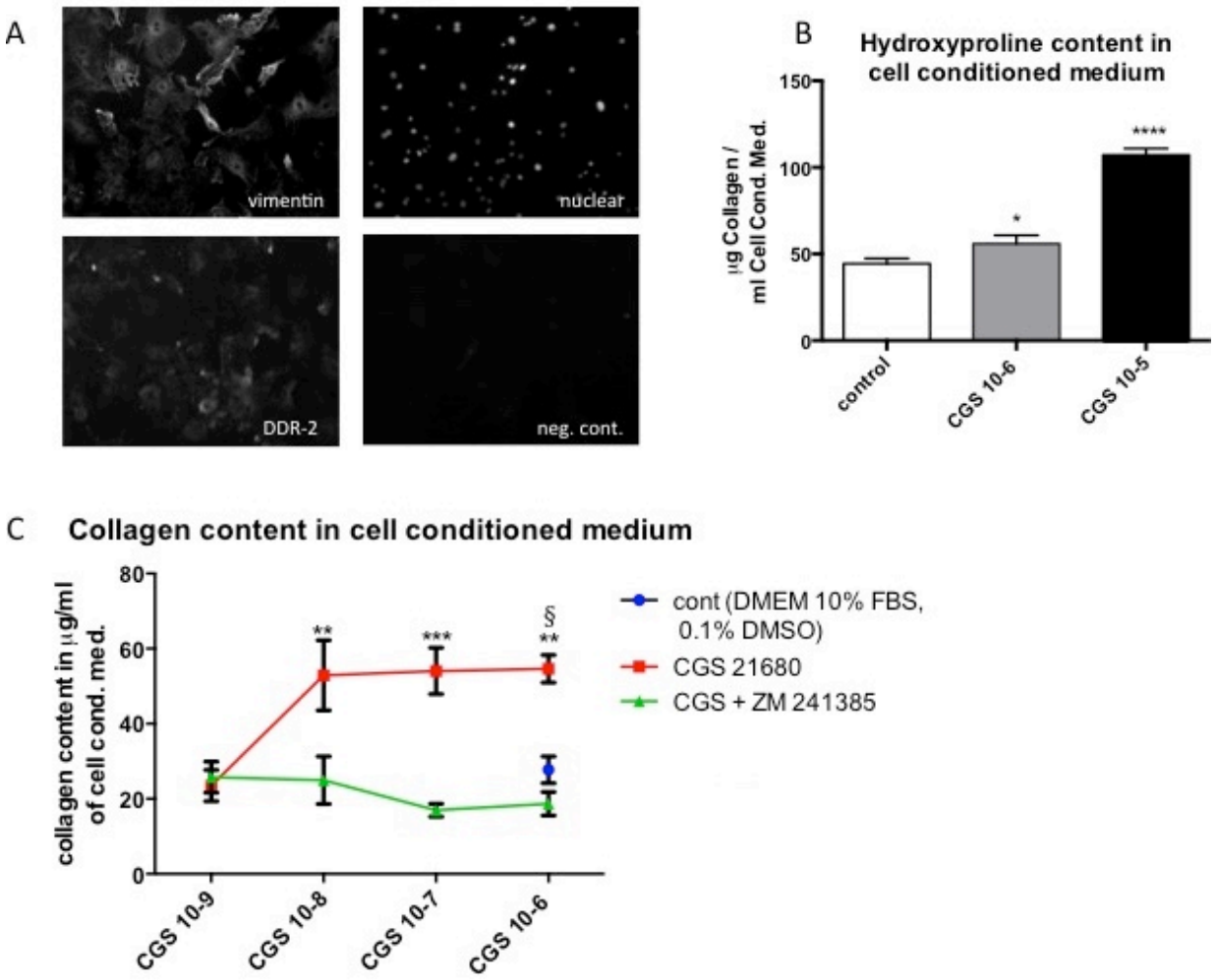


**Figure 4.3.: Adult mouse cardiac f**ibroblast cell stimulation experiments. The isolated cell population was characterized by immunofluorescence microscopy staining for DDR-2 and vimentin. At the time of experiments, at least 95% of the cells expressed both of these markers, and were considered cardiac fibroblasts (*A*). Hydroxyproline content in the CCM of CGS-21680 stimulated cardiac fibroblasts was dose-dependently increased. Maximal stimulation with CGS-21680 ($10^{-5}$ Molar) resulted in a highly significant ($p<0.0001$) increase in collagen content in the CCM (*B*). Sirius-red collagen measurements from CCM of stimulated cardiac fibroblasts demonstrated a significant, dose-dependent increase in collagen content in the cell-conditioned medium. This increase was inhibited by addition of the specific adenosine A2AR antagonist ZM-241385 (*C*).

### 4.3 Cardiac actin E99K mice crossbreeding with adenosine A2A receptor knock out mouse line

In order to investigate the role of adenosine A2AR signalling on myocardial fibrosis *in vivo*, crossbreeding experiments between adenosine A2AR knock-out (A2AR KO) mice and cardiac actin E99K mice were performed. The primary hypothesis of these experiments was that loss of the adenosine A2AR would abrogate fibroblast activation in actin E99K hearts. The potential resulting reduction of extracellular matrix production was investigated using the established experimental procedures that served to investigate the fibrotic phenotype of fibrotic models during the screening experiments. In addition to these, a potential effect on myocardial function was investigated by echocardiography and invasive measurements of left ventricular haemodynamics.

The breeding strategy to allow investigation of this hypothesis was designed to produce four groups of animals:

1. Cardiac actin (WT), A2A receptor (WT) (A2AR WT), (N=6)
2. Cardiac actin (WT), A2A receptor (KO, homozygous) (A2AR KO), (N=10)
3. Cardiac actin (E99K, heterozygous), A2AR WT, (N=7)
4. Cardiac actin (E99K, heterozygous), A2AR KO, (N=6)

Animals heterozygous for deletion of the adenosine A2AR were utilized for breeding in order to produce homozygous animals, but were not used for phenotypic experiments. Preliminary experiments had not demonstrated any effect of heterozygous loss of the adenosine A2AR on the phenotype of actin E99K hearts. The primary time-point for phenotyping and tissue collection of these groups was at 9 weeks of age.

### 4.3.1 Changes in morphometric measurements

Morphometric data was collected from the different groups, in order to compare basic physical differences between the genetic groups. No significant differences were found in body weight and tibia length between any of the groups (Figure 4.4, *A and B*). This indicates that there is no obvious impairment in gross physical development in mice as a result of the deletion of the adenosine A2AR or the presence of the actin E99K heart.

The hearts of cardiac actin E99K, A2AR WT mice demonstrated a significant increase in heart weight ($p<0.01$) compared to the heart weights of actin WT as well as A2AR WT animals. The heart weights of cardiac actin E99K, A2AR KO hearts were significantly ($p<0.05$) reduced compared to cardiac actin E99K, A2AR WT hearts and did not differ significantly from WT control hearts (Figure 4.4, *C*).

A functional impediment in either cardiac ventricle typically leads to congestion in the upstream organs, affecting the organ wet weights of the lung or the liver in case of the left- or right ventricular failure, respectively. As a potential marker of such cardiac congestion, lung and liver organ weights were investigated. Cardiac actin E99K, A2AR WT animals demonstrated a statistically significant ($p<0.0001$), near two-fold increase in lung weight compared to cardiac actin WT control animals. This marker of left-sided cardiac congestion was significantly ($p<0.001$) reduced in cardiac actin E99K, A2AR KO animals. No significant difference was found in liver weights between any of the groups, suggesting that any disruption of cardiac function does not affect the right ventricle to an extent that would cause significant congestion (Figure 4.4, *D and E*).

Normalization of heart, lung and liver weights to tibial length was carried out to relate organ weights to the physical development of the individual mice and revealed similar findings to the absolute values. The normalized heart weights of cardiac actin E99K, A2AR WT mice were significantly higher than the heart weights of actin WT A2AR WT mice. However, actin E99K, A2AR KO animals did not demonstrate a significant difference in normalized heart weight compared to actin WT, A2AR WT control mice. Normalized lung weights were significantly increased in cardiac actin E99K mice. In addition a significant reduction in normalized lung weight was observed in cardiac actin E99K, A2AR KO mice compared to actin E99K A2AR WT mice (Figure 4.4, *F-H*).

These results indicate that loss of the adenosine A2A receptor confers a potentially beneficial effect on the phenotypic development of cardiac actin E99K animals.

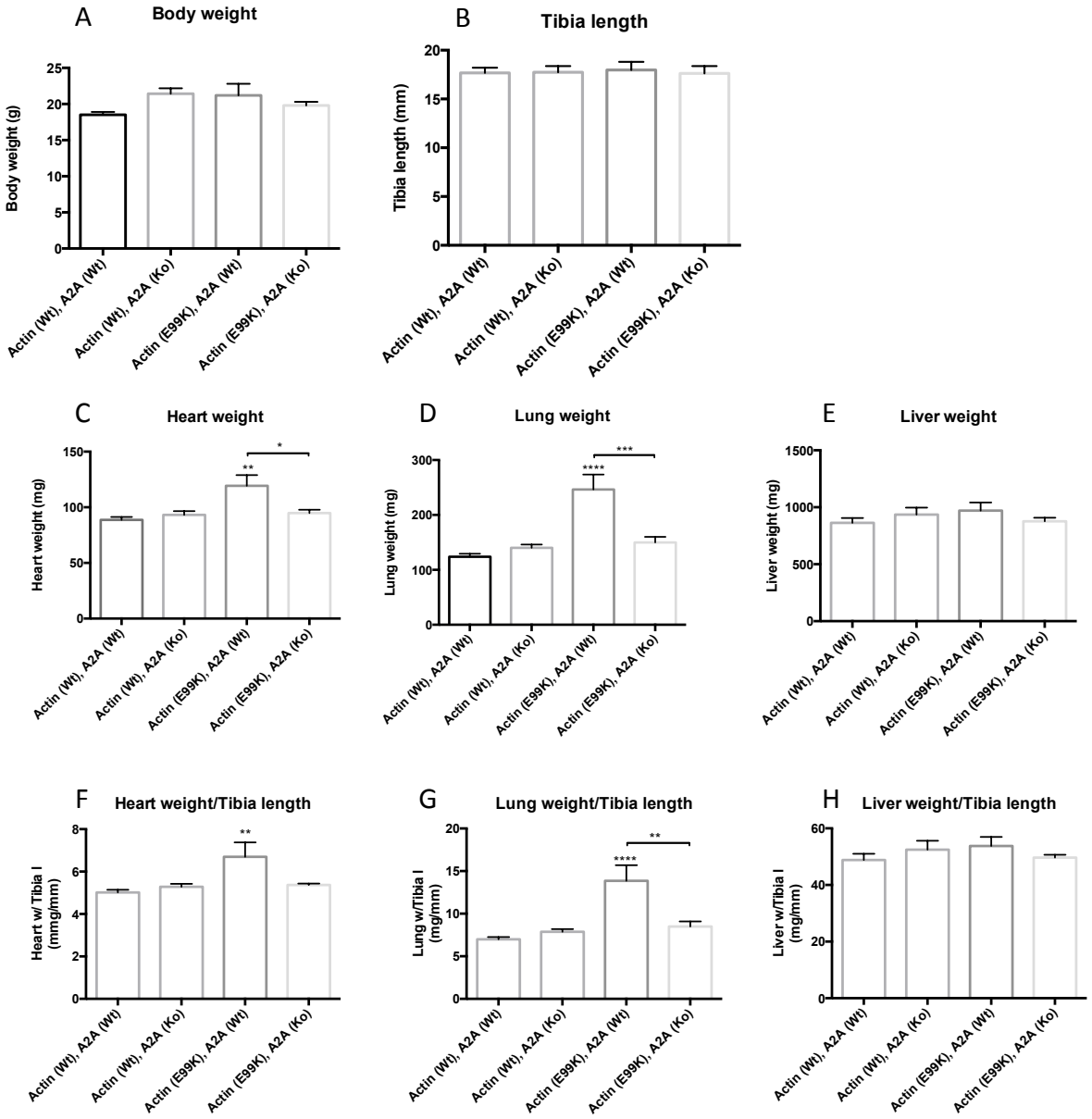


**Figure 4.4:** Morphometric measurements of absolute and normalized organ weights and tibia length. (*A&B*) No significant differences were found in body weight and tibia length between any of the genetic groups. (*C*) Actin E99K mice demonstrated a significant increase in heart weight ($p$<0.01) compared to the heart weights of actin and A2AR WT animals. The heart weights of cardiac actin E99K, A2AR KO hearts were significantly ($p$<0.05) reduced compared to cardiac actin E99K, A2AR WT hearts and did not differ significantly from WT control hearts. Cardiac actin E99K, A2AR WT animals demonstrated a significant ($p$<0.0001), two fold increase in average lung weight compared to actin WT control animals. Lung weights were significantly reduced ($p$<0.001) in cardiac actin E99K, A2AR KO mice compared to actin E99K, A2AR WT animals (*D*). No significant difference was found in liver weights between any of the groups (*E*). Normalization of heart, lung and liver weights to tibia length revealed similar findings (*F-H*). The normalized heart weights of cardiac actin E99K, A2AR WT mice were significantly higher than in actin WT A2AR WT mice. No significant difference in normalized heart weight was found in actin E99K A2AR KO and actin WT A2AR WT control mice (*F*). Normalized lung weights were significantly increased in cardiac actin E99K mice. Cardiac actin E99K, A2AR KO mice demonstrated a significant reduction of normalized lung weight compared to actin E99K A2AR WT mice (*G*).

### 4.3.2 Changes in myocardial collagen content and cardiac fibrosis

Evaluation of the fibrotic phenotype was conducted in order to investigate potential changes in myocardial fibrosis in cardiac actin E99K animals due to the deletion of the adenosine A2A receptor. Myocardial fibrosis was investigated by measurement of the hydroxyproline content and histologic examination of tissue sections from paraffin embedded heart tissue.

Hydroxyproline measurements from left ventricular tissues demonstrated a marked, statistically significant ($p$<0.0001) increase in collagen content of cardiac actin E99K, A2AR WT hearts compared to the collagen content in cardiac actin WT hearts. Conversely, the collagen content of cardiac actin E99K, A2AR KO hearts was significantly reduced ($p$<0.01) compared to cardiac actin E99K, A2AR WT hearts. The reduction of collagen content constituted a partial rescue, however, as the cardiac actin E99K, A2AR KO hearts still demonstrated a significantly higher collagen content than cardiac actin WT, A2AR WT animals (Figure 4.5).

Histologic examination by Sirius-red staining of paraffin embedded tissue sections revealed marked myocardial fibrosis in cardiac actin E99K, A2A WT hearts compared to cardiac actin WT controls. Cardiac actin E99K, A2AR KO hearts demonstrated markedly reduced interstitial fibrosis, compared to cardiac actin E99K A2AR WT hearts, providing additional evidence of a partial rescue of the fibrotic phenotype. This was also seen using computational quantification of the Sirius-red signal normalized to total tissue area. Significant myocardial fibrosis ($p$<0.001), i.e. a marked increase in Sirius-red signal per imaged cardiac tissue area, was identified in cardiac actin E99K, A2AR WT hearts. This fibrotic signal was significantly ($p$<0.05) reduced in cardiac actin E99K, A2AR KO hearts (Figure 4.5).

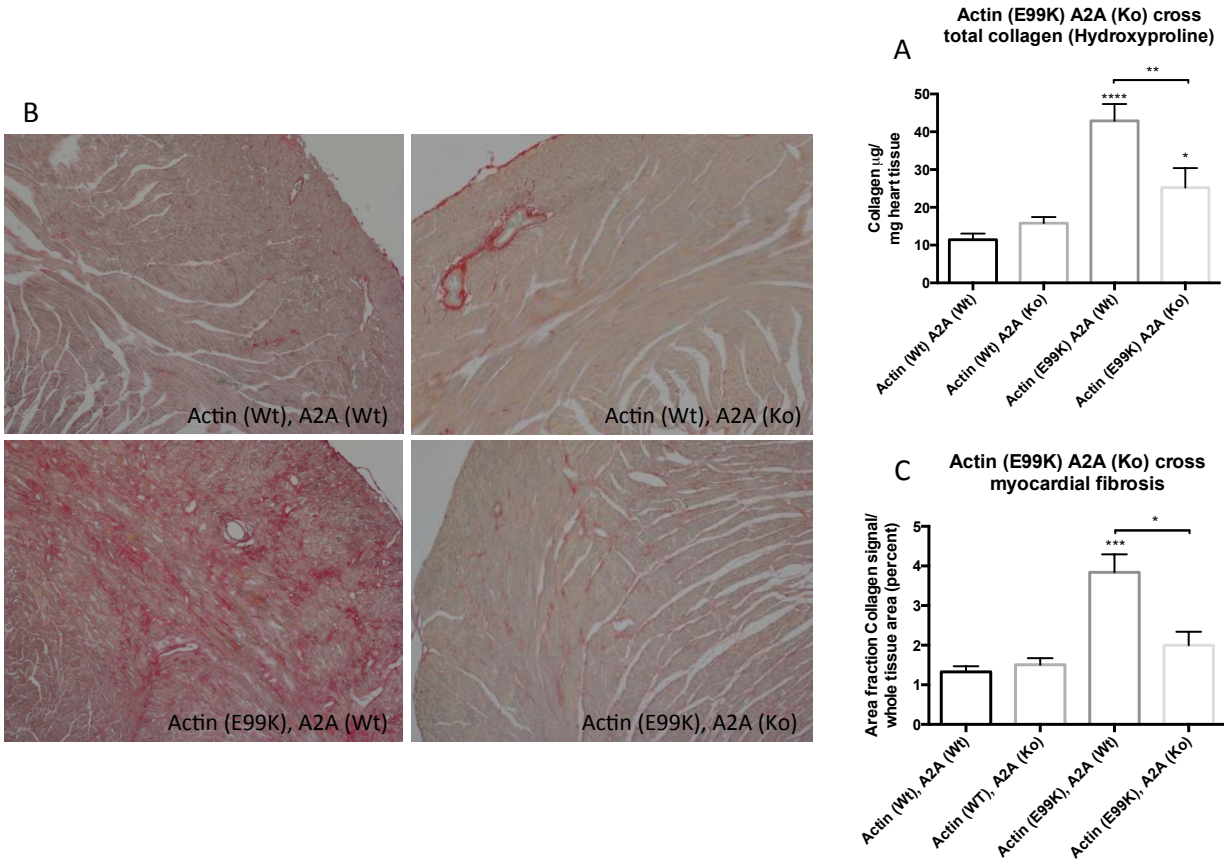


**Figure 4.5:** Evaluation of the fibrotic phenotype of E99K hearts in response to A2AR genetic deletion. (*A*) Hydroxyproline measurements revealed a marked and significant ($p<0.0001$) increase in tissue collagen content of actin E99K A2AR WT hearts. The collagen content of cardiac actin E99K A2AR KO hearts was reduced significantly ($p<0.01$). However, actin E99K, A2AR KO hearts demonstrated a significantly ($p<0.05$) higher collagen content than the hearts of cardiac actin WT, A2AR WT control animals. (*B*) Histologic examination (Sirius-red staining) revealed marked myocardial fibrosis in cardiac actin E99K, A2AR WT hearts compared to actin WT controls. Cardiac actin E99K, A2AR KO hearts demonstrated markedly reduced interstitial fibrosis compared to cardiac actin E99K A2AR WT hearts. Upon computational quantification (*C*) significant myocardial fibrosis ($p<0.001$) could be demonstrated in cardiac actin E99K, A2AR WT hearts. This fibrotic signal was significantly reduced ($p<0.05$) in cardiac actin E99K, A2AR KO hearts.

### 4.3.3 Changes in cardiac function on Echocardiography

In order to evaluate the effect of genetic adenosine A2A receptor deletion on the myocardial function of cardiac actin E99K animals, echocardiographic studies were performed.

Measurements of systolic function, such as left ventricular ejection fraction and fractional shortening did not reveal a statistically significant difference in any of the genetic groups, with only non-significant trends indicating a potential reduction in the average values of both of these parameters observed in cardiac actin E99K, A2AR WT hearts. No significant differences in systolic function were found between cardiac actin E99K, A2AR WT and actin E99K, A2AR KO hearts. In addition, a non-significant trend towards improved systolic function, measured by ejection fraction as well as fractional shortening, was observed in cardiac actin E99K, A2AR KO hearts compared to cardiac actin E99K hearts. (Figure 4.6, *A and B*).

Calculation of left ventricular mass from the echocardiographic images recapitulated the results obtained by morphometric evaluation of heart weights. The calculated left ventricular mass was significantly ($p<0.01$) reduced in cardiac actin E99K, A2AR KO hearts compared to actin E99K A2AR WT hearts. In addition, a significant reduction ($p<0.01$) in left ventricular end-diastolic volume was observed in cardiac actin E99K A2AR KO hearts, compared to cardiac actin E99K A2AR WT hearts (Figure 4.6, *C and D*).

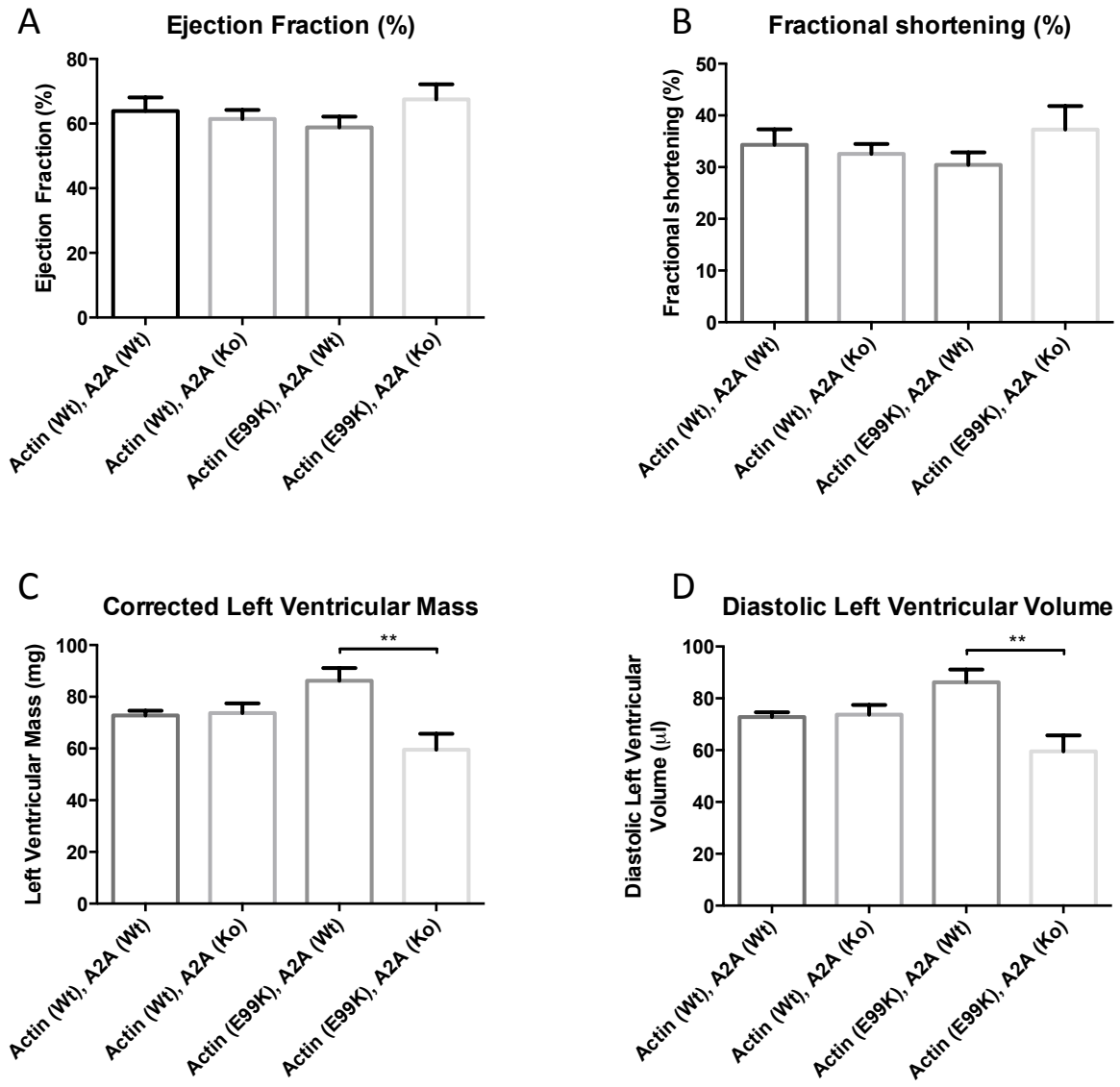


**Figure 4.6:** Myocardial function evaluated by echocardiography. (*A&B*) Measurements of systolic function, left ventricular ejection fraction and fractional shortening did not reveal a statistically significant difference between any of the genetic groups. (*C*) Calculation of the left ventricular mass demonstrated an increase in left ventricular mass in cardiac actin E99K hearts which was significantly ($p$<0.01) reduced in cardiac actin E99K, A2AR KO. Cardiac actin E99K A2AR KO hearts demonstrated a significant reduction ($p$<0.01) in end diastolic left ventricular volume, (*D*).

### 4.3.4 Changes in cardiac function in invasive haemodynamic measurements

In order to further delineate the effect of genetic deletion of the adenosine A2A receptor on the myocardial function of cardiac actin E99K animals, haemodynamic measurements of left ventricular pressures were conducted *in vivo*.

Intra-ventricular pressures were measured utilizing a manometric probe, which was inserted into the left ventricle through the aortic valve. Pressure measurements were conducted at baseline and - to investigate potential inotropic reserve - during two increasing dosages (4 and 16 ng/g BW/minute) of continuous dobutamine infusion. The maximal rate of pressure increase during systolic contraction (dP/dt max) was significantly reduced in cardiac actin E99K, A2AR WT mice compared to cardiac actin WT mice, indicating diminished systolic function. Conversely, no significant difference was found in this parameter between cardiac actin E99K, A2AR KO and cardiac actin WT control animals. Stimulation of the hearts by dobutamine infusion pronounced these differences further. Thus, upon stimulation with the highest dose of dobutamine the values for dP/dt max rates in cardiac actin E99K, A2AR KO mice were significantly higher ($p<0.05$) than cardiac actin E99K, A2AR WT mice. Comparably, the minimal rate of diastolic pressure decrease was significantly worse in cardiac actin E99K A2AR WT animals compared to cardiac actin WT animals. No significant alteration in diastolic pressure decrease rate was observed in cardiac actin E99K A2AR KO animals. In addition, upon maximal dobutamine stimulation, a significant improvement in diastolic pressure decrease rate of cardiac actin E99K A2AR KO animals was observed (Figure 4.7, *A*).

No significant differences in average heart rates were observed between any of the

groups, and all groups demonstrated a dose-dependent increase in heart rate upon dobutamine infusion (Figure 4.7, *B*).

Another indicator of diastolic function, the time constant of left ventricular relaxation, Tau, was markedly and significantly ($p<0.05$) increased in cardiac actin E99K, A2AR WT mice, compared to cardiac actin WT mice. No significant difference in relaxation time constant was observed between cardiac actin E99K, A2AR KO hearts and actin WT hearts (Figure 4.7, *C*).

In addition to dP/dt max, peak systolic left ventricular pressures and left ventricular developed pressure both served as indicators of systolic function. Left ventricular developed as well as maximal systolic pressures were significantly ($p<0.05$) decreased in cardiac actin E99K, A2AR WT hearts compared to cardiac actin WT, A2AR WT hearts. Further, cardiac actin E99K, A2AR KO mice demonstrated significantly ($p<0.05$) increased maximal systolic as well as developed left ventricular pressures (Figure 4.7, *D and E*).

The presented data indicates that the deletion of the adenosine A2A receptor confers a beneficial effect on the cardiac function of actin E99K mice.

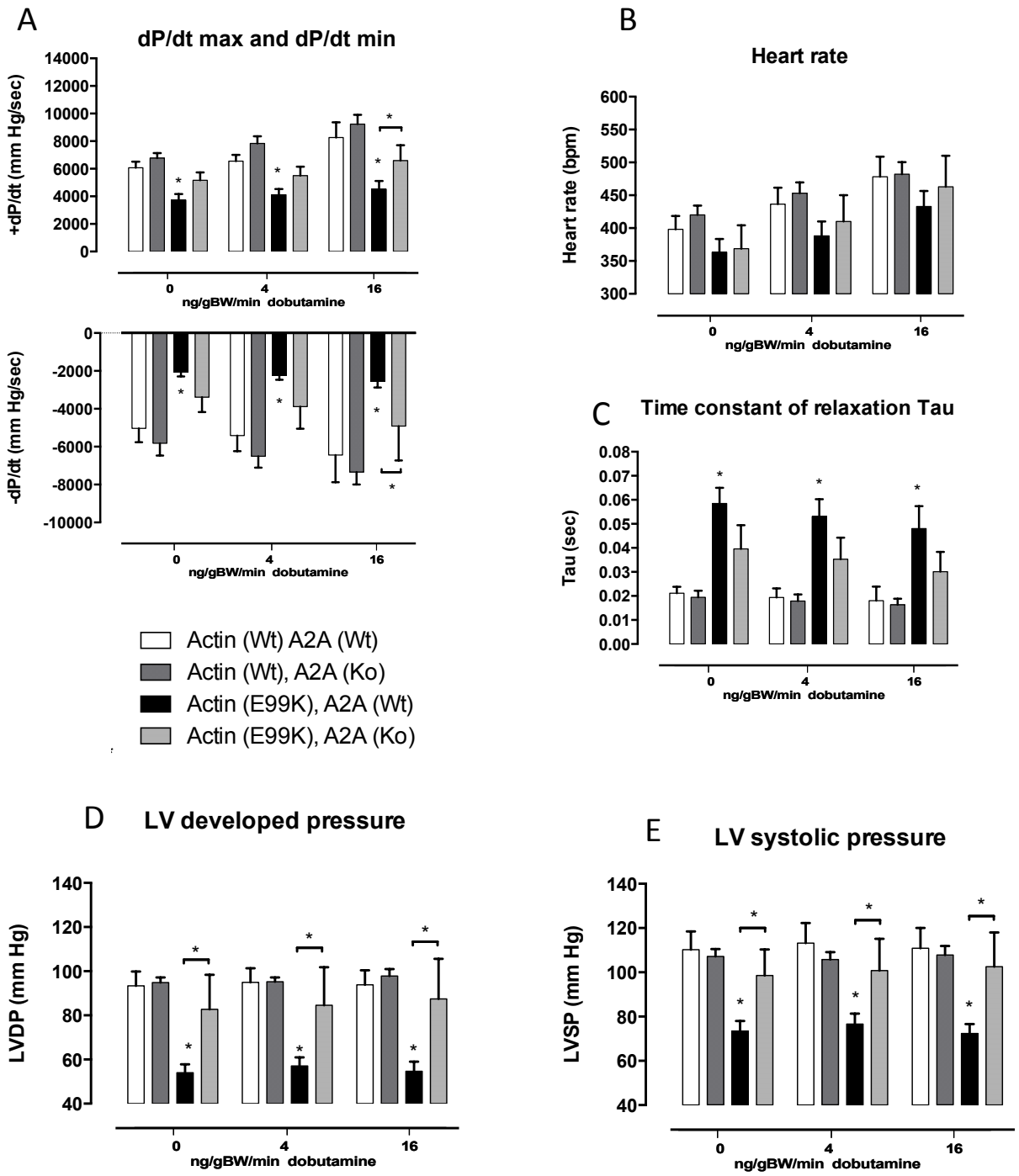


**Figure 4.7:** Invasive haemodynamic measurements of left ventricular pressures.. Intra-ventricular pressures were measured at baseline and during two increasing dosages (4 and 16 ng/gBW/minute) of continuous dobutamine infusion. (*A*) Maximal pressure increase rates (dP/dt max) were significantly reduced in cardiac actin E99K mice compared to cardiac actin WT mice. No significant difference was found in dP/dt max between cardiac actin E99K, A2AR KO and cardiac actin WT controls. Upon stimulation with 16 ng/gBW/minute of dobutamine, a significant increase in dP/dt max was found in cardiac actin E99K, A2AR KO hearts compared to cardiac actin E99K A2AR WT animals. Similarly, the minimal rate of diastolic pressure decrease (dP/dt min) was significantly worse in cardiac actin E99K A2AR WT animals, while no significant degradation was observed in cardiac actin E99K A2AR KO animals. Upon maximal dobutamine stimulation, a significant improvement of dP/dt min of cardiac actin E99K A2AR KO animals was observed. (*B*) No significant differences in heart rate were found between any of the groups.. (*C*) The time constant of left ventricular relaxation, Tau, was significantly ($p$<0.05) increased

in cardiac actin E99K, A2AR WT mice.. No significant difference was observed in relaxation time constant between cardiac actin E99K, A2AR KO hearts and actin WT hearts.. (*D&E*) Left ventricular developed and maximal systolic pressures were significantly ($p$<0.05) decreased in cardiac actin E99K A2AR WT hearts compared to cardiac actin WT hearts, while cardiac actin E99K A2AR KO mice demonstrated a significant ($p$<0.05) rescue of left ventricular pressures.

### 4.4 Treatment of cardiac actin E99K mice with the adenosine A2A receptor inhibitor ZM-241385

Studying the effect of the genetic loss of the adenosine A2A receptor in cardiac actin E99K mice demonstrated significant reduction in the fibrotic phenotype of this model, associated with functional improvements. In order to further verify the pathophysiological importance of the A2AR, a pharmacologic inhibition study was undertaken. In this experiment the specific adenosine A2AR inhibitor ZM241385, which had demonstrated an antagonistic effect on A2AR signalling in tissue culture experiments, was used. Mice were injected according to a treatment protocol that was previously established by Chan et al. which has been shown to inhibit the formation of tissue fibrosis by adenosine A2A receptor inhibition (Chan, Fernandez, et al., 2006; Chan, Montesinos, et al., 2006). Accordingly, mice were injected twice daily with 25mg/kg/day of ZM241385 diluted in PBS supplemented with 15% of DMSO and 15% of Cremophor. The same solution was used for vehicle treatments. Treatment of littermate control cardiac actin WT and E99K animals with either the drug or the vehicle solution resulted in four different treatment groups:

- Cardiac actin WT vehicle treated (N=5)
- Cardiac actin WT ZM-241385 treated (N=5)
- Cardiac actin E99K vehicle treated (N=4)
- Cardiac actin E99K ZM-241385 treated (N=4)

The treatment protocol was started at four weeks of age and administered continuously until the age of eight weeks. At that point phenotypic investigation of the treatment groups was initiated by invasive haemodynamic measurements and tissue harvest. Upon collection, the hearts of the animals were used for measurement of tissue collagen content and for histologic examination.

### 4.4.1 Changes in morphometric measurements

Morphometric measurements of absolute and normalized organ weights and tibia length were carried out at organ harvest. No significant differences were found in body weight or tibial length between any of the pharmacologic treatment groups, providing evidence for no obvious impairment in gross physical development due to prolonged ZM241385 treatment (Figure 4.8, A and *B*).

The hearts of vehicle and ZM241385 treated actin E99K mice demonstrated a significant increase in heart weight ($p<0.05$) compared to the heart weights of cardiac actin and A2AR WT animals. No significant difference in heart weight was found between vehicle and ZM241385 treated cardiac actin E99K mice. Further, both the vehicle and ZM241385 treated cardiac actin E99K animals also demonstrated a statistically significant ($p<0.01$ and $p<0.05$, respectively) increase in lung weight compared to cardiac actin WT control treated animals. In addition, no significant difference was found in liver weights between any of the treatment groups (Figure 4.8, C-*E*).

Normalization of organ weights to tibia length produced similar results. The normalized heart weights of vehicle and ZM241385 cardiac actin E99K mice were significantly higher than in vehicle treated cardiac actin WT mice. Normalized lung weights were significantly increased in vehicle and ZM241385 ($p<0.01$ and $p<0.05$, respectively) treated cardiac actin E99K mice. No significant difference was found in normalized liver weights between any of the treatment groups (Figure 4.8, F-H).
In conclusion, morphometric data from ZM241385 and vehicle treated cardiac actin E99K animals did not reveal significant treatment effects.

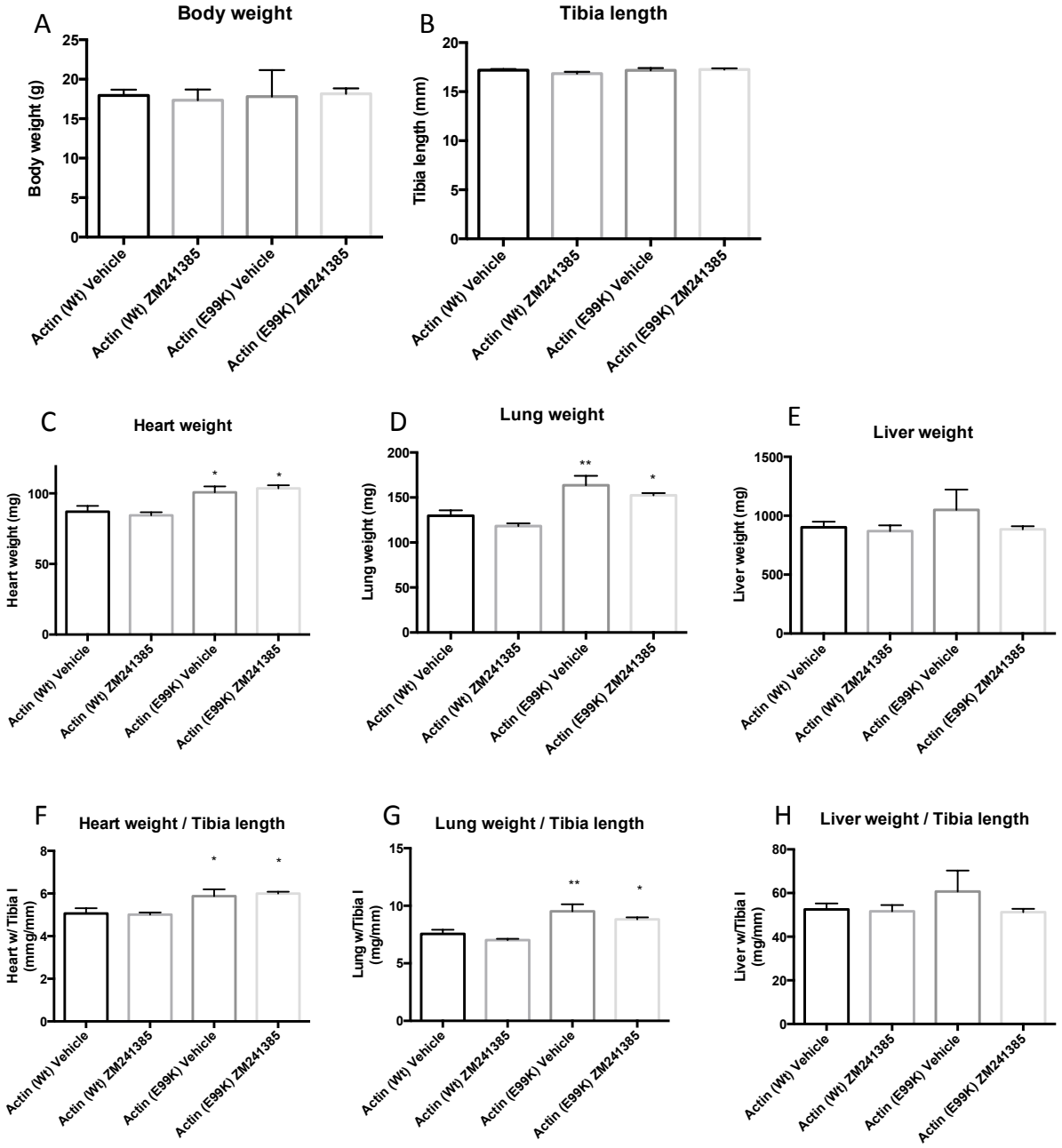


**Figure 4.8:** Morphometric measurements of absolute and normalized organ weights of E99K mice and controls in response to chronic treatment with A2AR inhibitor ZM241385. (*A&B*) No significant differences were found in body weight and tibia length. (*C*) Vehicle and ZM241385 treated cardiac actin E99K mice demonstrated a significant increase in heart weight ($p<0.05$) compared to the heart weights of cardiac actin E99K, A2AR WT animals. No significant difference in heart weight was found between vehicle and ZM241385 treated cardiac actin E99K mice. (*D&E*) Vehicle and ZM241385 treated cardiac actin E99K animals also demonstrated a statistically significant ($p<0.01$ and $p<0.05$, respectively), increase in lung weight (*D*). No significant difference was found in liver weights between any of the treatment groups (*E*). The normalized heart weights of vehicle and ZM241385 cardiac actin E99K mice were significantly higher than in vehicle treated cardiac actin WT mice (*F*). Normalized lung weights were significantly increased in vehicle and ZM241385 ($p<0.01$ and $p<0.05$, respectively) treated cardiac actin E99K mice (*G*). No significant difference was found in normalized liver weights between any of the treatment groups (*H*).

### 4.4.2 Changes in myocardial collagen content and cardiac fibrosis

Evaluation of the effect of vehicle and ZM241385 treatment on the fibrotic phenotype of cardiac actin WT and E99K hearts was conducted by measurement of the myocardial collagen content and histologic examination of cardiac tissue sections.

Hydroxyproline measurements from left ventricular tissue revealed a marked and statistically significant ($p$<0.0001) increase in tissue collagen content in vehicle as well as ZM241385 treated cardiac actin E99K hearts. Notably, measurement of the collagen content in ZM241385 treated cardiac actin E99K hearts revealed a modest but significant reduction ($p$<0.05) compared to vehicle treated cardiac actin E99K hearts, consistent with a partial rescue of the fibrotic phenotype (Figure 4.9).

Histologic examination of Sirius-red stained tissue sections revealed marked myocardial fibrosis in both ZM241385 treated cardiac actin E99K hearts. In addition, ZM241385 treated cardiac actin E99K hearts demonstrated reduced interstitial fibrosis, compared to vehicle treated cardiac actin E99K hearts. Upon computational quantification of Sirius-red signal normalized to total tissue area, significant myocardial fibrosis ($p$<0.0001) was demonstrated in vehicle treated cardiac actin E99K hearts, while ZM241385 treated cardiac actin E99K hearts demonstrated a significant ($p$<0.01) reduction in this fibrotic signal (Figure 4.9).

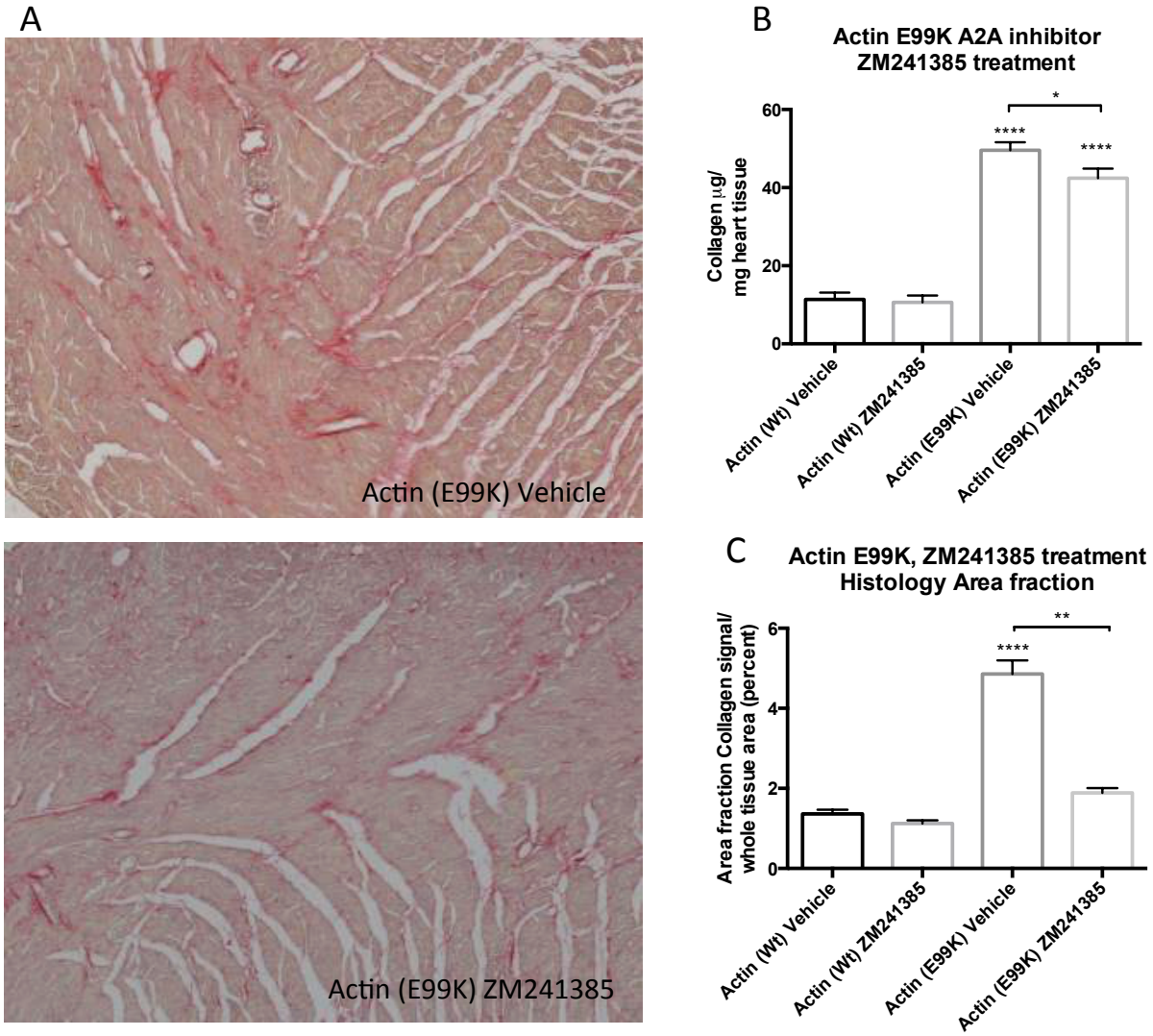


**Figure 4.9:** Evaluation of the fibrotic phenotype of vehicle and ZM241385 treated cardiac actin WT and E99K animals. (*A*) Hydroxyproline measurements from left ventricular tissue revealed a significant ($p<0.0001$) increase in tissue collagen content in vehicle as well as ZM241385 treated cardiac actin E99K hearts. The collagen content in ZM241385 treated cardiac actin E99K hearts was significantly reduced compared to vehicle treated actin E99K hearts ($p<0.05$). (*B*) Histologic examination (Sirius-red staining) revealed myocardial fibrosis in both vehicle and ZM241385 treated cardiac actin E99K hearts. ZM241385 treated cardiac actin E99K hearts demonstrated reduced interstitial fibrosis, compared to vehicle treated cardiac actin E99K hearts. Computational quantification (*C*) of Sirius-red signal revealed significant myocardial fibrosis ($p<0.0001$) in vehicle treated cardiac actin E99K hearts. This fibrotic signal was significantly ($p<0.01$) reduced in ZM24185 treated cardiac actin E99K hearts.

### 4.4.3 Changes in cardiac function in invasive haemodynamic measurements

In order to further assess the effect of pharmacologic adenosine A2A receptor inhibition on myocardial function of cardiac actin E99K hearts, haemodynamic measurements of left ventricular pressures were conducted. Intra-ventricular pressures were measured at baseline and, during the continuous infusion of two increasing dobutamine dosages (4 and 16 ng/gBW/minute) in order to investigate the chronotropic and inotropic reserve of the investigated hearts.

No significant difference was found in the average maximal pressure increase rate between all four of the pharmacological treatment groups. Similarly, the minimal rate of diastolic pressure decrease was not significantly altered between any of the treatment groups. Of note, a significant increase in heart rate was found between all vehicle treated and ZM241385 treated groups. This alteration in heart rate in response to ZM241385 potentially influences left ventricular contractility and intra-cardiac pressures and can thereby confound ready interpretation of the haemodynamic data. Regardless of baseline rate, however, all treatment groups demonstrated a dose-dependent increase in heart rate upon continuous dobutamine infusion (Figure 4.10, *A and B*).

Left ventricular developed and maximal systolic pressures were significantly ($p<0.05$) decreased in vehicle treated cardiac actin E99K hearts compared to vehicle treated cardiac actin WT hearts, while ZM241385 treated actin E99K hearts demonstrated a significant ($p<0.05$) partial rescue of left ventricular pressures (Figure 4.10, *C and E*).

In summary, while the improvement of left ventricular systolic and developed pressures could be interpreted as an improvement in systolic cardiac function in response to A2A inhibition in, the E99K model, the marked changes in heart rate in response to this agent and the close correlation of rate and function in the mouse heart make it difficult to draw a definite conclusion.

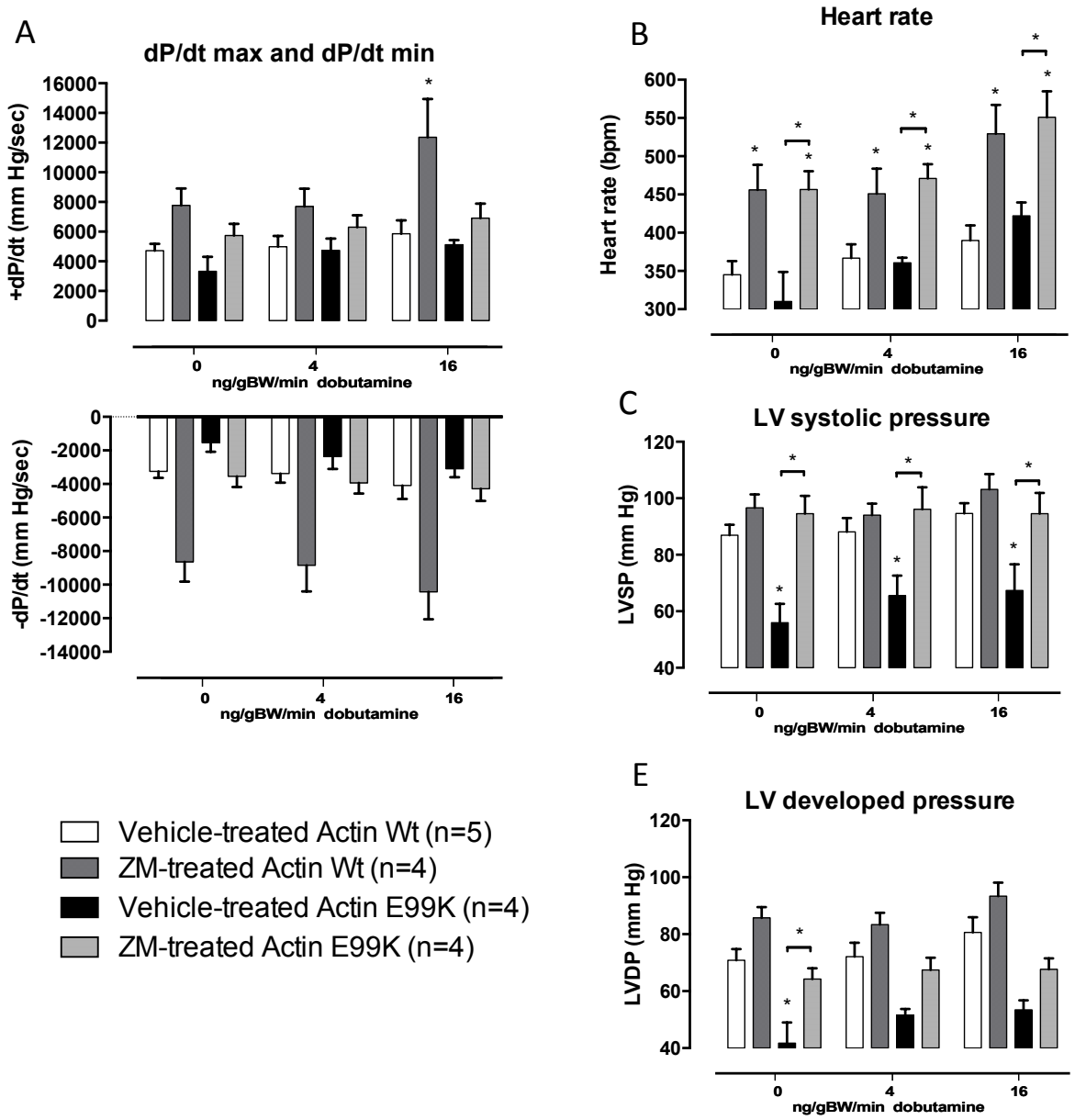


**Figure 4.10:** Haemodynamic measurements of left ventricular pressures.. Intra-ventricular pressures were measured at baseline and during increasing dosages (4 and 16 ng/gBW/minute) of dobutamine infusion. (*A*) No significant difference was found in maximal pressure increase rates (dP/dt max) in any of the pharmacological treatment groups. Similarly, the minimal rate of diastolic pressure decrease (dP/dt min) was not significantly altered between the treatment groups. (*B*) A significant increase in heart rate was found between the vehicle treated and ZM241385 treated groups, but all groups demonstrated a dose dependent increase in heart rate upon dobutamine infusion. (*C&D*) Left ventricular developed and maximal systolic pressures were significantly ($p$<0.05) decreased in vehicle treated cardiac actin E99K hearts compared to vehicle treated actin WT hearts, while ZM241385 treated cardiac actin E99K hearts demonstrated a significant ($p$<0.05) increase of left ventricular developed and systolic pressure.

## 4.5 Discussion

### 4.5.1 Primary conclusions of Results chapter two

1. Neonatal rat cardiac fibroblasts and adult mouse cardiac fibroblasts were successfully isolated and cultured.

2. Pharmacologic stimulation of cardiac fibroblasts with the adenosine A2A receptor agonist CGS induced increased production of fibrillar collagens.

3. Genetic loss (constitutive knockout) of the adenosine A2A receptor conferred a partial rescue effect on myocardial fibrosis in cardiac actin E99K hearts.

4. Pharmacologic inhibition of the adenosine A2A receptor resulted in a partial rescue of myocardial fibrosis in cardiac actin E99K hearts.

5. Abrogation of myocardial fibrosis was associated with corresponding improvements of cardiac function.

### 4.5.2 Summary of chapter findings and resulting conclusions – Cell experiments

In order to investigate the hypothesis that adenosine A2A receptor stimulation activates collagen production in cardiac fibroblasts, *in vitro* and *in vivo* experiments aiming to inhibit adenosine A2A receptor signalling were performed. These experiments served to provide evidence of a causal connection between adenosine A2A receptor signalling and cardiac fibroblast activation on a cellular level as well as in tissue.

Cardiac fibroblasts were successfully isolated and cultured from adult mouse hearts and neonatal rat hearts. This was achieved by collagenase digestion of the respective hearts followed by culture on plastic, which lead to fibroblast adhesion. Most other myocardial cell populations do not adhere to plastic and were therefore removed at the first change of medium. In addition, most cardiac cells other than fibroblasts, in particular cardiomyocytes and endothelial cells, have very limited proliferative potential under normal tissue culture conditions on plastic. As a result, after three passages the cells were considered as primary cardiac fibroblast cultures. This was further evidenced by immunofluorescence stainings for several cellular markers that are typically expressed on fibroblasts, including vimentin, discoidin domain receptor-2 (DDR-2) and collagen type-I. While vimentin is a very sensitive marker for fibroblasts staining a large majority of fibroblasts in most tissues it is also expressed in endothelial cells and therefore by itself not a specific marker. DDR-2 and collagen expression on cells isolated from the myocardium however are considered fibroblast specific markers. At the time the experiments were carried out more than 95% of the cells were expressing all these markers, and as a result were considered as fibroblasts isolated from the myocardium. However, one potential

disadvantage of such isolation protocols followed by the execution of *in vitro* experiments is that tissue culture growth on plastic under standard conditions by itself confers an activating stimulus on cardiac fibroblasts. As a result, stimulation experiments focusing on activating mechanisms can be hindered by the presence of background activation. Therefore, *in vitro* experiments on cardiac fibroblasts cannot be considered as entirely representative of the pathophysiologic conditions in the myocardial tissue and any positive findings need to be recapitulated by *in vivo* experiments.

Stimulation experiments of both neonatal rat cardiac fibroblasts and murine adult cardiac fibroblasts demonstrated that collagen production increases in cardiac fibroblasts upon stimulation with the adenosine A2A receptor agonist CGS-21680. This could be demonstrated in both investigated populations of cardiac fibroblasts. However a difference in amplitude of the stimulatory effect was observed between neonatal rat cardiac fibroblasts and murine adult cardiac fibroblasts. While neonatal rat cardiac fibroblasts demonstrated a modest, approximately 1.5 fold increase in collagen production, murine adult cardiac fibroblasts demonstrated an at least two fold increase in collagen content in the CCM. In both fibroblast cell populations the stimulatory effect of adenosine A2A receptor agonism could be demonstrated by two methods of collagen measurement. As a result this data demonstrates an important role for adenosine A2A receptor signalling in the activation of cardiac fibroblasts.

Further, the fact that this stimulatory response could be prevented by addition of the specific adenosine A2A receptor antagonist ZM241385 supports the hypothesis that this receptor is responsible for the stimulatory effect.

### 4.5.2 Summary of chapter findings and resulting conclusions – genetic experiment

As described in the first results chapter, the cardiac actin E99K mouse model develops a clear phenotype characterized by interstitial fibrosis. One of the primary aims of the experiments conducted in this chapter was to prevent the development of myocardial fibrosis in this model. In order to achieve this, the cardiac actin E99K mouse model was crossbred with a mouse line lacking a functional adenosine A2A receptor (Chen et al., 1999). While the cardiac actin E99K mouse model only exists in the form of heterozygous animals, the A2AR KO mice were bred to homozygosity. As a result, no adenosine A2A receptor dependent signalling could occur in these mice. Therefore this experiment aimed to provide evidence of a causal connection between adenosine A2A receptor signalling and the formation of myocardial fibrosis.

In order to produce the respective control and rescue mouse groups, a breeding protocol was planned and carried out over three generations in order to generate cardiac actin E99K animals that were also homozygous for the loss of the adenosine A2A receptor. Cardiac actin E99K, adenosine A2AR WT animals in this cohort demonstrated a clear fibrotic phenotype with a corresponding impairment in cardiac function. As a result, these animals served as an appropriate positive control, which recapitulated the phenotypic findings of pronounced cardiac fibrosis and corresponding myocardial dysfunction described in the first results chapter.

Cardiac actin E99K mice lacking the adenosine A2A receptor developed significantly less myocardial fibrosis than actin E99K animals sufficient in the adenosine A2A receptor. This was evidenced both by significantly less Sirius-red signal on histologic examination as well as by measurement of myocardial collagen content by means of

measuring myocardial hydroxyproline. This data clearly indicates that the adenosine A2A receptor is involved in the formation of myocardial fibrosis in the actin E99K mouse model. However, the fact that the rescue of fibrosis is partial and does not constitute a complete reversion to the state of cardiac actin WT hearts, indicates that other mechanisms, e.g. such as TGF-β, play an important role as well.

The reduction of myocardial fibrosis in cardiac actin E99K mice lacking the adenosine A2A receptor was associated with an improvement in myocardial function. This was evidenced by morphometric measurements as well as by the invasive measures of haemodynamic left ventricular pressures. The clear reduction in lung weight in actin E99K mice lacking the adenosine A2A receptor was consistent with a significant reduction in left sided cardiac congestion. This was also recapitulated by the fact that at haemodynamic assessment, the systolic and diastolic function of actin E99K mice lacking the adenosine A2A receptor was significantly improved. Both the maximal rates of pressure increase as well as the maximal developed left ventricular pressures were improved in cardiac actin E99K hearts lacking the adenosine A2A receptor, indicating improved systolic function. In addition, diastolic function was also improved, however this only reached statistical significance upon dobutamine stimulation.

In addition, a reduction of the modest hypertrophic phenotype was observed in cardiac actin E99K hearts upon adenosine A2A receptor knock out as far as heart weight measurements are concerned. This reduction was likely at least partially caused by the reduction of reactive myocardial hypertrophy of upstream myocardial compartments, in particular the left atrium and the right ventricle. All these

parameters point to the improvement of myocardial function of cardiac actin E99K animals caused by the deletion of adenosine A2A receptors.

In contrast, echocardiographic measurement revealed only minor changes in cardiac function. This was likely primarily due to the fact that the systolic function of cardiac actin E99K hearts did not appear significantly disrupted based on standard echocardiographic measurements. One potential explanation for this finding is that echocardiography is not a sensitive enough method to detect subtle systolic dysfunction in murine models for hypertrophic cardiomyopathy. However, calculations of left ventricular mass from echocardiographic images revealed similar findings to the ex vivo heart weight measurements, i.e. a reduction in cardiac mass in actin E99K mice lacking the adenosine A2A receptor.

In summary, the significant rescue of myocardial fibrosis in cardiac actin E99K hearts upon loss of the adenosine A2A receptor was associated with several indicators of improved myocardial function. This improvement of cardiac function could be due to the reduction in myocardial fibrosis. It has been suggested that diastolic as well as systolic myocardial function is connected to myocardial fibrosis. One potential factor is the hindering of cardiomyocyte widening during systolic contraction due to envelopment of individual or groups of cardiomyocytes by the endomysial collagen component (LeGrice et al., 2012). While this could be shown to be the case in cardiac actin E99K hearts in results chapter one, this was not formally investigated in cardiac actin E99K hearts lacking the adenosine A2A receptor.

A potential criticism of this experiment is that a systemic deletion of the adenosine

A2A receptor was used, rather than a cell specific conditional knock out in myocardial fibroblasts. In order to make a definite statement about the role of adenosine A2A receptor signalling in cardiac fibroblasts, a cell specific inhibition of this mechanism would be preferable. However, taking into account the cellular data demonstrating the effect of adenosine A2A receptor signalling on cardiac fibroblast activation and the clear partial rescue of the fibrotic phenotype, an effect on the cardiac fibroblast population seems likely. In addition, cardiomyocyte specific up-regulation of the adenosine A2A receptor conferred a beneficial effect on a transverse aortic constriction model of cardiac hypertrophy and fibrosis (Hamad et al., 2012). This paper demonstrates that cardiomyocyte specific adenosine A2A receptor signalling in the setting of hypertrophy and myocardial fibrosis is protective rather than maladaptive. Accordingly, it appears unlikely that the findings in this experiment are caused by cardiomyocyte specific inhibition of adenosine A2A receptor signalling. Furthermore, the applied systemic mode of genetic inhibition has the potential advantage of recapitulating a pharmacologic intervention, which was one of the basic aims of this experiment.

### 4.5.2 Summary of chapter findings and resulting conclusions – pharmacologic experiment

Pharmacologic inhibition experiments aiming to inhibit adenosine A2A receptor signalling in cardiac actin E99K animals were carried out using a chronic twice-daily injection regimen of the adenosine A2A receptor inhibitor ZM241385. The treatment period was followed by cardiac phenotyping at a similar time-point to the descriptive and genetic intervention studies. These pharmacologic experiments were conducted in order to further explore and seek to validate the findings from the previously described cross breeding study of cardiac actin E99K and adenosine A2A receptor knock out animals. In addition to demonstrating the effect of another modality of inhibition of adenosine A2A receptor signalling, a key aim of this experiment was to investigate whether this pathway is susceptible to pharmacologic modulation.

Pharmacologic intervention in genetic mouse models of hypertrophic cardiomyopathy is faced by several difficulties. In particular models that develop a phenotype from an early age, such as the cardiac actin E99K mouse model present difficulty for pharmacologic treatment. At the time-point the treatment regimen in this experiment was commenced, at four weeks of age, it is difficult to ascertain how much of the fibrotic phenotype had already developed. Even though four weeks of age was considered as a relatively early and therefore appropriate time-point it is likely that a substantial proportion of the fibrotic and hypertrophic phenotype had already developed prior to the initiation of treatment. While this experiment was planned and carried out with the aim to prevent the development of myocardial fibrosis, it is less likely that adenosine A2A receptor inhibition caused a regression of existing myocardial fibrosis.

These limitations, together with the difficulty of achieving complete receptor inhibition in the target tissue, likely underlie the less pronounced findings using the pharmacologic inhibitor than the genetic deletion experiments. Vehicle treated cardiac actin E99K animals developed a clear fibrotic and modest hypertrophic cardiac phenotype, comparable to the phenotype observed in untreated cardiac actin E99K animals. Upon treatment with the adenosine A2A receptor antagonist ZM241385, cardiac actin E99K animals did not demonstrate a significant reduction in heart or lung weight. However, a significant reduction in myocardial fibrosis was found in ZM241385 treated cardiac actin E99K hearts compared to vehicle treated controls upon histologic examination of cardiac tissue. In addition, a small but statistically significant reduction in myocardial collagen content was observed in ZM241385 treated cardiac actin E99K animals. As described above, it is unlikely that this data indicates that fibrosis is reversed in actin E99K hearts upon treatment, rather it likely inhibits the further accumulation of extracellular matrix.

The cardiac function of vehicle and ZM241385 treated actin E99K animals was investigated by the invasive measurement of left ventricular haemodynamic pressures. The left ventricular systolic as well as developed pressures were significantly reduced in vehicle treated cardiac actin E99K hearts, this reduction was absent in ZM241385 treated actin E99K hearts. However these results can only be interpreted with limitation, due to significantly different heart rates during the invasive measurement of intra ventricular pressures. It cannot be ruled out that these differences in basal heart rate influence intra-ventricular pressures and therefore no definitive statement on the myocardial function of ZM241385 treated cardiac actin E99K animals can be made. Adenosine signalling has been shown to have effects on

heart rate, in particular via adenosine A1 and A2A receptors (Yang, Chen, & Fredholm, 2009). As described, both these receptors are expressed in the heart, therefore the observed effect of adenosine A2A receptor inhibition on heart rate could be mediated directly via an intracardiac effect on these receptors. In addition however, adenosine receptor signalling is also crucial in the central regulation of heart rate and blood pressure, mostly via adenosine A1 receptors (Koeppen, Eckle, & Eltzschig, 2009). As a result, a central effect of ZM241385, albeit most likely unspecific cannot be excluded as explanation for the altered heart rates in drug treated animals compared to vehicle treated animals.

In conclusion, treatment of cardiac actin E99K mice with an adenosine A2A receptor antagonist abrogated myocardial fibrosis progression, with a potential improvement in myocardial function. These data recapitulate the findings from the genetic adenosine A2A receptor knock out experiments, even though the results of the pharmacologic intervention study are less pronounced. In addition, these results provide evidence that adenosine A2A receptor signalling is in principal susceptible to pharmacologic intervention, with the potential to inhibit fibrosis formation.

# 5. Results: Inhibiting adenosine A2A receptor signalling in pressure overloaded hearts (genetically & pharmacologically)

## 5.1 Introduction

To investigate whether adenosine signaling constitutes a conserved pathway in the development of MF in cardiac pathologies with left-ventricular hypertrophy, a well-established model of pressure overload, namely transverse aortic constriction was utilized. Banding of the aortic arch to a defined diameter leads to heart failure as well as the formation of MF after 5 weeks (Chapman et al., 1990; Heymans et al., 2005; Ying et al., 2009).

### 5.1.1 Hypothesis

The primary hypothesis of this investigation was that the findings on the role of adenosine signalling in the induction of myocardial fibrosis in the cardiac actin E99K mouse model would be reflected in a non-genetic pressure-overload model of MF. In particular, it was hypothesized that TAC experiments on animals lacking the adenosine A2A receptor would result in less myocardial fibrosis, compared to WT animals. In addition, it was hypothesized that pharmacologic inhibition of the adenosine A2A receptor would result in a similar rescue of the fibrotic phenotype.

### 5.1.2 Aims

As a result, the experimental aims of this chapter are

- To delineate the difference in the fibrotic and functional phenotype between TAC animals lacking the adenosine A2A receptor and WT TAC animals.
- To investigate the effect of pharmacologic inhibition of the adenosine A2A receptor on fibrosis formation in response to TAC.

## 5.2 Transverse aortic constriction on adenosine A2A receptor knock out mice

The primary hypothesis of this experiment was that the genetic deletion of the adenosine A2A receptor would confer a protective effect against myocardial fibrosis, due to TAC. In order to investigate this hypothesis, TAC experiments were conducted on adenosine A2AR KO animals. As control animals, sham operated animals as well as aortic-banded age-matched adenosine A2AR WT animals of identical genetic background (Balb/C) were used.

In order to investigate this hypothesis, operations were planned and conducted to produce four experimental groups of animals:

1. Sham operated, adenosine A2A receptor WT (A2AR WT) (N=8)
2. Sham operated, adenosine A2A receptor KO (A2AR KO) (N=6)
3. Aortic banded, adenosine A2A receptor WT (A2AR WT) (N=9)
4. Aortic banded, adenosine A2A receptor KO (A2AR KO) (N=9)

Both groups, i.e. adenosine A2AR KO and WT animals, underwent banding or sham operations at eight to nine weeks of age. In the fourth week after the operation phenotyping was initiated by echocardiography followed by invasive haemodynamic investigation and tissue harvest five weeks post operation.

### 5.2.1 Changes in morphometric measurements

Morphometric measurements of absolute and normalized organ weights and tibia length were conducted upon organ harvest, in order to compare basic physical differences between the distinct intervention groups. Body weight measurements revealed a significant ($p$<0.01) weight reduction of banded A2AR WT mice compared to sham operated A2AR WT animals, indicating a strong systemic effect of the banding operations. However, no significant reduction in bodyweight was observed in banded A2AR KO animals. No significant differences were found in tibia length between any of the experimental groups (Figure 5.1, *A and B*).

The hearts of banded A2AR WT and A2AR KO mice were characterized by a significant increase in heart weight ($p$<0.01) compared to the heart weight of sham operated A2AR WT animals. This finding provided evidence of a clear hypertrophic phenotype upon aortic banding. In addition, banded A2AR WT animals demonstrated a significant ($p$<0.001), more than two fold increase in average lung weight compared to sham operated A2AR WT control animals. This increase in lung weight was reduced in banded A2AR KO mice, albeit this reduction did not reach statistical significance. However, banded A2AR KO animals did demonstrate a significant increase in lung weight ($p$<0.05) compared to sham operated animals. Furthermore banded A2AR WT animals demonstrated significantly ($p$<0.05) reduced liver weights compared to sham operated A2AR WT animals as well as banded A2AR KO animals. No significant difference was found in liver weights between any of the remaining experimental groups. (Figure 5.1, *C-E*)

Normalization of heart, lung and liver weights to tibia length revealed similar findings. The normalized heart weights of banded A2AR WT and KO mice were significantly higher than average normalized heart weight of sham operated A2A receptor WT mice. Normalized lung weights were significantly increased in banded A2AR WT animals and A2AR KO animals, consistent with cardiac congestion post-TAC. However, the normalized lung weights of banded A2AR KO animals were significantly ($p$>0.05) reduced compared to normalized lung weights of banded A2AR WT animals. Average normalized liver weight was significantly decreased ($p$>0.05) in banded A2AR WT animals (Figure 5.1, *F-H*).

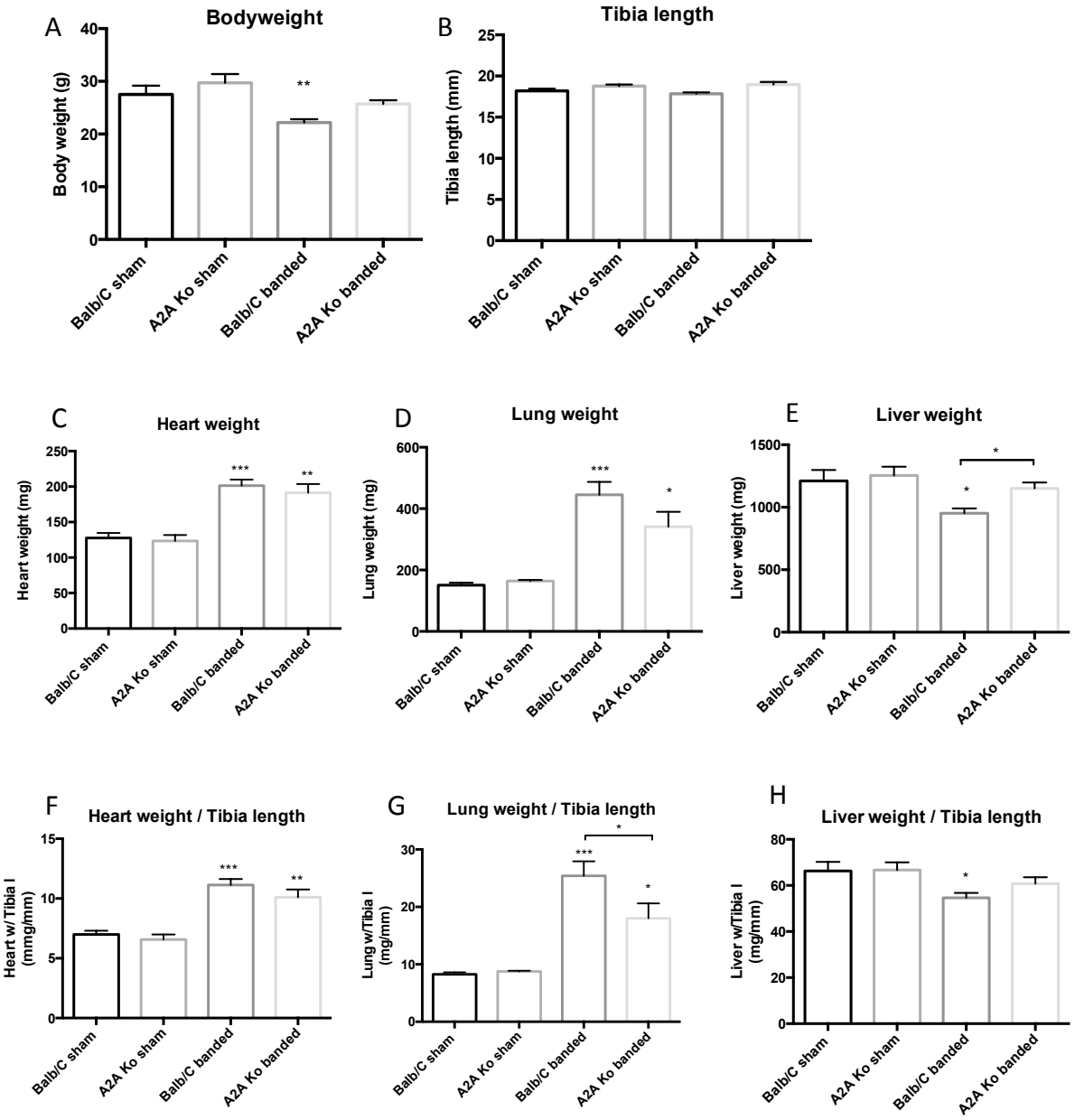


**Figure 5.1:** Morphometric measurements of absolute and normalized organ weights and tibia length. (*A*) Body weight measurements revealed a significant ($p$<0.01) weight reduction in banded A2AR WT mice, but no significant reduction in bodyweight in banded A2AR KO animals. (*B*) Tibia length did not differ between any of the treatment groups. (*C*) The hearts of banded A2AR WT and A2AR KO mice demonstrated a significant increase in heart weight ($p$<0.001 and $p$<0.01, respectively) compared to sham operated A2AR WT animals. Banded A2AR WT and KO animals demonstrated a significant ($p$<0.001) increase in lung weight compared to sham operated A2AR WT controls ($p$<0.05) (*D*). Banded A2AR WT animals demonstrated significantly reduced liver weights compared to sham operated A2AR WT animals as well as to A2AR KO mice (*E*). Heart weights, normalized to tibia length, of banded A2AR WT and KO mice were significantly higher than normalized heart weights of sham operated A2A receptor WT mice (*F*). Normalized lung weights were significantly increased in banded A2AR WT ($p$<0.001) animals and A2AR KO ($p$<0.05) animals. Also, the normalized lung weights of banded A2AR KO animals were significantly reduced ($p$<0.05) compared to banded A2AR WT animals (*G*). Normalized liver weights of banded A2AR WT animals were significantly decreased compared to sham operated A2AR WT animals.

### 5.2.2 Changes in myocardial collagen content and cardiac fibrosis

Evaluation of the fibrotic phenotype was conducted by measurement of myocardial collagen content as well by histologic investigation of paraffin embedded tissue sections. These experiments were carried out in order to determine the phenotype of hearts under pressure overload conditions and to demonstrate a potential effect of adenosine A2A receptor deletion on this phenotype.

Hydroxyproline measurements from left ventricular tissue aliquots of banded A2AR WT hearts revealed a marked, significant ($p<0.0001$) increase in tissue collagen content, indicating myocardial fibrosis. Conversely, the collagen content of banded A2AR KO hearts was significantly reduced ($p<0.01$) compared to banded A2AR WT hearts. The collagen content of banded A2AR KO hearts was reduced to the extent that these hearts did not demonstrate a significantly higher collagen content than sham operated A2AR WT hearts (Figure 5.2).

In support of these findings, histologic examination of Sirius-red stained tissue sections revealed marked myocardial fibrosis in banded A2AR WT hearts compared to sham operated A2AR WT hearts. Further, banded A2AR KO hearts demonstrated markedly reduced interstitial fibrosis. Semi-automated computational quantification of Sirius-red signal normalized to total tissue area, revealed significant myocardial fibrosis ($p<0.0001$) in banded A2AR WT hearts. This fibrotic signal was significantly ($p<0.0001$) reduced in banded A2AR KO hearts, and did not significantly differ from that of sham operated hearts (Figure 5.2).

In addition, immunofluorescence experiments against myocardial collagen were

conducted. Sham operated A2AR WT and KO hearts exhibited a thin, continuous signal of endomysial collagen comparable to the staining pattern of cardiac actin WT animals. Conversely, banded A2AR WT animals were characterised by a marked increase in endomysial collagen signal, enveloping individual cardiomyocytes with a thickened layer of collagen. This increase in endomysial collagen was markedly less pronounced in banded A2AR KO hearts. These immunofluorescence experiments demonstrated significant encasing of cardiomyocytes with thickened endomysial collagen in banded A2AR WT hearts, which was not present in banded A2AR KO animals (Figure 5.3).

Sham operated A2AR KO hearts did not demonstrate a significant difference in fibrotic phenotype from sham operated A2AR WT hearts. This indicates that under unchallenged conditions, the role of the adenosine A2AR in cardiac extra cellular matrix production and maintenance is likely to be limited. Conversely, the hearts of banded A2AR WT animals developed a pronounced fibrotic phenotype, which did not develop in the hearts of banded A2AR KO mice.

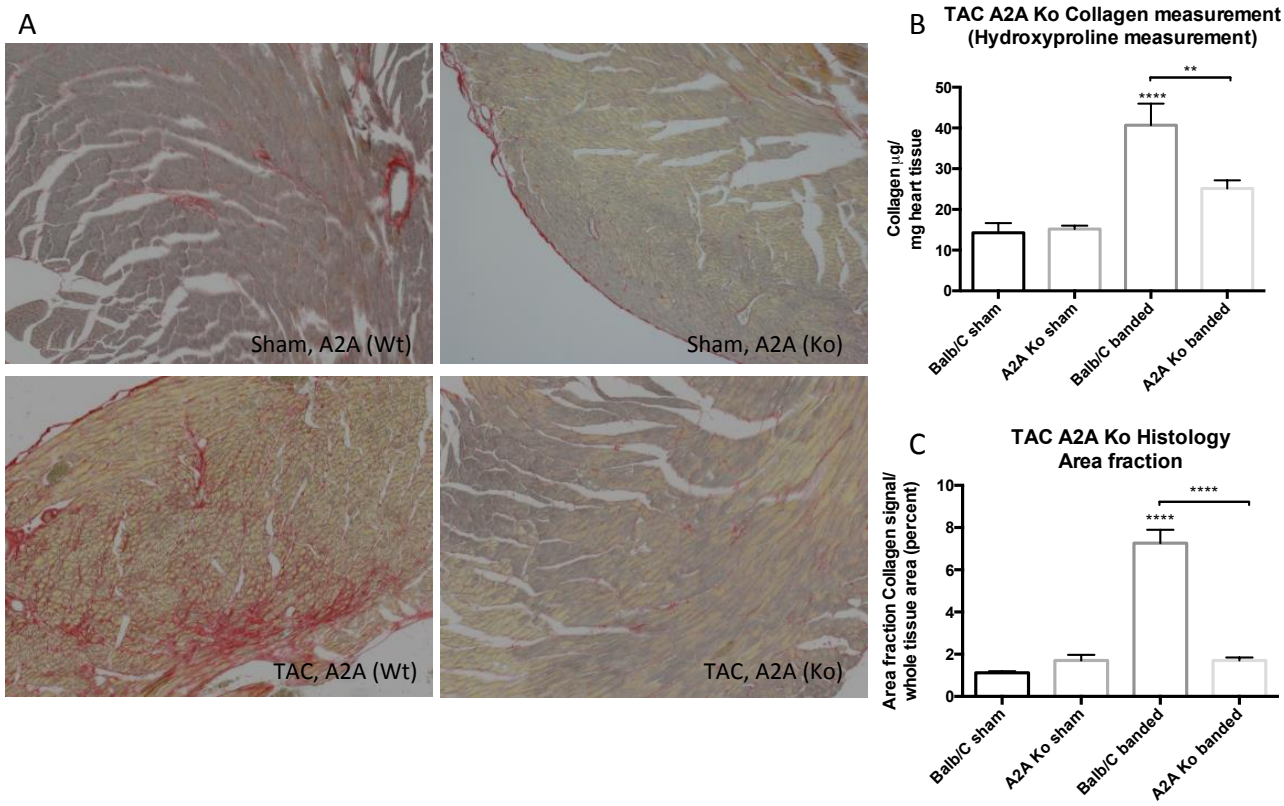


**Figure 5.2:** Evaluation of the fibrotic phenotype. (*B*) Hydroxyproline measurements from left ventricular tissue revealed a significant (p<0.0001) increase in tissue collagen content in banded A2AR WT hearts. The collagen content in banded A2AR KO hearts was reduced significantly ($p$<0.01) compared to banded A2AR WT hearts. A2AR KO hearts did not demonstrate a significantly higher collagen content than sham operated A2AR WT (Balb/C) hearts. (*A*) Histologic examination (Sirius-red staining) revealed marked myocardial fibrosis in banded A2AR WT (Balb/C) hearts (bottom row, left side) compared to sham operated A2AR WT hearts (top row, left side). Banded A2AR KO hearts (bottom row, right side) did demonstrate markedly reduced interstitial fibrosis. Computational quantification (*C*) of the Sirius-red signal revealed significant myocardial fibrosis ($p$<0.0001) in banded A2AR WT hearts. This fibrotic signal was significantly ($p$<0.0001) reduced in banded A2AR KO hearts. Sham operated A2AR KO animals did not differ significantly from sham operated A2AR WT animals.

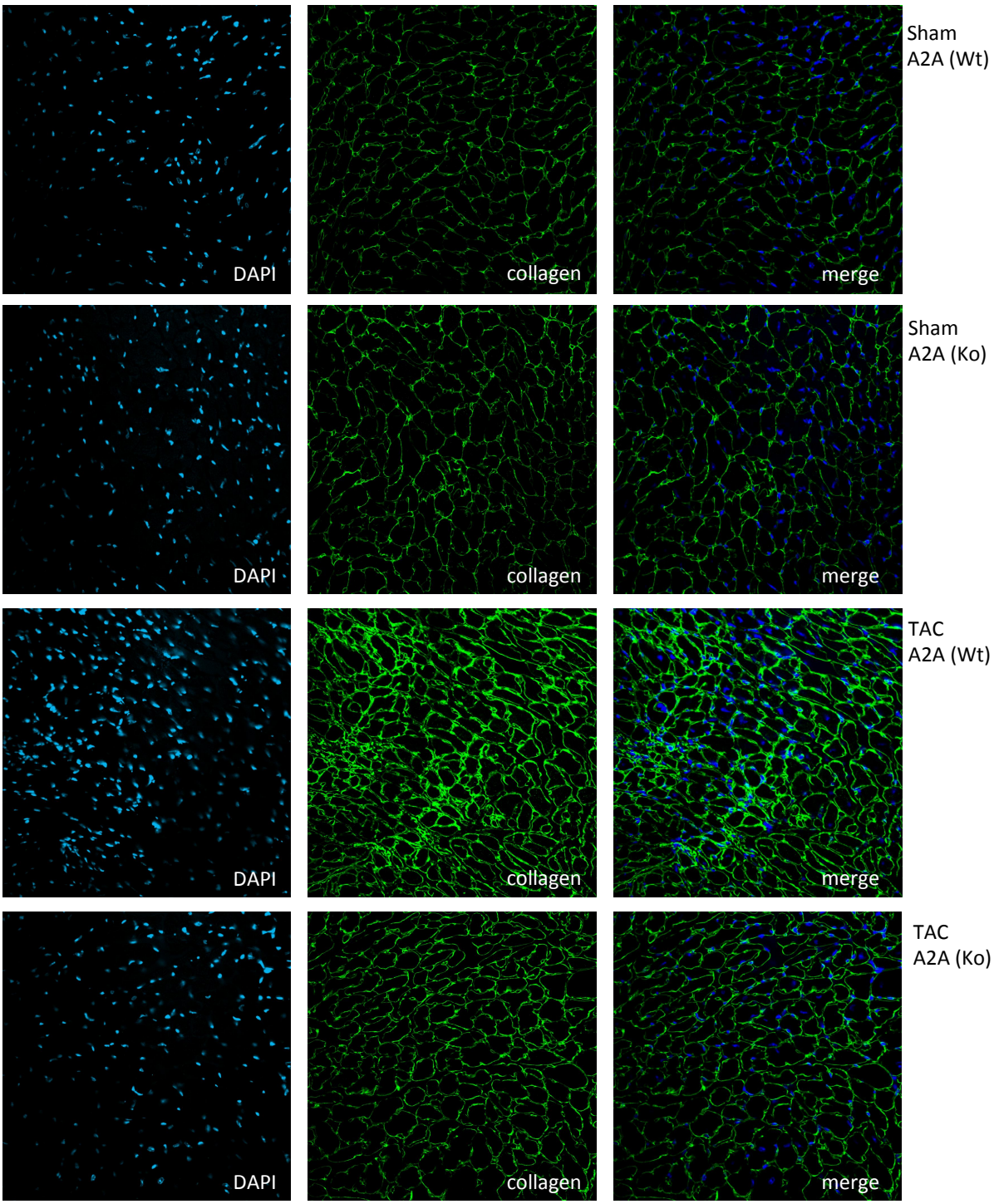


**Figure 5.3:** Immunofluorescence staining of myocardial collagen. Sham operated A2AR WT and KO hearts demonstrated a similar, faint but continuous signal of endomysial collagen.. Conversely, banded A2AR WT animals were characterised by a marked increase in endomysial collagen signal, enveloping individual cardiomyocytes. This increase in endomysial collagen was markedly less pronounced in banded A2AR KO hearts.

### 5.2.3 Changes in cardiac function on echocardiography

Echocardiographic investigations were conducted aiming to delineate the functional phenotype of banded and sham operated A2AR WT and KO animals *in vivo*. In particular, to investigate whether the pronounced reduction of myocardial fibrosis in banded A2AR KO hearts was accompanied by any improvement in cardiac function.

Echocardiography revealed a marked reduction in the systolic cardiac function of banded A2AR WT animals compared to sham operated animals. Banded A2AR WT animals demonstrated a significant reduction in ejection fraction, fractional shortening and fractional area change ($p<0.0001$, respectively), all of which constitute markers of systolic function. Banded A2AR KO animals demonstrated significantly ($p<0.001$) superior systolic function in all these parameters, compared to banded A2AR WT animals. However, banded A2AR KO animals demonstrated significantly worse systolic function than sham-operated A2AR WT animals ($p<0.01$). These findings indicate a partial rescue in cardiac function of mice undergoing transverse aortic constriction experiments, caused by the genetic deletion of the adenosine A2A receptor (Figure 5.4, A - C).

Upon calculation of left ventricular mass from echocardiographic images, both banded A2AR WT and A2AR KO animals demonstrated significant ($p<0.0001$) myocardial hypertrophy. These findings recapitulated the results from absolute *ex vivo* morphometric heart and lung weight measurements. Myocardial hypertrophy was observed in A2AR WT and KO animals, while cardiac dysfunction and resulting congestion was reduced in the hearts of A2AR KO animals (Figure 5.4, *D-H*).

Furthermore, at the time of echocardiography banded A2AR WT hearts had developed significant ventricular dilatation.. This was evidenced by a significant increase in diastolic left ventricular volume ($p<0.0001$). Banded A2AR KO animals demonstrated significantly less cardiac dilatation compared to banded A2AR WT hearts. The hearts from sham operated A2AR KO animals did not differ significantly from sham operated A2AR WT hearts, indicating that the adenosine A2A receptor plays a less important role in the myocardial function of unchallenged hearts (Figure 5.4, *E and F*).

In conclusion the results from echocardiographic investigations revealed that aortic banding leads to marked contractile dysfunction and ventricular dilatation in A2AR WT hearts, which was significantly improved in banded A2AR KO animals.

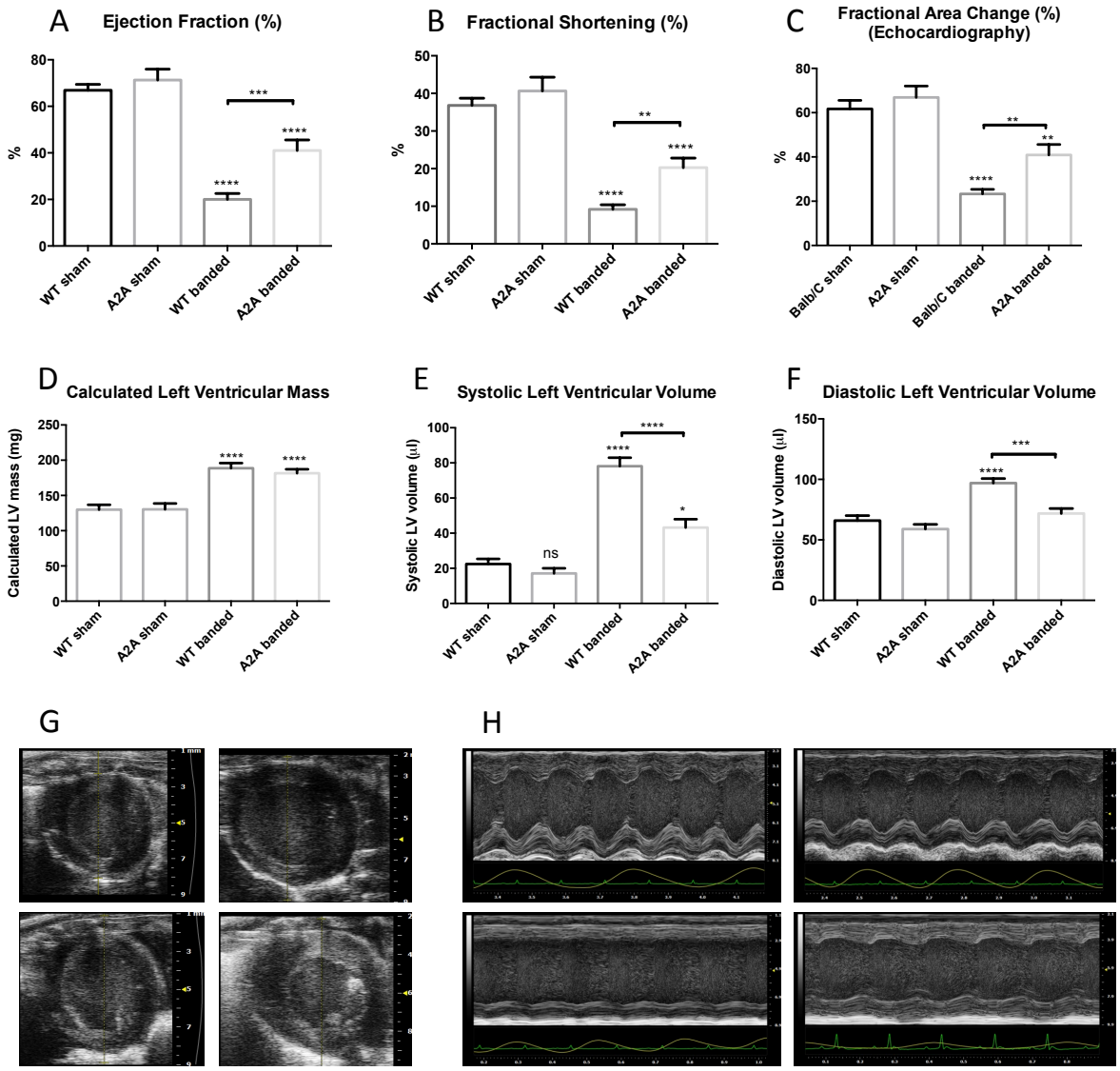


**Figure 5.4:** Echocardiographic investigation delineating the functional phenotype of banded A2AR WT and KO animals. Banded A2AR WT animals demonstrated a significant reduction of systolic function, evidenced by reduced ejection fraction (*A*), fractional shortening (*B*) and fractional area change (*C*) ($p$<0.0001, respectively). All three parameters were significantly increased ($p$<0.001) in banded A2AR KO animals indicating superior systolic function compared to banded A2AR WT animals. The systolic function of banded A2AR KO animals was still significantly reduced compared to sham operated hearts ($p$<0.01). Calculation of left ventricular mass revealed, significant ($p$<0.0001) myocardial hypertrophy in both banded A2AR WT and KO animals (*D*). Banded A2AR WT hearts developed significant ventricular dilatation,evidenced by a significant increase in diastolic left ventricular volume ($p$<0.0001). Banded A2AR KO animals demonstrated significantly smaller systolic and diastolic left ventricular volumes (*E&F*). Representative echocardiographic images (*G&H*) of sham operated A2AR WT (top row, left side), sham operated A2AR KO (top row, right side), banded A2AR WT (bottom row, left side), banded A2AR KO (bottom row, right side) hearts, depicting the short axis view (*G*) and left ventricular M-mode (*H*).

### 5.2.4 Changes in cardiac function by invasive haemodynamic measurement

In order to further delineate the effect of genetic deletion of the adenosine A2A receptor on myocardial function, haemodynamic measurements of left ventricular pressures were conducted. Intra-ventricular pressures were measured at baseline as well as during two increasing dosages (four and 16 ng/gBW/minute) of continuous dobutamine infusion, in order to investigate the contractile reserve of the hearts.

The maximal pressure increase rates of both banded A2AR WT and A2AR KO hearts were significantly reduced compared to sham operated A2AR WT hearts. In addition however, banded A2AR KO hearts demonstrated significantly higher pressure increase rates than banded A2AR WT animals, indicating an improvement in cardiac contractility. Stimulation of the hearts by dobutamine infusion served to pronounce the differences further. Similarly, the minimal rate of diastolic pressure decrease (dP/dt min) was significantly worse in banded A2AR WT and A2AR KO animals compared to sham operated A2AR WT animals. Further, banded A2AR KO animals demonstrated significantly improved rates of diastolic left ventricular pressure decrease, compared to banded hearts of A2AR WT hearts (Figure 5.5, *A*).

No significant differences in heart rate were observed between any of the groups, at baseline measurements. However, upon dobutamine infusion the heart rates of banded A2AR WT animals were significantly lower than other groups. (Figure 5.5, *B*).

Both, banded A2AR WT and KO hearts were characterized by increased end-diastolic left ventricular filling pressures. In addition, left ventricular systolic pressures revealed markedly improved systolic function in banded A2AR KO hearts compared

to banded A2AR WT hearts. The maximal systolic left ventricular pressure of banded A2AR KO hearts was significantly increased compared to sham operated hearts as well as to hearts of banded A2AR WT animals ($p<0.001$ and $p<0.01$, respectively). Accordingly, the left ventricular developed pressure of banded A2AR KO hearts was significantly higher than of banded A2AR WT hearts ($p<0.0001$) (Figure 5.5, *C* - *E*).

These findings demonstrate a clear improvement of systolic contractile function in pressure overloaded hearts in the setting of genetic deletion of the adenosine A2A receptor. By supporting the results obtained from echocardiography experiments, this dataset provides additional evidence for the crucial role of the adenosine A2A receptor in the formation of the cardiac phenotype in response to aortic banding.

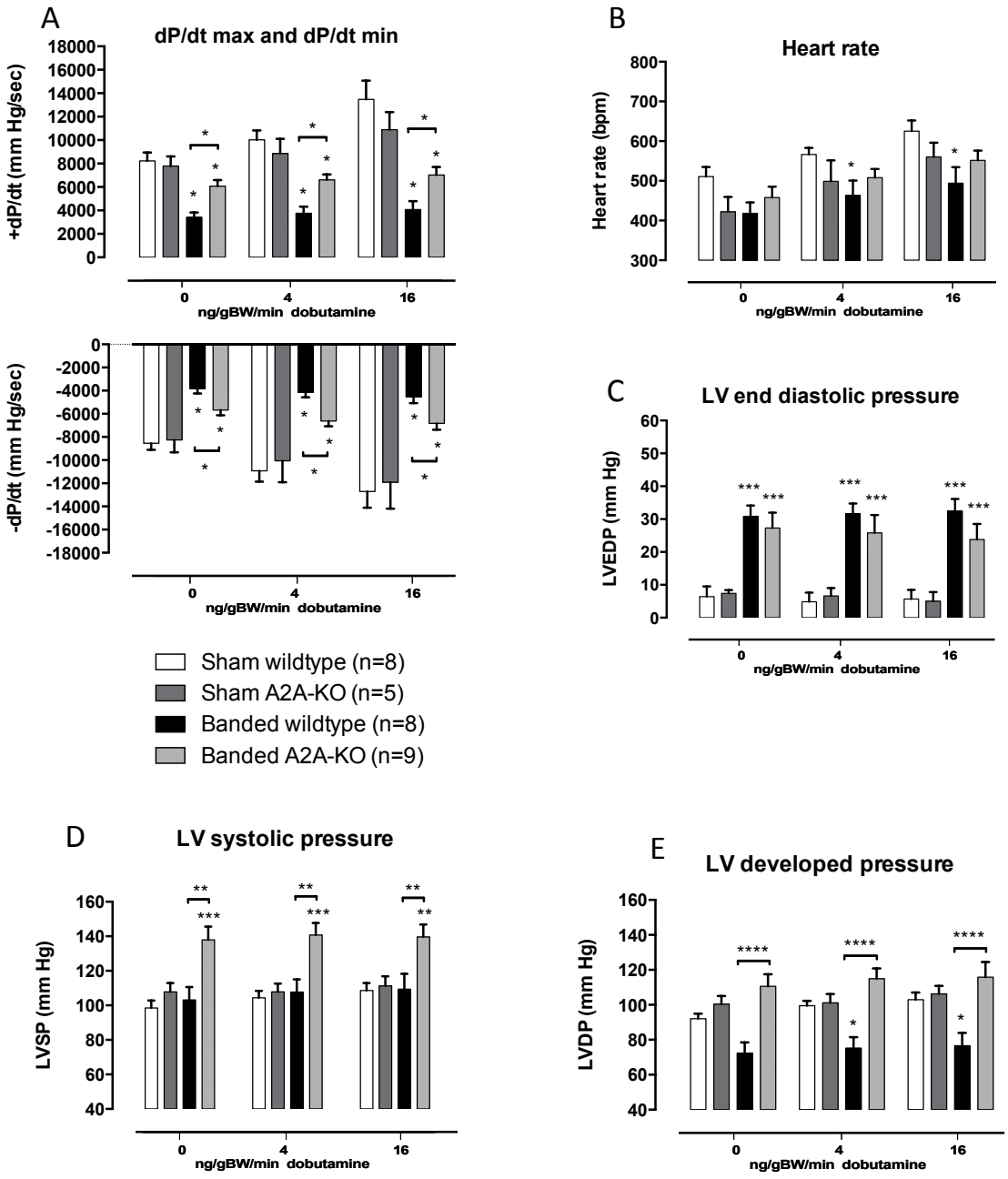


**Figure 5.5:** In order to further delineate myocardial function, invasive haemodynamic measurements of left ventricular pressures were conducted. (*A*) Maximal pressure increase rates (dP/dt max) were significantly reduced in both banded A2AR WT and A2AR KO hearts compared to sham operated A2AR WT hearts. However, banded A2AR KO hearts demonstrated significantly higher pressure increase rates than banded A2AR WT animals. Similarly, the minimal rate of diastolic pressure decrease (dP/dt min) was significantly worse in banded A2AR WT and A2AR KO animals compared to sham operated A2AR WT animals. Banded A2AR KO animals demonstrated significantly improved rates of diastolic left ventricular pressure decrease.. (*B*) No significant differences in heart rate were found between any of the groups, at baseline measurements, whereas upon dobutamine infusion the heart rates of banded A2AR WT animals were significantly reduced. (*C*) Both banded A2AR WT and KO hearts demonstrated increased diastolic left ventricular pressures. (*D&E*) Left ventricular systolic pressures revealed markedly superior systolic function in banded A2AR KO hearts.. (*D*) The maximal systolic left ventricular pressures of banded A2AR KO hearts were significantly increased compared to sham operated animals as well as banded A2AR WT animals ($p$<0.001 and $p$<0.01, respectively). (*E*) Accordingly, the left ventricular developed pressures of banded A2AR KO hearts was significantly higher than that of banded A2AR WT hearts ($p$<0.0001).

### 5.3 Treatment of pressure overloaded hearts with the adenosine A2A receptor inhibitor ZM-241385

As described above, the genetic deletion of the adenosine A2A receptor prevents the formation of myocardial fibrosis, with a corresponding compensation of cardiac function. Pharmacologic experiments, aiming to inhibit adenosine A2A receptor activation in TAC animals were conducted in order to further validate the findings from genetic deletion experiments. While full rescue of the cardiac actin E99K mouse model by pharmacologic treatment was impeded by an early onset of the cardiac phenotype, the treatment of TAC animals could be initiated at the time of operation. This mitigated the possibility of a cardiac phenotype developing before treatment initiation. As a result, the hypothesis of this experiment was that pharmacologic inhibition of the adenosine A2A receptor would inhibit the formation of myocardial fibrosis. In order to address this question, pressure overloaded animals were treated with the specific adenosine A2A receptor inhibitor ZM-241385. Starting on the day of transverse aortic constriction, at 9 weeks of age, a treatment regimen consisting of twice daily intra-peritoneal injections of ZM-241385 diluted in PBS (+15% DMSO & 15% Cremophor) was initiated. As controls , vehicle injected banded animals were used, resulting in two treatment groups:

1. Transverse aortic constriction (TAC), vehicle treatment (N=6)
2. Transverse aortic constriction (TAC), ZM-241385 treatment (N=5)

Treatment was continued for five weeks of daily injections followed by phenotyping with echocardiography during week four. At the end of the treatment period, invasive haemodynamic measurements followed by organ harvest were conducted and tissue analysis (i.e. the measurement of hydroxyproline and microscopy) was carried out.

### 5.3.1 Changes in morphometric measurements

As part of the investigation into the effect of pharmacologic adenosine A2A receptor inhibition on the cardiac phenotype caused by aortic banding, morphometric measurements were carried out. Absolute and normalized organ weights, body weight and tibia were evaluated in vehicle and ZM241385 treated banded animals.

Body weight measurements revealed no significant difference between ZM241385 and vehicle treated mice. In addition, no significant difference was found in tibial length between any of the treatment groups. The average heart weight of ZM241385 treated TAC mice was significantly ($p<0.05$) reduced compared to the heart weights of banded vehicle treated animals. ZM241385 treatment of banded animals was also associated with a reduction in average lung weight compared to vehicle treated animals, although this did not reach statistical significance. No significant difference was found in liver weights between the two treatment groups (Figure 5.6, *A* - *E*).

Normalization of heart, lung and liver weights to tibia length demonstrated similar findings. The average normalized heart weight of ZM241385 treated banded mice was significantly reduced, compared to the average normalized heart weight of vehicle treated mice. Normalized lung weights were not significantly different in banded vehicle treated animals compared to ZM241385 treated TAC animals. However, a non-significant trend towards a reduction in the normalized lung weight of banded ZM241385 treated animals was observed. Average normalized liver weights of ZM241385 treated, banded animals were not significantly different from vehicle treated TAC animals (Figure 5.6, *F* - *H*).

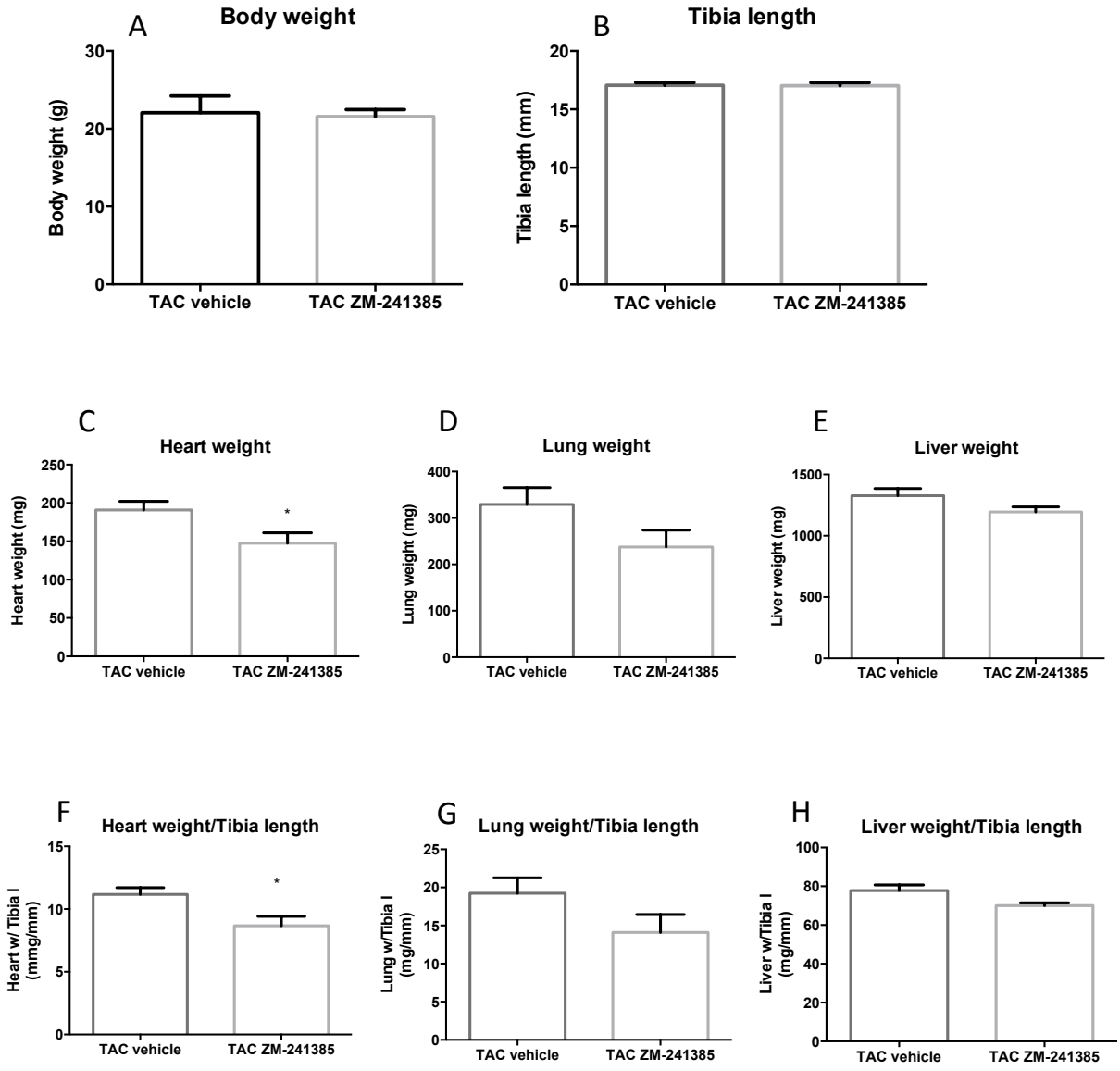


**Figure 5.6:** Morphometric measurements of absolute and normalized organ weights and tibia length. Body weight (*A*) and tibia length (*B*) measurements revealed no significant differences between ZM241385 and vehicle treated TAC mice. (*C*) The average heart weight of ZM241385 treated TAC mice was significantly ($p<0.05$) reduced compared to the heart weights of vehicle treated TAC animals. ZM241385 treatment of banded animals induced a reduction in average lung weight compared to vehicle treated animals, although this did not reach statistical significance (*D*). No significant difference was found in liver weights between the two treatment groups (*E*). The average normalized heart weight of ZM241385 treated banded mice was significantly reduced, compared to the average normalized heart weight of vehicle treated TAC mice (*F*). Normalized lung weights were not significantly different in banded vehicle treated animals compared to ZM241385 treated TAC animals. (*G*). Average normalized liver weights of ZM241385 treated, banded animals were not significantly different from vehicle treated TAC animals (*H*).

### 5.3.2 Changes in myocardial collagen and cardiac fibrosis

Evaluation of myocardial fibrosis was carried out to investigate whether pharmacologic inhibition of the adenosine A2A receptor resulted in modification of the fibrotic phenotype of TAC hearts.

Total collagen content measurements from left ventricular tissue aliquots revealed that ZM241385 treated TAC animals had a significant ($p<0.05$) decrease in myocardial collagen content compared to vehicle treated animals (Figure 5.7).

In addition, histologic examination using Sirius-red stained tissue sections revealed marked interstitial myocardial fibrosis in the cardiac tissue of vehicle treated, TAC animals.. Compared to these hearts, those from ZM241385 treated, TAC animals demonstrated markedly reduced interstitial myocardial fibrosis (Figure 5.7).

Semiautomatic computational quantification of the Sirius-red signal normalized to total tissue area, revealed a significantly ($p<0.0001$) reduced fibrosis signal in hearts of banded, ZM241385 treated animals compared to vehicle treated TAC animals (Figure 5.7).

These results suggest that the adenosine A2A receptor mediated pro-fibrotic effect is susceptible to pharmacologic intervention and therefore constitutes a potentially promising target for pharmacologic modulation of fibrosis formation in response to cardiac pressure overload.

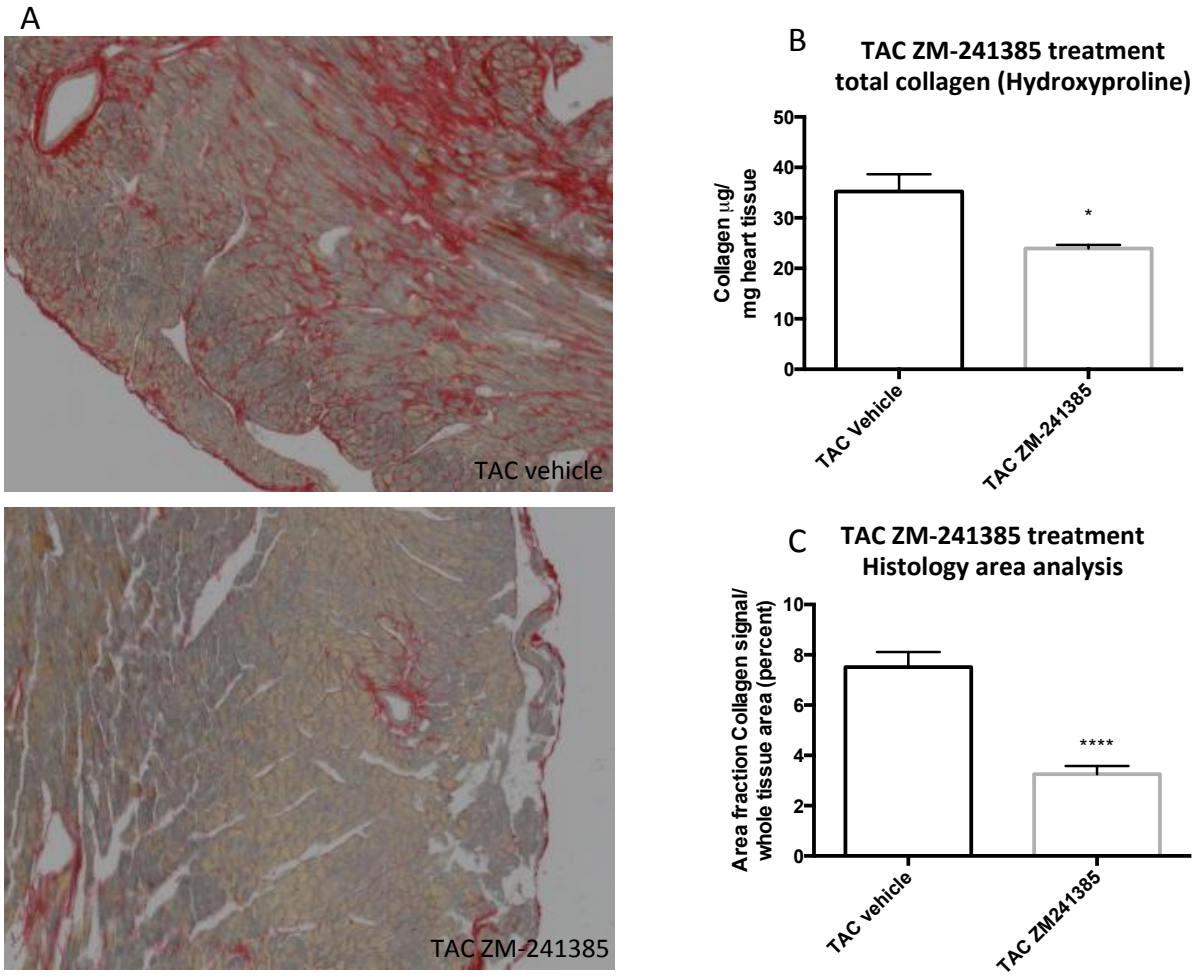


**Figure 5.7:** Evaluation of the fibrotic phenotype. (*B*) Hydroxyproline measurements showed a significant ($p<0.05$) decrease in the myocardial collagen content of ZM241385 treated TAC animals compared to vehicle treated animals. (*A*) Histologic examination (using Sirius-red staining) revealed marked myocardial fibrosis in the hearts of vehicle treated, TAC animals (top image). Compared to that ZM241385 treated TAC animals (bottom image) demonstrated markedly reduced interstitial myocardial fibrosis. Computational quantification (*C*) of Sirius-red signal revealed significantly ($p<0.0001$) reduced fibrosis in hearts of banded ZM241385 treated animals compared to vehicle treated banded animals.

### 5.3.3 Changes in cardiac function on echocardiography

Echocardiography was carried out in order to delineate the effect of ZM241385 treatment on the cardiac function of TAC animals.

Evaluation of left ventricular systolic function did not reveal a statistically significant difference between vehicle treated and ZM241385 treated TAC animals. Upon evaluation of fractional area change, a two dimensional marker for systolic function, a trend towards improved systolic function was observed, however this did not reach statistical significance (Figure 5.8, *A* - *C*).

Calculation of left ventricular mass from echocardiographic images revealed no significant difference in cardiac hypertrophy between ZM241385 and vehicle treated TAC animals on echocardiography. In addition, vehicle treated TAC animals did appear more dilated on echocardiography, compared to ZM241385 treated animals. While the reduction of left ventricular systolic volume did not reach statistical significance, the left ventricular end-diastolic volume was significantly ($p<0.05$) reduced in ZM241385 treated TAC hearts compared to vehicle treated controls (Figure 5.8, *D* - *F*).

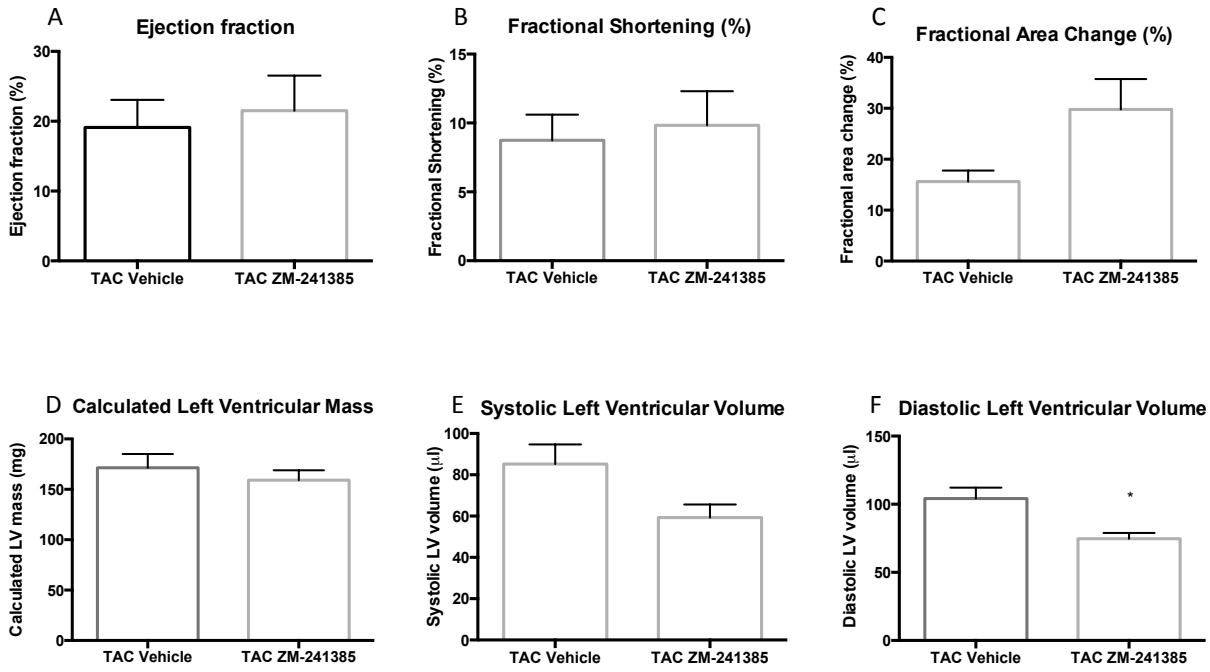


**Figure 5.8:** Echocardiographic investigations were carried out in order to delineate the effect of ZM241385 treatment on the cardiac function of TAC animals. (*A-C*) Evaluation of left ventricular systolic function did not reveal a statistically significant difference between vehicle and ZM241385 treatment. (*C*) Fractional area change demonstrated a non-significant trend towards improved systolic function... (*D*) The calculated left ventricular mass revealed no significant difference in cardiac hypertrophy between ZM241385 and vehicle treated TAC animals... (*E&F*) Vehicle treated TAC animals more dilated on echocardiography, compared to ZM241385 treated animals. The reduction of left ventricular systolic volume (*E*) did not reach statistical significance, however the diastolic left ventricular volume (*F*) of ZM241385 treated TAC hearts was significantly ($p<0.05$) reduced compared to vehicle treated controls.

### 5.3.4 Changes in cardiac function in invasive haemodynamic measurements

In order to further delineate the effect of pharmacologic adenosine A2A receptor inhibition on the myocardial function of TAC hearts, haemodynamic measurements of were conducted. In order to investigate basic cardiac function as well as the chronotropic and inotropic reserve intra-ventricular pressures were measured at baseline and during the continuous infusion of two increasing dobutamine dosages (4 and 16 ng/gBW/minute).

No significant difference was found in the average maximal pressure increase rate between all the pharmacological treatment groups. Similarly, the minimal rate of diastolic pressure decrease was not significantly altered between the two treatment groups. Also, no significant change in heart rate was found between the vehicle treated and ZM241385 treated groups. All treatment groups demonstrated a dose dependent increase in heart rate upon continuous dobutamine infusion.

In addition, left ventricular diastolic as well as the left ventricular developed and maximal systolic pressures were not significantly altered between vehicle and ZM241385 treated TAC.

In conclusion, the treatment of TAC hearts with the adenosine A2A receptor antagonist ZM241385 did not demonstrate a significant effect on left ventricular haemodynamics.

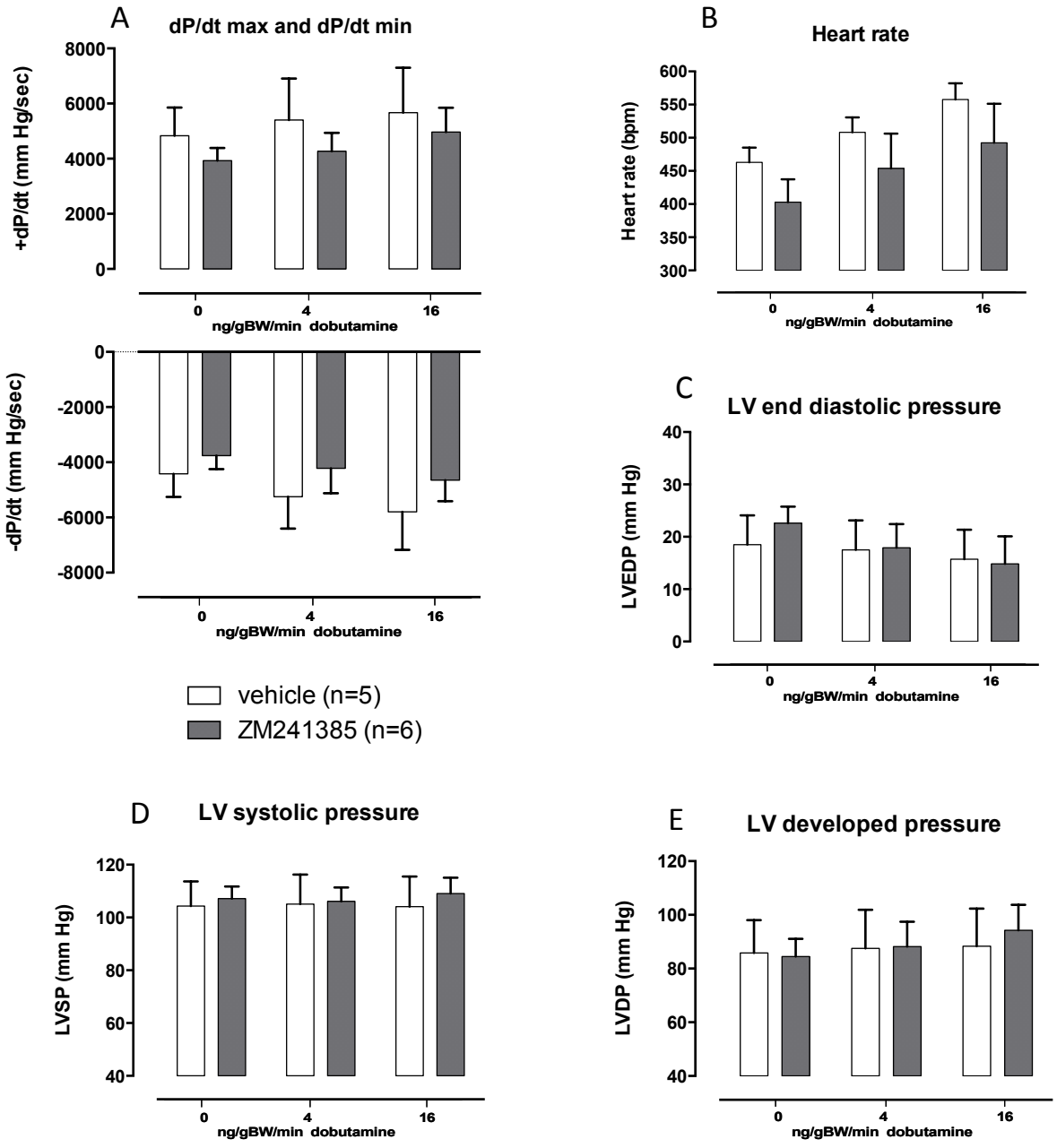


**Figure 5.9:** Haemodynamic measurements of left ventricular pressures. Intra-ventricular pressures were measured at baseline and during increasing dosages (4 and 16 ng/gBW/minute) of dobutamine infusion. (*A*) No significant difference was found in the maximal pressure increase rates (dP/dt max) the pharmacological treatment groups. Similarly, the minimal rate of diastolic pressure decrease (dP/dt min) was not significantly altered between the treatment groups. (*B*) No significant change in heart rate was found between the vehicle treated and ZM241385 treated groups, all groups demonstrated a dose dependent increase in heart rate upon dobutamine infusion. (*C-E*) Left ventricular diastolic, developed and maximal systolic pressures were unchanged between vehicle treated and ZM241385 treated TAC hearts.

## 5.4 Discussion

### 5.4.1 Primary conclusions of Results chapter three

1. Transverse aortic banding leads to significant and consistent development of myocardial fibrosis and cardiac hypertrophy in control animals.

2. Genetic loss of the adenosine A2A receptor did not demonstrate a significant effect on sham-operated animals.

3. Genetic deletion of the adenosine A2A receptor significantly reduced the formation of myocardial fibrosis in response to aortic banding.

4. The reduction in myocardial fibrosis was associated with marked preservation of systolic and diastolic cardiac function.

5. Pharmacologic inhibition of the adenosine A2A receptor significantly reduced the development of cardiac fibrosis caused by TAC.

### 5.4.2 Summary of chapter findings and resulting conclusions – genetic experiment

The principal objective of this experiment was to delineate the effect of genetic loss of the adenosine A2A receptor on the cardiac phenotype of mice undergoing TAC surgery. As delineated in the previous results chapter, the genetic loss of the adenosine A2A receptor resulted in a marked reduction of cardiac fibrosis in the cardiac actin E99K mouse model for hypertrophic cardiomyopathy. In addition, the reduction of myocardial fibrosis in actin E99K hearts was associated with a significant improvement of contractile cardiac function and reduced pulmonary congestion. The primary hypothesis of the experiments described in this chapter was that the findings relating to the role of adenosine signalling in the induction of myocardial fibrosis in actin E99K hearts would be equally applicable to an acquired (pressure-overload) model of myocardial fibrosis. In order to address this question, aortic banding operations were conducted on adenosine A2AR KO mice and compared to banded adenosine A2AR WT animals.

The cardiac phenotype ensuing upon transverse aortic constriction is characterized by the development of hypertrophic and fibrotic changes and the eventual progression to frank heart failure (K. T. Weber et al., 1988; Ying et al., 2009). As a result, the TAC mouse model was considered an appropriate model to investigate the role of adenosine A2A receptor signalling as a key pathway in myocardial fibrosis formation.

Four experimental groups of animals were produced in this experiment, sham operated A2AR WT mice, sham operated A2AR KO mice, banded A2AR WT mice, and banded A2AR KO hearts. Banded A2AR WT animals developed a consistent

clear hypertrophic and fibrotic phenotype, that reflected the phenotype described in publications (Moens et al., 2008; Ying et al., 2009). In addition the hearts of banded A2AR WT mice were characterized by a marked reduction of systolic function on echocardiography, in addition to systolic and diastolic dysfunction upon haemodynamic measurement of left ventricular pressures. Banded A2AR KO animals demonstrated markedly less interstitial cardiac fibrosis compared to banded A2AR WT animals. This was evidenced by a reduction of myocardial collagen content upon hydroxyproline measurement as well as upon histologic examination.

Interestingly, the reduction of myocardial fibrosis in banded A2AR KO hearts was not associated with a reduction in cardiac hypertrophy. Both absolute and normalized heart weights were significantly increased in A2AR WT and KO hearts and did not differ significantly between these two groups. The fact that both banded A2AR WT and KO animals developed marked cardiac hypertrophy indicates that the stimulus caused by the aortic banding operation was similar in these two groups.

The reduction of myocardial fibrosis in banded A2AR KO hearts was associated with a significant improvement of myocardial function, compared to banded A2AR WT hearts. This was demonstrated by echocardiographic investigation as well as by left ventricular haemodynamic pressure measurements. At echocardiography, banded A2AR WT hearts appeared dilated and functionally decompensated, which was reinforced by findings of decreased left ventricular systolic and developed pressures. Conversely, the hearts of banded A2AR KO animals demonstrated lower left ventricular volumes and better systolic function. Accordingly, invasive haemodynamic measurements revealed compensated systolic function of banded A2AR KO animals.

Indeed, the maximal systolic pressure of banded A2AR KO animals was increased beyond the levels of sham operated control animals, to the extent that left ventricular developed pressure levels were comparable to those of sham operated animals.

Conversely to the pronounced rescue effect observed in systolic parameters between banded A2A WT and KO hearts, end diastolic pressures did not differ significantly between these two groups. While the rate of diastolic relaxation (dP/dtmin) was significantly improved in banded A2A KO hearts, indicating faster diastolic relaxation, the diastolic filling pressures were not significantly improved. This data generally indicates that the rescue effect conferred by the abrogation of the adenosine A2A receptor is more prominent in systolic than diastolic parameters. However, volume parameters, in particular end-diastolic volumes were not investigated during the haemodynamic investigations, which could have potentially elucidated a rescue effect in diastolic parameters further.

Sham operated A2AR KO animals did not demonstrate significant differences to sham operated A2AR WT animals in any of the experiments aiming to delineate the phenotype of these animals. This suggests that the role of the adenosine A2A receptor is limited in such relatively unchallenged hearts.

In conclusion, these results indicate a crucial role of the adenosine A2A receptor in the formation of myocardial fibrosis caused by pressure overload. Furthermore, in combination with the results of the previous chapter these findings indicate a conserved role for the adenosine A2A receptor in myocardial fibrosis formation. Thus, the genetic deletion of the adenosine A2A receptor demonstrated a similar

protective effect on a disease model caused by a sarcomeric mutation and in a cardiac pressure overload model. These two findings potentially indicate that the adenosine A2A receptor constitutes a crucial signalling mechanism in the formation of myocardial fibrosis in a range of cardiac pathologies, in particular in combination with cardiac hypertrophy.

In addition, the observed reduction of myocardial fibrosis in banded A2AR KO hearts was associated with markedly improved systolic and diastolic cardiac function. The association of cardiac dysfunction and myocardial fibrosis has been commonly observed (Kong et al., 2014). In particular myocardial fibrosis is believed to play an important role in the development of diastolic dysfunction (Kai, Kuwahara, Tokuda, & Imaizumi, 2005). However, as far as systolic dysfunction is concerned, a clear causal connection between fibrosis and dysfunction has not been described in the literature. As described in the previous results chapter, a potential contributing factor to the development of systolic dysfunction is the encasement of individual or groups of cardiomyocytes by a thickened layer of endomysial collagen (LeGrice et al., 2012). Immunofluorescence experiments revealed a marked increase in endomysial collagen signal in banded A2AR WT animals, which was observed to be less prominent in banded A2AR KO animals. This finding demonstrates an association of systolic dysfunction and thickening of the endomysial collagen layer. Even though this does not provide evidence for a causal connection, it supports the possibility of a role for endomysial collagen in systolic dysfunction.

Finally, analogous to the crossbreeding experiment performed between cardiac actin E99K and A2AR KO animals, the systemic nature of the adenosine A2A receptor

knock out used in the animals undergoing TAC surgery is a potential cause for criticism. The adenosine A2A receptor targeted in this experiment is not specifically deleted in cardiac fibroblasts, but in all cells. As a result a definite conclusion that the prevention of the fibrotic phenotype is mediated via cardiac fibroblasts cannot be drawn. However, the myocardial collagen content and myocardial fibrosis in banded A2AR KO hearts is almost normalized to the levels of sham operated animals. In addition, cardiac hypertrophy was unaltered between A2AR WT and KO animals. As a result, cardiomyocytes are less likely than cardiac fibroblasts to be the primary effector cell population mediating the effect of the adenosine A2AR KO. This is further supported by the published description that a cardiomyocyte-specific up-regulation of the adenosine A2A receptor has a *protective* effect on TAC animals (Hamad et al., 2012). Further studies will be needed to characterize the seemingly divergent effects of cardiomyocyte and fibroblast adenosine A2A receptor signalling in the heart.

### 5.4.3 Summary of chapter findings and resulting conclusions – pharmacologic experiment

The genetic deletion of the adenosine A2A receptor demonstrated a clear protective effect on the fibrotic phenotype of TAC hearts. In order to investigate whether this effect can be replicated by pharmacologic intervention, a treatment study on TAC hearts was carried out using the adenosine A2A receptor antagonist ZM241385. As described in the previous results chapter, pharmacologic intervention aiming to modulate the phenotype of a genetic mouse model can be limited by the early development of the phenotype. In contrast, in the case of aortic banding, pharmacologic intervention can be initiated at the time of the operation, obviating the risk of development of an abnormal cardiac phenotype before pharmacologic treatment.

To investigate whether pharmacologic adenosine A2A receptor inhibition modulates the fibrotic phenotype of TAC operated mice, TAC operated mice were allocated to either a ZM241385 treatment group or a vehicle treated control group. As described in the previous results chapter, ZM241385 treatment did not demonstrate an effect on cardiac actin WT animals. Accordingly, the generation of sham-operated treatment controls was not deemed justified from a welfare perspective.

Vehicle treated TAC animals developed cardiac hypertrophy as well as clear myocardial fibrosis. Upon ZM241385 treatment, banded animals developed significantly less myocardial fibrosis as evidenced by both myocardial collagen content and histologic examination. This indicated that adenosine A2A receptor signalling is in principal susceptible to pharmacologic modulation. Investigation of left ventricular contractile function did not, however, demonstrate a clear difference

between ZM241385 and vehicle treated animals. At echocardiography upon measurement of the fractional area change, there was a non-significant trend towards an improvement in the left ventricular systolic function of ZM241385 treated animals. In addition, the hearts of ZM241385 treated TAC mice appeared less dilated on echocardiography, supported by the finding of significantly reduced left ventricular end-diastolic volume compared to vehicle treated animals. While these are indicators of a mild improvement of cardiac function, invasive left ventricular pressure measurements did not reveal a significant difference in myocardial function in terms of invasive pressures, between ZM241385 and vehicle treated TAC animals.

Surprisingly, the change in heart rate, observed in ZM241385 treated actin WT and E99K animals, was not found in ZM241385 treated TAC animals. TAC mice have been shown to exhibit a progressive decline in heart rate over time after banding (Sedej et al., 2014). As a result, the increasing effect on heart rate conferred by ZM241385 treatment could be negated in TAC animals by a general heart rate lowering mechanism. In addition, haemodynamic measurements are not optimised to investigate intrinsic heart rates as the necessity for deep anaesthesia and the possibility of blood loss during surgical preparation can alter heart rates. Other investigations, such as electrocardiograms on conscious or lightly anaesthetized mice and the delineation of intrinsic heart rates in Langendorff perfused hearts would be required to obtain a definite result on the effects of adenosine A2A receptor signalling on heart rates.

In conclusion, this experiment demonstrated a significant reduction of myocardial fibrosis in ZM241385 treated TAC hearts compared to vehicle treated hearts.

However the marked improvement of cardiac function observed in banded A2AR KO animals was not reproduced by pharmacologic adenosine A2A receptor inhibition. This apparent discrepancy can potentially be explained by a weaker inhibitory effect of the pharmacologic antagonist compared to a genetic deletion. The utilized pharmacologic agent ZM241385 was characterized by very poor solubility. As a result, even though the drug solution was made up freshly every 48 hours, precipitation of the drug during storage as well as within the peritoneal cavity could not be excluded for certain. Therefore the continuous maintenance of sufficient inhibitor levels cannot be guaranteed. Furthermore, another possibility is that the pharmacologic inhibitor affected different cell populations differently to the genetic KO. Cardiomyocyte specific up-regulation of the adenosine A2A receptor has demonstrated a protective effect on a TAC mouse model (Hamad et al., 2012). Accordingly, it is theoretically possible that pharmacologic inhibition of the adenosine A2A receptor on cardiomyocytes partially cancels out the beneficial effect of a reduction of myocardial fibrosis. Further pharmacologic studies are required in order to pinpoint the effect of pharmacologic adenosine A2A receptor inhibition on different myocardial cell populations and to define an optimal pharmacologic agent.

# 6. General Discussion

The thesis in hand focused on the description of myocardial fibrosis and the mechanisms initiating the formation of myocardial fibrosis. The specific hypothesis of this project was that myocardial interstitial adenosine is up-regulated in times of metabolic stress as an autocrine and paracrine danger signal. Interstitial adenosine, as in other tissues, stimulates neighbouring fibroblasts via adenosine A2A receptor activation.

In order to address this hypothesis, the fibrotic phenotype of five genetic mouse models of inherited cardiomyopathy was delineated. Interestingly, even though all these models had been described as developing myocardial fibrosis in the literature, they demonstrated vastly different fibrotic phenotypes. This finding provides evidence that the current binary fashion in which cardiac fibrosis is typically described in scientific publications falls short to describe the heterogeneous nature of fibrotic lesions. These descriptive experiments were conducted to gain insight into the different patterns of myocardial fibrosis formation in different murine models. On the other hand, they also served as screening experiments aiming to find a mouse model with a consistent and pronounced fibrotic phenotype.

From these screening experiments emerged the transgenic cardiac actin E99K model that developed a clear and consistent fibrotic phenotype. The cardiac actin E99K model can also be considered as representative for the human disease, as it recapitulates the phenotype of human mutation carriers. As a result the cardiac actin E99K mouse model was chosen for further descriptive experiments and for subsequent rescue experiments. The detailed description of the cardiac actin E99K

mouse model demonstrated marked architectural, cellular and functional abnormalities. A significant increase in cardiac fibroblast numbers as well as a significantly thicker endomysial collagen layer was associated with a striking reduction in myocardial function. Furthermore, this fibrotic phenotype was also associated with a significant disruption of myocardial energetics, evidenced by a reduced PCr to ATP ratio upon nuclear magnetic resonance spectroscopy. In addition, interstitial adenosine levels measured by microdialysis correlated significantly with myocardial collagen content in cardiac actin E99K hearts. These experiments were descriptive in nature and did not provide evidence of a causal connection between adenosine and myocardial fibrosis. However the aforementioned results do support the hypothesis that in metabolically stressed hearts adenosine can contribute to myocardial fibrosis formation.

In order to provide evidence of a causal connection between adenosine A2A receptor signalling and myocardial fibrosis formation cellular stimulation experiments and *in vivo* inhibition experiments were conducted.

Cardiac fibroblasts, isolated and cultured from neonatal as well as adult murine hearts, demonstrated a significant up-regulation of collagen production upon stimulation with a specific adenosine A2A receptor agonist. Further, addition of a specific adenosine A2A receptor inhibitor abrogated the stimulatory response. These *in vitro* experiments provided proof of principle that the activation of adenosine A2A receptor signalling activates cardiac fibroblasts to increase collagen production or secretion.

This was further investigated by *in vivo* experiments aiming to inhibit adenosine receptor signalling. Crossbreeding experiments between cardiac actin E99K and adenosine A2AR KO animals were conducted. The results of phenotyping experiments on the resulting intercrossed animal cohorts demonstrated that a genetic deletion of the A2A receptor results in a significant reduction of myocardial fibrosis in cardiac actin E99K hearts. This reduction in myocardial fibrosis was associated with a corresponding improvement of cardiac function, indicated by improved pressures on left ventricular haemodynamic investigation. This data provides evidence that the adenosine A2A receptor plays a decisive role in the formation of myocardial fibrosis in a mouse model for hypertrophic cardiomyopathy.

Next, the question whether the role of adenosine A2A receptor signalling was limited to our model for hypertrophic cardiomyopathy, or represented a key node in a conserved pathophysiological pathway contributing to several cardiac pathologies, was addressed. In order to answer this question, A2AR KO mice underwent aortic banding operations in order to develop a pressure overload induced cardiac phenotype, which includes myocardial fibrosis. Banded A2AR KO animals developed markedly reduced myocardial fibrosis, which was again associated with a significant rescue of cardiac function, on echocardiography and invasive measurement of haemodynamics. This recapitulated the findings from cardiac actin E99K, adenosine A2AR KO crossbreeding experiments, as it indicated the crucial role of the adenosine A2A receptor in the formation of cardiac fibrosis. Further, the pronounced improvement of cardiac function caused by the loss of the adenosine A2A receptor reiterated the findings from cardiac actin E99K hearts. These results provide evidence that the role of the adenosine A2A receptor in the formation of myocardial

fibrosis is not only limited to hypertrophic cardiomyopathy, but extends to another clinically relevant model of myocardial fibrosis and cardiac hypertrophy, i.e. pressure overload.

Finally, the potential for pharmacologic modulation of myocardial fibrosis by targeting adenosine A2A receptor signalling was investigated. To test the hypothesis that pharmacologic inhibition of the adenosine A2A receptor would replicate the findings from the genetic ablation experiment, actin E99K as well as TAC animals were treated with a specific A2A receptor antagonist. Treatment with the pharmacologic A2A receptor antagonist did result in a significant reduction of myocardial fibrosis in both models of cardiac fibrosis. However, the corresponding improvement of myocardial function was less pronounced than that caused by the genetic deletion of adenosine A2A receptors. This indicates on the one hand that the adenosine A2A receptor pathway is susceptible to pharmacologic intervention, and on the other that the formation of myocardial fibrosis can be prevented by such an approach. Even though the drug treatment experiment did not fully recapitulate the very marked functional results observed in the genetic studies, the treatment effect was promising. In addition, the pharmacologic studies conducted on both actin E99K and TAC animals were potentially underpowered to demonstrate a functional rescue effect and will require additional experiments to allow for definite results.

Adenosine A2A receptor manipulation may contribute to further understanding of pathophysiological pathways in the development and progression of cardiac disease. Further, the results of this study suggest that the adenosine A2A receptor represents an excellent therapeutic target. Of note, new A2A receptor antagonists are currently

being developed, for example for the treatment of neurological diseases such as Parkinson disease, and so will be available clinically.

## 6.1 Future directions

While much evidence has been obtained that indicates the role of the adenosine A2AR in MF formation, a definitive confirmation on the source of its ligand adenosine requires further study. Accordingly, further experiments are planned aiming to further delineate the primary source and effect of interstitial adenosine.

The ecto-nucleotidases, CD39, which hydrolyses ATP to AMP, and CD73, which hydrolyses AMP to adenosine, are believed to be crucial regulators of adenosine concentrations in the interstitial myocardium and therefore of adenosine signalling (Bönner et al., 2012). To delineate the role of CD39 and CD73 in the actin E99K and the TAC mouse models, pharmacologic inhibition experiments will be conducted. The well described CD39 inhibitor sodium polyoxotungstate (Grenz et al., 2007; Müller et al., 2006) will be used in TAC experiments and on E99K mice, compared to vehicle control and the effects on the phenotype of these models and in particular on MF will be investigated. In addition, the specific CD73 inhibitor, adenosine 5'-(α,β-methylene)diphosphate (APCP) (Synnestvedt et al., 2002) will be similarly used to evaluate the role of CD73 in TAC and in cardiac actin E99K mice.

In addition, Panx-1 channels are believed to be a major source of extracellular nucleotides in the myocardium (Dolmatova et al., 2012). In order to delineate the role of Panx-1 in MF, pharmacologic inhibition experiments using probenecid, which has been shown to inhibit Panx-1 channels (Silverman, Locovei, & Dahl, 2008), will be conducted.

These experiments aim to pinpoint crucial effectors regulating adenosine

concentration in the myocardium.

Further, as already discussed above a potential criticism of the genetic ablation experiments in this investigation is that the deletion of the adenosine A2A receptor is systemic rather than a cell specific conditional knock out in myocardial fibroblasts. However, the cardiomyocyte specific up-regulation of the adenosine A2A receptor conferred a beneficial effect on a TAC model of cardiac hypertrophy and fibrosis (Hamad et al., 2012). Further, the heterogeneity of the CF population (Krenning et al., 2010) makes the choice of a Cre recombinase mouse line encompassing the majority of CFs fairly difficult. However, Takeda et al. could demonstrate a CF specific Krüppel-like factor 5 deletion using a periostin-cre line (Takeda et al., 2010). Accordingly, we are currently planning to attempt generating a conditional adenosine A2AR KO mouse by crossing a mouse line with a “floxed” adenosine A2AR (Bastia et al., 2005) with the periostin-cre line. The resulting potentially fibroblast specific conditional adenosine A2A receptor knockout mice will then undergo TAC in order to investigate its effect on MF.

Finally, as described above, several drugs targeting the adenosine A2AR are currently being developed and have gone through Phase I-III studies for the treatment of Parkinson’s disease. These drugs potentially represent good candidates for repositioning as modulators of MF. Non-invasive technologies for potential endpoint investigations of MF, particularly MRI technologies such as late gadolinium enhancement and T1-mapping have been developed and are available in Oxford. As a result the initiation of a clinical trial using these agents is currently being considered.

## Bibliography


Abrahams, C., Janicki, J. S., & Weber, K. T. (1987). Myocardial hypertrophy in Macaca fascicularis. Structural remodeling of the collagen matrix. *Laboratory Investigation*, *56*(6), 676–83.

Acton, S. E., Astarita, J. L., Malhotra, D., Lukacs-Kornek, V., Franz, B., Hess, P. R., … Turley, S. J. (2012). Podoplanin-rich stromal networks induce dendritic cell motility via activation of the C-type lectin receptor CLEC-2. *Immunity*, *37*(2), 276–89. doi:10.1016/j.immuni.2012.05.022

Adam, O., Theobald, K., Lavall, D., Grube, M., Kroemer, H. K., Ameling, S., … Laufs, U. (2011). Increased lysyl oxidase expression and collagen cross-linking during atrial fibrillation. *Journal of Molecular and Cellular Cardiology*, 1–8. doi:10.1016/j.yjmcc.2010.12.019

Aksentijević, D., Lygate, C. a, Makinen, K., Zervou, S., Sebag-Montefiore, L., Medway, D., … Neubauer, S. (2010). High-energy phosphotransfer in the failing mouse heart: role of adenylate kinase and glycolytic enzymes. *European Journal of Heart Failure*, *12*(12), 1282–9. doi:10.1093/eurjhf/hfq174

Alberts, B., Johnson, A., Lewis, J., Raff, M., Roberts, K., & Walter, P. (2002). The extracellular matrix of animals. In *Molecular biology of the cell* (fourth edi., pp. 1090–1113). New York: Garland Science.

Ali, S. R., Ranjbarvaziri, S., Talkhabi, M., Zhao, P., Subat, A., Hojjat, A., … Ardehali, R. (2014). Developmental Heterogeneity of Cardiac Fibroblasts Does Not Predict Pathological Proliferation and Activation. *Circulation Research*. doi:10.1161/CIRCRESAHA.115.303794

Anderson, K. R., Sutton, M. G., & Lie, J. T. (1979). Histopathological types of cardiac fibrosis in myocardial disease. *The Journal of Pathology*, *128*(2), 79–85. doi:10.1002/path.1711280205

Arber, S., Hunter, J. J., Ross, J., Hongo, M., Sansig, G., Borg, J., … Caroni, P. (1997). MLP-deficient mice exhibit a disruption of cardiac cytoarchitectural organization, dilated cardiomyopathy, and heart failure. *Cell*, *88*(3), 393–403. Retrieved from http://www.ncbi.nlm.nih.gov/pubmed/9039266

Arts, T., Costa, K. D., Covell, J. W., & McCulloch, A. D. (2001). Relating myocardial laminar architecture to shear strain and muscle fiber orientation. *American Journal of Physiology. Heart and Circulatory Physiology*, *280*, 2222–2229.

Ashrafian, H., Docherty, L., Leo, V., Towlson, C., Neilan, M., Steeples, V., … Dear, T. N. (2010). A mutation in the mitochondrial fission gene Dnm1l leads to cardiomyopathy. *PLoS Genetics*, *6*(6), e1001000. doi:10.1371/journal.pgen.1001000

Ashrafian, H., Redwood, C., Blair, E., & Watkins, H. (2003). Hypertrophic

cardiomyopathy:a paradigm for myocardial energy depletion. *Trends in Genetics : TIG*, *19*(5), 263–8. doi:10.1016/S0168-9525(03)00081-7

Barasch, E., Gottdiener, J. S., Aurigemma, G., Kitzman, D. W., Han, J., Kop, W. J., & Tracy, R. P. (2011). The relationship between serum markers of collagen turnover and cardiovascular outcome in the elderly: the Cardiovascular Health Study. *Circulation. Heart Failure*, *4*(6), 733–9. doi:10.1161/CIRCHEARTFAILURE.111.962027

Bastia, E., Xu, Y.-H., Scibelli, A. C., Day, Y.-J., Linden, J., Chen, J.-F., & Schwarzschild, M. a. (2005). A crucial role for forebrain adenosine A(2A) receptors in amphetamine sensitization. *Neuropsychopharmacology : Official Publication of the American College of Neuropsychopharmacology*, *30*(5), 891–900. doi:10.1038/sj.npp.1300630

Beer, M., Seyfarth, T., Sandstede, J., Landschütz, W., Lipke, C., Köstler, H., … Neubauer, S. (2002). Absolute concentrations of high-energy phosphate metabolites in normal, hypertrophied, and failing human myocardium measured noninvasively with (31)P-SLOOP magnetic resonance spectroscopy. *Journal of the American College of Cardiology*, *40*(7), 1267–74. Retrieved from http://www.ncbi.nlm.nih.gov/pubmed/12383574

Bing, O., Fanburg, B., Brooks, W., & Matsushita, S. (1978). The Effect of the Lathyrogen Beta-Amino Proprionitrile (BAPN) on the Mechanical Properties of Experimentally Hypertrophied Rat Cardiac Muscle. *Circulation Research*, *43*(4), 632. doi:10.1161/01.RES.43.4.632

Birkler, R. I. D., Støttrup, N. B., Hermannson, S., Nielsen, T. T., Gregersen, N., Bøtker, H. E., … Johannsen, M. (2010). A UPLC-MS/MS application for profiling of intermediary energy metabolites in microdialysis samples--a method for high-throughput. *Journal of Pharmaceutical and Biomedical Analysis*, *53*(4), 983–90. doi:10.1016/j.jpba.2010.06.005

Blair, E., Redwood, C., Ashrafian, H., Oliveira, M., Broxholme, J., Kerr, B., … Watkins, H. (2001). Mutations in the gamma(2) subunit of AMP-activated protein kinase cause familial hypertrophic cardiomyopathy: evidence for the central role of energy compromise in disease pathogenesis. *Human Molecular Genetics*, *10*(11), 1215–20. Retrieved from http://www.ncbi.nlm.nih.gov/pubmed/11371514

Bläsche, R., Ebeling, G., Perike, S., Weinhold, K., Kasper, M., & Barth, K. (2012). Activation of P2X7R and downstream effects in bleomycin treated lung epithelial cells. *The International Journal of Biochemistry & Cell Biology*, *44*(3), 514–24. doi:10.1016/j.biocel.2011.12.003

Bönner, F., Borg, N., Burghoff, S., & Schrader, J. (2012). Resident cardiac immune cells and expression of the ectonucleotidase enzymes CD39 and CD73 after ischemic injury. *PloS One*, *7*(4), e34730. doi:10.1371/journal.pone.0034730

Boor, P., & Floege, J. (2012). The renal (myo-)fibroblast: a heterogeneous group of cells. *Nephrology, Dialysis, Transplantation : Official Publication of the European Dialysis and Transplant Association - European Renal Association*, *27*(8), 3027–36.

doi:10.1093/ndt/gfs296

Borg, T. K., & Caulfield, J. B. (1981). The collagen matrix of the heart. *Federation Proceedings*, *40*(7), 2037–41. Retrieved from http://www.ncbi.nlm.nih.gov/pubmed/7227559

Borrello, M. A., & Phipps, R. P. (1996). Differential Thy-1 expression by splenic fibroblasts defines functionally distinct subsets. *Cellular Immunology*, *173*(2), 198–206. doi:10.1006/cimm.1996.0268

Bours, M. J. L., Swennen, E. L. R., Di Virgilio, F., Cronstein, B. N., & Dagnelie, P. C. (2006). Adenosine 5'-triphosphate and adenosine as endogenous signaling molecules in immunity and inflammation. *Pharmacology & Therapeutics*, *112*(2), 358–404. doi:10.1016/j.pharmthera.2005.04.013

Brilla, C. G. (2000). Aldosterone and Myocardial Fibrosis in Heart Failure. *Herz*, *25*(3), 299–306. doi:10.1007/s000590050024

Brilla, C. G., Zhou, G., Matsubara, L., & Weber, K. T. (1994). Collagen Metabolism in Cultured Adult Rat Cardiac Fibroblasts: Response to Angiotensin II and Aldosterone. *Journal of Molecular and Cellular Cardiology*, *26*, 809–820. Retrieved from http://www.sciencedirect.com/science/article/pii/S0022282884710984

Brown, R. D., Ambler, S. K., Mitchell, M. D., & Long, C. S. (2005). The cardiac fibroblast: therapeutic target in myocardial remodeling and failure. *Annual Review of Pharmacology and Toxicology*, *45*(1), 657–87. doi:10.1146/annurev.pharmtox.45.120403.095802

Camelliti, P., Borg, T. K., & Kohl, P. (2005). Structural and functional characterisation of cardiac fibroblasts. *Cardiovascular Research*, *65*(1), 40–51. doi:10.1016/j.cardiores.2004.08.020

Campanholle, G., Ligresti, G., Gharib, S. a, & Duffield, J. S. (2013). Cellular mechanisms of tissue fibrosis. 3. Novel mechanisms of kidney fibrosis. *American Journal of Physiology. Cell Physiology*, *304*(7), C591–603. doi:10.1152/ajpcell.00414.2012

Chan, E. S. L., & Cronstein, B. N. (2010). Adenosine in fibrosis. *Modern Rheumatology / the Japan Rheumatism Association*, *20*(2), 114–22. doi:10.1007/s10165-009-0251-4

Chan, E. S. L., Fernandez, P., Merchant, a a, Montesinos, M. C., Trzaska, S., Desai, A., … Cronstein, B. N. (2006). Adenosine A2A receptors in diffuse dermal fibrosis: pathogenic role in human dermal fibroblasts and in a murine model of scleroderma. *Arthritis and Rheumatism*, *54*(8), 2632–42. doi:10.1002/art.21974

Chan, E. S. L., Montesinos, M. C., Fernandez, P., Desai, A., Delano, D. L., Yee, H., … Cronstein, B. N. (2006). Adenosine A(2A) receptors play a role in the pathogenesis of hepatic cirrhosis. *British Journal of Pharmacology*, *148*(8), 1144–55. doi:10.1038/sj.bjp.0706812

Chapman, D., Weber, K. T., & Eghbali, M. (1990). Regulation of fibrillar collagen types I

and III and basement membrane type IV collagen gene expression in pressure overloaded rat myocardium. *Circulation Research*, *67*(4), 787–794. doi:10.1161/01.RES.67.4.787

Chen, J. F., Huang, Z., Ma, J., Zhu, J., Moratalla, R., Standaert, D., … Schwarzschild, M. a. (1999). A(2A) adenosine receptor deficiency attenuates brain injury induced by transient focal ischemia in mice. *The Journal of Neuroscience : The Official Journal of the Society for Neuroscience*, *19*(21), 9192–200. Retrieved from http://www.ncbi.nlm.nih.gov/pubmed/19703429

Cho, J. R., Park, S., Choi, B. W., Kang, S.-M., Ha, J.-W., Chung, N., … Rim, S.-J. (2010). Delayed Enhancement Magnetic Resonance Imaging Is a Significant Prognostic Factor in Patients With Non-Ischemic Cardiomyopathy. *Circulation Journal*, *74*(3), 476–483. doi:10.1253/circj.CJ-09-0446

Cohn, J. N., Goldstein, S. O., Greenberg, B. H., Lorell, B. H., Bourge, R. C., Jaski, B. E., … White, B. G. (1998). A dose-dependent increase in mortality with vesnarinone among patients with severe heart failure. *The New England Journal of Medicine*, *339*, 1810–1816. Retrieved from http://www.nejm.org/doi/full/10.1056/NEJM199812173392503

Cohn, J. N., & Tognoni, G. (2001). A RANDOMIZED TRIAL OF THE ANGIOTENSIN-RECEPTOR BLOCKER VALSARTAN IN CHRONIC HEART FAILURE. *New England Journal of Medicine*, *345*(23), 1667–1675. Retrieved from http://www.nejm.org/doi/full/10.1056/nejmoa010713

Costa, K. D., Takayama, Y., McCulloch, A. D., & Covell, J. W. (1999). Laminar fiber architecture and three-dimensional systolic mechanics in canine ventricular myocardium. *American Journal of Physiology. Heart and Circulatory Physiology*, *267*, 595–607. Retrieved from http://ajpheart.physiology.org/content/276/2/H595.short

Crabos, M., Roth, M., Hahn, A. W., & Erne, P. (1994). Characterization of Angiotensin II Receptors in Cultured Adult Rat Cardiac Fibroblasts. Coupling to Signaling Systems and Gene Expression. *Journal of Clinical Investigation*, *93*, 2372–2378. doi:10.1172/JCI117243.ing

Creemers, E. E., & Pinto, Y. M. (2011). Molecular mechanisms that control interstitial fibrosis in the pressure-overloaded heart. *Cardiovascular Research*, *89*(2), 265–72. doi:10.1093/cvr/cvq308

Cronstein, B. N. (2011). Adenosine receptors and fibrosis: a translational review. *F1000 Biology Reports*, *3*(October), 21. doi:10.3410/B3-21

Dobaczewski, M., Chen, W., & Frangogiannis, N. G. (2011). Transforming growth factor (TGF)-β signaling in cardiac remodeling. *Journal of Molecular and Cellular Cardiology*, *51*(4), 600–6. doi:10.1016/j.yjmcc.2010.10.033

Dolmatova, E., Spagnol, G., Boassa, D., Baum, J. R., Keith, K., Ambrosi, C., … Duffy, H. S. (2012). Cardiomyocyte ATP release through pannexin 1 aids in early fibroblast

activation. *American Journal of Physiology. Heart and Circulatory Physiology*, *303*(10), H1208–18. doi:10.1152/ajpheart.00251.2012

Dweck, M. R., Joshi, S., Murigu, T., Alpendurada, F., Jabbour, A., Melina, G., … Prasad, S. K. (2011). Midwall fibrosis is an independent predictor of mortality in patients with aortic stenosis. *Journal of the American College of Cardiology*, *58*(12), 1271–9. doi:10.1016/j.jacc.2011.03.064

Dzeja, P., & Terzic, A. (2009). Adenylate kinase and AMP signaling networks: Metabolic monitoring, signal communication and body energy sensing. *International Journal of Molecular Sciences*, *10*(4), 1729–72. doi:10.3390/ijms10041729

Esposito, a, De Cobelli, F., Perseghin, G., Pieroni, M., Belloni, E., Mellone, R., … Maschio, a Del. (2009). Impaired left ventricular energy metabolism in patients with hypertrophic cardiomyopathy is related to the extension of fibrosis at delayed gadolinium-enhanced magnetic resonance imaging. *Heart (British Cardiac Society)*, *95*(3), 228–33. doi:10.1136/hrt.2008.142562

Fan, D., Takawale, A., Lee, J., & Kassiri, Z. (2012). Cardiac fibroblasts, fibrosis and extracellular matrix remodeling in heart disease. *Fibrogenesis & Tissue Repair*, *5*(1), 15. doi:10.1186/1755-1536-5-15

Frangogiannis, N. G., Dewald, O., Xia, Y., Ren, G., Haudek, S., Leucker, T., … Entman, M. L. (2007). Critical role of monocyte chemoattractant protein-1/CC chemokine ligand 2 in the pathogenesis of ischemic cardiomyopathy. *Circulation*, *115*(5), 584–92. doi:10.1161/CIRCULATIONAHA.106.646091

Fredholm, B. B. (2007). Adenosine, an endogenous distress signal, modulates tissue damage and repair. *Cell Death and Differentiation*, *14*(7), 1315–23. doi:10.1038/sj.cdd.4402132

Germack, R., & Dickenson, J. M. (2005). Adenosine triggers preconditioning through MEK/ERK1/2 signalling pathway during hypoxia/reoxygenation in neonatal rat cardiomyocytes. *Journal of Molecular and Cellular Cardiology*, *39*(3), 429–42. doi:10.1016/j.yjmcc.2005.06.001

Gödecke, S., Stumpe, T., Schiller, H., Schnittler, H.-J., & Schrader, J. (2005). Do rat cardiac myocytes release ATP on contraction? *American Journal of Physiology. Cell Physiology*, *289*, 609–616. doi:10.1152/ajpcell.00065.2005.

Goldsmith, E. C., Hoffman, A., Morales, M. O., Potts, J. D., Price, R. L., McFadden, A., … Borg, T. K. (2004). Organization of fibroblasts in the heart. *Developmental Dynamics : An Official Publication of the American Association of Anatomists*, *230*(4), 787–94. doi:10.1002/dvdy.20095

Grenz, A., Zhang, H., Hermes, M., Eckle, T., Klingel, K., Huang, D. Y., … Eltzschig, H. K. (2007). Contribution of E-NTPDase1 (CD39) to renal protection from ischemia-reperfusion injury. *FASEB Journal : Official Publication of the Federation of American Societies for Experimental Biology*, *21*(11), 2863–73. doi:10.1096/fj.06-7947com

Hagood, J. S., Miller, P. J., Lasky, J. A., Tousson, A., Guo, B., Fuller, G. M., & McIntosh, J. C. (1999). Differential expression of platelet-derived growth factor-α receptor by Thy-1- and Thy-1+ lung fibroblasts. *American of Physiology-Lung*, *277*, L218–L224. Retrieved from http://ajplung.physiology.org/content/277/1/L218.short

Hamad, E. a, Zhu, W., Chan, T. O., Myers, V., Gao, E., Li, X., … Feldman, A. M. (2012). Cardioprotection of controlled and cardiac-specific over-expression of A(2A)-adenosine receptor in the pressure overload. *PloS One*, *7*(7), e39919. doi:10.1371/journal.pone.0039919

Hanley, P. J., Young, A. A., LeGrice, I. J., Edgar, S. G., & Loiselle, D. S. (1999). 3-Dimensional configuration of perimysial collagen fibres in rat cardiac muscle at resting and extended sarcomere lengths. *The Journal of Physiology*, *517 ( Pt 3*, 831–7. Retrieved from http://www.pubmedcentral.nih.gov/articlerender.fcgi?artid=2269383&tool=pmcentrez&rendertype=abstract

Headrick, J. P., Matherne, G. P., & Berne, R. M. (1992). Myocardial Adenosine Formation During Hypoxia: Effects of Ecto-5'-Nucleotidase Inhibition. *Journal of Molecular and Cellular Cardiology*, *303*, 295–303. Retrieved from http://www.sciencedirect.com/science/article/pii/002228289293166H

Heineke, J., Wollert, K. C., Osinska, H., Sargent, M. a, York, A. J., Robbins, J., & Molkentin, J. D. (2010). Calcineurin protects the heart in a murine model of dilated cardiomyopathy. *Journal of Molecular and Cellular Cardiology*, *48*(6), 1080–7. doi:10.1016/j.yjmcc.2009.10.012

Heymans, S., Lupu, F., Terclavers, S., Vanwetswinkel, B., Herbert, J.-M., Baker, A., … Moons, L. (2005). Loss or inhibition of uPA or MMP-9 attenuates LV remodeling and dysfunction after acute pressure overload in mice. *The American Journal of Pathology*, *166*(1), 15–25. doi:10.1016/S0002-9440(10)62228-6

Ho, C. Y., López, B., Coelho-Filho, O. R., Lakdawala, N. K., Cirino, A. L., Jarolim, P., … Seidman, C. E. (2010). Myocardial fibrosis as an early manifestation of hypertrophic cardiomyopathy. *The New England Journal of Medicine*, *363*(6), 552–63. doi:10.1056/NEJMoa1002659

Hudsmith, L. E., & Neubauer, S. (2008). Detection of myocardial disorders by magnetic resonance spectroscopy. *Nature Clinicla Practice Cardiovascular Medicine*, *5*, S49–S56.

Hulmes, D. J. S. (2008). Collagen Diversity, Synthesis and Assembly. In P. Fratzl (Ed.), *Collagen Structure and Mechanics* (pp. 15–41). Potsdam, Germany: Springer Science+Business Media, LLC.

Intrigila, B., Melatti, I., Tofani, A., & Macchiarelli, G. (2007). Computational models of myocardial endomysial collagen arrangement. *Computer Methods and Programs in Biomedicine*, *86*(3), 232–44. doi:10.1016/j.cmpb.2007.03.004

Iwanaga, Y., Aoyama, T., Kihara, Y., Onozawa, Y., Yoneda, T., & Sasayama, S. (2002).

Excessive activation of matrix metalloproteinases coincides with left ventricular remodeling during transition from hypertrophy to heart failure in hypertensive rats. *Journal of the American College of Cardiology*, *39*(8), 1384–1391. doi:10.1016/S0735-1097(02)01756-4

Janicki, J. S., & Brower, G. L. (2002). The role of myocardial fibrillar collagen in ventricular remodeling and function. *Journal of Cardiac Failure*, *8*(6 Suppl), S319–25. doi:10.1054/jcaf.2002.129260

Jugdutt, B. I., & Amy, R. W. M. (1986). Healing after myocardial infarction in the dog: Changes in infarct hydroxyproline and topography. *Journal of the American College of Cardiology*, *7*(1), 91–102. doi:10.1016/S0735-1097(86)80265-0

Kaczmarek-Hájek, K., Lörinczi, E., Hausmann, R., & Nicke, A. (2012). Molecular and functional properties of P2X receptors--recent progress and persisting challenges. *Purinergic Signalling*, *8*(3), 375–417. doi:10.1007/s11302-012-9314-7

Kai, H., Kuwahara, F., Tokuda, K., & Imaizumi, T. (2005). Diastolic Dysfunction in Hypertensive Hearts: Roles of Perivascular Inflammation and Reactive Myocardial Fibrosis. *Hypertension Research*, *28*(6), 483–490.

Kalluri, R., & Zeisberg, M. (2006). Fibroblasts in cancer. *Nature Reviews. Cancer*, *6*(5), 392–401. doi:10.1038/nrc1877

Kanzaki, Y., Terasaki, F., Okabe, M., Fujita, S., Katashima, T., Otsuka, K., & Ishizaka, N. (2010). Three-dimensional architecture of cardiomyocytes and connective tissue in human heart revealed by scanning electron microscopy. *Circulation*, *122*(19), 1973–4. doi:10.1161/CIRCULATIONAHA.110.979815

Koeppen, M., Eckle, T., & Eltzschig, H. K. (2009). Selective Deletion of the A1 Adenosine Receptor Abolishes Heart-Rate Slowing Effects of Intravascular Adenosine <italic>In Vivo</italic>. *PLoS ONE*, *4*(8), e6784. Retrieved from http://dx.doi.org/10.1371%2Fjournal.pone.0006784

Kong, P., Christia, P., & Frangogiannis, N. G. (2014). The pathogenesis of cardiac fibrosis. *Cellular and Molecular Life Sciences : CMLS*, *71*(4), 549–74. doi:10.1007/s00018-013-1349-6

Koumas, L., Smith, T. J., Feldon, S., Blumberg, N., & Phipps, R. P. (2003). Thy-1 expression in human fibroblast subsets defines myofibroblastic or lipofibroblastic phenotypes. *The American Journal of Pathology*, *163*(4), 1291–300. doi:10.1016/S0002-9440(10)63488-8

Krenning, G., Zeisberg, E. M., & Kalluri, R. (2010). The origin of fibroblasts and mechanism of cardiac fibrosis. *Journal of Cellular Physiology*, *225*(3), 631–637. doi:10.1002/jcp.22322.The

Kuusisto, J., Kärjä, V., Sipola, P., Kholová, I., Peuhkurinen, K., Jääskeläinen, P., … Laakso, M. (2012). Low-grade inflammation and the phenotypic expression of myocardial fibrosis in hypertrophic cardiomyopathy. *Heart (British Cardiac Society)*, *98*(13),

1007–13. doi:10.1136/heartjnl-2011-300960

Kuwahara, F., Kai, H., Tokuda, K., Kai, M., Takeshita, A., Egashira, K., & Imaizumi, T. (2002). Transforming Growth Factor-beta Function Blocking Prevents Myocardial Fibrosis and Diastolic Dysfunction in Pressure-Overloaded Rats. *Circulation*, *106*(1), 130–135. doi:10.1161/01.CIR.0000020689.12472.E0

Laurent, G. J. (1987). Dynamic state of collagen: pathways of collagen degradation in vivo and their possible role in regulation of collagen mass. *The American Journal of Physiology*, *252*(1 Pt 1), C1–9. Retrieved from http://www.ncbi.nlm.nih.gov/pubmed/3544859

LeGrice, I. J., Pope, A. J., Sands, G. B., Whalley, G., Doughty, R. N., & Smaill, B. H. (2012). Progression of myocardial remodeling and mechanical dysfunction in the spontaneously hypertensive rat. *American Journal of Physiology. Heart and Circulatory Physiology*, *303*(11), H1353–65. doi:10.1152/ajpheart.00748.2011

Lijnen, P., & Petrov, V. (2000). Induction of cardiac fibrosis by aldosterone. *Journal of Molecular and Cellular Cardiology*, *32*(6), 865–79. doi:10.1006/jmcc.2000.1129

Lu, D., & Insel, P. a. (2014). Cellular mechanisms of tissue fibrosis. 6. Purinergic signaling and response in fibroblasts and tissue fibrosis. *American Journal of Physiology. Cell Physiology*, *306*(9), C779–88. doi:10.1152/ajpcell.00381.2013

Lu, D., Soleymani, S., Madakshire, R., & Insel, P. a. (2012). ATP released from cardiac fibroblasts via connexin hemichannels activates profibrotic P2Y2 receptors. *FASEB Journal : Official Publication of the Federation of American Societies for Experimental Biology*, *26*(6), 2580–91. doi:10.1096/fj.12-204677

Lygate, C. a, Fischer, A., Sebag-Montefiore, L., Wallis, J., ten Hove, M., & Neubauer, S. (2007). The creatine kinase energy transport system in the failing mouse heart. *Journal of Molecular and Cellular Cardiology*, *42*(6), 1129–36. doi:10.1016/j.yjmcc.2007.03.899

Macchiarelli, G., & Ohtani, O. (2001). Endomysium in left ventricle. *Heart (British Cardiac Society)*, *86*(4), 416. Retrieved from http://www.pubmedcentral.nih.gov/articlerender.fcgi?artid=1729923&tool=pmcentrez&rendertype=abstract

Macchiarelli, G., Ohtani, O., Nottola, S. a, Stallone, T., Camboni, a, Prado, I. M., & Motta, P. M. (2002). A micro-anatomical model of the distribution of myocardial endomysial collagen. *Histology and Histopathology*, *17*(3), 699–706. Retrieved from http://www.ncbi.nlm.nih.gov/pubmed/12168777

Mallat, A., & Lotersztajn, S. (2013). Cellular mechanisms of tissue fibrosis. 5. Novel insights into liver fibrosis. *American Journal of Physiology. Cell Physiology*, *305*(8), C789–99. doi:10.1152/ajpcell.00230.2013

Maron, B. J., Wolfson, J. K., Epstein, S. E., & Roberts, W. C. (1987). Morphologic evidence for “small vessel disease” in patients with hypertrophic cardiomyopathy. *Zeitschrift*

*Fur Kardiologie*, *76 Suppl 3*, 91–100.

Maron, M. S., Olivotto, I., Harrigan, C., Appelbaum, E., Gibson, C. M., Lesser, J. R., … Maron, B. J. (2011). Mitral valve abnormalities identified by cardiovascular magnetic resonance represent a primary phenotypic expression of hypertrophic cardiomyopathy. *Circulation*, *124*(1), 40–7. doi:10.1161/CIRCULATIONAHA.110.985812

Marotta, M., & Martino, G. (1985). Sensitive spectrophotometric method for the quantitative estimation of collagen. *Analytical Biochemistry*, *150*(1), 86–90. Retrieved from http://www.ncbi.nlm.nih.gov/pubmed/4083486

Maslov, M., Chacko, V., Stuber, M., Moens, A., Kass, D., Champion, H., & Weiss, R. (2007). Altered high-energy phosphate metabolism predicts contractile dysfunction and subsequent ventricular remodeling in pressure-overload hypertrophy mice. *American Journal of …*, *6568*(292), 387–391. doi:10.1152/ajpheart.00737.2006.

Merante, F., Tein, I., Benson, L., & Robinson, B. H. (1994). Maternally inherited hypertrophic cardiomyopathy due to a novel T-to-C transition at nucleotide 9997 in the mitochondrial tRNA(glycine) gene. *American Journal of Human Genetics*, *55*(3), 437–446.

Meyer, T. E., Chung, E. S., Perlini, S., Norton, G. R., Woodiwiss, a. J., Lorbar, M., … Dobson, J. G. (2001). Antiadrenergic Effects of Adenosine in Pressure Overload Hypertrophy. *Hypertension*, *37*(3), 862–868. doi:10.1161/01.HYP.37.3.862

Moens, A. L., Takimoto, E., Tocchetti, C. G., Chakir, K., Bedja, D., Cormaci, G., … Kass, D. a. (2008). Reversal of cardiac hypertrophy and fibrosis from pressure overload by tetrahydrobiopterin: efficacy of recoupling nitric oxide synthase as a therapeutic strategy. *Circulation*, *117*(20), 2626–36. doi:10.1161/CIRCULATIONAHA.107.737031

Möllmann, H., Nef, H. M., Kostin, S., von Kalle, C., Pilz, I., Weber, M., … Elsässer, A. (2006). Bone marrow-derived cells contribute to infarct remodelling. *Cardiovascular Research*, *71*(4), 661–71. doi:10.1016/j.cardiores.2006.06.013

Mubagwa, K., & Flameng, W. (2001). Adenosine, adenosine receptors and myocardial protection: an updated overview. *Cardiovascular Research*, *52*(1), 25–39. Retrieved from http://www.ncbi.nlm.nih.gov/pubmed/11557231

Müller, C. E., Iqbal, J., Baqi, Y., Zimmermann, H., Röllich, A., & Stephan, H. (2006). Polyoxometalates--a new class of potent ecto-nucleoside triphosphate diphosphohydrolase (NTPDase) inhibitors. *Bioorganic & Medicinal Chemistry Letters*, *16*(23), 5943–7. doi:10.1016/j.bmcl.2006.09.003

Nag, A. C. (1980). Study of non-muscle cells of the adult mammalian heart: a fine structural analysis and distribution. *Cytobios*, *28*(109), 41–61. Retrieved from http://www.ncbi.nlm.nih.gov/pubmed/7428441

Neubauer, S. (2007). The failing heart—an engine out of fuel. *New England Journal of*

*Medicine*, *356*, 1140–51. Retrieved from http://www.nejm.org/doi/full/10.1056/nejmra063052

Neubauer, S., Horn, M., Cramer, M., Harre, K., Newell, J. B., Peters, W., … Kochsiek, K. (1997). Myocardial Phosphocreatine-to-ATP Ratio Is a Predictor of Mortality in Patients With Dilated Cardiomyopathy. *Circulation* , *96* (7 ), 2190–2196. Retrieved from http://circ.ahajournals.org/content/96/7/2190.abstract

Neubauer, S., Horn, M., Pabst, T., Gödde, M., Lübke, D., Jilling, B., … Ertl, G. (1995). Contributions of 31P-magnetic resonance spectroscopy to the understanding of dilated heart muscle disease. *European Heart Journal*, *16*, 115–118. Retrieved from http://eurheartj.oxfordjournals.org/content/16/suppl_O/115.short

Neubauer, S., Krahe, T., Schindler, R., Horn, M., Hillenbrand, H., Entzeroth, C., … Lackner, K. (1992). 31P magnetic resonance spectroscopy in dilated cardiomyopathy and coronary artery disease. Altered cardiac high-energy phosphate metabolism in heart failure. *Circulation*, *86*(6), 1810–1818. doi:10.1161/01.CIR.86.6.1810

Neumann, S., Huse, K., Semrau, R., Diegeler, A., Gebhardt, R., Buniatian, G. H., & Scholz, G. H. (2002). Aldosterone and D-Glucose Stimulate the Proliferation of Human Cardiac Myofibroblasts In Vitro. *Hypertension*, *39*(3), 756–760. doi:10.1161/hy0302.105295

Nishida, M., Sato, Y., Uemura, A., Narita, Y., Tozaki-Saitoh, H., Nakaya, M., … Kurose, H. (2008). P2Y6 receptor-Galpha12/13 signalling in cardiomyocytes triggers pressure overload-induced cardiac fibrosis. *The EMBO Journal*, *27*(23), 3104–15. doi:10.1038/emboj.2008.237

O'Hanlon, R., Grasso, A., Roughton, M., Moon, J. C., Clark, S., Wage, R., … Prasad, S. K. (2010). Prognostic significance of myocardial fibrosis in hypertrophic cardiomyopathy. *Journal of the American College of Cardiology*, *56*(11), 867–74. doi:10.1016/j.jacc.2010.05.010

Oberst, L., Zhao, G., Park, J. T., Brugada, R., Michael, L. H., Entman, M. L., … Marian, a J. (1998). Dominant-negative effect of a mutant cardiac troponin T on cardiac structure and function in transgenic mice. *The Journal of Clinical Investigation*, *102*(8), 1498–505. doi:10.1172/JCI4088

Packer, M., Bristow, M. R., Cohn, J. N., Colucci, W. S., Fowler, M. B., Gilbert, E. M., & Shusterman, N. H. (1996). The effect of carvedilol on morbidity and mortality in patients with chronic heart failure. *The New England Journal of Medicine*, *334*(21), 1349–1355. Retrieved from http://www.nejm.org/doi/full/10.1056/NEJM199605233342101

Pfeffer, M. a, Braunwald, E., Moyé, L. A., Basta, L., Brown, E. J., Cuddy, T. E., … Hawkins, M. C. (1992). Effect of captopril on mortality and morbidity in patients with left ventricular dysfunction after myocardial infarction: results of the survival and ventricular enlargement. *The New England Journal of Medicine*, *327*(10), 669–677. Retrieved from http://www.nejm.org/doi/full/10.1056/NEJM199209033271001

Pfeffer, M. a, Swedberg, K., Granger, C. B., Held, P., McMurray, J. J., Michelson, E. L., … Yusuf, S. (2003). Effects of candesartan on mortality and morbidity in patients with chronic heart failure: the CHARM-Overall programme. *The Lancet*, *362*(9386), 759–766. doi:10.1016/S0140-6736(03)14282-1

Phipps, R. P., Penney, D. P., Keng, P., Quill, H., Paxhia, A., Derdak, S., & Felch, M. E. (1989). Characterization of Two Major Populations of Lung Fibroblasts: Distinguishing Morphology and Discordant Display of Thy 1 and Class II MHC. *American Journal of Respiratory Cell and Molecular Biology*, *1*(1), 65–74. doi:10.1165/ajrcmb/1.1.65

Plaksej, R., Kosmala, W., Frantz, S., Herrmann, S., Niemann, M., Störk, S., … Weidemann, F. (2009). Relation of circulating markers of fibrosis and progression of left and right ventricular dysfunction in hypertensive patients with heart failure. *Journal of Hypertension*, *27*(12), 2483–91. doi:10.1097/HJH.0b013e3283316c4d

Pope, A. J., Sands, G. B., Smaill, B. H., & LeGrice, I. J. (2008). Three-dimensional transmural organization of perimysial collagen in the heart. *American Journal of Physiology. Heart and Circulatory Physiology*, *295*(3), H1243–H1252. doi:10.1152/ajpheart.00484.2008

Porter, K. E., & Turner, N. a. (2009). Cardiac fibroblasts: at the heart of myocardial remodeling. *Pharmacology & Therapeutics*, *123*(2), 255–78. doi:10.1016/j.pharmthera.2009.05.002

Povlsen, J. A., Løfgren, B., Dalgas, C., Birkler, R. I. D., Johannsen, M., Støttrup, N. B., & Bøtker, H. E. (2013). Protection against Myocardial Ischemia-Reperfusion Injury at Onset of Type 2 Diabetes in Zucker Diabetic Fatty Rats Is Associated with Altered Glucose Oxidation. *PloS One*, *8*(5), e64093. doi:10.1371/journal.pone.0064093

Pula, B., Witkiewicz, W., Dziegiel, P., & Podhorska-Okolow, M. (2013). Significance of podoplanin expression in cancer-associated fibroblasts: a comprehensive review. *International Journal of Oncology*, *42*(6), 1849–57. doi:10.3892/ijo.2013.1887

Purslow, P. P. (2008). The extracellular matrix of skeletal and cardiac muscle. In P. Fratzl (Ed.), *Collagen Structure and Mechanics* (pp. 325–357). Potsdam, Germany: Springer Science+Business Media, LLC.

Regan, C. P., Anderson, P. G., Bishop, S. P., & Berecek, K. H. (1997). Pressure-independent effects of AT1-receptor antagonism on cardiovascular remodeling in aortic-banded rats. *American Journal of Physiology. Heart and Circulatory Physiology*, *272*(5), H2131–H2138. Retrieved from http://ajpheart.physiology.org/content/ajpheart/272/5/H2131.full.pdf

Riteau, N., Gasse, P., Fauconnier, L., Gombault, A., Couegnat, M., Fick, L., … Couillin, I. (2010). Extracellular ATP is a danger signal activating P2X7 receptor in lung inflammation and fibrosis. *American Journal of Respiratory and Critical Care Medicine*, *182*(6), 774–83. doi:10.1164/rccm.201003-0359OC

Robinson, T. F., Geraci, M. a., Sonnenblick, E. H., & Factor, S. M. (1988). Coiled perimysial fibers of papillary muscle in rat heart: morphology, distribution, and changes in

configuration. *Circulation Research*, *63*(3), 577–592. doi:10.1161/01.RES.63.3.577

Rossi, M. a., Abreu, M. a., & Santoro, L. B. (1998). Connective Tissue Skeleton of the Human Heart : A Demonstration by Cell-Maceration Scanning Electron Microscope Method. *Circulation*, *97*(9), 934–935. doi:10.1161/01.CIR.97.9.934

Sadoshima, J., & Izumo, S. (1993). Molecular characterization of angiotensin II--induced hypertrophy of cardiac myocytes and hyperplasia of cardiac fibroblasts. Critical role of the AT1 receptor subtype. *Circulation Research*, *73*(3), 413–423. doi:10.1161/01.RES.73.3.413

Sakaguchi, T., Sawa, Y., Kitakaze, M., Suzuki, K., Nishimura, M., Kaneda, Y., & Matsuda, H. (2000). Ecto-5'-nucleotidase plays a role in the cardioprotective effects of heat shock protein 72 in ischemia-reperfusion injury in rat hearts. *Cardiovascular Research*, *47*(1), 74–80. Retrieved from http://www.ncbi.nlm.nih.gov/pubmed/10869532

Schieffer, B., Wirger, a., Meybrunn, M., Seitz, S., Holtz, J., Riede, U. N., & Drexler, H. (1994). Comparative effects of chronic angiotensin-converting enzyme inhibition and angiotensin II type 1 receptor blockade on cardiac remodeling after myocardial infarction in the rat. *Circulation*, *89*(5), 2273–2282. doi:10.1161/01.CIR.89.5.2273

Scholzen, T., & Gerdes, J. (2000). The Ki-67 Protein : From the Known and Unknown. *Journal of Cellular Physiology*, *182*, 311–322.

Schorb, W., Booz, G. W., Dostal, D. E., Conrad, K. M., Chang, K. C., & Baker, K. M. (1993). Angiotensin II is mitogenic in neonatal rat cardiac fibroblasts. *Circulation Research*, *72*(6), 1245–1254. doi:10.1161/01.RES.72.6.1245

Schroeder, M., Ali, M., Hulikova, A., Supuran, C. T., Clarke, K., Vaughan-Jones, R. D., … Swietach, P. (2013). Extramitochondrial domain rich in carbonic anhydrase activity improves myocardial energetics. *Proceedings of the …*, *110*(10). doi:10.1073/pnas.1213471110/-/DCSupplemental.www.pnas.org/cgi/doi/10.1073/pnas.1213471110

Sedej, S., Schmidt, A., Denegri, M., Walther, S., Matovina, M., Arnstein, G., … Pieske, B. (2014). Subclinical abnormalities in sarcoplasmic reticulum Ca2+ release promote eccentric myocardial remodeling and pump failure death in response to pressure overload. *Journal of the American College of Cardiology*, *63*(15), 1569–1579. doi:10.1016/j.jacc.2013.11.010

Silverman, W., Locovei, S., & Dahl, G. (2008). Probenecid, a gout remedy, inhibits pannexin 1 channels. *American Journal of Physiology. Cell Physiology*, *295*(3), C761–7. doi:10.1152/ajpcell.00227.2008

Sinclair, C. J., Shepel, P. N., Geiger, J. D., & Parkinson, F. E. (2000). Stimulation of nucleoside efflux and inhibition of adenosine kinase by A1 adenosine receptor activation. *Biochemical Pharmacology*, *59*(5), 477–83. Retrieved from http://www.ncbi.nlm.nih.gov/pubmed/10660114

Song, W., Dyer, E., Stuckey, D. J., Copeland, O., Leung, M.-C., Bayliss, C., … Marston, S. B. (2011). Molecular mechanism of the Glu99lys mutation in cardiac actin (ACTC gene) that causes apical hypertrophy in man and mouse. *The Journal of Biological Chemistry*, *286*(31), 27582–27593. doi:10.1074/jbc.M111.252320

Souders, C. a, Bowers, S. L. K., & Baudino, T. a. (2009). Cardiac fibroblast: the renaissance cell. *Circulation Research*, *105*(12), 1164–76. doi:10.1161/CIRCRESAHA.109.209809

Støttrup, N. B., Løfgren, B., Birkler, R. D., Nielsen, J. M., Wang, L., Caldarone, C. A., … Nielsen, T. T. (2010). Inhibition of the malate-aspartate shuttle by pre-ischaemic aminooxyacetate loading of the heart induces cardioprotection. *Cardiovascular Research*, *88*(2), 257–66. doi:10.1093/cvr/cvq205

Stypmann, J., Engelen, M. a, Troatz, C., Rothenburger, M., Eckardt, L., & Tiemann, K. (2009). Echocardiographic assessment of global left ventricular function in mice. *Laboratory Animals*, *43*(2), 127–37. doi:10.1258/la.2007.06001e

Sun, Y., & Weber, K. T. (2010). Animal Models of Cardiac Fibrosis. In J. Varga, D. A. Brenner, & S. H. Phan (Eds.), *Fibrosis Research* (pp. 273–290). Totowa, New Jersey: Humana Press Inc.

Synnestvedt, K., Furuta, G. T., Comerford, K. M., Louis, N., Karhausen, J., Eltzschig, H. K., … Colgan, S. P. (2002). Ecto-5′-nucleotidase (CD73) regulation by hypoxia-inducible factor-1 mediates permeability changes in intestinal epithelia. *Journal of Clinical …*, *110*(7), 993–1002. doi:10.1172/JCI200215337.Introduction

Takeda, N., Manabe, I., Uchino, Y., Eguchi, K., Matsumoto, S., Nishimura, S., … Nagai, R. (2010). Cardiac fibroblasts are essential for the adaptive response of the murine heart to pressure overload. *The Journal of Clinical Investigation*, *120*(1), 254–265. doi:10.1172/JCI40295

Teekakirikul, P., Eminaga, S., Toka, O., Alcalai, R., Wang, L., Wakimoto, H., … others. (2010). Cardiac fibrosis in mice with hypertrophic cardiomyopathy is mediated by non-myocyte proliferation and requires Tgf-$\beta$. *The Journal of Clinical Investigation*, *120*(10), 3520. doi:10.1172/JCI42028DS1

Varga, J., Brenner, D. A., & Phan, S. H. (2010). *Fibrosis Research. Methods and Protocols*. (J. M. Walker, C. Tirpak, & M. Caravella, Eds.). Totowa, New Jersey: Humana Press Inc.

Vaughn, B. P., Robson, S. C., & Burnstock, G. (2012). Pathological roles of purinergic signaling in the liver. *Journal of Hepatology*, *57*(4), 916–20. doi:10.1016/j.jhep.2012.06.008

Vial, C., Owen, P., Opie, L. H., & Posel, D. (1987). Significance of release of adenosine triphosphate and adenosine induced by hypoxia or adrenaline in perfused rat heart. *Journal of Molecular and Cellular Cardiology*, *19*(2), 187–97. Retrieved from http://www.ncbi.nlm.nih.gov/pubmed/2883323

Vignier, N., Schlossarek, S., Fraysse, B., Mearini, G., Krämer, E., Pointu, H., … Carrier, L.

(2009). Nonsense-mediated mRNA decay and ubiquitin-proteasome system regulate cardiac myosin-binding protein C mutant levels in cardiomyopathic mice. *Circulation Research*, *105*(3), 239–48. doi:10.1161/CIRCRESAHA.109.201251

Virchow, R. (1858). *Die Cellularpathologie in ihrer Begruendung auf physiologische und pathologische Gewebelehre.* (A. Hirschwald, Ed.). Berlin, Germany: Verlag von August Hirschwald.

Von Gise, A., & Pu, W. T. (2012). Endocardial and epicardial epithelial to mesenchymal transitions in heart development and disease. *Circulation Research*, *110*(12), 1628–45. doi:10.1161/CIRCRESAHA.111.259960

Wallis, J., Lygate, C. A., Fischer, A., ten Hove, M., Schneider, J. E., Sebag-Montefiore, L., … Neubauer, S. (2005). Supranormal Myocardial Creatine and Phosphocreatine Concentrations Lead to Cardiac Hypertrophy and Heart Failure: Insights From Creatine Transporter–Overexpressing Transgenic Mice . *Circulation* , *112* (20 ), 3131–3139. Retrieved from http://circ.ahajournals.org/content/112/20/3131.abstract

Walsh, K. B., Zhang, J., Fuseler, J. W., Hilliard, N., & Hockerman, G. H. (2007). Adenoviral-mediated expression of dihydropyridine-insensitive L-type calcium channels in cardiac ventricular myocytes and fibroblasts. *European Journal of Pharmacology*, *565*(1-3), 7–16. doi:10.1016/j.ejphar.2007.02.049

Watkins, H., Ashrafian, H., & Redwood, C. (2011). Inherited cardiomyopathies. *The New England Journal of Medicine*, *364*(17), 1643–56. doi:10.1056/NEJMra0902923

Weber, K. T. (1989). Cardiac interstitium in health and disease: the fibrillar collagen network. *Journal of the American College of Cardiology*, *13*(7), 1637–52. Retrieved from http://www.ncbi.nlm.nih.gov/pubmed/2656824

Weber, K. T., Janicki, J. S., Shroff, S. G., Pick, R., Chen, R. M., & Bashey, R. I. (1988). Collagen remodeling of the pressure-overloaded, hypertrophied nonhuman primate myocardium. *Circulation Research*, *62*(4), 757–765. doi:10.1161/01.RES.62.4.757

Weber, K. T., Sun, Y., Bhattacharya, S. K., Ahokas, R. a, & Gerling, I. C. (2013). Myofibroblast-mediated mechanisms of pathological remodelling of the heart. *Nature Reviews. Cardiology*, *10*(1), 15–26. doi:10.1038/nrcardio.2012.158

Westermann, D. (2012). Does inflammation trigger fibrosis in hypertrophic cardiomyopathy: a burning question? *Heart (British Cardiac Society)*, *98*(13), 965–6. doi:10.1136/heartjnl-2012-301730

Wynn, T. a, & Ramalingam, T. R. (2012). Mechanisms of fibrosis: therapeutic translation for fibrotic disease. *Nature Medicine*, *18*(7), 1028–40. doi:10.1038/nm.2807

Xu, X., Fassett, J., Hu, X., Zhu, G., Lu, Z., Li, Y., … Chen, Y. (2008). Ecto-5'-nucleotidase deficiency exacerbates pressure-overload-induced left ventricular hypertrophy and dysfunction. *Hypertension*, *51*(6), 1557–64.

doi:10.1161/HYPERTENSIONAHA.108.110833

Yang, J.-N., Chen, J.-F., & Fredholm, B. B. (2009). Physiological roles of A1 and A2A adenosine receptors in regulating heart rate, body temperature, and locomotion as revealed using knockout mice and caffeine. *American Journal of Physiology - Heart and Circulatory Physiology*, *296*(4), H1141–H1149. Retrieved from http://ajpheart.physiology.org/content/296/4/H1141.abstract

Ying, X., Lee, K., Li, N., Corbett, D., Mendoza, L., & Frangogiannis, N. G. (2009). Characterization of the Inflammatory Fibrotic Response in a Mouse Model of Cardiac Pressure Overload. *Histochemistry and Cell …*, *131*(4), 471–481. doi:10.1007/s00418-008-0541-5.Characterization

Zak, R. (1974). Development and proliferative capacity of cardiac muscle cells. *Circulation Research*, *35*(2), suppl II:17–26. Retrieved from http://www.ncbi.nlm.nih.gov/pubmed/4276486

Zeisberg, E. M., Tarnavski, O., Zeisberg, M., Dorfman, A. L., McMullen, J. R., Gustafsson, E., … Kalluri, R. (2007). Endothelial-to-mesenchymal transition contributes to cardiac fibrosis. *Nature Medicine*, *13*(8), 952–61. doi:10.1038/nm1613

Zeisberg, M., & Kalluri, R. (2013). Cellular mechanisms of tissue fibrosis. 1. Common and organ-specific mechanisms associated with tissue fibrosis. *American Journal of Physiology. Cell Physiology*, *304*(3), C216–25. doi:10.1152/ajpcell.00328.2012

Zhang, W., ten Hove, M., Schneider, J. E., Stuckey, D. J., Sebag-Montefiore, L., Bia, B. L., … Clarke, K. (2008). Abnormal cardiac morphology, function and energy metabolism in the dystrophic mdx mouse: an MRI and MRS study. *Journal of Molecular and Cellular Cardiology*, *45*(6), 754–60. doi:10.1016/j.yjmcc.2008.09.125